EVALUATION OF PLANT ROOT ON THE PERFORMANCE OF EVAPOTRANSPIRATION (ET) COVER SYSTEM

By

MD JOBAIR BIN ALAM

Presented to the Faculty of the Graduate School of

The University of Texas at Arlington in Partial Fulfillment

of the Requirements

for the Degree of

DOCTOR OF PHILOSOPHY

THE UNIVERSITY OF TEXAS AT ARLINGTON

OCTOBER 2017

Acknowledgements

First, I would like to express my sincere gratitude to my supervisor, Dr. Sahadat Hossain, for being so generous with his time and providing direction, inspiration, assistance, and unconditional support throughout my graduate studies. Without his continuous guidance and support, this dissertation would not have been completed.

I would also like to express my special thanks to Dr. Melanie Sattler, Dr. Xinbao Yu, and Dr. Saiful M Chowdhury for sharing their precious time and valuable suggestions, and for participating as members of my committee.

I am thankful to my undergraduate supervisor Dr. A.B.M. Badruzzaman for encouraging me for higher studies and achieving my goal. Funding from the City of Denton Landfill made this research possible, for which I am very grateful. Special thanks go to Vance Kemler and David Dugger for their support during all the stages of this research.

Lucas Hoyos and Cory Rauss worked as a team and assisted in all stages of this research, and their efforts are much appreciated. I would like to thank Dr. Brett DeVries for his valuable suggestions and assistance during this research. My heartiest appreciation to Rezaul Haque, Ferdous Intaj, Dr. Sadik Khan, Dr. Istiaque Hasan, Dr. Shahed Manzur and Dr. Zahangir Alam for their continuous encouragement over the phone. I would also like to thank my dearest friends, Rakib Ahmed, Arindam Dhar, Asif Ahmed, and Abu Hasan for their valued friendship and many good times.

I sincerely express my gratitude to my beloved wife, Naima Rahman, for her cooperation, perseverance, sacrifice, and endless support throughout my graduate studies, and my sisters, Sharmin Alam and Farhana Alam, for their support.

Finally, I would like to dedicate this dissertation to my parents for their infinite love, encouragement, and extraordinary support. I am truly blessed to be a part of their family.

October 17, 2017

Abstract

EVALUATION OF PLANT ROOT ON THE PERFORMANCE OF

EVAPOTRANSPIRATION (ET) COVER SYSTEMS

Md Jobair Bin Alam, PhD

The University of Texas at Arlington, 2017

Supervising Professor: MD. Sahadat Hossain

The performance of an evapotranspiration (ET) cover for a landfill exceeds that of a conventional landfill final cover. Its low percolation and high evapotranspiration rely on the properties of unsaturated soils, the energy demands of plants, and the atmosphere. Plant roots pull water out of the cover soil and release it into the environment, thus managing water in a much more natural way than the conventional cover, where water is controlled by creating a physical barrier. Therefore, plant roots are a significant component in the optimization of ET cover performance. In recent years, a great deal of effort has been made to understand the effectiveness of the ET cover system in different regions of the United States. However, comprehensive studies, through field monitoring and model prediction, on the plant root and its effect on the performance of the ET cover are very limited. No research incorporating a thorough study on plant roots has been conducted in the semi-humid region of Texas to evaluate the performance of ET covers. Therefore, the motivation of this study was to develop a methodical approach to investigating below-ground biomass (roots) and to evaluate their effect on the performance of the ET cover.

Six instrumented field-scale test sections (Lysimeter) of soil cover (three on the flat section and three on the slope section), made of 3 ft. thick compacted clay overlain by 1 ft. thick topsoil, were constructed at the City of Denton Landfill, TX and monitored for three and one-half years. Three different types of vegetation were planted in the test sections. Eight acrylic plastic tubes (minirhizotron) were installed in the six test sections to

determine the root zone depth, root distribution and assess the root dynamics. Root images were captured from minirhizotrons to quantify the roots in terms of length through image analysis. A systematic approach was undertaken for enhancing the image quality before quantification. Traditional root sampling and electrical resistivity imaging on the cover were conducted to verify the results obtained from the minirhizotron. To evaluate the changes in the soil properties, a field soil water characteristic curve (FSWCC) was developed, based on the instrumentation results. A Guelph permeameter was used to determine the time-dependent saturated hydraulic conductivity of the cover soil.

Measured root depth and distribution was found to be limited to certain depths. The maximum root depth found was for Bermuda grass (nearly 20 inches). Soil density was found to be a resistive factor for root growth. Field evapotranspiration (ET) from water balance measurements was found short of potential evapotranspiration (PET) due to the lack of adequate root depth. Bermuda grass was found to perform relatively better than other grasses in terms of annual transpiration. No significant difference was observed in the annual percolation (45 mm to 80 mm) of all the lysimeters throughout the monitoring period. The major pulse of percolation occurred during high intensity rainfall.

Finally, the water balance of the lysimeters was simulated, using the UNSAT-H code. A forward model with a conservative approach and field-fit simulation were conducted to compare the field water balance. Field-fit simulation yielded results that were close to those of the field-monitored results. A parametric study was conducted to evaluate the climatological parameters and the critical soil and plant parameters. Parametric study revealed that increased root depth is more important than shallow root depth with high density to reduce annual percolation. Annual precipitation with frequent high intensity events causes the major increment in annual percolation. Saturated and unsaturated hydraulic properties also play significant roles in the amount of annual percolation.

Table of Contents

List of Illustrations

List of Tables

Chapter 1

Introduction

1.1 Background

The government of the United States and other private concerns spend trillions of dollars to undertake the mammoth task of cleaning up landfills and waste disposal sites across the country. The single most expensive part of this task is closing these landfills and waste disposal sites and maintaining them after closure. The fundamental element of landfill closure is the efficient design and construction of the final cover that is intended to isolate the underlying waste material from the environment.

The U.S. Environmental Protection Agency (EPA) recommends a prescriptive cover that is used throughout the United States, but they have shown little regard for regional and local meteorological conditions. The most common design of the final cover (compacted soil layer or barrier layer) recommended by the EPA experiences countless problems, including desiccation cracking, due to extensive loss of moisture during the summer, and deterioration resulting from freeze/thaw cycles. Desiccation occurs from several complex mechanisms and is a significant failure mode for compacted soil, especially in arid environments (Suter et al. 1993). The EPA of California made known that compacted clay barrier layers fail with no regard of climate and site geology (Mulder and Haven 1995). Incorporating geosynthetic material (i.e., geomembrane) in prescriptive cover design brought a remarkable solution, but did not fully resolve the problem. Geosynthetic materials are used in conventional landfill covers, but there are some flaws, and they have increased construction cost and design complexity. Most importantly, the database for evaluating the long-term durability of the geosynthetic material is very limited. In accordance with the EPA design guidance document for final landfill covers, a barrier soil layer composed of natural soil and geomembrane is not effective, as the soil that is

compacted wet of optimum moisture content will dry and crack, and will eventually make a preferential flow path for the water to move into the cover soil (EPA 1991). Prescriptive covers are problematic, expensive, and difficult to construct (Dwyer 2000, Hauser et al. 2001). It is obvious from observation that the performance of landfill covers diminishes with the passage of time. Normally, the moisture intrusion through the cover soil is not measured, and it ultimately plays the main role in a leaching problem. All over the world, there is evidence of ground water contamination through landfill leachate, and a poorly designed final cover contributes to this problem. Adequate design and a properly-constructed landfill final cover can alleviate the problem.

The evapotranspiration cover system (ET Cover), also known as the water balance cover, has several advantages over the prescriptive or conventional landfill cover (EPA 2003; Benson et al. 2005; ITRC 2003). It is simpler to construct, less costly to maintain, and its performance is expected to improve with time (Albright et al. 2004, Hauser 2008). The basic principal of an ET cover system is that it stores precipitation during the rainy season and releases it into the environment during the dry period by means of evaporation from the top cover soil and transpiration from the vegetation (Barnswell and Dwyer 2011, Benson et al. 2002, Khire et al. 2000, Malusis and Benson 2006, and Stormont and Morris 1998, Albright et al. 2004, 2010; Bohnhoff et al. 2009). Thus, it minimizes the percolation of water into the waste mass under the cover. The ET cover is also justifiable because it can be constructed with natural on-site materials, and the local vegetation harmonizes with local climatological and soil conditions. Most importantly, it can be constructed by locally-available labor, at low construction cost, and without sophisticated equipment (Benson and Bareither 2012). Unlike a prescriptive cover, the soil of an ET cover is minimally compacted, allowing the low-hydraulic-conductivity-barrier layer to restrict percolation. A lower compaction effort promotes the storage capacity of the soil and reduces the potential for

desiccation cracking and freeze/thaw effects (Othman et al. 1994; Albright et al. 2006). It also promotes vigorous growth of the plant roots, which is necessary for sufficient transpiration (Goldsmith et al. 2001). The healthy root system removes water from the soil (transpiration) beyond the influence of surface evaporation (Andraski 1997; Dwyer 2001; Gee et al. 2002; Albright et al. 2004).

There are basically two choices for ET covers: monolithic covers and capillary barriers (Albright et al. 2004). Monolithic covers are single layers of soil that store water. The capillary barriers consist of a fine-grained soil layer overlaying a coarser grained soil. The interface between the two soil layers forms a capillary break which allows the fine-grained soil to store a greater amount of water than the same thickness of one soil layer (Khire et al. 2000).

1.2 Problem Statement

Although the ET cover system has greater potential to deliver higher performance than the conventional cover system, there are some uncertainties that remain unaddressed. The first is that the system is relatively new, and its performance largely depends on site-specific factors, such as climate, vegetation, and soil conditions. The most important of these is the vegetation, as the rate of transpiration or water removal from the ET cover relies on the plant root characteristics. Therefore, monitoring and understanding the vegetation characteristics; plant root system; root distribution, density, and depth is important for the performance evaluation of the ET cover system.

The EPA, TCEQ, and other state regulators are actively searching for final covers to replace the currently used prescriptive covers, but they need reliable data which establishes that the performance of an alternative cover exceeds that of the prescriptive cover. At the same time, many state regulatory agencies and the EPA are looking for design tools (computer programs) that can accurately analyze the cover performance. So

far, little progress has been made. According to the Environmental Protection Agency (EPA), Office of Solid Waste and Emergency Response, Technology Innovation Program, more than 20 full-scale ET covers have been constructed in the United States; however, descriptions of the design, construction, and performance of them are limited. In Texas, according to the water balance cover guidance document (TCEQ 2012), the percolation at the bottom of the ET cover should not be more than 4 mm/year for a 30-year period. So far in Texas, there is only one study on the ET cover. It is of one in the Chihuahuan desert in Sierra Blanca, an arid region in west Texas (Scanlon et al. 2005), where a capillary barrier ET cover was constructed and monitored for four years. No field scale monolithic ET cover study has been conducted yet; therefore, the dataset that is available is not adequate to flawlessly evaluate the ET cover performance in the field. Moreover, accuracy of the design tools has not been proven, as comparison studies could not be executed with field performance due to the lack of data.

A research project was started in the City of Denton Landfill, Texas in June 2014, to address the effectiveness of the ET cover. Six large-scale lysimeters (40 feet by 40 feet) were constructed in the study area. Different kinds of sensors and instrumentation were installed to monitor and analyze the typical water balance parameters of the ET cover. Three different kinds of vegetation were planted in the study area. Construction and instrumentation in the study area was completed in October 2014. Instrumented data monitoring began in October 2014 and is currently in progress.

Studies conducted over the past few years were focused on the effects of various climatological conditions and soil types on the critical performance indicators of the ET cover. However, field scale vegetation monitoring and laboratory investigations were not performed due to the complexity of the subject and the intensive labor that would be required. Therefore, most of the vegetation input for numerical model predictions was

based on literature. Extensive characterization of vegetation (plant roots) is needed for conducting long-term performance evaluations and for efficiently incorporating the numerical model to compare the field performance and model prediction. Therefore, monitoring and accumulation of both field and lab scale data, along with information on meteorological factors and soil properties, should be continued for an extended period.

1.3 Objective of the Study

The overall objective of the current study is to evaluate the effect of plant root growth on the performance of the ET cover, including modeling the ET cover system and investigating the critical parameters for optimum ET cover performance. The specific tasks to accomplish the objective of the study include:

1. Selection of full scale study area
2. Comprehensive experimental study of ET cover soil
3. Performance monitoring of the instrumented study area
4. Methodical investigation of the vegetation and root growth in the ET cover
5. Numerical modeling of the ET cover system
6. Optimization and calibration of preliminary modeling with field performance results
7. Study of on the different parameters to determine the sensitivity of the critical parameters

The flow diagram of the current research is presented in Figure 1.1.

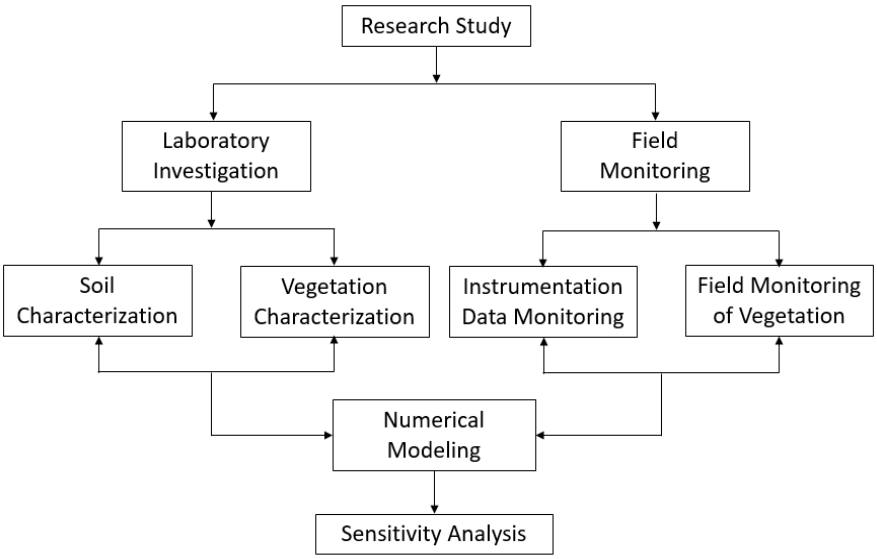

Figure 1.1 Flow chart of research activities undertaken in the current study

1.4 Thesis Organization

The thesis is divided into seven chapters that can be summarized as follows:

Chapter 1 provides an introduction and presents the problem statement and objective of the study.

Chapter 2 presents a literature review on the evapotranspiration (ET) cover system. It contains descriptions of different landfill cover types, the basic components of the ET cover and its mechanism, effects of soil properties and vegetation characteristics on the optimum performance of the ET cover, methodologies for root measurements, and performance prediction of the ET cover through numerical modeling. Finally, a few case studies are presented on the results of performance monitoring and an evaluation of model-predicted ET cover performance.

Chapter 3 describes the research methodologies of this study, including the selection of the study area, collection of soil samples and characterization, field monitoring

methods and laboratory investigation techniques of vegetation, details of field instrumentation, determination of in-situ hydraulic characteristics, and selection of a numerical modelling tool. This chapter also presents the geophysical investigation of the study area, using a resistivity imaging technique.

Chapter 4 presents the detailed characterization results of ET cover soil, which is comprised of the index properties (grain size distribution, Atterberg limits, and specific gravity), mechanical properties (moisture-density relationship), and hydraulic properties. It also includes the suction-moisture relationship, or the soil water characteristic curve (SWCC).

Chapter 5 presents the detailed results of in-situ root investigation and analysis and establishes a methodical root analysis system, using a minirhizotron-based image analysis. This chapter also presents the results of root characterization obtained from the traditional method, as well as a description of the geophysical investigation of the root zone.

Chapter 6 focuses on the instrumentation results and performance evaluation of the ET cover system. The chapter describes the water balance performance of the test sections and the effect of vegetation on the overall performance of the cover system. It also includes the development of a field evaluation curve, based on the field-monitored plant characteristics and water balance component.

Chapter 7 establishes a numerical study on the performance of the ET cover. It presents a comparison of field monitoring results and model-evaluated outcomes, and predicts ET cover performance. A parametric evaluation on the effect of different vegetation parameters and soil hydraulic properties of ET cover was performed, and the results of the field study and the numerical analysis are presented.

Chapter 8 summarizes the main conclusions drawn from the current research and provides recommendations for future work.

Chapter 2

Literature Review

2.1 Final Cover System of Landfill

A landfill final cover is a multi-layered system composed of various materials. It is considered the most significant component of the landfill, since environmental degradation is deemed to be largely associated with the failure of the final cover system. Final cover is constructed over landfill to achieve three primary goals; namely, waste isolation, infiltration minimization, and control of fugitive gas emissions (Hauser et al. 2004). There are two basic types of final cover systems: conventional or prescriptive final covers, and alternative final covers. The following section describes the two types of cover systems.

2.1.1 Conventional / Prescriptive Landfill Cover

A conventional or prescriptive cover consists of several layers, such as compacted clay, geomembranes or geosynthetic clay, a drainage layer, and a topsoil layer (Figure 2.1a) (USEPA, 1991, 1993, and 1996). The main concept of a conventional cover is to construct a soil layer that has low saturated hydraulic conductivity to prevent the infiltration of precipitation into the waste mass. These layers have been termed as barrier layers or infiltration layers. The cover systems with barrier layers are referred to as resistive covers (Benson 1997). Under the Resource Conservation and Recovery Act (RCRA), a final cover for a Subtitle “D” landfill which contains municipal solid waste (MSW) must have a saturated hydraulic conductivity of 1×10^{-7} cm/sec or be equal to the saturated hydraulic conductivity of the bottom liner. The cover system also must minimize the water infiltration through the MSW by incorporating an infiltration layer constructed with a minimum of 450-mm of earthen material (Figure 2.1b). Finally, a 150-mm soil layer must be placed on the top to minimize the erosion by efficient vegetation growth.

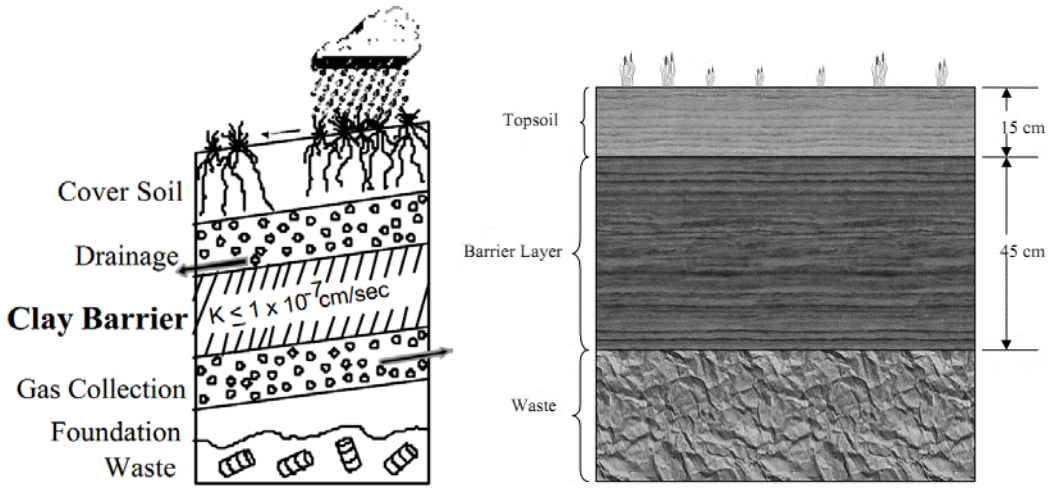

Figure 2.1 (a)Typical conventional landfill cover (b) RCRA Subtitle "D" cover (EPA, 1991)

The conventional cover system has disadvantages, the most important of which are degradation due to environmental exposure, performance reduction with time, and high cost and difficulty of construction (Dwyer 2000a, Hauser et al. 2001). According to Gross et al. (2001), many problems are associated with prescriptive cover designs, resulting in uncontrolled water flux and erosion. From the construction perspective, controlling the required moisture content and density, uniform compaction throughout the cover section, and bonding between layers, and achieving the targeted saturated permeability is difficult. Though a conventional cover is designed to have lower saturated hydraulic conductivity, saturated conditions are rarely achieved, especially in dry regions. The cover system is seldom saturated, and water movement within the cover system occurs under unsaturated condition. The compacted soil layers desiccate due to extensive moisture loss and form cracks (Figure 2.2) in the cover which, in turn, create irreversible changes in soil hydraulic characteristics. This problem of desiccation was overlooked for many years (Suter et al., 1993, Mulder and Haven, 1995). Several studies have also suggested that compacted soil layers are susceptible to burrowing animals (Pratt 2000, Bowerman and Redente 1998,

Johnson and Blom 1997, Hakonson 1986) and are affected by freeze-thaw action, which develops macropores and eventually increases the saturated hydraulic conductivity of the cover (Benson and Othman 1993).

Figure 2.2 Failure mode of prescriptive landfill cover

2.1.2 Alternative Cover

Two types of alternatives have been suggested. The first one is the modified prescriptive cover, where most of the essential design principles are retained by replacing the compacted soil layer with a geosynthetic clay liner (GCL). The main advantage of a GCL is that it eliminates the difficult construction of the compacted soil layer. The second alternative cover is independent of the barrier layer and relies upon the water storage capability of the cover soil and subsequent removal through evapotranspiration. Presently, this type of alternative cover is predominantly utilized across the United States. The latter cover type is also known as evapotranspiration (ET) covers, store-and-release covers, or water balance (WB) covers. For simplicity of reference, “ET cover” will henceforth be used to denote the alternative cover. Section 2.2 describes the ET cover.

2.2 Water Balance or Evapotranspiration (ET) Cover

The ET cover system is an updated landfill final cover system (EPA 2003; Benson et al. 2005; ITRC 2003). The main idea of the ET cover is that it works with the natural processes to create a better performing landfill cover (Benson et al. 2000), endowing it with

a greater potential for long-term successful performance when compared to the performance of a conventional cover (Benson et al. 2002). An ET cover consists of a surface layer of vegetation, underlain by a storage layer to hold precipitation during periods of low evapotranspiration. The basic concept of an ET cover is to store precipitation during the rainfall season and release it into the environment during the dry period by means of evaporation from the top cover soil and transpiration from the vegetation (Barnswell and Dwyer 2011, Benson et al. 2002, Khire et al. 2000, Malusis and Benson 2006, and Stormont and Morris 1998, Albright et al. 2004, 2010; Bohnhoff et al. 2009). Consequently, it minimizes percolation from the bottom of the cover. The schematic of the ET cover concept is illustrated in Figure 2.3.

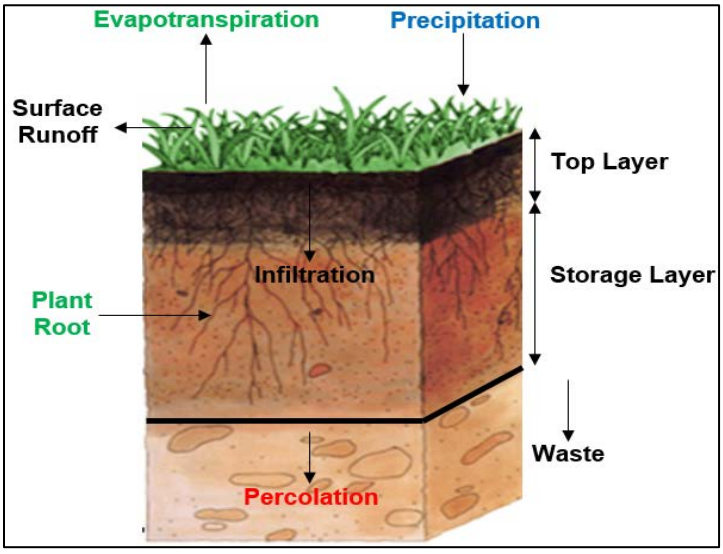

Figure 2.3 Schematic of ET cover concept

The mechanism of the ET cover that manages the water balance does not exclusively rely on the physical characteristics of a single design element, such as lower saturated hydraulic conductivity. It relies mostly on the integrated system of the cover components, which consists of soil and plants. The function of the soil is to store water and support robust plant growth that can keep harmony with local climatology, whereas the

roots of the plants transpire the stored water. The soil water storage (SWS) and transpiration is a concurrent process to limit the percolation; however, the processes depend on the active seasons (Figure 2.4). During the growing season, evapotranspiration is at its maximum due to active root growth, and SWS is minimal. The process has minimal efficiency during the inactive period (late fall and winter). Thus, the performance of an ET cover largely relies on the efficient root growth into the cover system. Therefore, the soil of an ET cover is not compacted heavily to obtain low hydraulic conductivity; instead, a lower compaction effort is ensured for efficient root growth, which promotes the storage capacity of the soil and reduces the potential for desiccation cracking and freeze/thaw effects (Othman et al. 1994; Albright et al. 2006).

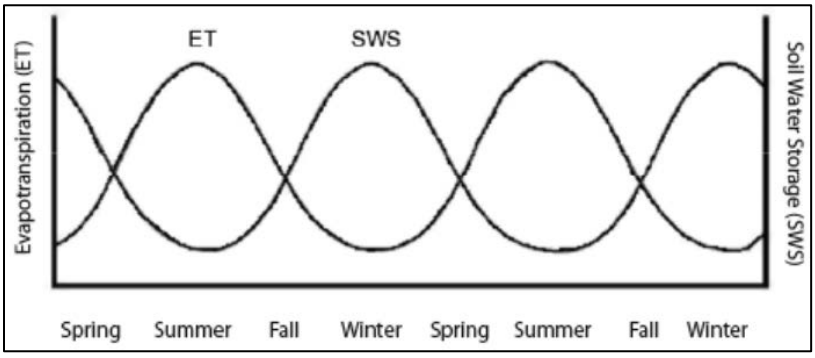

Figure 2.4 Typical seasonal cycle of transpiration and SWS of ET cover

2.2.1 Mass Balance Equation of ET Cover

The key component of an ET cover design is the water balance analysis, which is a mass balance approach that is used to evaluate the cover performance. The general concept of water balance of the ET cover is that the equilibrium of the input of water (precipitation) into the cover system will be maintained by the summation of the output components. The components of the water balance cover are illustrated in Figure 2.5. The water balance equation of an ET cover can be written as follows:

$$P = R + S + P_r + E + T$$

Here, P = Precipitation

R = Surface Runoff

S = Soil Water Storage (SWS)

P_r = Percolation

E = Evaporation

T = Transpiration

Precipitation (P) is defined as rainfall, snowmelt, or any other irrigation applied to the ET cover surface. The performance of the ET cover significantly depends on the magnitude and distribution of precipitation with time. Surface runoff (R) is the portion of the precipitation which falls on the cover but does not infiltrate, rather flows over the surface. Surface runoff is also referred to as overland flow. SWS is the volume of water stored in the pore spaces of the cover soil. A change in the SWS indicates a change in the soil volumetric moisture content. Evaporation (E) is defined as the conversion of liquid (stored water) to the gas phase and subsequent removal from the top of the cover. The water released from the deeper layer of the cover through the actions of plant roots is termed as transpiration (T).

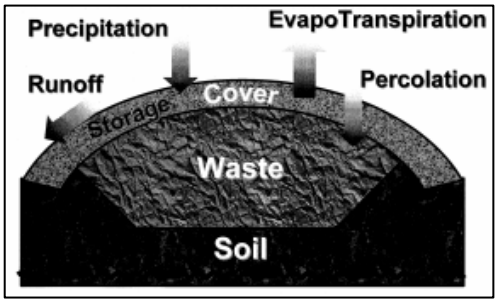

Figure 2.5 Water balance for ET cover

Percolation (P_r) is the most critical parameter of water balance analysis. It is defined as the volume of water seeping through the base of the ET cover system.

Percolation is a complex process in the ET cover system. When precipitation hits the cover soil, the movement of water obeys the laws of gravity, capillarity, and suction (Brooks et al. 2003; Hillel, 2004). After the infiltration of the precipitated water into the cover, the length of the wetted part increases and the suction gradient decreases. As water keeps infiltrating, the suction at the top becomes negligible. At this point, gravity is the only force causing the water to move downward (Hillel, 2004). It eventually reaches the bottom of the cover and completes the percolation process.

2.2.2 Types of ET Cover

There are two basic types of ET cover systems: monolithic covers and capillary barriers (Albright et al. 2004). A monolithic cover (Figure 2.6 a) consists of a single layer of fine-textured soil. A capillary barrier system (Figure 2.6 b) is comprised of two layers of soil: a fine-grained soil layer placed over a coarser-grained soil. The interface of the two soil types acts as a capillary break, which allows the fine-grained soil layer to hold a greater amount of water than an equally thick monolithic cover (Khire et al. 2000).

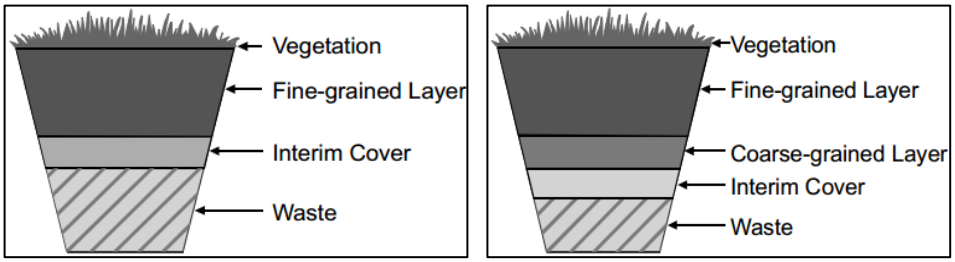

Figure 2.6 (a) Monolithic ET cover (b) Capillary barrier ET cover

2.2.3 Effectiveness of ET Cover System

The major components of the ET cover system are soil and plants, and the optimum performance (minimal percolation) of the ET cover system largely depends on the ideal field behavior of these two components. Climatological conditions are the main factors which affect the performance of ET cover. Among the climatological factors, precipitation

(P) and air temperature are considered the most critical factors to consider during the design procedure. Annual precipitation is used to determine the amount of water to be stored in the ET cover system (Benson 2004), and air temperature is an indicator for potential evapotranspiration (PET). Benson (2006) revealed that an ET cover can be effective in those regions where P: PET does not exceed 0.75. In other words, an ET cover is more effective in arid and semi-arid regions, where the dry season exists for extended periods and the rainfall amount is reasonable (Nativ 1991, Nyhan et al. 1990, Hakonson et al 1994, Stormont 1997, Ward and Gee 1997, Dwyer 1997). In arid and semi-arid regions, PET may significantly exceed P; therefore, percolation rarely occurs. In contrast, in humid regions, P may significantly exceed PET, and percolation is likely to occur. Some researchers have suggested, however, that an ET cover can also be effective in humid regions (Abichou et al., 2005, Albright et al., 2004). Some climatic zones are characterized by an excess of precipitation and a lack of evaporative demand. The soil characteristics and plants of an ET cover in this region may not be suitable to minimize the percolation (Albright et al. 2004). Figure 2.7 shows a map of arid, semi-arid, and humid regions of the US, along with the higher and lower percolation zones.

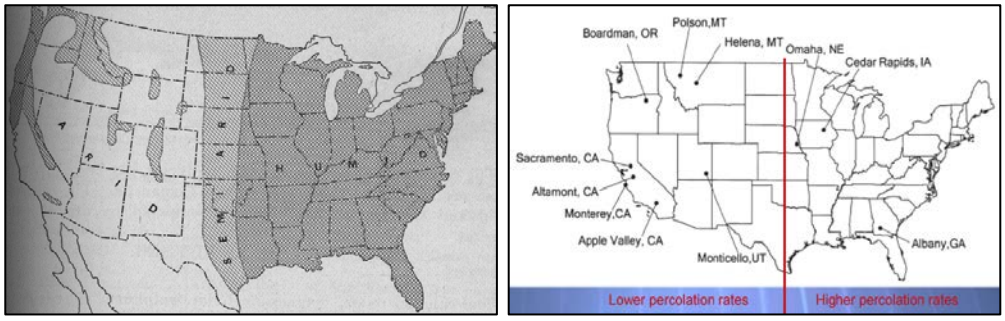

(a) (b)

Figure 2.7 (a) Map showing arid, semi-arid, and humid regions of the US (b) Regions of lower and higher percolation rates (Albright et al., 2004)

The best performance of ET covers can be achieved when the evapotranspiration (ET) component is the greatest. The evapotranspiration (ET) component is affected by plant species and their physical properties, such as above-and-below-ground biomass (Ben-Gal et al. 2003) and leaf area (Vertessy et al. 1995; Cortina et al. 2005). Climatological parameters such as temperature, solar radiation, humidity, and wind speed also affect the ET component (Montero et al. 2001). Soil properties are a major element of ET cover because they influence the root water uptake. In general, fine-grained soils are the primary choice for ET covers (Gurdal et al. 2003) since they have greater storage capacity than coarse-grained soil (Saxton et al. 2005) and the thickness of the ET cover is designed based on the water storage capacity of the soil to limit percolation. In humid regions, the ET cover needs to be thicker than it does in arid regions (Albright et al. 2004). Unfortunately, increased thickness also involves inflated costs for construction, resulting in ET cover construction in humid regions always being a challenge.

2.2.4 Importance of Choosing the Right Vegetation for an ET Cover

The basic concepts of removing the water from the ET cover are the evaporation (E) and transpiration (T) processes. Optimal T is largely dependent on the vegetation rooting depth; therefore, it is essential to select the right vegetation. The following vegetation characteristics are considered appropriate for an ET cover:

- Native to the region
- Perennial
- Rapid growth rate
- Adapted to various soil condition
- Extensive root system
- Functional over entire growing season

Since the ET cover is gaining popularity because of its better performance, many state regulatory agencies are permitting its construction. The overall performance of the ET cover system depends on rooting depths and distribution. Therefore, choosing the right vegetation for the ET cover system is crucial for long-term success. There are several evidences of designing and constructing ET covers, using both warm and cool season grasses to lengthen the duration of growing period. However, according to the report by Aquaterra Environmental Solutions, Inc., Overland Park, Kansas, in most cases, using a combination of warm and cool season grasses doesn't work well.

The warm season grasses, which are commonly known as native or prairie grasses, generally have deeper root systems. The root depth of this type of grass can be 2 to 8 feet. Consequently, the transpiration fraction of the water balance equation is greater in warm season grasses. But, the major shortcoming of warm season grasses is that they have a shorter growing period. In contrast to the warm season grasses, cool season grasses like fescue, rye, brome, etc. have a longer growing season, but have the shallow rooting depth. Typical rooting depth of this type of grass is 2 to 8 feet. The main problem associated with mixing the warm and cool season grasses for the ET cover system is that the cool season grasses can out-compete the warm season grasses over time. This is due to two main reasons: cool-season grasses grow quicker in the spring time than the warm-season grasses, and cool-season grasses are moisture "hogs" and steal necessary moisture away from the warm-season grasses (Ohlenbusch, 2004). Obviously, this means that the combination of these two types of grasses in the ET cover system will not serve the long-term purpose.

Warm-season grass seeds usually germinate in soil above 55 degrees Fahrenheit (°F); cool-season grass seeds are able to germinate at a lower temperature, ranging from 45 to 50 °F. The cool-season seeds get a head start, and the warm-season grass roots fail

to penetrate as deep as they should and cannot handle the drought, as most of the moisture is used by the cool-season grasses. Additionally, cool-season grasses act torpidly during the most crucial period at the end of summer (July and August). Over a long period (five to ten years), the planted mixed vegetation of cool-and-warm-season grasses in the ET cover will be only cool season grasses. Therefore, few years after germination of the seeds, the ET cover sites will have predominantly shallow root systems. In the wetter or humid climates, water balance models will not pass the infiltration criteria unless the rooting depth is more than 1 foot.

Over time, native grasses have adapted to surviving in adverse environments, such as the heavy drought period in mid-summer. These types of plants can change the soil's infiltration behavior, water holding capacity, carbon sequestration and turnover, and nutrient retention and uptake to extend its survival time (Dierks, 2007). The warm-season grasses can endure much more severe environments that are common in a closed landfill cover. The heterogenic characteristics of the warm-season grasses, like varying heights, dead and dying stalks, and plant litter stimulate them to treat water as an essential resource for their survival. The native grasses are actively engaged in the recycling of water by continuously capturing, storing, and reusing the precipitation. Therefore, native species are highly recommended by most of the researchers for the ET cover system, as they are compatible with native environmental conditions.

2.2.5 Advantage of ET Cover over Prescriptive Cover

The ET cover system offers several advantages over the conventional cover type. The most substantial advantage is the significant cost savings. Considerable costs of conventional cover construction are associated with purchasing, hauling, and placement of the materials. The cost further increases for transportation of the material where clayey soil is not locally available. On the other hand, ET cover construction is carried out with

locally available soil and native vegetation. Approximately, $50,000 to $75,000 per acre can be saved by using the ET cover (Benson et. al, 2000). The placement of geomembranes and compaction of hydraulic barriers are time-consuming and labor-intensive. Another attractive feature of the ET cover is that it provides more flexibility for converting an existing landfill to newly-developed bio-cell technology (Abichou, 2003). ET covers are also advantageous with respect to performance standards. While the performance of conventional covers decreases with time due to the reduction in hydraulic conductivity, the performance of ET covers increases due to increased storage capacity with time and removal of water with increased root depth and evapotranspiration. The expected life span of an ET cover may be thousands of years due to its operation in the natural processes. On the contrary, the life span of a conventional cover is often uncertain (Abichou, 2001). The cost of maintaining an ET cover is much less than that of the conventional cover, and the ET cover is also less susceptible to slope failure and erosion, as the vegetation system offers better slope stability.

2.3 ET Cover Soil Profile: Water Flow and Retention

2.3.1 Soil Compaction

Soil compaction is one of the major important factors for optimum ET cover performance. In a prescriptive cover, the main purpose of compaction is to attain lower hydraulic conductivity. A high compaction level in the prescriptive design initially produces less infiltration. However, this type of cover undergoes seasonal changes of moisture at significant depths due to seasonal variations of precipitation and evapotranspiration, especially after a few wet-dry cycles (Khire et al., 1997). The compacted soil barrier is also susceptible to desiccation cracking that increases the hydraulic conductivity of the soil. Benson et al., (1993) reported that soil compacted at wet of optimum moisture content experienced an increase in hydraulic conductivity by a factor of three, after four wet-dry

cycles. All of the negative impacts of the prescriptive cover are overcome in the water balance cover or ET cover. Unlike a prescriptive cover, the soil of an ET cover is not significantly compacted to obtain lower hydraulic conductivity. Rather, a lower compaction effort is ensured to promote the water storage capacity of the soil and reduce the potential for desiccation cracking and freeze/thaw effects (Othman et al.1994; Albright et al. 2006). In addition, a higher compaction level significantly impedes the plant root growth (Kuchenbuch and Ingram 2004) and water uptake by plants (Arvidsson 1999). Therefore, obtaining a favorable compaction level in ET cover soil is necessary to have adequate soil water storage capacity and less hydraulic conductivity, and to promote effective root growth.

The effect of pore size distribution or soil bulk density plays an important role in soil water retention. In compacted soil, soil particles are pressed together, thereby reducing the pore space between them (Figure 2.8). Heavily compacted soil contains very few large pores and a smaller total pore volume, and consequently a greater density. Therefore, with higher soil density, the amount of pore space decreases the hydraulic conductivity and water holding capacity of the soil (Radford et al. 2001; Mooney and Nipattasuk 2003).

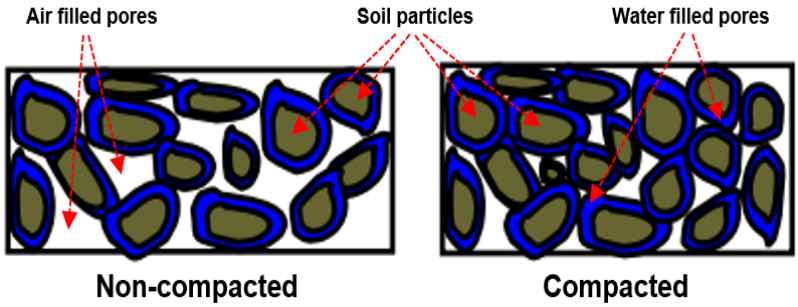

Figure 2.8 Effect of compaction on pore space (Modified from Neil Hansen, 2003)

Joseph (2010) conducted a study to observe the effect of soil density on the field capacity of soils at different compaction levels. The results obtained from his study are shown in Figure 2.9 and clearly explain that the field capacity decreases with an increase

in the relative density. Although the change in compaction does not greatly affect the field capacity, the density does have some influence on the water retention capability of the soil.

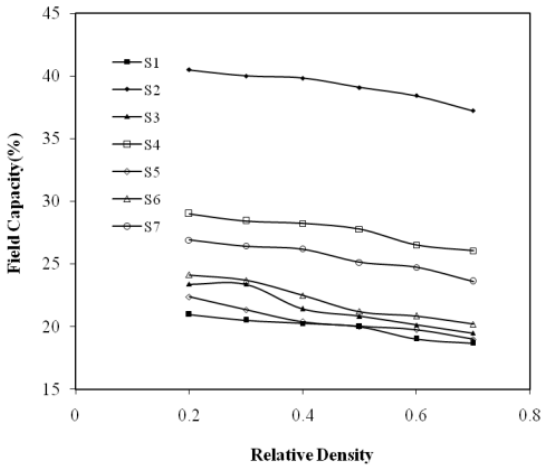

Figure 2.9 Variation of field capacity with relative density (Joseph, 2010)

Obtaining an acceptable field density is necessary for the effective performance of all of the components of an ET cover. The acceptable range of density and the water content of the soil effective for an ET cover is referred to as an acceptable compaction zone (ACZ) (Dwyer et al. 1999). Dwyer (1999) suggested determining the goal density of the soil, using the ASTM standard. The root-limiting bulk density also needs to be checked. The allowable dry unit weight or the soil density during construction should be based on the ACZ and root-limiting density. Figure 2.10 shows the typical ACZ for the soil in Los Alamos, New Mexico, based on the research of the Los Alamos National Laboratory (LANL). The ET cover soil placed within the boundary of ACZ during construction is less susceptible to desiccation and, consequently, shrinkage cracking, and there is less change in volume due to wet-dry cycles (Daniel and Wu 1993). There is little change in hydraulic conductivity of the soil placed in the ACZ (Benson et al. 1993).

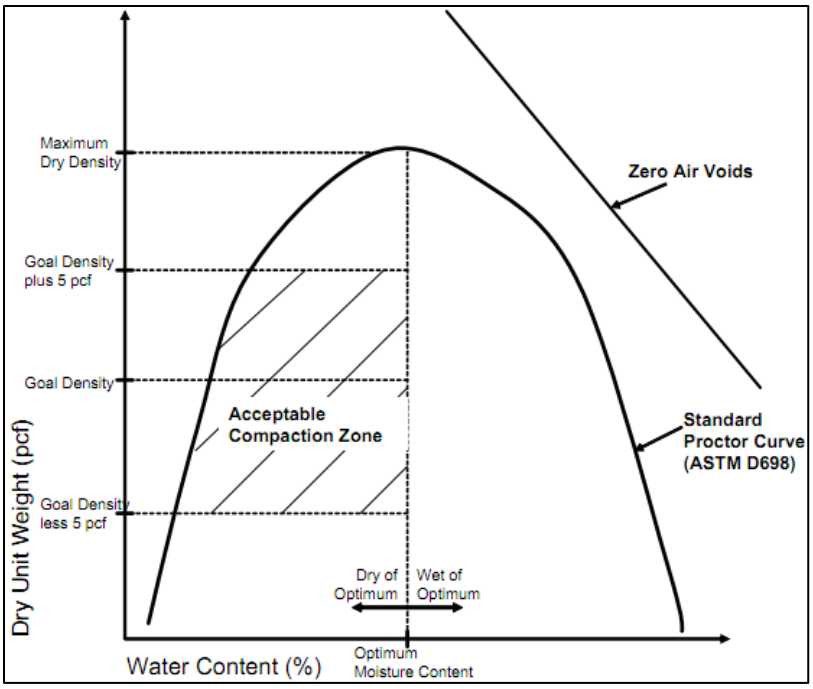

Figure 2.10 Acceptable compaction zone (ACZ) for soil placement for LANL cover system (Dwyer 2007)

2.3.2 Behavior of Water Flow at Saturated Condition

The saturated hydraulic characteristics describe the maximum flow rate of water through a soil at a given state of energy. When there is a heavy precipitation event, the cover system will either have water storage needs beyond its capacity or will be at fully saturated condition. The flow of water at saturated condition can be described by the simple principle of Darcy. According to Darcy's law, the flow rate through a soil Q is,

$$Q = \mathrm{K}_s \times \frac{\Delta H}{L} \times A$$

Where, K_s = saturated hydraulic conductivity, ΔH = difference in hydraulic potential, L = length of flow path through the cover and A = cross sectional area of the cover through which flow occurs. Figure 2.11 shows the concept of water flow through the cover system at saturated condition.

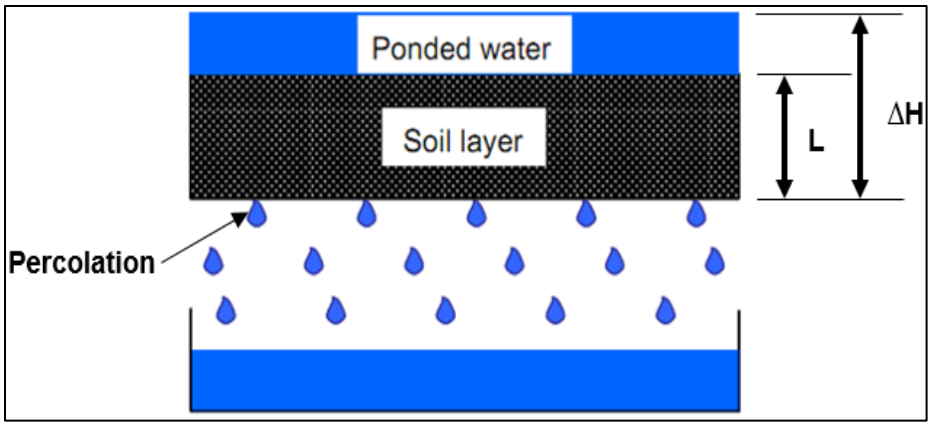

Figure 2.11 Concept of saturated hydraulic conductivity (modified from Albright et al., 2004)

2.3.3 Unsaturated Soil Properties

2.3.3.1 Soil Water Suction

A water balance cover remains in an unsaturated condition most of the time. In the unsaturated soil, moisture in the soil pores is in tension, and the pressure is referred to as the negative pore water pressure or soil suction (ψ).

The concept of soil suction is important in designing a water balance cover system. Figure 2.12 shows a conceptual illustration of suction, with the water pressure in a capillary tube below and above the free water surface. The water pressure below the free water surface is positive and increases with depth. In the capillary tube, water is held by capillary forces which is the negative pressure, or suction. ψ is a function of radius (r) of the capillary tube. Mathematically ψ is expressed in the form of the following equation.

$$\psi = \frac{2\sigma \cos\beta}{r}$$

Like the illustration, in the water balance cover, water is retained in the soil due to the action of capillary forces which develop suction in the soil. Adsorptive forces between

the water molecules and the surface of the solid particles also contribute to retaining water in the unsaturated soil of the water balance cover.

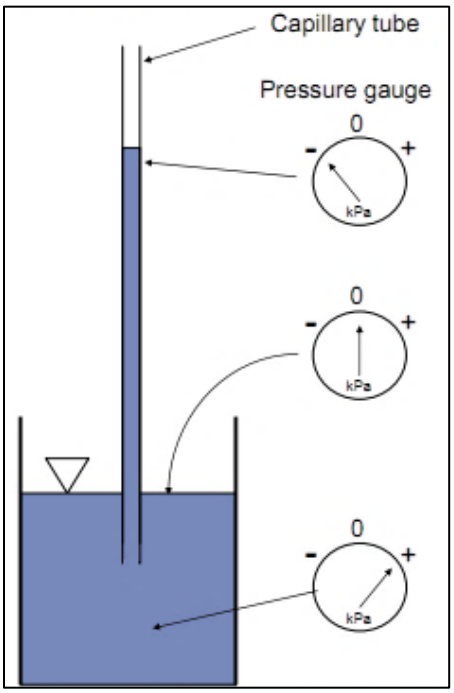

Figure 2.12 Soil suction concept (Albright et al. 2004)

Soil suction is inversely proportional to the volumetric moisture content (θ). θ is defined as the volume of water per total volume of soil. It decreases when the applied forces are large enough to overcome the capillary forces; therefore, the moisture content decreases as the suction on the pore water increases. Conversely, when the suction is reduced, the moisture content increases and water fills larger pores.

2.3.3.2 Soil Water Storage

One of the significant purposes of the ET cover system is to store precipitation in the soil profile and thus minimize the flow through the bottom of the cover. A brief explanation of the soil water storage concept is given in the following section, according to the conceptual description by Albright et al. (2004).

Two types of soils are subjected to saturation: one is clean sand with relatively large particles, and the other one is silty sand with finely-textured, well-graded soil (Figure 2.13). The percentage of soil pore spaces varies with the soil type. Fine-grained soils generally have a higher volume of pores. For this illustration, each type of soil was assigned a pore volume of 40%, and the remaining 60% was comprised of the soil grains. Hence, both soils had a porosity value of 0.4.

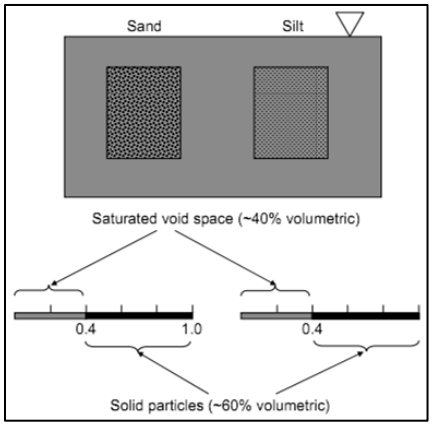

Figure 2.13 Schematic illustration of void space concept

The two types of soil were taken out of the water and allowed to drain freely (Figure 2.14). Water continued to drain from the soils until enough suction developed in the pore water to hinder the gravitational force that causes drainage. As instinctive properties, more water drains from sand than from silt. Because the sandy soil has larger pores, it can develop small suctions to retain water within the pore volume. The water that remained in the sand was about 10% of the total soil volume, whereas for the silty sand, the water was almost 44% of the total soil volume. (These numbers are arbitrary, but do approximate actual soils and are meant to demonstrate concepts, Albright et al., 2004.) These soils were in the equilibrium condition, and the water content at this condition is referred to as the field capacity water content (θ_{FC}). In practice, θ_{FC} is the water content corresponding to the suction of 33 KPa.

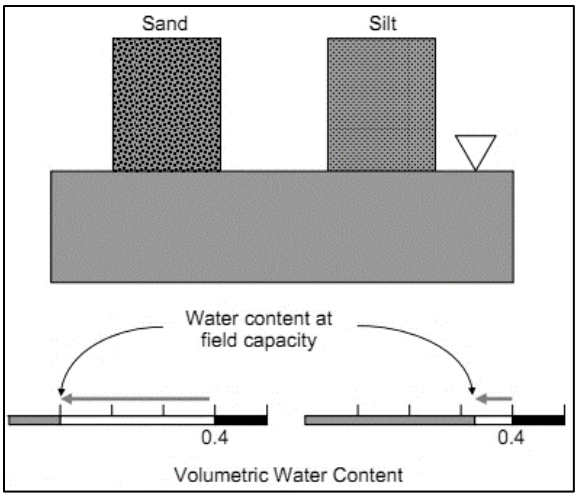

Figure 2.14 Schematic illustration of field capacity concept

The root system of plants removes additional water via the transpiration process (Figure 2.15). This process continues under ambient temperature as long as water is available. As soon as transpiration stops, the soil moves into the wilting point condition, and the water content is referred to as the wilting point water content (θ_{WP}). At the wilting point condition, the water content of sand is lower than that of silt. The wilting point is often assigned as the water content at a suction of 1,500 KPa.

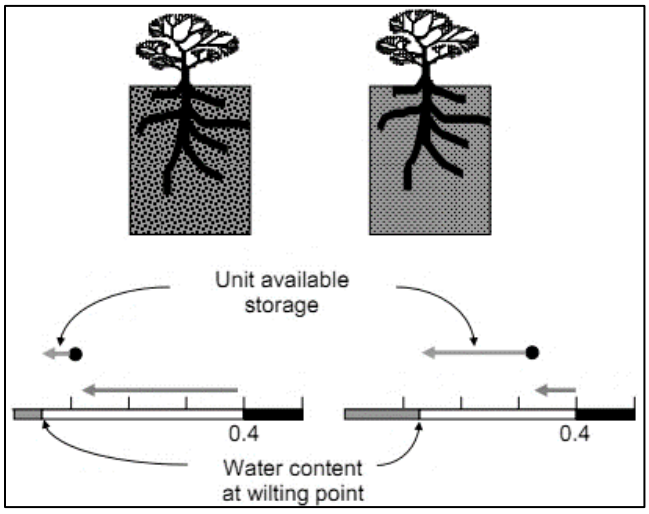

Figure 2.15 Schematic illustration of wilting point concept

2.3.3.3 Soil Water Characteristic Curve (SWCC)

The soil water characteristic curve (SWCC) is the continuous relationship between the soil moisture and suction. It is a graphical representation of the mathematical relationship that describes the status of soil moisture as a function of suction at different pore size distributions (Figure 2.16).

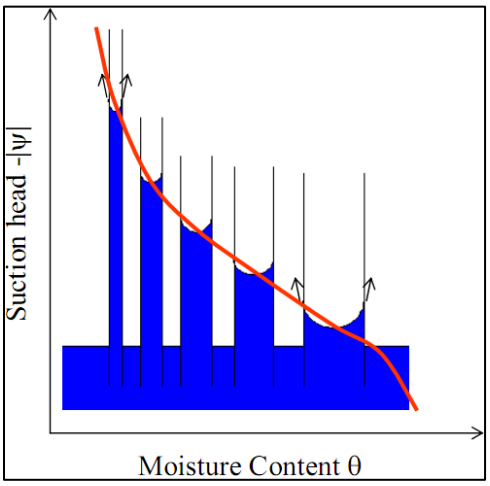

Figure 2.16 The shematic of the relationship between pore diameter and suction at which water is held in pores of various sizes

The suction level at which the largest pores tend to desaturate is called the air entry suction (Ψ_a). Suction values lower than the air entry values describe the fully saturated condition of the soil. At zero suction, the water content is referred to as the saturated water content (Θ_s). At the driest condition of the soil, the water content is called the residual water content (Θ_r). SWCC also defines the field capacity (Θ_{FC}) and the wilting point (Θ_{WP}) of the soil (Figure 2.17). Θ_{FC} is the water content at which the soil can no longer retain water and Θ_{WP} is the water content at which plants are no longer capable of removing water from the soil. Typically, Θ_{FC} corresponds to a suction value of 33 KPa, and Θ_{WP} is the moisture content corresponding to the suction of 1500 KPa. However, Θ_{FC} and Θ_{WP} are subjected to changes at different climatological conditions.

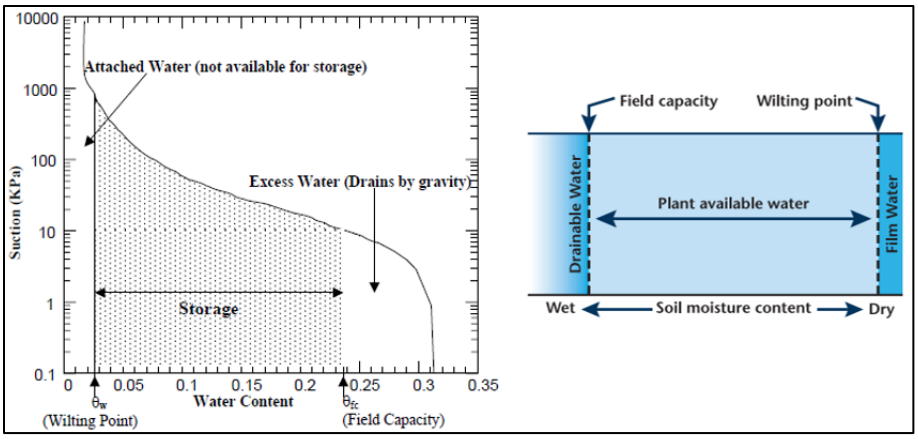

Figure 2.17 Plant available water and drainable water in relation to FC and WP

The SWCC is usually described with different parameters that fit the function, based on the test data. The most functional relationship used is the Van Genuchten equation (Van Genuchten 1980).

$$\theta = \theta_r + (\theta_s - \theta_r)\left\{\frac{1}{1+(\alpha\psi)^n}\right\}^m$$

Where Θ_s and Θ_r are the saturated and residual water content. α and n are Van Genuchten parameters. α is inversely related to the air entry suction for drying or water entry suction for wetting (Figure 2.18). The n parameter describes the slope of the SWCC. For a properly measured SWCC, Θ_r should be close to or equal to zero.

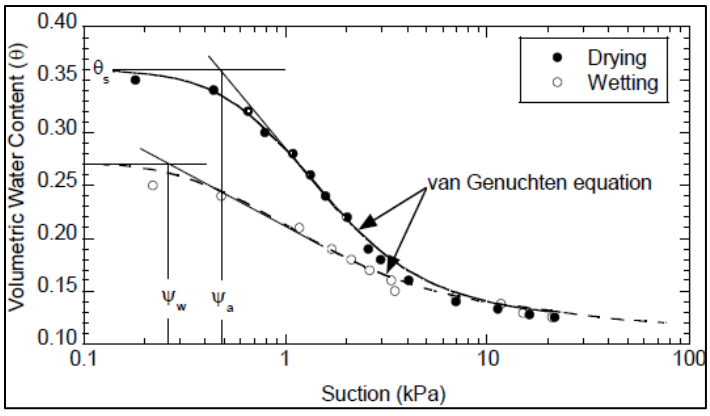

Figure 2.18 Example of SWCC showing fit to Van Genuchten equation

2.3.3.4 Unsaturated Hydraulic Conductivity

When soil begins desaturating, pore volumes which were fully occupied with water under saturated conditions become partially saturated or filled with air. There are basically three different types of soil moisture (Figure 2.19). The first one is gravitational moisture, which occurs when water flows under gravitational forces. The second one is capillary moisture, which occurs when plants consume water. The third one is hygroscopic moisture, which occurs when the water exists as thin films which are connected through grain-to-grain contacts. At very low moisture content in the soil, the hydraulic conductivity decreases as the channels that transmit water through the soil become smaller and convoluted.

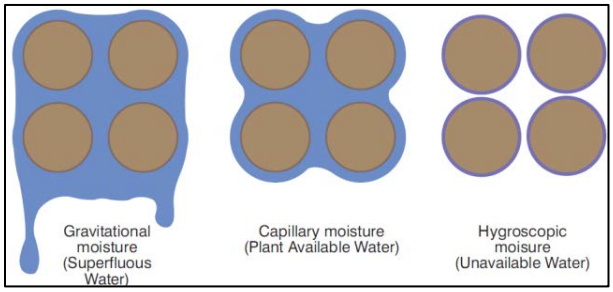

Figure 2.19 Types of moisture in soil

Unsaturated hydraulic conductivity (K_w) is a function of both void ratio (e) and water content (w) or degree of saturation (S). K_w can be expressed as a function of three parameters: Kw = f (e,w), Kw = f (S,e), Kw = f (S,w). Determining unsaturated hydraulic conductivity is difficult, expensive, and time consuming. The duration of the test increases with a decrease in the water content. Unsaturated conductivity can be valued with greater accuracy as it can be measured (Benson and Gribb 1997). The parameters θs, θr, α, n are used to describe the SWCC and to predict the unsaturated hydraulic conductivity as a function of soil water suction. Van Genuchten (van Genuchten, 1980) proposed the following equation to estimate the unsaturated hydraulic conductivity:

$$K_{\psi} = K_{sat} \times \frac{\left\{1 - (\alpha\psi)^{(n-1)}[1 + (\alpha\psi)^{n}]^{-m}\right\}^{2}}{[1 + (\alpha\psi)^{n}]^{\frac{m}{2}}}$$

The Van Genuchten parameters α and n have a significant effect on the unsaturated hydraulic conductivity. Figure 2.20 depicts the effect of the parameters on the hydraulic conductivity of unsaturated soil. As α parameter decreases, the breakpoint extends and the hydraulic conductivity begins declining. When the n parameter decreases, it increases the slope of the SWCC and eventually decreases the rate at which conductivity declines.

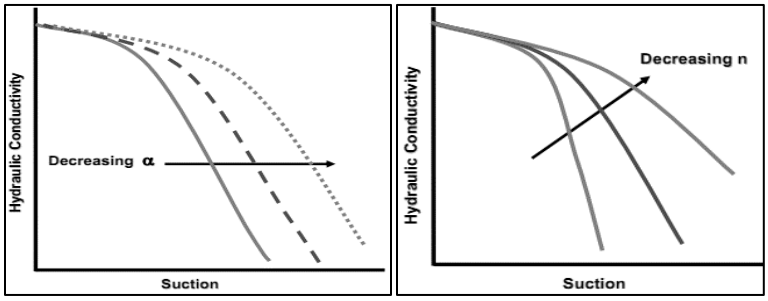

Figure 2.20 Effect of α and n parameters on hydraulic conductivity (Modified from Albright et al. 2004)

The movement of water in unsaturated soil is due to its response to suction gradients. Total soil water potential is the sum of two components: the soil water pressure head and the elevation head. Water flows in the soil, under the influence of gravity, from higher elevations to lower elevations in the entire soil profile, or from points of high water pressure to points of low water pressure, which is lower suction to higher suction. The components from gravity and pressure determine the direction of flow. A soil surface that is dry, after the evaporation process, draws water upward because the suction gradient is higher than the downward gradient due to the difference in elevation.

Two concepts are important in the unsaturated flow of water: unit gradient and equilibrium gradient. When there is no difference in the suction value across the vertical

segment of a soil profile, the flow of water is the hydraulic conductivity of the soil, and it is considered a unit gradient condition. When the soil is saturated and there is no ponding water on the surface, and the rate at which water gets out of the base of the soil profile equals the saturated hydraulic conductivity, it is considered a unit gradient condition.

When there is no movement of water across the vertical segment of the soil profile, the equilibrium gradient condition is in action. As there is no movement of water in the equilibrium gradient condition, the gradient in total soil water potential is zero.

2.3.3.5 Field Variations of SWCC

Hydraulic characteristics of soil may change in the field (Albright et al. 2009). Laboratory determined hydraulic properties of soil analyzed at a certain compaction may differ in the field due to hysteresis; alterations in soil structures due to freeze thaw cycles, wet-dry cycles, bio intrusion (root growth and death, burrowing fauna); and other pedogenic processes. These processes generally lower the density of soils and form large pores. These-post construction changes in the soil structure are more often found in clayey soils than in coarse-grained soil and eventually result in a smaller water storage capacity. In the laboratory, Albright and Benson (2009) measured the SWCC of different soil samples from the ACAP sites. The conventional laboratory-measured SWCCs were found to be lower than those measured in the field (Figure 2.21). Nearly all of the lab-dried SWCC points fell below the 1:1 equality line. The SWCC results, obtained from the undisturbed soil samples from the ACAP test sections in the as built condition, were significantly different from the samples collected after several years of exposure to the environment. Benson et al. (2007) showed that saturated volumetric water content (Θ_s) tends to increase with time, as density decreases with time, and soils placed at higher Θ_s during construction exhibit minor changes in Θ_s.

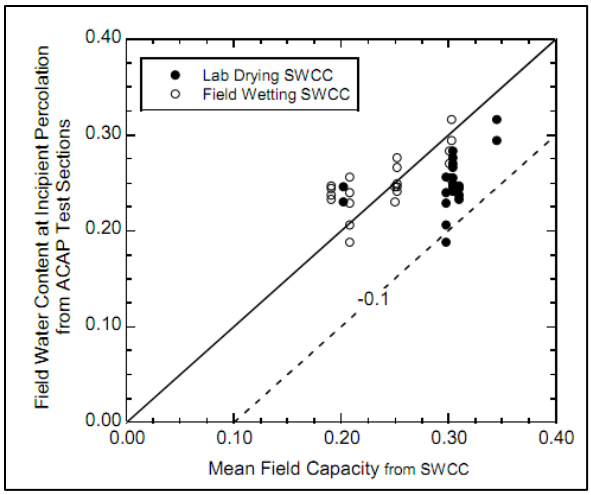

Figure 2.21 Relationship between field capacity water content from SWCCs and the water content at incipient drainage from test section data (Albright et al. 2009)

The unsaturated hydraulic parameters (α and n) of soils change over time due to the field exposure. The α parameter generally increased after a few years of exposure, indicating the generation of larger pores within the soil. The n parameter generally decreased in the ACAP sites. The changes of the n parameter were relatively small due to the range over which n can vary in natural soils.

Based on the changes of saturated and unsaturated hydraulic parameters of varied soils in the ACAP sites, Apiwantragoon (2007), developed a correction method for the application of laboratory-based SWCC in the field. He applied a scaling factor to the VG parameters (α and n) obtained from the laboratory-measured SWCC so that the laboratory-based SWCC can be representative of the field condition. Figure 2.22 shows the laboratory-based SWCC and the SWCC after the correction factor was applied. Apiwantragoon proposed a multiplying scaling factor of 1.3 for less-plastic soils and 12.9 for high-plastic soils. For the n parameter, he used a multiplying factor of 1.1 and 1.2 for less-plastic and high-plastic soils, respectively.

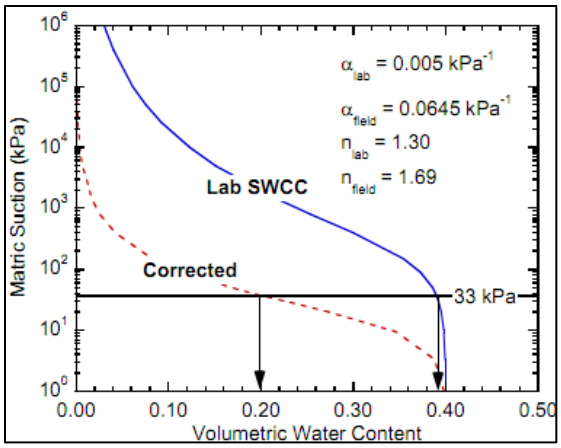

Figure 2.22 Correction procedure applied to a laboratory-based SWCC (Albright 2009)

Figure 2.23 depicts the corrected SWCC, after the scaling factor suggested by Apiwantragoon was applied. Data from field sensors was obtained during monitoring period for the first two years. The solid line represents the corrected average laboratory SWCC, and the dashed lines correspond to the upper bounds and lower bounds of corrected SWCC from laboratory measurements. A good agreement was found between the field-measured SWCCs and the corrected SWCCs. Alam et al. (2017) developed a field based soil water characteristic curve (FSWCC) to evaluate the percolation of flat and slope section ET cover (Figure 2.23 b). Alam et al. (2017) measured the unsaturated hydraulic conductivity based on the FSWCC and assessed percolation relating the unsaturated hydraulic conductivity. Ahmed et al. (2017) also developed a field based soil water characteristic curve (FSWCC) to evaluate the moisture distribution in unsaturated subgrade.

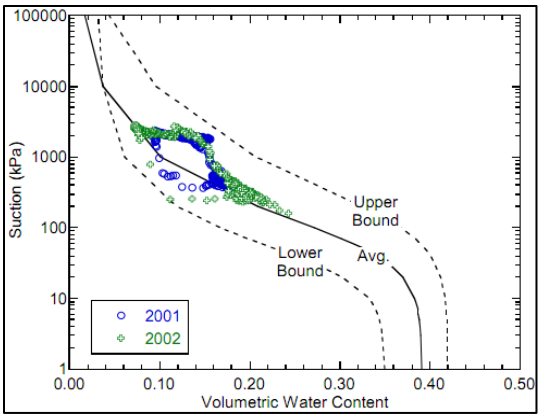

(a)

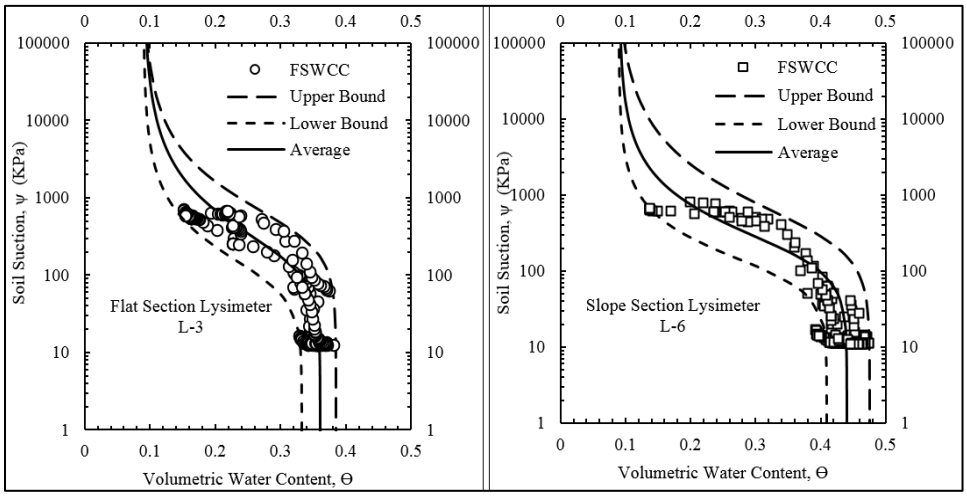

(b)

Figure 2.23 (a) Corrected laboratory-measured SWCCs data from co-located sensors in an ACAP site (b) field based SWCC for flat and slope section vegetated lysimeter soil (Alam et al. 2017)

2.4 ET Cover Vegetation: Water Store-Release and Root Growth Concepts

2.4.1 Basic Concept of Plant Transpiration

The process of transpiration is a natural and complex phenomenon. Transpiration is the evaporation of water from plants, and it is one of the main mechanisms that contributes to the release of water from a water balance cover. The water stored by the

cover transpires when water vapor transfers from the stomatal cavities on the leaf surface into the atmosphere. Other mechanisms can affect water movement through plants, but the dominating driving force is the transpiration process. This process is the interplay of energy and water between soil, plant roots, leaf surfaces, and the atmosphere.

Plant transpiration relies upon the matric potential gradients. Figure 2.24 shows the large difference in matric potential between the soil and the atmosphere. The term matric potential is also referred to as water potential, which is the force or potential energy that acts on water in soil and plants. Water potential in soil and plants primarily depends on three physical and chemical energy forces:

$$\Psi_{tot} = \Psi + \Psi_0 + \Psi_z$$

Where ψ_{tot} is the total water potential, ψ is the matric potential, ψ_0 is the osmotic potential, and ψ_z is the gravitational potential. These components contribute to the total potential (or head) in soil water.

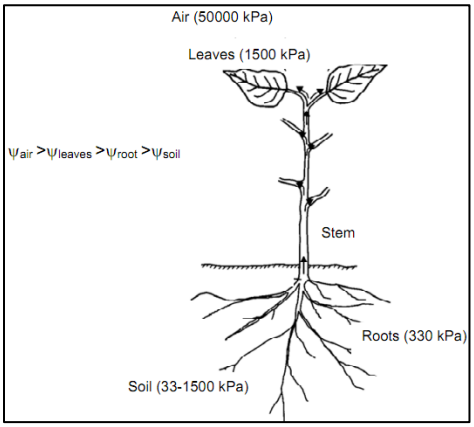

Figure 2.24 Typical soil-plant-atmosphere water potential variation (Hillel, 1998)

In arid regions, the difference between soil moisture and atmospheric humidity can be as large as 1000 atmospheres (bars) (Hillel 1998). The major portion of the entire potential difference occurs between the plant leaves and the atmosphere. The higher the soil-plant-atmosphere potential gradient is, the more effective the water balance cover

system is. Therefore, the vegetated cover system or ET cover system is very effective in climates where potential evapotranspiration (PET) is greater than the precipitation.

Water usually enters the plants through the hairs of young root tips or through cracks in the root cortex of older roots. Once the water enters a plant, it is forced to move through resistant cell membranes. The movement of water becomes more dynamic as soon as the water enters the xylem. Water keeps moving in the xylem, through vascular cell walls and through spaces between mesophyll cells, and lastly into sub-stomatal cavities in leaves where it transpires - vaporizes and passes through the stomatal pores and into the atmosphere. Although, there is a significant resistance to flow throughout the entire soil-plant-atmosphere process, stomates are the principal controller of water movement (Figure 2.25). Factors controlling the opening and closing of stomate pores basically control the transpiration process of a plant. Stomates on the leaf surface allow intrusion of carbon dioxide to diffuse into the sub-stomatal cavity in response to light and CO_2 concentrations.

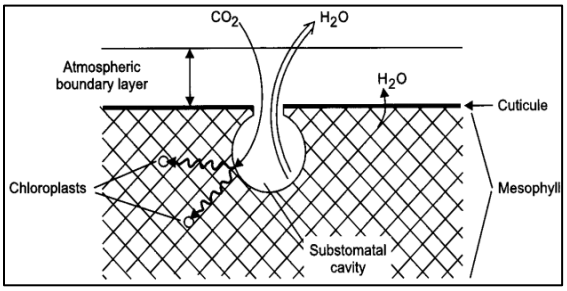

Figure 2.25 Schematic of the leaf surface and stomates. (Modified from Albright 2009)

The water release from the water balance cover is a combination of transpiration through plant roots and evaporation from the soil surface. It is confined to the rate of potential evapotranspiration (PET). PET is the theoretical maximum rate at which evapotranspiration (ET) occurs in a given climatic condition and represents the energy

available for evaporation. Actual evapotranspiration is less than or equal to PET. The most common method to compute PET is the Penman-Monteith equation:

$$PET = \frac{(\delta / \xi) J_n + 0.35\left[(e_s - e)(0.5 + U/100)\right]}{\delta / \xi + 1}$$

Where, e = atmospheric vapor pressure at 2 m above ground surface,

e_s = saturated vapor pressure corresponding to the air temperature,

U = the wind velocity at 2 m above ground surface,

ξ = psychrometric constant,

δ = rate of change in e_s with temperature,

J_n = net solar radiation.

The equation clearly specifies that PET increases as the solar radiation, air temperature, and wind speed increase and the relative humidity decreases. Thus, an ET cover is very effective in the arid and semi-arid regions, where less cloud cover, higher air temperatures, and greater wind velocity tend to have greater potential to evaporate water than in humid regions.

2.4.2 Vegetation Effect on Runoff-Infiltration-Precipitation Process

Surface runoff is one of the water balance components of an ET cover system. Surface runoff refers to the portion of the precipitation that travels over the vegetative cover toward other surface water features like ponds, lakes, streams, rivers, etc. Runoff occurs after the intensity of rainfall exceeds the demands of interception, evaporation, infiltration, and surface storage capacity. Infiltration is the intrusion of precipitated water into the soil cover through the surface. Water that moves downward through the soil profile beyond the depth of the cover is called percolation. When the intensity of the rainfall exceeds the infiltration rate, or when the cover soil becomes fully saturated, the excess rainfall starts ponding on the soil surface. The water fills the depressions in the soil caused from the

irregularities in the soil surface. The water that is held in this manner is called the surface storage. After the end of a precipitation event, the water held in the surface storage will either infiltrate the cover soil or evaporate and transpire through the vegetation roots. When the volume of water from the precipitation exceeds the capacity of the volume of surface storage, surface runoff occurs.

In arid and semi-arid regions, surface runoff occurs primarily from intense precipitation of limited areal extent and of short duration, falling on the unsaturated soils (Fletcher, 1961; Osborn and Reynolds, 1963). In general, the intensity and amount of precipitation, evapotranspiration, existing soil moisture, topography, and soil hydraulic characteristics affect surface runoff (Gautam et al., 2000). Vegetation has a significant influence on infiltration, and therefore, on surface runoff. The runoff is essentially the difference between the amount of precipitation and the portion of it that is intercepted by vegetation or absorbed by the soil (Gregory, 1984). The plant canopy helps delay the onset of soil saturation and the runoff process via transpiration (Gray and Leiser, 1982). Root systems penetrate the soil, keeping the soil medium porous and unconsolidated. Organic matter improves permeability. The above-ground biomass of the in-situ vegetation protects the soil surface from the impact of rain, thereby reducing the disintegration of particles. It also provides surface roughness that eventually obstructs the flow of water on the surface. This reduces the velocity of flow, providing additional time for the water to be infiltrated. In areas of light vegetation, the infiltration is more dominant than the interception by vegetation. On the other hand, if the vegetation is dense enough, a brief or light rainfall may not be able to make the soil wet beneath the plants, and a major fraction of the precipitation water will be intercepted by the foliage of plants. Once the rain stops, the stored water in the leaves slowly runs down the stem and evaporates into the atmosphere. Therefore, dense vegetation is of high importance for optimal performance of the ET cover.

From different studies, it has been recognized that the runoff and infiltration process are influenced by the slope of the landscape, soil texture, and vegetation cover. Nyhan et al. (1997) and Nyhan (2005) conducted the only study that evaluates, in a systematic manner, the effect of slope on the water balance performance of the ET cover system. They presented the increase in runoff quantity as a factor of 4 when the slope increased 5 to 25%.

In a study by Chen et al. (2006), it was shown that vegetation has a strong effect on surface runoff. One of the major objectives of the study was to evaluate the effect of different types of vegetation on the surface runoff. They reported that pine woodlands produced the largest surface runoff, followed by sloping croplands, alfalfa, semi-natural grasslands, and shrublands. The low volume of surface runoff of shrublands and semi-natural grasslands was reported as mainly due to the robust ground coverage and slightly lower soil bulk density than under pine woodlands.

In a study by Nagase et al. (2012), it was shown that a significant difference exists in the amount of runoff between different vegetation types. They found that grasses are most effective for reducing the amount of runoff, followed by forbs and sedum. Nagase et al. (2012) suggested planting grasses and forbs which have a tall height, large diameter, and large shoot and root biomass for reduction of runoff.

2.4.3 Vegetation Response to Soil Moisture Dynamics of ET Cover

Soil moisture dynamics are the central component of the hydrological cycle (Legates et al. 2011). In an evapotranspiration cover system, soil moisture dynamics are mainly determined by evaluating moisture intrusion into the cover, percolation from the bottom of the cover, evaporation from the soil surface, transpiration from the distributed root zone, and the root water uptake process. The relationship between vegetation rooting depth and distribution and the soil moisture is a vital theme of the hydrological balance of

an ET cover system. Soil moisture movement, both across the landscapes and within the soil profiles, is principally controlled by the interactive actions of precipitation and vegetation response at a macroscopic scale, especially in arid and semi-arid regions.

2.4.3.1 Effect of Vegetation on Soil Water Dynamics

The ET cover system is recognized as a key factor in controlling the patterns of soil moisture distribution. Under robust vegetation, an ET cover can control the rate of infiltration, surface runoff, and evapotranspiration. The ET cover system constructed under different climatological conditions with different native plants will have varying degrees of above-ground biomass and different rooting depths. The above-ground biomass determines how much precipitated water will be intercepted and how much water will be infiltrated into the ground (Brooks et al. 2003; Chang 2006). The root depth of the vegetation determines the rate of evapotranspiration from the cover soil. Healthy vegetation in the ET cover also deposits organic matter on the soil surface and extracts organic matter through the root water uptake process. This process enhances the infiltration rate of precipitated water, improves the soil moisture-holding capacity, and reduces the amount of surface runoff or increases the time for runoff to occur. Therefore, soil moisture dynamics are strongly influenced by the presence of vegetation.

Salve et al. (2011) reported that the hydrological processes caused by the rainfall effect vary significantly with different vegetation types and duration of growing season. Vegetative covers are considered the most vital factor that affects the soil hydrology and reduces surface erosion. In an ET cover system, the presence of robust vegetation and amount of precipitation are important factors which influence the soil water dynamics.

Soil water is divided into available and non-available water for plants. Field capacity is the upper end of the available water, and wilting point is the lower end of the available water. To meet the evapotranspiration needs, the roots of the plants need to grow

quickly to absorb water from the deeper depths of the cover soil. If the soil moisture is less than the preliminary wilting point, it becomes difficult for the plants to uptake water and impedes the normal growth of the plants, thereby impacting the water dynamics of the soil.

2.4.3.2 Effect of Precipitation

Precipitation directly influences the soil moisture dynamics. After a rainfall event, the precipitation water that reaches the ground moves into the soil, ponds on the soil surface, or flows over the soil surface, depending on the status of the existing soil moisture. The rainfall water that enters the soil and is not absorbed travels either downwards or laterally (Brooks et al., 2003). As soon as the rainfall enters the cover soil, it directly affects the water content of the soil before leaving the cover system by means of evapotranspiration or root water uptake, or by moving downward due to the influence of gravity. In accordance with Brooks et al. (2003), the rate of precipitation at which it enters the cover soil depends on several soil characteristics and the soil surface condition. The intensity of the rainfall event and the existing soil moisture status control the cover soil response to precipitation.

The pattern of precipitation also influences the soil moisture dynamics. Unless external irrigation is applied, rainfall is the only source of water replenishment to sustain plant growth in an ET cover system. The characteristics or patterns of rainfall, such as frequency, amount, intensity, and seasonal changes in rainfall events affect the temporal and spatial dynamics and distributions of soil water (Wilson et al. 2004; Salve et al. 2011; Yao et al. 2013). According to a study by Li et al. (2013), the amount of precipitation significantly affects surface soil moisture in soils under shrub-encroached grasslands.

2.4.4 Plant Response to Soil Properties

Many researchers have shown in different studies that there are two main factors that cause the failure of a vegetative cover. One is insufficient depth of cover soil, which

leads to an inadequate water storage capacity, and the other one is high soil density that results in low water-holding capacity and causes poor root growth (Anderson, 1997 and Warren et al. 1996). In compacted soil, roots do not penetrate well, eventually resulting in a malformed, shallow root system. Therefore, the selection of the correct soil and its placement during construction of the ET cover is vital because the plants' growth largely depends on the soil properties. The efficiency of an ET cover is ensured by the optimization of all the factors that control the plant growth, except for soil water supply. The concept is to make the soil water content a limiting factor for the plants multiple times during the natural growing season. Soil water storage should be minimal at the beginning of the critical events so that the cover soil can have the capability to store enough precipitation. The important characteristics of plant root growth and distribution in the soil are described in the following section.

2.4.4.1 Environmental Factors Affecting Root Growth

It is important to identify the role of roots in expelling water from the ET cover because the roots control the removal of water from the cover soil's deepest layer. Rendig and Taylor (1989) stated that the roots serve many functions. The plants are supplied with water and nutrients that have been absorbed by roots in both deep and shallow layers. Consequently, the deeper the roots can penetrate the cover soil, the more water and nutrients can be extracted from the deeper layer. The roots absorb water from many types and conditions of soil, from moist soil to partially dry soil, and soil zones of different biological, chemical, and physical properties. Plants are anchored in the soil by their roots, and roots and shoots are mutually dependent. Therefore, if the above-ground biomass is reduced, there is usually a reduction of root biomass also. Parts of the root system may die from a water stress condition in response to soil drying in any layer; simultaneously, new roots may grow rapidly in another moist soil layer.

Nutrient and salinity levels of the soil strongly affect vegetation growth. The soil layers need to provide nutrients to promote vegetation growth and maintain a robust root system. Low-nutrient or high-salinity levels can have detrimental effects on vegetation growth, and supplemental nutrients may need to be added to promote vegetation growth, thereby increasing the cost. For example, in a monolithic ET cover at Fort Carson, Colorado, bio solids were added as nutrients to increase organic matter and provide a slow release of nitrogen to enhance vegetation growth, as nitrogen is a key element for root growth. In addition, topsoil promotes growth of vegetation and reduces erosion. For ET covers, the topsoil layer is generally a minimum of six inches thick (McGuire, England, and Andraski 2001). Under favorable conditions, some plant roots have been found to grow 2 cm (0.8-inch) each day. However, there are some factors that hinder the robust root growth, and they eventually restrict the rate of water and nutrient uptake through the roots (Hauser and Gimon 2004). The factors that limit the root growth include the following, per Rendig and Taylor (1989);

- High soil strength and corresponding physical factors
    1. Soil density
    2. Particle size distribution
    3. Soil moisture content
- Unacceptable soil p^H
- Soil temperature (too high or too low)
- Salinity of the soil solution
- Deficiency of soil oxygen
- Chemical toxicity
- Allelopathic toxicants

2.4.4.2 Effect of Soil Density on Root Growth

The drying of each soil layer is controlled by the mass and distribution of living plant roots. Figure 2.26 demonstrates the possible root distribution patterns. If the soil layers are sufficiently moist, roots typically develop like the solid line-1 in Figure 2.26 (a). Most of the roots are found near the surface. Later, during the drying period, as the soil starts drying from the surface, the root distribution patterns changes to the condition like the dotted line-2. During and after the dry period, active root systems are found in the deeper layer of the cover soil. Many plant roots die in limiting conditions, but regeneration of roots is found again in different soil layers in response to the changes in the condition of the soil profile (Camp et al. 1996; Stewart and Nielsen, 1990; and Merva, 1995).

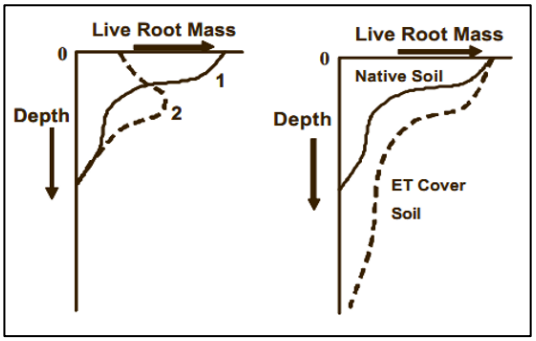

Figure 2.26 Root distribution in response to (a) soil water and (b) soil tilth and density

It is crucial, for an effective ET cover, to have a favorable soil condition that allows the rapid growth of roots to remove water after heavy precipitation. Under a responsive condition, root growth rate may exceed 2 cm/day vertically and 0.5 cm/day laterally. Russell 1977) reported a growth rate up to 6 cm/day based on his investigation. Unfavorable soil density is a major cause of restricting root growth rate and lowers the potential depth of rooting. In addition to impeding the root development, high bulk density of soil results in a reduction of the soil water-holding capacity (Radford et al. 2001; Mooney and Nipattasuk

2003). Under many native conditions, root growth rate is found limited due to high density. This can be overcome in the ET cover by placing soil at the appropriate density. Figure 2.26 (b) illustrates the root distribution in a native soil with higher density and in a correctly-placed ET cover, using the same soil and placed to achieve optimum soil density. Deep rooting and good soil tilth permit fast and complete removal of water stored in the cover soil (Hauser 2004). At many natural sites, soil properties limit the rooting depth rather than the plant's properties. Therefore, the soil condition for effective root growth should be optimized throughout the entire depth of the ET cover so that all of the vegetative landfill cover has rooting depth to the bottom of the cover depth.

In most soils, root growth is reduced when soil bulk density exceeds 1.5 g/cm^3, and the bulk density values above 1.7 g/cm^3 potentially prevent the development of root growth (Eavis, 1972; Monteith and Banath, 1965; Taylor et al. 1966; Jones, 1983; Timlin et al. 1998; and Gameda et al. 1985). According to the United States Department of Agriculture (USDA) and Natural Resources Conservation Services (NRCS), there is a limit of bulk density beyond which root growth is restricted. Table 2.1 shows the ideal and restricting bulk densities for root growth for different soil types. Optimum bulk densities for soils depend on the particle size distribution. Sandy soil is better than clayey soil at the same density for root growth. However, due to lower water-holding capacity and higher hydraulic conductivity of sandy soil than clayey soil, an ET cover is not recommended for sandy soil. The presence of organic matter in the top soil and greater biological activity can enable roots to grow satisfactorily despite higher densities.

Table 2.1 Ideal and root restricting bulk densities, USDA (1999) and NRCS

Soil Texture	Ideal Bulk Density	Bulk Density restricts root growth
	g/cm^3	
Sand, loamy sand	<1.60	>1.80
Sandy loam, loam	<1.40	>1.80
Sandy clay loam, clay loam	<1.40	>1.75
Silt, silt loam	<1.30	>1.75
Silty clay loam	<1.40	>1.65
Sandy clay, silty clay	<1.10	>1.58
Clay	<1.10	>1.47

A study by Keisling, Batchelor, and Porter (1995) revealed that root growth in compacted soils is constrained because roots can sustain a maximum pressure above which they are not able to expand in soils. They recorded 300 psi penetration resistance, which roots can overcome. In many cases in high-compacted zones, the development of cracks and fissures allows roots to grow through them. However, roots have also been found to concentrate in areas above or beside the compacted zone (Figure 2.27).

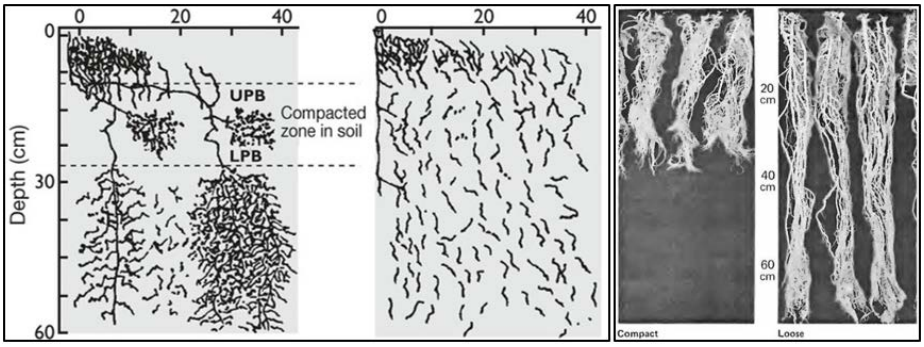

(a) (b) (c)

Figure 2.27 Effects of compaction on root distribution. Roots occupy a larger soil volume in (a) uncompacted soil than in (b) compacted soil (Keisling,T. C., J.T. Batchelor, and O.A. Porter. 1995) (c) Depth of alfalfa roots in loosened soil and comapcted dense soil (G.R. Saini, 1980)

2.4.4.3 Effect of Soil Moisture and Suction on Root Growth

Both a deficiency and an excess of soil water can limit root growth. Soil water itself is not directly detrimental to roots, as shown by its dynamic growth in well-aerated nutrient solutions, but an excess of water in the soil displaces the air from the non-capillary pore space and creates an oxygen deficiency that may lessen the root growth and functioning and cause the roots to die. A severe insufficiency of soil water commonly brings about a reduction in root growth. When permanent wilting appears, very little or no root growth occurs. Due to a deficiency of soil water, the absorption of minerals is greatly inhibited. Kaufmann (1968) reported that the root growth of Loblolly and Scotch pine seedlings in a slowly-drying soil was diminished to about 25% of the rate at field capacity at a soil water potential of 0.6 to 0.7 MPa. It was also reported that the growth of shoots was reduced even more dramatically than the growth of roots in drying soil.

Teskey and Hinckley (1981) reported that at the soil water potential of 0.1 MPa, root elongation in the Missouri oak-hickory forest was found to be the greatest, but the number of growing root tips was somewhat greater in drier soil. A study by Vartanian (1981) showed that drying soil reduced the root elongation but increased the number of new lateral roots in Sinapis Alba. Above a soil temperature of 17^{o}C in an experiment by Teskey and Hinckley, the soil water potential was found to be the dominant limiting factor for root growth. But below 17^{o}C, temperature was most often the only limiting factor. During this study, optimum soil temperatures and soil water potential were never found simultaneously; either the temperature or the soil water potential was always the limiting factor. Waring and Schlesinger (1985) quoted numerous experimentations signifying that plant roots, especially tree roots, grow very slowly at a soil water potential below -0.7 MPa, but Logsdon et al. (1987) presented the growth of maize crop roots at -1.09 MPa. According

to Newman (1966), flax root growth was reduced when the soil water potential was found -0.7 MPa, but some growth was observed in soil drier than -2.0 MPa.

2.4.5 Rate and Periodicity of Root Growth

The elongation rate of roots varies widely among species, as it is affected by the season; by changes in soil condition, like variation of water content, aeration, and temperature; and the influence of the shoot environment that affects the supply of carbohydrates. Weaver (1925) showed that the principal roots of a maize crop grow 5 to 6 cm per day for 3 to 4 weeks after sown. A growth rate of 10 to 12 mm per day is said to be usual in grasses, but 3 to 5 mm rate of growth is more common in tree roots (Barney, 1951; Reed, 1939; Wilcox, 1962). Several studies have shown that roots sometimes elongate more rapidly at night than during the day (Lyr and Hoffman, 1967; Reed, 1939). Such behavior is most likely to occur when high rates of transpiration produce daytime water stress.

According to Reich et al. (1980), flushes of oak root growth occur between flushes of shoot growth in a constant environment. Lyr and Hoffman, 1967; Romberger, 1963 have shown that seasonal cycles in root growth of perennial grass is at least partly related to soil temperature. Turner (1936) and Reed (1939) observed root growth every month of the year in Loblolly and Shortleaf pine, with the most growth occurring in the spring and summer and the least growth occurring during the winter period. In Figure 2.28, it is obvious that the periods of slow root growth in the winter coincided with periods of low soil moisture. In the study by Teskey and Hinckley (1981), they found that in the Missouri Oak-Hickory forest, optimum soil temperatures and water potential never occur simultaneously.

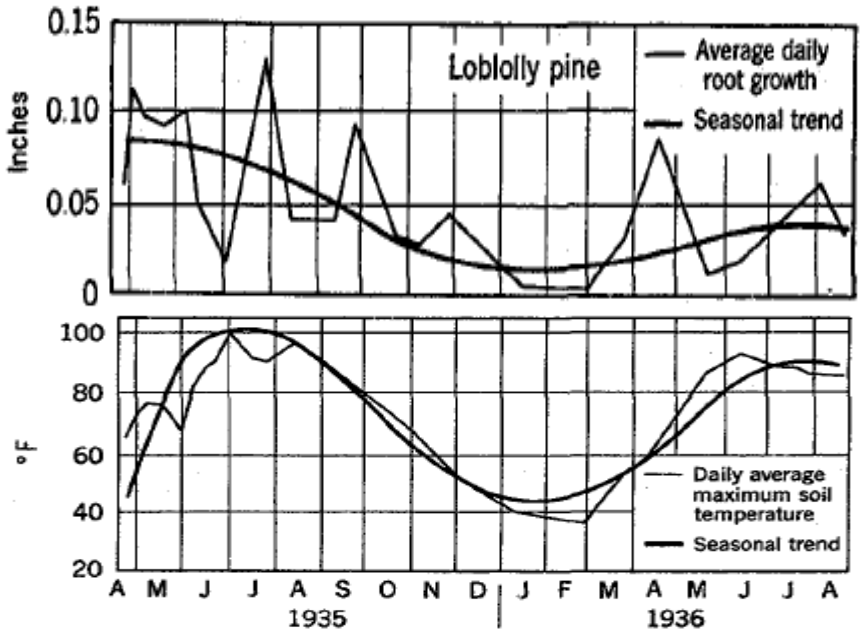

Figure 2.28 Effects of soil temperature and water content on growth of roots of Shortleaf pine (Kramer 1983, after Reed 1939)

Roots extend into previously unoccupied soil as additional water and nutrients come available. The ability of roots to continue growing is known as root growth potential (RGP) and is very important to the success of the water balance of an ET cover. In field conditions, water supply, fertilization, density of seedlings, and time affect the capacity of plants to generate new roots and hold more water, resulting in subsequent transpiration from the deeper depths.

2.4.6 Plant Root Water Uptake Principles

Two basic components are important to explain root water uptake principles: rhizosphere and bulk soil. Rhizosphere is the zone, within the bulk soil and surrounded by plant roots, where the biological and chemical activities are more concentrated. Respiration, gas exchange, and nutrient and moisture use are influenced by roots in the rhizosphere. The rhizosphere zone is about 1 mm wide, but has no distinct edge. Bulk soil

is that part which is not directly affected by the active functioning of the living plant roots. However, bulk soil may be transformed to rhizosphere over time, due to pedogenic effect. A schematic of root water uptake is shown in Figure 2.29.

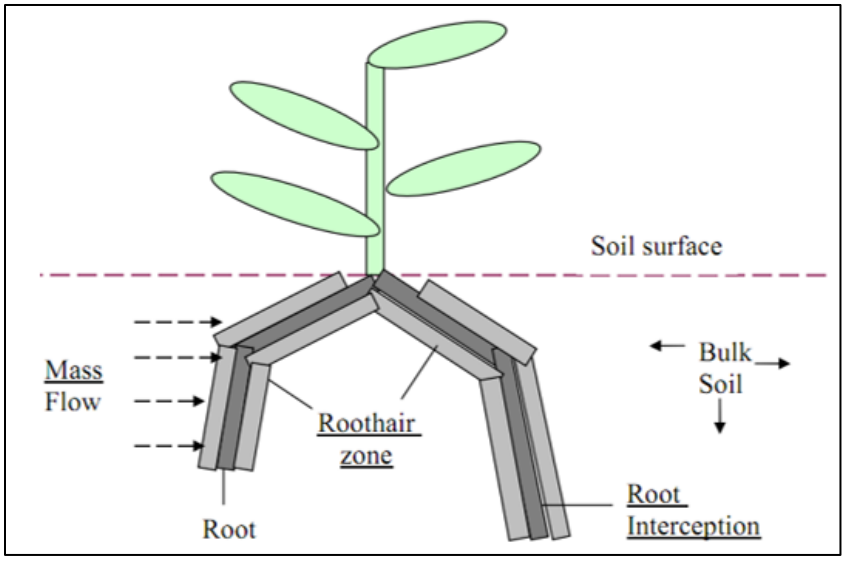

Figure 2.29 Basic components contributing to root water uptake (Modified from Schleiff, 2006)

After a precipitation event, water content increases in the bulk soil, as well as in the rhizospheric zone. The rate of root water uptake remains high as long as there is enough water in close contact with the roots and root hair. As soon as soil water from the root hair starts depleting, a soil water potential gradient develops between the bulk soil and rhizosphere, initiating the mass flow of the soil solution from the bulk soil to the rhizosphere, or the root surface or the root hair zone. The spatial distribution of roots in the soil determines the ability of plants to take up soil water and nutrients to sustain plant growth and development. A higher volume of root hair results in a higher rate of water uptake from the soil. Many studies on root water uptake have confirmed that deeper root systems enable plants to have easy access to water, whereas water is not available for shallow root

systems. Literature suggests that deeper root systems typically develop typically in drier environments. Different studies have found a significant difference in the root water uptake depths under different rooting patterns (Nippert and Knapp, 2007). Asbjornsen et al. (2007, 2008) reported that Big Bluestem grass takes water only from the top 20 to 30 cm of the soil. Canadell et al. (1996) and Jackson et al. (1996) conducted a survey on the patterns of root distribution and depth. Globally, roots of vegetation in the desert extend to a maximum depth of 13.4 m. Results of their survey revealed that almost 31% of the total root biomass is below 0.3 m. They also reported that 35% of the root biomass is below 0.3 m depth in temperate forests. However, root water uptake varies among different plant types and is strongly influenced by the availability of soil water. Araki and Iijima (2005), found, in their study, that the dryness of the top soil significantly affects the root water uptake. The basic principle of an ET cover system is to release water in the environment by means of transpiration through the plant roots and evaporation from the surface. Therefore, getting more water released into the atmosphere from the cover system requires deeper spatially-distributed root systems. Hence, root morphology or structure must be considered as an important factor for the design of evapotranspiration cover systems.

2.5 Methods of Root Study

Root growth and measurements have been studied for many years, and knowledge pertaining to exact root development, position, distribution, and penetration depth is very significant (Weaver et al. 1922). Weaver and Burner (1927) executed a thorough and extensive study on the size of the root systems in the United States, and Kutschera (1960) did a detailed investigation of root systems in Europe. However, as roots are underground and difficult to study, there is limited literature available. Nonetheless, even a small consideration of the functions of roots indicates that physiologically dynamic root systems are as vital as energetic shoots for successful plant growth because root and

shoot growth are so mutually dependent that one cannot get ahead without the other. Therefore, a good understanding and knowledge of plant root distributions and structure and root water uptake patterns have become increasingly important for developing modern and environmentally friendly practices for the sustainable solution for landfill final cover. This is especially true for the evapotranspiration cover (ET Cover), where the main mechanism relies on the plant water dynamics. The root structure is a central factor for soil-plant-water dynamics because it affects the pathway and resistance to water and solute movement, while the extent of the root systems affects the volume of soil available as a source of water and mineral nutrients. Factors affecting root growth and root functioning were investigated by McMichael and Persson (1991) and Waisel et al. (1991), Epstein (in Hashimoto et al. 1990), Feldman (1984), and Zimmermann et al. (1992), and in a review by Aesbacher et al. (1994)

In a vegetative landfill cover system, knowledge of roots is of paramount importance, as the in-situ root depth and distribution of roots significantly control the release process (transpiration) of water which is stored in the soil during the precipitation event (Barnswell and Dwyer 2011, Benson et al. 2002, Khire et al. 2000, Malusis and Benson 2006, and Stormont and Morris 1998, Albright et al. 2004, 2010; Bohnhoff et al. 2009). There are several methods for measuring the root system. Every method has different techniques and uses different equipment, and they all have benefits and drawbacks. The advantages and disadvantages of the different methods which are frequently applied are listed in Table 2.2.

Table 2.2 Frequently-used methods for measuring and analyzing root systems

Method	Information type	Destructive Method	Advantage	Disadvantage
Photographs or Drawings	Qualitative, 2D root morphology	✗	easy and rapid process, viewing exact root structure	tedious, blurry photographs, qualitative information only, root overlap, no statistical inference
Trench/Window	2D spatial root distribution	✓	Easy recording of root data, repeated same point measurement	Static, limited 2D area, destruction of roots during digging
Pinboards/Monoliths	Length, weight, diameter, distribution pattern	✓	provides natural arrangements of roots	labor intensive, skilled labor, loss of fine roots
Augure/Core	Length, weight, diameter, distribution pattern	✓	easy and straight forward method	requires large number of samples, labor intensive, time consuming, limited sampling depth
Rhizotron, Minirhizotron and Mesorhizotron	Dynamic 2D information, root growth and turnover	✗	repeated measurements at same point, accurate	expensive, labor intensive, time consuming

2.5.1 Field Monitoring Methods of Measuring Root Growth

Several methods are used to measure root growth in the field. McDougall (1916) used the horizontal and vertical glass plate method. Schuurman and Goedewaagen (1965) described the method of monoliths, soil cores, and profile walls. Most recently, Smit et al., (2000) used the rhizotrons, minirhizotrons, or transparent walls/windows method for root measurement. Some of the methods for root study are described in the following section.

2.5.1.1 Trench, Photographs and Drawings

The trench method of measuring roots is one of the oldest methods. Weaver et al. (1922) first used this method by digging a trench along the side of the plant to a depth of five feet. The width of the trench was determined, based on the condition of the site and how convenient it was for digging the trench. The major advantage of the method was that

the entire root system was visible after the excavation of the trench; however, this method also has some drawbacks. Excavating large trenches often destroyed the roots, and photographs taken at different times were often blurry, which didn't allow the viewers to observe the finer roots. Therefore, Weaver et al. (1922) suggested drawing life-sized images of the root system, as closely as possible to the exact measurements of the root system. Figure 2.30 shows a schematic drawing of the trench method.

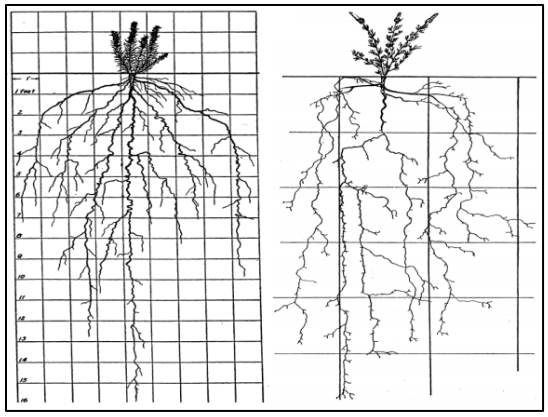

Figure 2.30 Root systems analysed by excavation and drawing (Weaver, 1919; 1920)

In 1979, Lore Kutschera (in Austria) added some improvements to the Weaver method. She investigated a wide range of grasses in Europe and proposed to excavate trenches on the south side of the plants, allowing her to shade the exposed roots with her body and prevent the sun from shining directly into her eyes. Day-to-day records of in-situ root images are possible with this method; however, it does not provide information on the total root system extension (Neumann et al. 2009). This highly destructive method for root measurement is not recommended at all for ET cover studies.

2.5.1.2 Pinboards and Monoliths

The pinboard method provides a complete depiction of root structures; however, the field installation of this method is time consuming. The pit has to be excavated against the plant, then the excavated wall is smoothed. The pinboard is then placed and pressed

against the wall. A steel cable is used so that the soil surrounding the pinboard is cut away, and the plant roots are still held by the pin when the pinboard is pulled away (Schuurman et al. 1971). Kono et al. (1987) and Kano-Nakata et al. (2011) quantitatively and qualitatively measured the root system using a “root box-pinboard”, and found this method to be an easy and effective method of root quantification. However, this method is not recommended for the ET cover, as the box used in this method limits the root growth (Kono et al. 1987).

2.5.1.3 Augurs and Cores

Core sampling, using an augur, measures root development in the field. A soil and root sample are extracted from the landscape, and the root sample is separated from the soil. These separated roots are then quantified, and the root growth is expressed as volume; diameter; weight; surface area; root length density (RLD), which is root length per unit soil volume; and root mass density (RMD), which is root mass per unit soil volume (Barnett et al. 1983 and Bohm, 1979). The main advantages of this method are that only a portion of the roots needs to be collected and the equipment required is inexpensive. In some other methods, like deep-pit digging, the equipment required is quite expensive, but it is possible to measure the actual root growth precisely. However, as this method utilizes a destructive method for root quantification, and there is great potential for human error, it is not recommended to use for the ET cover system.

2.5.1.4 Rhizotron, Minirhizotron and Mesorhizotron

Rhizotrons are commonly used for root measurement. Rogers (1969) designed the first rhizotron, which was constructed in the East Malling district of Kent, England. The word rhizotron came from the Greek words rhizos for root and tron for instrument, and is an underground facility or structure for viewing and measuring plant roots through transparent surfaces that may be in contact with the natural soil (Klepper et al. 1994). It is one of the

earliest non-destructive techniques for observing root growth in soil which allows repetitive measurements of root systems at a large field-scale. Rhizotrons have several advantages and limitations (Taylor et al. 1990). The major advantage is that successive measurements can be made on the same individual root so that the rate of length increment of the root can be observed (Taylor et al. 1990). Sensors and cameras are installed to measure soil conditions and record photography. Plant roots growing along the transparent wall can easily be traced, and the speed of root growth and root density can be determined (Glinski et al. 1993). However, the major disadvantage of this method is associated with its cost and operation process (Taylor et al. 1990). In a project at Auburn, Alabama in 1969, almost $40,000 was spent to construct the rhizotron, and the cost of operating it for the first 13 years was near $50 -100,000. The operating cost included updating the computer system and control system (Huck et al. 1982). The cost of constructing the rhizotrons would be considerably higher today (Taylor et al. 1990). Huck and Taylor (1982) cited more disadvantages of rhizotrons. During its installation, the structure and the environment of the soil changes, and the surface from which to view the root may not be representative. Klepper et al. (1994) suggested changing the soil after the rhizotron research, as populations of worms, fungi, bacteria and insects are very likely to grow.

The minirhizotron was proposed by Bates (1937) as a more viable alternative to rhizotrons. Bates used a mirror and a battery-operated lamp to observe roots intersecting in a glass tube in the ground. Later, the minirhizotron technique was improved upon by other researchers to create the modern minirhizotron. The modern minirhizotron uses a color video camera, where images can be recorded in videos or photographs which have better quality due to the application of modern technology (Smit et al. 2000, Dannoura et al. 2008, Taylor et al. 1990, Patena et al. 2000). A schematic of the minirhizotron with a data acquisition system is shown in Figure 2.31.

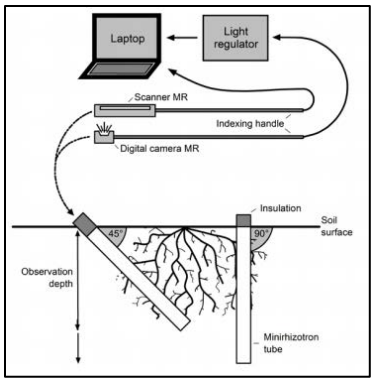

(a)

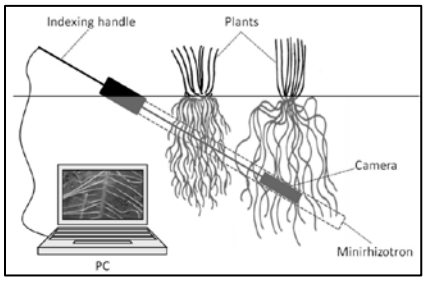

(b)

Figure 2.31 Schematic diagram of minirhizotron tubes (a) in both angled and vertical position (Modified from: Rewald and Ephrath, 2013) (b) Vamerali et al. (2012)

Minirhizotron is one of the best methods for studying roots. It is only destructive during the installation, it gives the same point measurement for root measurement, and it only takes about 30 minutes to install (Taylor et al. 1990). Though it takes a substantial amount of time to collect the pictures from the tubes and analyze them (Ingram et al. 2001), it is the best way to measure the root growth and density. For an ET cover study, the minirhizotron technique can be used to measure root growth, as using this method will keep the maximum integrity of the ET cover.

2.5.2 Digital Imaging

Digital imaging is the advanced method for the characterization of plant roots. It includes photographs or videos of the roots, scanned images of roots, or scanned drawings of root tracings. Ottman and Timm (1984) predicted the root length and area of an onion's

roots at definite root segments by using a computer program that analyzed images from photographs. In the rhizotron, minirhizotron, or other transparent wall design method for root measurement, there is usually an option to capture digital images or recorded videos of the roots. These digital images are examined for the measurement of the root length and density, using the computer tools. The quantification of roots, using photo electronic methods followed by an analysis of the image, has several advantages (Lesley et al., 2015). Image analysis is less time consuming and less dependent on human judgement. The distribution of the roots can be directly imaged with the digital camera when they are grown in a minirhizotron or transparent substrate (Downie et al. 2012, Bucksch et al. 2014). With the advancement of technology, photographs or scanned images are now used to evaluate several root measurements. Digital images have several key features and contain several layers of information that make the root study more precise (Lobet et al. 2013, Wang et al. 2015). The resolution of digital images and the automated analysis method makes the root measurements more productive (Pound et al. 2013)

Several commercial and free computer programs are available for root analysis, using digital images. Lobet et al. (2013) stated that there are 19 commonly-used programs for root analysis. The most common computer programs include WinRHIZO Tron, RootReader 2D, ImageJ, EZ-Rhizo, RootLM, and WinRHIZO. Some of these programs can determine the complex measurements of the roots, such as density, angles, total area, root order, and root intensity distribution with depth and branching (Zhu et al. 2011). Many research publications are available in the agricultural sector where image analysis via software has been extensively used (Lobet et al. 2013).

In the evapotranspiration cover system, studies on below-ground biomass are very limited, and root measurements, using image analysis, have not been conducted yet.

Image analysis is the most suitable tool for root analysis for the ET cover because it is a quick and precise method which is less prone to human error.

2.5.2.1 Advantages and Disadvantages of using Software for Image Analysis

WinRHIZO (Regents Instruments, Quebec City, Canada) is a program that was developed based on an optical scanner which produces high-quality images (Arsenault et al. 1995). It can be used for several root measurements, such as total root length, projected area, surface area, root tips, branching points, and root length at different intervals preferred by user (Arsenault et al. 1995). Per Fang et al. (2012), WinRHIZO is comparatively cheap and can be used for both large and small-scale studies. The major disadvantages of WinRHIZO is that it is sometimes unable to detect the finer roots, and the root system must be washed before scanning, which could cause the loss of some fine roots.

Benjamin and Nielson (2004) used the software Sigma-Scan™ to determine the root surface area. Another software program developed for root study is the ROOTEDGE. This program can measure the areas, perimeters, lengths, and widths of digitized roots (Kasper et al. 1997). It can perform basic image processing; however, ROOTEDGE assumes that the roots in the image will be black, on a white background.

Cornell University (Ithaca, NY, USA) developed the software RootReader 2D for the quantification of root growth (Clark et al. 2013). RootTrace, RE GR Analysis, Kine-Root, and Root FlowRT are sophisticated software that are used to determine the plant root system and focus on analyzing root growth. These programs are also capable of measuring the effects of temperatures and nutrient availability on root growth (Zhu et al. 2001).

Though the computer program for image analysis for root measurement is advantageous, the precision level is not always up to the mark. In a study by Kano-Nakata

et al. (2011), root length measured from the digital photography was found to be underestimated due to the overlapping of the roots. Ottman and Timm (1984) could not differentiate between viable and non-viable roots and organic materials, using an image analyzer. The process of translating qualitative information from observations to quantitative data is often tedious and time consuming.

2.5.2.2 Application of X-ray CT and NMRI

X-ray-computed tomography (CT) and nuclear magnetic resonance imaging (NMRI) offer additional techniques that are both non-invasive and non-destructive for measuring 3D root systems. The new approaches allow for the study of root growth, undisturbed, over time. To produce a 3D image with the CT method, X-rays are used to measure the photo-electrical absorptions or scattering to scan the roots growing in soil/substrate contained in PVC tubes (Heeraman et al. 1997). Rotated between an X-ray source and a detector, the sample is additionally recorded with a series of 2D projections, from which a 3D volume dataset may be constructed (Metzner et al. 2015). Unique to the X-ray CT scanning technique, it can be used for 3D visualization and quantification, with resolution ranging from 10 to 500 μm (Garbout et al. 2013). Lateral root development or root elongation rates have been included in recent applications. While the entire root system within its environment can be measured, allowing for non-destructive measurements, a major issue is with surrounding structures of the roots, such as water-filled pores. This can lead to low contrast, hindering straightforward segmentation of the roots from the background (Metzner et al. 2015). Studies conducted by Tracy et al. (2015) reported that 1,200 image projections were captured for each CT-measured-planted container. From the CT image data, the root system models can be used to quantify root length, volume, surface area, mean diameter, root tip diameter, and vertical root depth (Tracy et al. 2015). Long scan times are necessary for higher quality images. Daly et al.

(2015) produced 1,440 projection images after scanning a sample, rotating all around for 105 min. The use of high-resolution scanners with the CT method may lead to a wider use of CT in plant sciences (Metzner et al. 2015). Beyond plant roots, this method can be utilized in measuring rhizosphere hydraulic properties or in the characterization of soil aggregate properties.

Using photon signal intensities, the NMRI method measures spatial array, producing an image of the root system (Brown et al. 1991). When the NMRI method is applied, it is vital to differentiate protons in the roots from protons in soil for accurate measurement of the images of the root system, as protons are abundant in living tissues. Most soils, unfortunately, are unsuitable for NMRI imaging (Brown et al. 1991). 3D datasets of samples are produced from strong magnetic fields and radio frequency fields (Metzner et al. 2015). The CT scan may take longer to produce segmented images than the NMRI imaging, but because of its higher resolution, it is advantageous for finely-graduated root diameters (Metzner et al. 2015). Roots may appear thicker in the NMRI than in the CT, caused by the much coarser spatial resolution of the NMRI (Metzner et al. 2015). Metzner et al. (2015) reported that the thinnest roots detected with the NMRI were 250 μm in diameter. Despite precise and accurate measurement of the root system, NMRI or X-ray CT method is still very rare in ET cover study because of its sensitivity and requirement for skilled labor. Moreover, the NMRI method is expensive, and the system is complicated. Therefore, the NMRI method is not usually recommended for root study in ET cover systems.

2.5.2.3 ImageJ Software

One of the fundamental tasks for the evaluation of ET cover performance is the quantification of root length and root surface area, and distribution of root intensity at different depths of the in-situ root profile. The available methods for root quantification are

highly destructive, tedious, and time consuming. Several commercially-available image analysis software have been designed specifically for root studies, but most of them are expensive and very sensitive in operation. However, there are other programs which can be alternative solutions for root studies. ImageJ (Abramoff et al. 2004, Rasband 2011) is a license-free open source program developed at the National Institute of Health in the United States. It is a powerful and user-friendly program which can be customized for various root measurements, and it offers an inexpensive alternative to commercial software. Many researchers have performed root system analysis using ImageJ software. Bottema (2000) and Lobet et al. (2011) suggested a method to extract dynamic root traits with a shape descriptor using ImageJ. Basu and Pal (2012) described the method of root segmentation from the background using ImageJ. The ImageJ program was proved to be a powerful tool for studying root systems.

2.5.3 Geophysical Methods in Root Study

Little research has been done on the assessment of the effect of plant roots on the ET cover system. There are several methods described in literature, but most of them are destructive methods which preclude root measurements at the same location. Moreover, because destructive methods are labor intensive and time consuming, they often yield results of low resolution. Hence, due to the lack of information on root distribution, poor sampling occurs, resulting in high variability in root measurements (Tardieu 1988, Amato and Ritchie 2002). Other more sophisticated methodologies are non-destructive and precise, but they require quantifying the qualitative data, which takes a considerable amount of time. An example of one of these methods is the minirhizotron method. As an alternative to the current methodologies, geophysical methods are now widely used as an effective way of root monitoring and quantification.

2.5.3.1 Application of Electrical Resistivity Imaging (ERI) Technique

The electrical resistivity imaging (ERI) technique is a non-destructive and non-invasive geophysical method to measure root biomass (Al Hagrey, 2007; Amato et al. 2008). This subsurface geophysical investigation is a promising method because it provides concentrated spatial data and nearly instant depth coverage (Tabbagh et al. 2000). The ERI method has the capability of detecting resistive areas in the root zone (Al Hagrey et al. 2004), and extensive destructive sampling confirmed that variations of electrical resistivity (ρ) are related to plant roots (Amato et al. 2008; Lazzari et al. 2008; Zenone et al. 2008, Panissod et al. 2001, Loperte et al. 2006, Morelli et al. 2007).

Many researchers have conducted resistivity surveys in the vadose root zone and have established relationships between root biomass and soil resistivity. Amato et al. (2008) showed a strong effect of root biomass on soil resistivity under an Alder (Alnus glutinosa) stand (Figure 2.32 a). Amato et al. (2008) suggested that the effects of roots must be considered when soil resistivity data is interpreted and calibrated for other purposes. Paglis (2013) generated a high-resolution 2D electrical resistivity tomography along a soil transect under a Coffee tree. He compared the results with destructive soil sampling and concluded that soil resistivity is quantitatively related to root biomass (Figure 2.32 b), and the ERI method provides the basis for in-situ detection of root biomass. Rossi et al. (2011) used multi-electrode soil electrical resistivity tomography for mapping root biomass distribution. Destructive sampling, like root mass density (RMD) and root length density (RLD), was also measured for the coarse and fine roots. They found a significant correlation between electrical resistivity and RMD, especially for the coarse roost (Diameter > 2 mm). They recommended using the ERI method as a proxy for RMD.

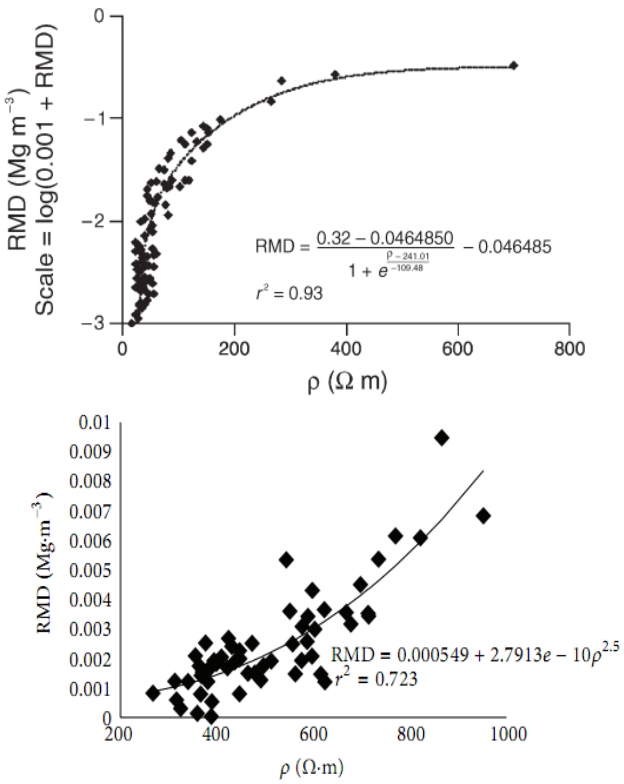

Figure 2.32 Root dry mass per unit soil volume (RMD) as a function of soil electrical resistivity (ρ), (a) (Amato et al. 2008) and (b) Paglis (2013)

Researchers have also attempted to quantify the root zone moisture uptake in contrasting vegetation types and determine the zone of evapotranspiration (ET). Jayawickreme et al. (2008) quantified the large seasonal differences in root-zone moisture dynamics for both forests and grasslands (Figure 2.33). They demonstrated that ERI is a quick and easy method to use to quantify the active zones of water uptake for different levels of soil water. Conventional methods for the estimation of root water uptake are restricted to a one-dimensional approach. In contrast, ERI gives both horizontal and vertical profiles, which are more closely linked to field scale behavior. Robinson et al. (2012) showed that electrical resistivity is consistent with the hydraulic redistribution (HR), mostly hydraulic lift (HL) within the vadose root zone. They concluded that the spatial information

from the ERI method is much more complete, and that it would have been difficult to obtain the necessary information through standard sampling.

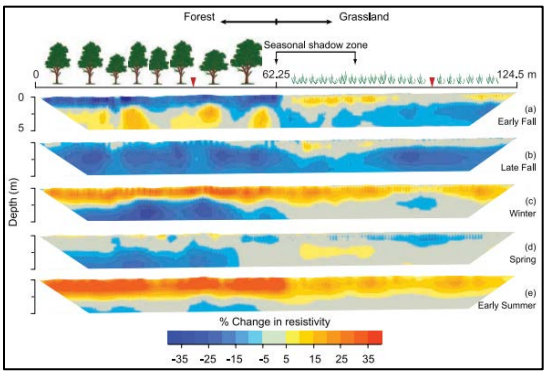

Figure 2.33 Subsurface imaging of root zone moisture (Jayawickreme et al. 2008)

2.5.3.1.1 Theory of ERI Method

To measure the electrical resistivity in the root zone, a minimum of four electrodes are required. The electric current is injected through two current electrodes, and the resulting voltage is measured through the pair of potential electrodes. Figure 2.34 depicts the schematic of four-point electrode configurations to measure electrical resistivity. Here, C_1, and C_2 are the current electrodes, and P_1, and P_2 are the potential electrodes. The apparent specific electrical resistivity (ρ_a) is measured in Ω-m units.

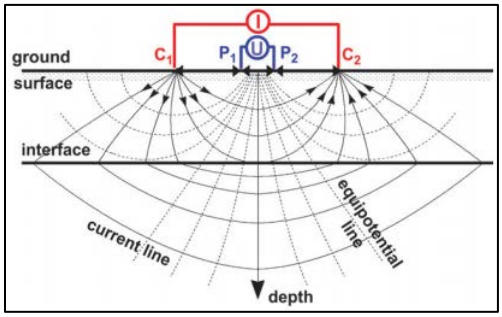

Figure 2.34 Configuration of four-point electrodes (modified from Hagrey 2007)

Several configurations of electrodes can be used to measure the resistivity. The Wenner array uses equally-spaced electrodes and a dipole-dipole configuration, dipole

offset, and its n-multiple of the dipole-dipole offset. Figure 2.35 illustrates the dipole-dipole array configuration.

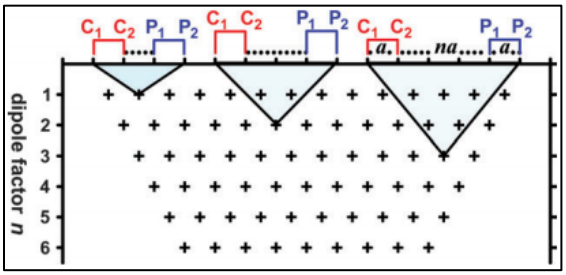

Figure 2.35 Acquisition of 2D apparent resistivity pseudosection using dipole-diploe array

A resistivity imaging survey is conducted by using electrodes distributed along an individual profile. The distribution of electrodes depends on the size of the profile and the required resolution. If the spacing among the electrodes increases, the depth of penetration increases. The pseudosection obtained from the survey gives a qualitative image of the subsurface distribution of resistivity. The resistivity profile is then inverted to a 2D or 3D model to obtain the in-situ actual resistivity value (Loke and Barker, 1995, 1996). A finite difference algorithm is used to develop of the relationship repeatedly until a predefined threshold value is obtained.

2.5.3.2 Ground Penetrating Radar (GPR) Method

Ground penetrating radar (GPR) is a 3D non-destructive geophysical method being rapidly developed in root research (Luster et al. 2009). GPR uses high-frequency radio waves in the soil, and the differences in dielectric constants between materials result in the contrast of the developed image (Zhu et al. 2011). The GPR method can provide both 2D and 3D live images (al Hagrey, 2007). Al Hagrey (2007) developed a methodology using GPR and produced root images growing in the field from the data on soil moisture distribution. Though GPR is a promising method of root study, researchers have confirmed that it could be highly dependent on the soil type and texture.

2.6 Field Determination of Hydraulic Conductivity of ET Cover

Hydrologic properties of soil play an important role in quantifying the moisture movement in an ET cover system. Hydraulic properties of soils, such as saturated and unsaturated hydraulic conductivity and the soil water characteristic curve (SWCC), significantly impact the percolation rate into the underlying waste (Khire et al. 1997, Ogorzalek et al. 2008, Bohnhoff et al. 2009). Over time, the hydraulic conductivity of the ET cover soil changes due to the change in soil structure in response to natural environmental processes, such as freeze-thaw cycling, wet-dry cycling, and plant root intrusion (Chamberlain and Gow 1979, Beven and Germann 1982, Suter et al. 1993, Albrecht and Benson 2001). These changes in soil formation need to be considered in the design of an ET cover for optimum performance. Benson and Albright (2009) showed that regardless of the as-built saturated hydraulic conductivity (K_s), a few years after the construction, due to the field exposure, K_s typically ranges between 1×10^{-5} and 1×10^{-3} cm/sec for most soils (Figure 2.36). Unsaturated hydraulic conductivity is also very important for long-term performance evaluation because soils in the ET cover are generally unsaturated (Khire et al. 1994a, and 1995). Moreover, the unsaturated hydraulic conductivity function is important for the accurate simulation of the ET cover system. Very limited data is available in the literature regarding the unsaturated hydraulic properties of compacted fine-grained soils of ET cover systems (Meerdink 1994, Tinjum 1995). Hence, determination of field scale hydraulic conductivity is important for evaluating the long-term cover performance.

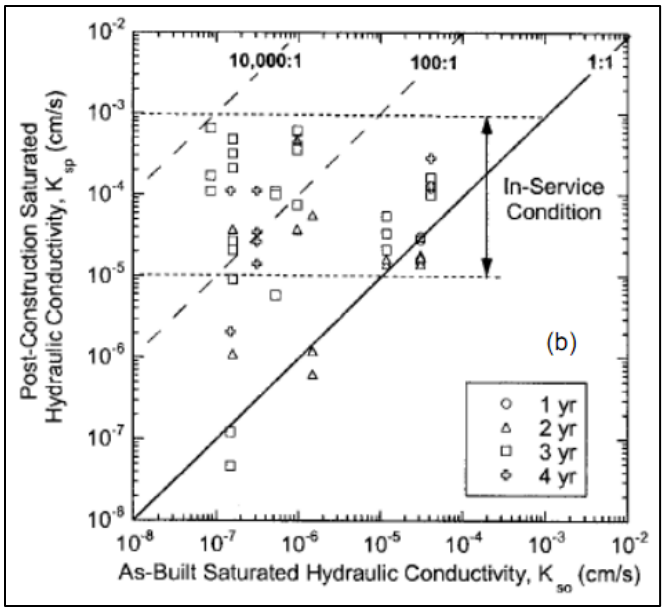

Figure 2.36 Changes in saturated hydraulic conductivity after field exposure (ACAP Project, Benson et al. 2007)

2.6.1 Determination of Saturated Hydraulic Conductivity

Common methods used to determine the saturated hydraulic conductivity in the ET cover system are two stage borehole test (TSB), sealed double ring infiltrometer (SDRI), open double ring infiltrometer (ODRI), Guelph permeameter (GP), and tension infiltrometer (TI). A short description of these methods is given in the following section.

2.6.1.1 Two Stage Borehole (TSB)

The concept of the TSB method depends on the wetted zone in the soil. The vertical and horizontal saturated conductivity varies, based on the geometry of the TSB equipment (Daniel, 1989). The test is conducted in two stages, and two equations are used to determine the vertical and horizontal conductivities. TSB equipment is installed in the field by drilling a hole, placing the casing, and then sealing the annular space between the casing and hole with suitable grout. The TSB equipment used in an ACAP site is shown in Figure 2.37.

The major limitation of the TSB method is a smear zone of the sidewall during drilling, which can often provide misleading readings. Another limitation is that the test cannot be conducted at the ground level or near the surface of a shallow depth.

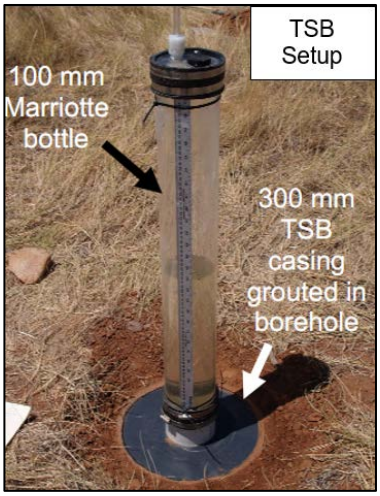

Figure 2.37 In-situ hydraulic conductivity measurement with TSB permeameter (ACAP project, Albright et al. 2004)

2.6.1.2 Sealed Double Ring Infiltrometer (SDRI)

The SDRI test determines the low infiltration rates of fine-grained soils. It has been designed to measure the actual volume of water flowing through the soil mass over a fixed period. The SDRI test is typically conducted with 25 mm tubing and a Marriott bottle. For the ODRI test, an inner ring with a 305 mm diameter is typically used. SDRI test equipment used in the ACAP project is shown in figure 2.38.

The major drawbacks of the SDRI method are that it cannot be used on slopes unless a flat trench is cut, which adds to the cost; The installation procedure is time consuming and difficult; the monitoring method is labor intensive; and repetitive tests are difficult.

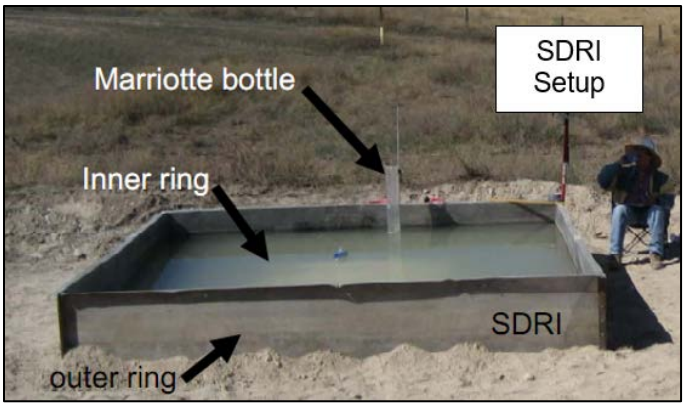

Figure 2.38 In-situ hydraulic conductivity measurement with SDRI permeameter (ACAP project, Albright et al. 2004)

2.6.1.3 Guelph Permeameter (GP)

The GP method is a widely-applied method that is used to determine the most important soil hydraulic properties (Elrick & Reynolds, 1992a). It is a user-friendly instrument that can quickly and accurately measure the in-situ hydraulic conductivity. Depending on the soil type, this equipment can be used to measure the hydraulic conductivity in 0.5 to 2 hours, at depths ranging from 0.5 ft. to 2.5 ft. The GP test method involves drilling small, vertical, and cylindrical holes of radius a (unit mm). The steady state flow (Q_s) rate (unit mm^3/h) is determined by maintaining a constant depth of ponding in the hole. The flow rate in GP is measured visually by taking the reading of the water level in the GP reservoir. The time interval between two consecutive readings is kept constant and typically ranges from 15 seconds to 60 minutes, depending on the soil types. The standard time interval is 120 seconds (Soil moisture Equipment Corp. 1987). Figure 2.39 shows the field application of GP.

The major advantage of GP is that the equipment is easy to operate and takes less time than either the TSB or SDRI method. The results obtained from GP are also more reliable than other methods. GP can be used in both flat and slope sections, and the testing

is less destructive than that of the TSB and SDRI methods. It is also possible to use GP at surface shallow depths.

Figure 2.39 In-situ hydraulic conductivity measurement with GP

2.6.2 Determination of Unsaturated Hydraulic Conductivity

The hydraulic conductivity of unsaturated soil is of increasing concern for geotechnical and geo-environmental engineers. The ET cover system requires special attention in measurement of unsaturated hydraulic conductivity since long-term performance of the ET cover system cannot be effectively evaluated without considering the unsaturated behavior of the soil. Direct measurement of unsaturated permeability in the lab, with collected soil specimens, is labor intensive and time consuming. There are limited methods available for in-situ determination of unsaturated permeability of soil. Richards and Weeks (1953) introduced a method named 'Instantaneous Profile Method' (IPM), which measures unsaturated hydraulic conductivity in the field. Later on, several other researchers (Bruce and Klute, 1956, Watson 1966, Hamilton et al. 1981, Daniel 1983, Malicki et al. 1992) modified the method. Meerdink et al. (1996) applied this method for the evaluation of unsaturated soil behavior of two landfill final covers: the Greater Wenatchee Regional Landfill in East Wenatchee, Washington; and the Live Oak Landfill in Conely, Georgia.

The IPM method uses the simple Darcy's law in the following manner:

$$K\Psi = \frac{v}{\frac{\partial h}{\partial z}}$$

Where, K_ψ is the hydraulic conductivity at suction ψ, v is the discharge velocity, h is the hydraulic head and z is the depth below the ground, ∂h/∂z is the vertical suction gradient.

2.7 Water Balance Modeling

Numerical models have served as an important tool for the design, prediction, and performance evaluation of ET cover systems. The National Research Council established the Committee on Ground Water Modeling Assessment (CGWMA) to review the precision of various numerical models for the water balance cover and the extent to which regulatory agencies can make their decisions based on the model predictions (Schwartz et al. 1990). CGWMA concluded that models are more certain than the real scenario. It is to be remembered that numerical models are the mathematical representation of real-world conceptual models, the real-world behavior.

Several models have been used for the prediction of water balance cover, but most of them do not include all of the features required to effectively predict the water balance performance. Some general vadose zone models describe the water movement through unsaturated soil. Researchers often fail to come to a consensus due to a lack of understanding and limited database available for the vadose zone regarding the selection and application of an apposite model for the water balance design (Albright, W.H., Gee, G.W., Wilson, G.V. & Fayer, M. J. 2002). Most complexities arise in trying to understand the physical and hydrologic processes in the vadose zone, as well as other processes (vegetation and climate). Therefore, selection of the appropriate water balance model is vital.

2.7.1 Models Available for Water Balance Cover Design

The EPA, TCEQ and other state regulatory agencies allow design and construction of alternative landfill covers if they are capable of controlling erosion and minimizing the rate of infiltration to an acceptable limit. Therefore, a computer-based simulation of a water balance cover design is highly recommended to meet the regulations for the acceptability of the alternative (ET) cover (e.g., Morris and Stormont 1998). Several simulation codes are available for the design and verification of a water balance cover. An extensive review was conducted for the available models for landfill final covers by Nixon et al. (1997). Based on their review, 13 codes (CREAMS, HSSWDS, HELP, MULTIMED, SOILINER, HRS, HARM, DRASTIC, PCLTF, NCAPS, DPM, RELRISK, RCRASTD) were compared. Among these codes, HELP is by far the most popular code because of its simple algorithms. Later, the codes HYDRUS-2D, UNSAT-H, LEACHM and EPIC Model gained popularity among researchers and consultants for their wide range of features and greater accuracy. According to the US EPA, the most widely used and recommended models for ET cover designs are as follows:

- UNSAT-H
- HELP
- HYDRUS-1D
- EPIC
- LEACHM
- VADOSE/W
- SHAW

2.7.2 Advantage of UNSAT-H Model

All the models for the water balance design of ET cover systems have some advantages and limitations. The hydrologic evaluation of landfill performance (HELP)

simulation code (Schroeder et al. 1994) is the most commonly used computer tool for the assessment of ET cover design. The New Mexico Environmental Department (1996) used the HELP model to compare the equivalent or lower flux rate of alternative covers to a prescriptive design under the same climatic and operational conditions (Dwyer 2003). Khire et al. (1997) simulated the earthen final cover of the Live Oak Landfill in Atlanta, GA and the Greater Wenatchee Regional Landfill in East Wenatchee, Washington. However, the HELP program is not theoretically reliable for the assessment of the ET covers. A major shortcoming of this program is that it assumes a unit gradient for the unsaturated flow of the cover soil. It does not consider the influence of suction gradients on water movement, like water being drawn upward in response to evaporation. Another major drawback is that HELP assumes that any layer that is assigned as a barrier layer is always saturated, which is not the case at all (Dwyer 2003).

LEACHM was developed for agricultural use and is a very popular water balance program among soil scientists. It simulates the one-dimensional Richard's equation. Nevertheless, this code is no longer supported by developers, so regulators have stopped relying on it for water balance modeling for landfill covers. Not much information could be obtained on the application of LEACHM to alternative covers.

The EPIC model, developed as an agricultural support tool, was identified as the most comprehensive code that incorporates most of the critical features (Albright et al. 2002). It embodies the most rigorous algorithm regarding the plant growth process; however, it requires an extensive list of plant characteristics which are not typically evaluated in water balance covers. Therefore, EPIC is not considered pertinent for the assessment of water balance modeling.

A water balance model for landfill covers in arid, semi-arid, and especially humid or semi-humid regions should include the constitutive algorithms for surface fluxes, a

systematic method for the management of runoff, an organized algorithm to handle time-based and depth-dependent soil water uptake by plant roots, an aptitude to account for vapor flow and hysteresis in soil hydraulic properties, and multidimensional flow that accounts for suction-based anisotropy (Khire et al, 1997). The existing models available for water balance modeling are not capable of including all of these elements. Furthermore, the multidimensional models that are currently accessible do not consider the suction-based anisotropy or vapor flow, and some of the existing models experience serious computational complications and malfunctions during the simulation of flow in soils. The computational snags are specifically austere when sporadic applications of water, comparable to meteorological conditions in arid, semi-arid, and humid regions, are made to the surface. Therefore, considering all of the negative impacts, the one-dimensional model, UNSAT-H, is considered the best solution for simulating the water balance. It includes most of the features that are theoretically believed to have critical impacts on the water balance of monolithic ET cover systems, such as surface fluxes, runoff, vapor flow, temporal and depth-dependent root water uptake, etc. It is also computationally all-encompassing for the conditions that generally are prevalent in the ET cover system in the field. UNSAT-H also has the greatest flexibility of choosing between Van Genuchten (VG) and Brooks and Corey (BC) water retention functions, the Haverkamp function, and other polynomial functions to fit water retention data.

2.7.3 Unsaturated Soil Water and Heat Flow Model (UNSAT-H)

UNSAT-H was developed as a one-dimensional, finite-difference computer program by Fayer and Jones (1990), and can simulate the water balance, as well as soil heat flow of landfill covers (Fayer 2000). UNSAT-H solves Richards' equation and Fourier's heat conduction equation to simulate water flow and heat flow. The form of Richard's equation solved by UNSAT-H is:

$$\frac{\partial \theta}{\partial \psi}\frac{\partial \psi}{\partial t} = -\frac{\partial}{\partial z}\left[KT\frac{\partial \psi}{\partial z} + K\psi + qVT\right] - S(z,t)$$

Where, Ψ = matric suction; t = time; z = vertical coordinate; K_Ψ = unsaturated hydraulic conductivity;

$$K_T = K_\Psi + K_{V\Psi}$$

$K_{V\Psi}$ = isothermal water vapor conductivity (Fayer and Gee 1992); q_{VT} = thermal vapor flux density; and S (z, t) = sink term represents water uptake by vegetation

The UNSAT-H approach to analyzing water flow in earthen covers has distinctive differences from that of the HELP approach. Figure 2.40 shows a schematic illustration of how UNSAT-H computes the water balance. The precipitation experienced on the landfill cover is separated by UNSAT-H into infiltration and overland flow. The quantity of water infiltrating depends on the infiltration capacity of the soil profile immediately prior to the rainfall (e.g. total available porosity). Thus, the fraction of precipitation shed as flow is dependent upon the saturated and unsaturated hydraulic conductivities of the final cover's soil characteristics. If the infiltration capacity is exceeded by the rate of precipitation, the excess water is shed as surface runoff. UNSAT-H does not consider absorption or interception of water by the plant canopy, or the effect of slope and slope length when computing surface runoff.

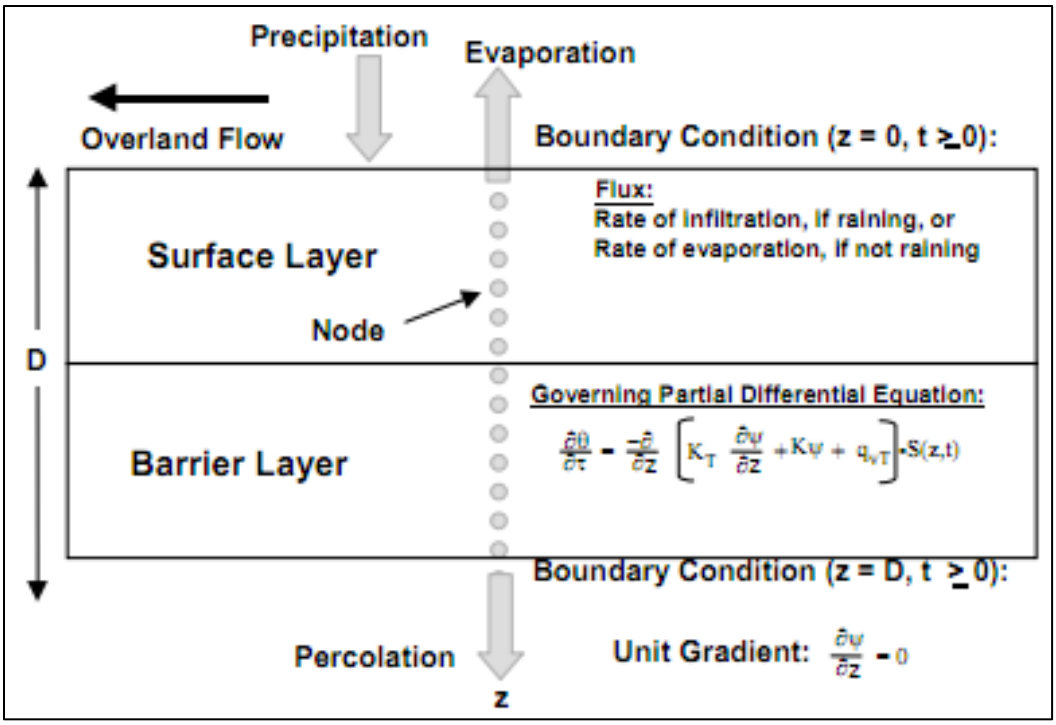

Figure 2.40 Schematic representation of water balance computation by UNSAT-H (modified from Dwyer 2001)

During an UNSAT-H simulation, water that has infiltrated a soil profile moves upward or downward because of gravity and matric potential (Figure 2.40). Evaporation is computed using Fick's law. Water removal by transpiration of plants is treated as a sink term in Richards' equation (Figure 2.40). A modified form of Penman's equation, given by Doorenbos and Pruitt (1977), is used to compute PET from daily wind speed, relative humidity, net solar radiation, and daily minimum and maximum air temperatures. The soil water storage is computed by integrating the water content profile. Flux from the lower boundary is via percolation (Figure 2.40). UNSAT-H does not compute lateral drainage, as it is a one-dimensional program.

2.7.3.1 Infiltration

UNSAT-H simulates infiltration by a two-step process. First, infiltration is set equal to the precipitation rate during each time step. Second, if the surface soil saturates, using a Dirichelt condition (with the surface node saturated), the solution of the time step is repeated. The infiltration rate is the resulting flux from the surface into the profile.

2.7.3.2 Runoff

The UNSAT-H model does not explicitly simulate runoff, but rather equates runoff to the precipitation rate that is more than the infiltration rate.

2.7.3.3 Soil Water and Heat Flow

The UNSAT-H model simulates liquid water flow, using the Richards' equation, Frick's law for water vapor diffusion, and the Fourier equation for sensible heat flow. Convective airflow is not considered in the model. There are many options when describing soil-water retention, including linked polynomials, the Haverkamp function, the Brooks and Corey function, and the van Genuchten function, as well as several special functions that account for the water retention of very dry soils. The van Genuchten function can also be treated hysterically. Linked polynomials, the Haverkamp model, the Mualem model, and the Burdine model are options for describing hydraulic conductivity.

2.7.3.4 Evaporation

In simulating evaporation, the UNSAT-H model employs two alternatives. One alternative is the isothermal mode which employs the PET concept. User-supplied daily values of PET or daily weather data are used in code calculations for the daily PET values, using the Penman equation. The code attempts to apply the potential evaporation rate during each time step. If the soil surface dries to or above a user-defined matric potential limit, the time step is re-solved, using a Dirichlet condition at the surface. Given this situation, at the matric potential limit, the surface potential would be held constant while

the evaporation is set equal to the flux from below. In the thermal mode, UNSAT-H calculates evaporation as a function of the difference of the vapor density between the soil and the reference height (the height at which air temperature and wind speed are measured) and the resistance to vapor transport. Air temperature, wind speed, and atmospheric stability are some of the several factors used in the function for resistance to vapor transport.

2.7.3.5 Transpiration

The effects of plant transpiration, using the PET concept, are simulated in the UNSAT-H model. There is no provision for simulating both water and heat flow under a plant canopy. The PET is separated into potential evaporation and potential transpiration, given plant information supplied to the code. The root zone is where the potential transpiration will be applied, using the root distribution to apportion it among the computational nodes that have roots. The suction head of the node is the dependent factor when dealing with the withdrawal of water from a certain node. Suction head values provided by the user to define the potential transpiration rate of a node will be reduced. Transpiration cannot remove any water below the minimum value, commonly known as the wilting point. Transpiration is reduced to zero when all nodes with roots reach this level of suction head.

2.7.4 UNSAT-H Input Parameters

2.7.4.1 Boundary Condition

Boundary condition specifications are determined by the flow of water across the surface and the lower boundary of the selected cover profile. For infiltration occurrences, a maximum hourly flux (commonly 1 cm/hr.) is set for the upper boundary. During evaporation, the surface condition can be modeled as a flux that requires daily weather data. Applicable weather data should be selected based on the desired design life of the

cover system. Potential evaporation (E_ρ) and potential transpiration (T_ρ) are partitioned from PET when using the UNSAT-H program. Potential evaporation is estimated or derived from daily weather parameters (Fayer 2000). Potential transpiration is calculated by using a function (Equation 6.1) that is based on the value of the assigned LAI and an equation developed by Ritchie and Burnett (1971) for cotton and grain sorghum:

$$T_p = PET\ [a + b\ (LAI)^c], \text{ where } d \leq LAI \leq e$$

Here: a, b, c, d and e are fitting parameters;

A = 0.0, b = 0.52, c = 0.5, d = 0.1, e = 2.7 (Fayer 2000)

2.7.4.2 Vegetation Data

Vegetation properties have a significant role in predicting the water balance. The set of parameters required in UNSAT-H are the leaf area index (LAI), rooting depth and density, and root growth rate, as well as the suction head value that corresponds to the soil's field capacity, wilting point, and water content above which plants do not transpire because of anaerobic conditions. Based on the user's desired or worst-case scenarios, a percentage of bare area must be determined. Desired or expected plants on the cover and the final cover profile are used in the representative assumption of the maximum rooting depth (Foxx et al. 1984, Weaver 1920). The root length density (RLD) describes the distribution of roots with depth and is assumed to follow an exponential function:

$$RLD = a \times e^{(-bz)} + c$$

Where, a, b and c are fitting parameters; Z = depth below surface. Typical RLD curves is shown in figure 2.41. Fayer (2000) suggests the parameters used for the RLD functions are: a = 0.315, b = 0.0073, and c = 0.076 for cheat grass. He also recommends the root depth be established as a function of time.

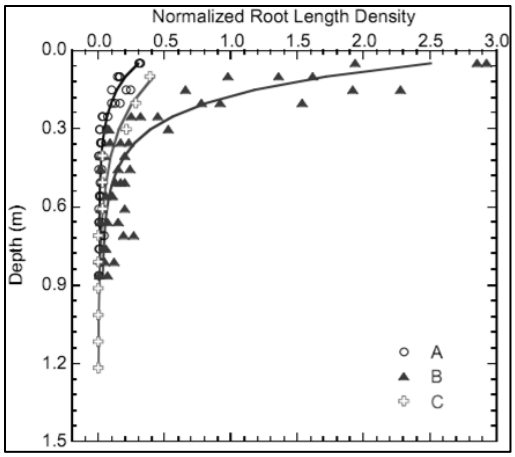

Figure 2.41 RLD function to fit root density for a monolithic cover (Modified from Albright et al. 2009)

LAI is a non-negative value and can be greater than 1. UNSAT-H uses LAI in partitioning PET into potential transpiration (PT) and potential evaporation (PE). The Ritchie-Burnett-Ankeny function is generally used for the partitioning. The equation is as below;

$$\mathrm{PT} = 0.52 \times \mathrm{PET}\sqrt{\mathrm{LAI}}$$

LAI can vary seasonally and is affected by meteorological factors. But for modeling, the seasonal variation of LAI is represented by a linear function. The typical LAI function used in UNSAT-H is shown in Figure 2.42.

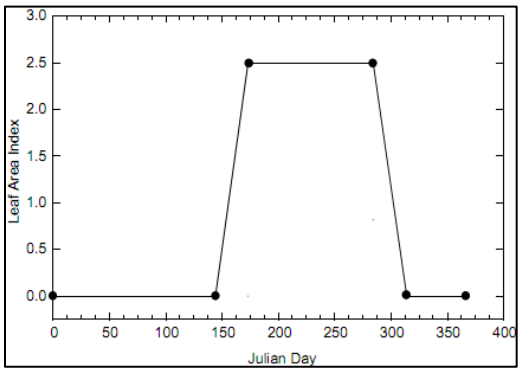

Figure 2.42 Typical LAI function used in UNSAT-H

2.7.4.3 Soil Properties

The input of soil properties in UNSAT-H includes the saturated hydraulic conductivity and parameters that describe the soil water characteristic curve (SWCC). The hydraulic properties have a strong influence on the water balance prediction of ET covers (Ogorzalek et al. 2007, Bohnhoff et al. 2009). Therefore, careful determination of the hydraulic properties and SWCC are important to reflect the field condition.

Unsaturated hydraulic conductivity can be described with a variety of equations, but the most commonly used is the Van Genuchten-Maulem function. Figure 2.43 illustrates the Van Genuchten-Maulem unsaturated hydraulic conductivity function for different soil types.

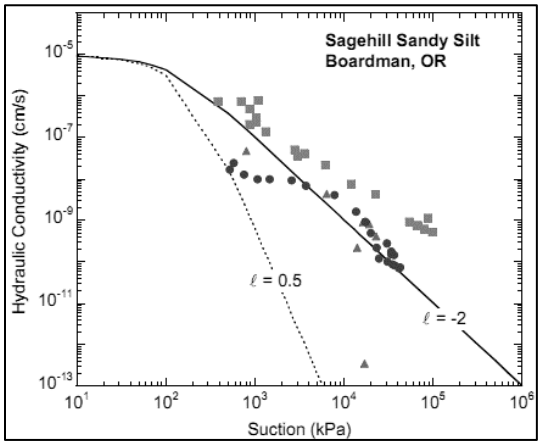

Figure 2.43 Unsaturated hydraulic conductivity predicted with Van Genuchten-Maulem equation (Modified from Benson et al. 2009)

2.8 Selected Studies on ET Cover: Field Monitoring

Several researchers and state regulators have attempted to evaluate the field performance of ET covers in the United States, resulting in more than 20 field scale ET cover studies. The largest study is the Alternative Cover Assessment Program (ACAP), which included 13 construction and monitoring sites that were under different

meteorological conditions and were of assorted soil types. The major studies conducted on ET cover performances are shown in Figure 2.44. It is to be noted that most of the studies were conducted in the western region of the United States; very few are evident in the eastern part. Some of the research was of long duration, and some were of short duration. Some of the case studies will be presented in the following section.

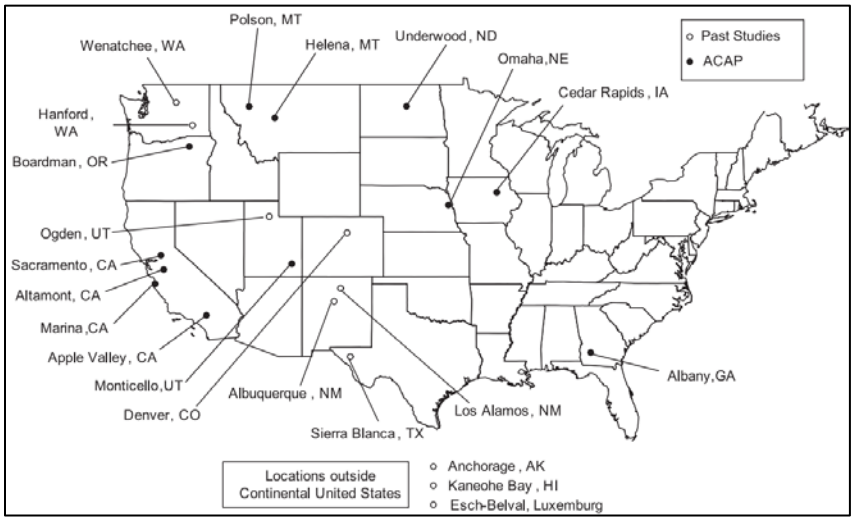

Figure 2.44 Field sites in US EPS's ACAP project and past studies

2.8.1 Long Term ET Cover Study

ET cover studies that are considered long-term are ones in which the sites are monitoring for more than 15 years. Two selected studies are described in the following section.

2.8.1.1 Great Plains Water Balance

A study by Cole and Mathews (1939) describes the monitoring results of the water balance of the Great Plains for almost 30 years, from 1907 to 1936. During the study period water balance investigations were performed on five locations within the Great Plains. Two locations were continuously monitored, while the other locations provided limited measurements of the water balance in native sods. The two locations that logged

full-time measurement were Mandan, North Dakota, which had silty clay loam, and North Platte, Nebraska, which had a very fine sandy loam. At Mandan, soil-water records were completed for 21 years on native sod, while at North Platte, soil-water records were completed for 25 years. Monitoring results from these water balance measurements showed that water did not permeate past the root zone depths. No evidence was found that water percolated past root zone depths at any of the five sites during the 30-year period. Native plants grew throughout the year on native sod, removing water stored in the soil quickly because of the evapotranspiration covers. This study confirmed that there was no water movement past the root zone despite the unplanted period, when water accumulates in the soil.

2.8.1.2 Pawnee National Grasslands

Sala et al. (1992) studied the soil-water balance of grasslands in northeastern Colorado for more than 30 years. The soil at the site was characterized as sandy loam. The annual average precipitation during the study period was almost 327 mm. The conclusion of the study, from the field monitoring results, was that the soil profile within the potential root depth of native grasses was rarely filled with water. The water removal mechanism was like the ET cover concept. No deep percolation was observed below 135 cm during 30 years of monitoring.

2.8.2 Short-Term ET Cover Study

The short-term ET cover studies refer to monitoring the field performance for two to seven years. Some of the case studies are described in this section.

2.8.2.1 Lakeside Reclamation Landfill, Oregon

In 1990, the Lakeside Reclamation Landfill was approved for ET cover capping, using poplar trees. A comparison study was made between covers of non-RCRA grasses and covers planted with poplar trees (Jarrell et al. 1995). Soil moisture was monitored for

both test sections at different depths to compare the performances of poplar trees and the grasses. Litch et al. (2001) recorded that the root depth of the poplar tree at the site was 4 feet, and the grass roots only reached 1.5 feet, at their maximum. Jarrell et al. (1995) concluded that water removal for the ET cover was higher than for the grass-only cover. They also concluded that at lower depths of the soil, water removal was effective due to the deep growth of poplar roots. Percolation rates from the ET cover test pads were found to be lower than the grass-only cover due to higher root density and a more efficient water removal mechanism.

2.8.2.2 Bluestem Landfill Site No. 2 - Marion, Iowa

A performance-based study was conducted for two years (from 1995 to 1996) at the Bluestem Landfill in Marion, Iowa (Licht et al. 2001). The study compared an ET cover and a clay cover. The clay cover test pad was designed and constructed based on the IOWA regulations, and had a compacted clay layer with hydraulic conductivity of 10^{-7} cm/sec and only grass as the vegetation. The ET cover vegetation was mixed with grass and poplar trees. Time domain reflectometry (TDR) was used to measure the soil moisture. Based on the sensors' results, at lower depths, the soil moisture fluctuation underneath the ET cover was higher, which was the result of water removal due to the root depth of the poplar (Licht et al. 2001).

2.8.2.3 Alternative Cover Assessment Program (ACAP)

The Alternative Cover Assessment Program (ACAP) was conducted across the United States at 12 sites for the evaluation of field scale hydrology of the ET cover system. Varied climates were represented in the ACAP sites, ranging from arid to humid, with annual precipitation from 119 to 1263 mm/year. Fifteen test sections of drainage lysimeters with dimensions of 10 m × 20 m were constructed for direct monitoring of the water balance for 3-6 years. The locations of the ACAP test sections are shown in Figure 2.45.

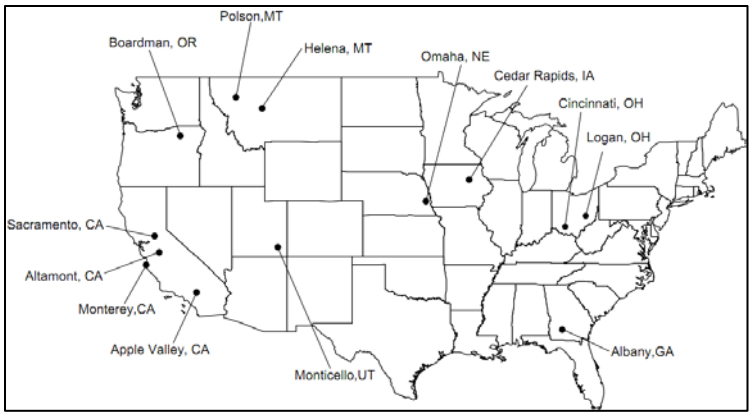

Figure 2.45 Location of ACAP sites

Plant communities in the ACAP sites consisted of grasses, grasses and shrubs, or grasses and trees to encourage evapotranspiration and evaluate the potential of different plant types. A wide range of root distributions was recorded from the ACAP field sites. The RLD functions from the ACAP sites are shown in Figure 2.46.

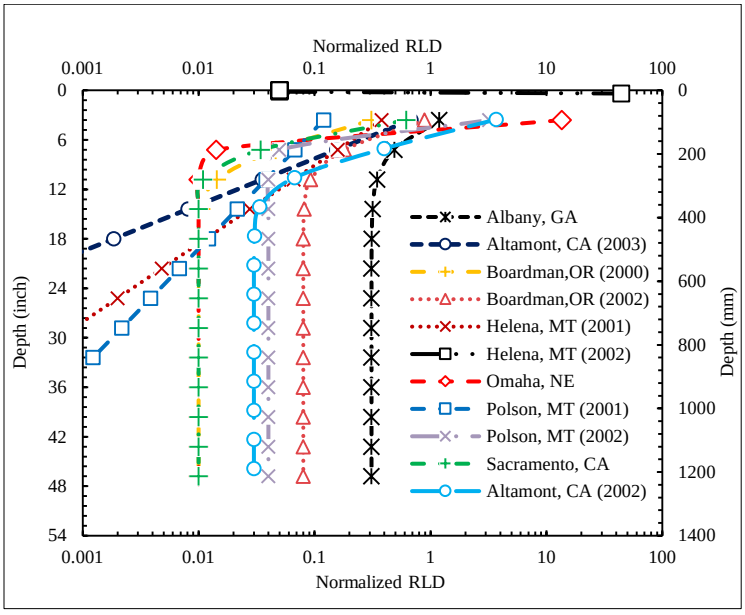

Figure 2.46 RLD function fitted with 4-8 years of measured data during peak growing season (Generated from Apiwantragoon et al. 2014)

From the field water balance analysis of the ACAP sites, percolation was found to range from 0 to 225 mm/year (Apiwantragoon et al. 2014) (Figure 2.47). This annual percolation was 0 to 34% of the annual precipitation. Apiwantragoon et al. (2014) reported that annual percolation from these sites was significantly affected by annual precipitation, preferential flow, and storage capacity of the cover soil. Evapotranspiration was found to be the largest component of the water balance analysis (more than 60% of annual precipitation). Evapotranspiration was mainly affected by water availability, energy demand as characterized by potential evapotranspiration, and type of root characteristics of the plant community. Surface runoff was the smallest component (less than 16%) in the ACAP sites. Its occurrence depended on the field saturated hydraulic conductivity and intensity of precipitation.

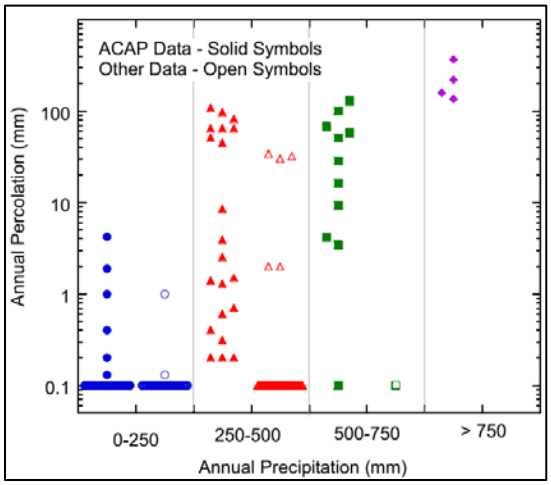

Figure 2.47 Annual percolation for ACAP covers (Apiwantragoon et al. 2014)

2.8.2.4 Evapotranspiration Cover in Northwestern Ohio

A study was conducted in northwestern Ohio to evaluate the annual percolation in a wetter region with average annual precipitation of 830 mm/year (Barnswell et al. 2011). Per the Ohio Environmental Protection Agency (OEPA 2003), the maximum allowable annual percolation rate is 320 mm/year. To address this issue, six drainage lysimeters

were constructed that were 1.52 m in diameter and 1.52 m deep. Ten types of plant species were assessed in this study. Immature and mature plant mixtures of warm-and-cool-season species were evaluated. The preliminary results from the study indicated that an ET cover may be effective in wetter regions, such as northwestern Ohio. The cover with a mature plant mixture produced lower rates of percolation than the cover of an immature plant mixture (Figure 2.48). The dredged sediment used in the cover soil provided sufficient water storage and supported efficient plant growth. However, the non-growing season was a concern because of the lack of an evapotranspiration mechanism to release water, causing the soil water to increase further due to further precipitation. Overall, the ET cover in northwestern Ohio was found effective with respect to percolation criteria set by OEPA (2003), and plant species played an important role in lowering the annual percolation.

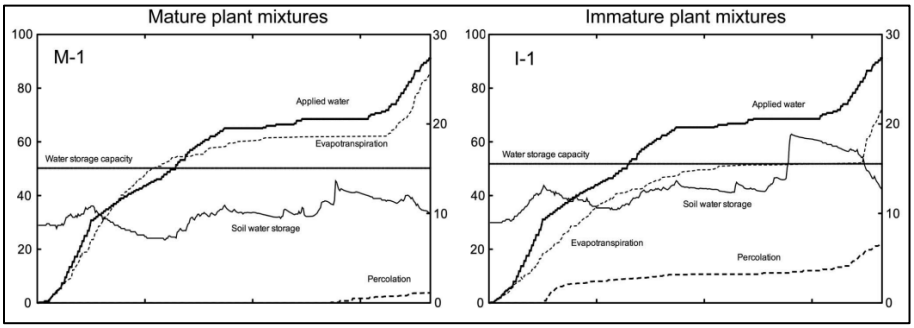

Figure 2.48 Water balance results of ET cover of mature and immature plant mixes (Barnswell et al. 2011)

2.8.2.5 Chihuahuan Desert Radioactive Waste Disposal Site

A performance evaluation of a capillary barrier ET cover in Sierra Blanca, Texas for the proposed radioactive waste disposal site in the Chihuahuan desert, representing the arid region, was conducted for 4 years (from 1997 to 2001) (Scanlon et al. 2005). Prototype pan lysimeters (Figure 2.49) were installed on a tract of land known as the Faskin Ranch. The constructed test plots had the most extensive and intensive monitoring

facilities, and according to Scanlon et al. (1997), the monitoring system was designed for 30 years' operation. The measured storage capacity of the cover soil was 100 mm. The apparent storage capacity of the cover soil was low because of low annual rainfall during the monitoring period.

Figure 2.49 Pan Lysimeters in Sierra Blanca Site

Several conclusions were drawn based on the results of four years of monitoring. The drainage estimated from the pan lysimeters ranged from 0.4-0.5 mm/year and corresponded to both precipitation and applied irrigation. From the water balance study, it was found that vegetation plays a critical role in controlling the water balance of the cover system since rapid changes in water storage were observed during the monitoring period. The sensitivity analysis, based on model evaluation, indicated that the water balance of the ET cover system is most sensitive to the presence and absence of vegetation. The change in hydraulic properties were also found to be sensitive to the water balance of the test section.

2.9 Selected Application of UNSAT-H Model

Many researchers have attempted to simulate the water balance, modeling the ET cover with the UNSAT-H model. Fayer et al. (1992) and Fayer and Gee (1997) predicted matric potential, soil water storage, and percolation based upon the UNSAT-H model, and

compared the predicted results with field data from eight instrumented lysimeters in Hanford, Washington. The eight lysimeters were basically capillary barriers, consisting of a 150-cm thick surface layer (silt loam) overlying 10 cm thick layers of sand and gravel. Moisture content and deep percolation were continuously monitored from these lysimeters. The predicted percolation by UNSAT-H was almost equal to the measured percolation during the study period. Fayer and Gee (1997) reported that the model was sensitive to the hydraulic conductivity function and the prediction was further improved when they applied the hysteresis.

Khire and Mijares (2000) reported, based on their UNSAT-H model, that the capillary break introduced by non-woven geotextiles in the capillary barrier ET cover significantly affects the water balance when equivalent hydraulic conductivity of the cover soil ranges between 10^{-3} to 10^{-4} cm/sec.

Benson, Khire and Bosscher (2000) conducted water balance simulation with the unsaturated flow model UNSAT-H at four locations in arid and semi-arid regions (Wenatchee, Washington; Denver, Colorado; Phoenix, Arizona; and Nevada, Reno). The climatic conditions of each of the locations was distinctly different. The main objective of the simulation was to assess the effects of layer thickness, unsaturated hydraulic properties, and the meteorological condition. There was good agreement between the model prediction and the field response. Based on their extensive simulation, the main outcomes of the study were as follows:

- Thicker surface layers generally yield smaller amounts of percolation because of higher storage capacity.
- Long term water accumulation and percolation may occur if deep-rooted vegetation is not present.

- Surface layers with lower saturated permeability generate more runoff and less infiltration, and, eventually, less percolation.

Khire et al. (1997) predicted the water balance for two sites: one in a humid region and the other in a semi-arid climatic zone. Both test sections had an on-site water balance monitoring system. Khire et al. (1997) reported that the predicted percolation, based on the UNSAT-H simulation, was 0.2 cm and 3 cm of the actual percolation in the semi-arid and humid sites, respectively. The predicted evapotranspiration was within 5 cm at the semi-arid site and 2 cm at the humid site.

Wilson et al. (1999) used the UNSAT-H, model along with other two water balance models, HYDRUS-2D and HELP, to predict the percolation at the Hanford site. UNSAT-H predicted the most accurate percolation, which was within 0.25 cm of the actual percolation. HYDRUS-2D's simulated percolation was 0.5 cm of the actual, while HELP overestimated the measured percolation by 6.7 cm.

Khire et al. (1999) compared the field performance of a capillary barrier ET cover with the UNSAT-H model. The simulation results showed that UNSAT-H underpredicted the surface runoff (within 10 cm); the soil water storage was predicted within 3 cm of the measured storage.

Scanlon et al. (2005) performed an evaluation of an ET cover in Sierra Blanca, Texas and Albuquerque, New Mexico, using water balance monitoring and short-term and long-term water balance simulation with UNSAT-H. The field water balance of the sites was reproduced by the water balance simulation. Based on the field water balance results, they reported that it is possible to simulate the effect of critical precipitation events with UNSAT-H. They also reported that the hydraulic conductivity impacts the simulated water balance. The sensitivity analysis indicated that the simulated water balance is most sensitive to the presence or absence of vegetation, especially at the Texas site.

2.10 Limitations in Previous ET Cover Studies

Previous studies indicated that an ET cover system could be a suitable final cover system where weather conditions are favorable. Most of the studies focused on the effects of different weather conditions and soil characteristics. Though plant root is one of the determinant components for optimum ET cover performance, the effects of the roots were not considered in many of the studies conducted for performance evaluation. Plant roots were characterized in a few studies; however, no studies have been done on in-depth characterization of plant roots throughout the monitoring period of water balance covers. Many studies assume plant root data based on literature in evaluating and predicting water balance performance. Very limited studies are evident where performance indicators (e.g. percolation, evapotranspiration) of ET covers were assessed in response to the plant root effect. This is because of the complexity of root studies and time constraints. Additionally, in most of the numerical simulations conducted for performance prediction and evaluation in comparison with field ET cover results, the input of vegetation was based on literature. Therefore, a study is required to establish a systematic way to characterize in-situ roots to effectively evaluate the performance of ET covers and to simulate the cover performance with an in-situ database.

Chapter 3

Materials and Methods

3.1 Introduction

An extensive laboratory experimental program was developed to investigate the geotechnical properties of the evapotranspiration cover (ET cover) soil. The test specimens for the laboratory tasks were prepared with disturbed soil. The rudimentary geotechnical properties of the soil specimens were determined using conventional geotechnical tests with disturbed soil specimens. Disturbed soil specimens were also used to characterize the unsaturated soil behavior (SWCC).

To evaluate the performance of different types of vegetation in the different lysimeters, a methodical investigation program was developed. Both laboratory exploration and field monitoring of vegetation were incorporated in the vegetation study. The laboratory assessment of vegetation was to determine the (a) root length, (b) root length density (RLD), and (c) root mass density (RMD). Field monitoring included (a) time-dependent root depth monitoring, using the minirhizotron technique; (b) root distribution; and (c) image analysis.

Electrical resistivity tests were conducted monthly on the ET cover. The frequency of the tests was increased during the summer, to quantify the potential depth of evapotranspiration, detect in-situ roots, and verify root depth measurement.

A complete test plan was developed to determine the in-situ hydraulic conductivity. The tests were conducted in all of the lysimeters, at two different depths. The test depths included (a) 6 inches from the surface and (b) 12 inches from the surface.

Field instrumentation results were obtained from the site at regular intervals to compute and evaluate the water balance components. Numerical modeling was conducted to simulate the ET cover system and future performance predictions. The obtained data

from the laboratory investigation and field monitoring was extensively used for the numerical simulation. The test methodologies considered in this current study are summarized in Figure 3.1.

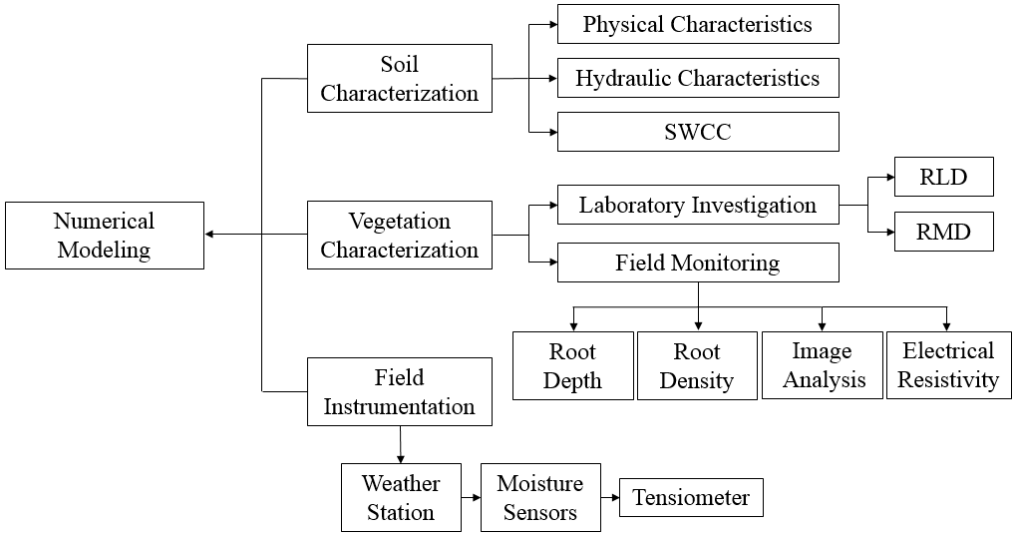

Figure 3.1 Flow diagram for test methodology

3.2 Selection of Study Area

A large-scale field test was conducted, whereby six different ET covers (lysimeters) were built side-by-side. The physical arrangement allowed for direct comparison of different vegetative cover designs under the same climatic conditions with similar soil types. The lysimeters were constructed at the City of Denton MSW Landfill, Denton, Texas. Texas has three climatic regions. Western Texas is an arid region, eastern Texas is a humid region, and the middle part of Texas is typically a semi-arid or semi-humid region (Figure 3.2a). The study area was in the semi-humid region.

The construction of the lysimeters started in June 17th, 2014, and after 4.5 months of extensive earth work and instrumentation, was completed in November 1st, 2014. The test lysimeters were located on top of an existing landfill cell (cell-1), with intermediate cover. Figure 3.2 (b, c) shows the location of the study area.

Figure 3.2 (a) Geographical location of City of Denton Landfill (b) Location of the study area (c) Footprint of Denton landfill

3.2.1 Description of the Study Area: ET Cover (Lysimeter)

Six large-scale lysimeters with dimensions of 40 ft. × 40 ft. × 4 ft. were constructed. Three of them were constructed on a flat surface with 2% slope, and three of them were constructed on a slope section, with 25% slope. The lysimeters were covered with 3 ft. of compacted clay, overlain by a 1 ft. vegetation surface layer. Figure 3.3 shows the plan and section of the lysimeters.

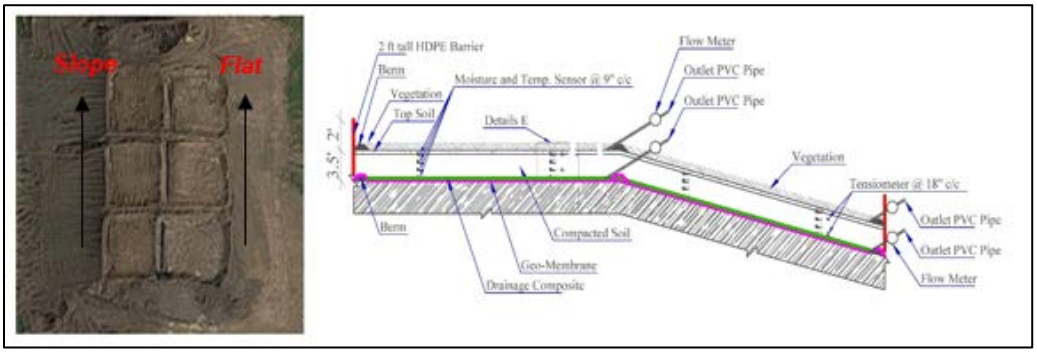

(a) (b)

Figure 3.3 (a) Plan view of the lysimeters (b) section schematic

A four ft. tall embankment was constructed of clayey soil so that the lysimeter pits could be excavated without being in contact with the underlying waste mass. After the construction of the embankment, the soil was excavated again in the lysimeter locations. The excavated areas were approximately 12 m x 12 m (40 ft. x 40 ft.) and nearly 0.9-m (3 ft.) deep. Subgrades of the excavated areas were compacted to provide an adequate surface for placement of the geomembrane. The geomembrane was placed on the subgrade and along the sidewalls of the excavations. To effectively collect the percolated water through the ET cover system, a percolation collection system (HDPE pipe) was installed along the lowest side of each lysimeter. Geocomposite drains were placed, overlaying the geomembrane at the bottom of the lysimeters, and geotextile was placed along the sidewalls. 0.9 m (3 ft.) of compacted clay was placed in each lysimeter in an approximately 0.2 m (12 inch) lift to obtain the required 95% maximum dry density (MDD). The soil was wetted and compacted with a sheep-footed compactor. Compaction of soil for each of the lysimeters was performed at dry of optimum (95% of the MDD at dry side) rather than wet of optimum as currently recommended by the EPA (1991). Dry-side compaction was performed to limit the potential for desiccation cracking in the compacted soil layer. It also made construction easier and provided for more initial soil water storage capacity due to the lower initial saturation. A nuclear density gauge (NDG) was used to measure the required compaction level in the lysimeter. Clay berms were installed on both sides of the exposed vertical geomembrane, along the lysimeter perimeters. The berms were installed to deter the runoff from flowing into or out of the lysimeters. The runoff collection systems (HDPE pipe) were constructed with a procedure similar to the percolation collection systems. Approximately one foot of topsoil was placed, overlaying the compacted clay layer and berms in each lysimeter. The topsoil was compacted relatively lower than the storage layer to allow effective vegetation growth.

3.2.2 Instrumentation of Different Lysimeters

An extensive instrumentation was implemented at the test section after the construction of the lysimeters. Water balance data was obtained for each of the lysimeters from December 2014. The continuous data monitoring included soil moisture and temperature, soil suction, surface runoff, percolation, precipitation, barometric pressure, relative humidity, wind speed and direction, and solar radiation. The details of the on-site instrumentation are provided in Table 3.1. All of the water balance data measurements were made with an automated monitoring system to obtain continuous performance results of all of the lysimeters. A complete description of the instrumentation, monitoring plan, and data acquisition system can be found in Brett DeVries (2016).

Table 3.1 Instrumentation Detail

Sl. No	Sensors and Instrumentation	Quantity	Purpose
1	Moisture and Temperature Sensors	48	Moisture Content and Temperature
2	Tensiometers	12	Soil Suction
3	Dosing Siphon	6	Runoff Quantification
4	Pressure Transducer	6	Time Dependent Runoff Quantification
5	Rain Gauge	6	Quantification of Percolation
6	Weather Station	1	Rainfall, Barometric Pressure, Relative Humidity, Wind Speed and Direction and Solar Radiation

Field measurements of soil moisture and soil suction are necessary for monitoring the moisture fluxes through the cover (Feng 1999). Lee (1999) stated that variations of soil moisture are the results of changes in the soil matric suction caused by infiltration and evaporation. Soil moisture sensors, temperature sensors, and tensiometers were installed to maintain continuous soil moisture, temperature, and suction status at various depths of

the ET cover system. Soil water storage and in-situ SWCC were also measured by the instrumentation. A total of 48 moisture and temperature sensors and 12 tensiometers were installed in the ET cover. A detail description of the installation of the sensors is given in Section 3.5.

Surface runoff was collected from each of the lysimeters through the runoff collection pipe (HDPE) that was connected to the runoff collection tank located at the bottom of the slope-section lysimeters. The runoff water was routed through a dosing siphon and pressure transducers to the collection tank for the automated acquisition of time-dependent quantity of runoff. For each of the lysimeters, there was one runoff collection tank, instrumented with a dosing siphon and pressure transducers.

Percolation (infiltrated water from the bottom of the cover soil) was collected through the percolation collection pipe (HDPE), which accumulated in the percolation collection tank. The percolated water was routed through the instrumentation, which consisted of a tipping-bucket rain gauge to quantify the volume of percolation. Each lysimeter had a separate percolation collection tank. Figure 3.4 shows the on-site runoff and percolation collection tanks.

Figure 3.4 Surface runoff and percolation collection tanks in the study area (Modified from Brett Devries, 2016)

A complete weather station was installed at the site to effectively monitor the meteorological data. Precipitation, air temperature, relative humidity, wind speed and direction, and solar radiation are continually monitored by the weather station, which has an automatic data recording system. The on-site weather station is shown in Figure 3.5.

Figure 3.5 On-site weather station

3.2.3 Vegetation of the ET Cover System

Plant communities within the study area are subjugated by the native grasses, such as a mix of native trails, perennial wildflower mix, and caliche; mix of upland switchgrass, perennial wildflower mix, and caliche; and Bermuda grass and hulled common Bermuda grass (grade 90/80). The six lysimeters were intentionally planted with these three different types of grasses on both the flat and sloped lysimeters. Lysimeters 1 and 4 were topped with mix of native trails, perennial wildflower mix, and caliche. Lysimeters 2 and 5 were topped with mix of upland switchgrass, perennial wildflower mix, and caliche; and lysimeters 3 and 6 were covered with Bermuda grass (Table 3.2). Lysimeters 3 & 6, used for Bermuda grass and hulled common Bermuda grass, were 40 ft. × 20 ft. The details are shown in Figure 3.6.

Table 3.2 Vegetation Detail

Lysimeters	Vegetation Details	Designation ID	Extent of Vegetation
3 and 6	Common Bermuda Grass and Hulled Common Bermuda Grass (Grade 90/80)	BG/HBG	50% in Lysimeters 3 and 6
2 and 5	Mix of Upland Switchgrass, Perennial Wildflower Mix, and Caliche	SG	100% in Lysimeters 2 and 5
1 and 4	Mix of Native Trail, Perennial Wildflower Mix, and Caliche	NT	100% in Lysimeters 1 and 4

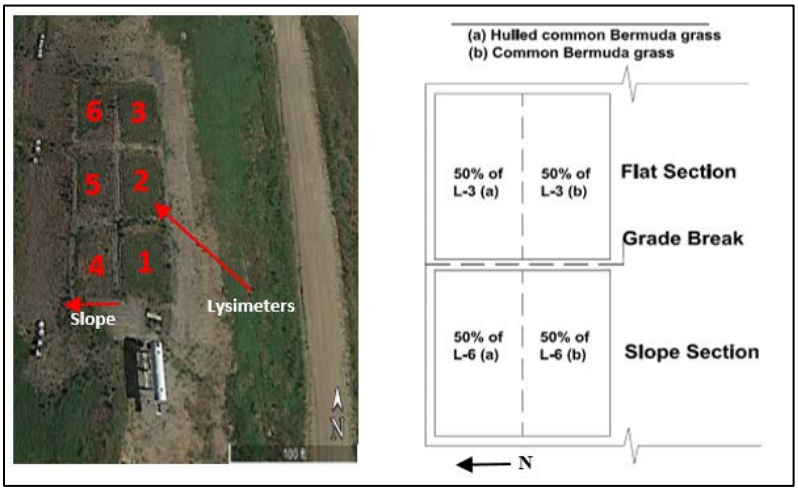

(a) (b)

Figure 3.6 (a) Vegetative lysimeters (b) vegetation details of lysimeter 3 & 6

3.3 Collection of Soil Samples & Determination of Geotechnical Properties

The soil samples were collected from all six lysimeters, at different depths, during construction of the ET cover. All of the lysimeters were constructed with three feet of compacted soil layer, overlain by one foot of vegetation layer. The three feet of compacted soil layer were built in three lifts, with a placement of one foot of soil dirt followed by compaction with a sheep foot roller. From each of the soil lifts, three buckets (20 litter/bucket) of disturbed soil samples were collected (Figure 3.7) and shipped to the

laboratory for the geotechnical investigation. Disturbed samples were also utilized for the determination of the SWCC of the soil. Undisturbed soil specimens, along with the vegetation, were collected with a 75-mm sample corer one year after the construction of the lysimeters for the determination of plant root distribution and bulk density.

Figure 3.7 Soil sample collection (disturbed soil sample)

Eighteen buckets, each with a 20-liter capacity, were utilized for the investigation of geotechnical properties of the ET cover soil. For ease of representation, soil samples were designated in accordance with the lysimeter number and depth, as presented in Table 3.3.

Table 3.3 Designation of soil samples

Lysimeter	Sample ID	Designation	Lysimeter	Sample ID	Designation
Lysimeter 1	Top Soil	L1-Top	Lysimeter 4	Top Soil	L4-Top
	1st Lift	L1-1		1st Lift	L4-1
	2nd Lift	L1-2		2nd Lift	L4-2
	3rd Lift	L1-3		3rd Lift	L4-3
Lysimeter 2	Top Soil	L2-Top	Lysimeter 5	Top Soil	L5-Top
	1st Lift	L2-1		1st Lift	L5-1
	2nd Lift	L2-2		2nd Lift	L5-2
	3rd Lift	L2-3		3rd Lift	L5-3
Lysimeter 3	Top Soil	L3-Top	Lysimeter 6	Top Soil	L6-Top
	1st Lift	L3-1		1st Lift	L6-1
	2nd Lift	L3-2		2nd Lift	L6-2
	3rd Lift	L3-3		3rd Lift	L6-3

An experimental program was developed to determine the geotechnical properties of the soil specimens. The laboratory investigation included a) physical properties, b) hydraulic properties, and c) a soil suction study. Geotechnical investigations performed on the soil specimens are summarized in Table 3.4

Table 3.4 Experimental test program on the soil samples

Name of Test	Test Method
Grain size distribution	ASTM D 422-63
Specific gravity	ASTM D 854-00
Atterberg limits	ASTM D 4318
Standard Proctor Compaction	ASTM D 698
Hydraulic Conductivity	ASTM D 5084
Soil Water Characteristic Curve	ASTM D 6836-02

3.3.1 Grain Size Distribution

Particle size distribution of the samples was determined per the ASTM D422-63 standard test method. The soil samples were oven dried at 100-110^{o} C temperature for 24 hours. The soil aggregate of the oven-dried samples was broken by a mortar-and-rubber-covered pestle, and an approximate 500 gm sample was measured for the sieve analysis. The soil sample was subjected to wet sieving, using a #200 sieve with flowing water, until the leached water was completely clean. The retained and leached samples were dried in the oven at 100-110^{o} C temperature for 24 hours or until it reached the constant weight. After that, the retained soils were sieved, using #4, #10, #30, #40, #60, #100, and #200 US standard sieves. The mass of retained samples in each sieve was determined after completion of the test. The soil passed through the #200 sieve during wash sieving was utilized in the hydrometer test.

3.3.2 Atterberg Limits

Atterberg limit tests were performed on the soil specimens per the ASTM D4318 standard method. Samples passing through #40 sieve were considered in the test. After

addition of water, the soil sample was chopped, stirred, and kneaded repeatedly until a uniform soil paste was prepared. A portion of the soil was placed in the Cassagrande liquid limit device, and a groove was cut at the center of the cup. The cup of the device was lifted and dropped at a rate of 2 drops/second until the groove was around 10 mm. The test was repeated for four times, and the number of blows was plotted against the moisture content. The moisture content corresponding to 25 blows was considered as the liquid limit of the specimen.

For the determination of plastic limit, water was added to the soil and kneaded repeatedly. The soil masses were rolled in the glass plate until threads of about 3 mm were formed. When the threads were broken at 3 mm diameter, they were put in the moisture cans. Samples were dried in the oven at 100-110^{o} C temperature for 24 hours or until constant weight was gained. The moisture content at this condition was considered as plastic limit of the specimen.

3.3.3 Specific Gravity

Specific gravity of the collected soil samples was measured according to ASTM D 854-00 standard test method. Approximately 50 gm of soil mass was weighted after passing through a #10 sieve. After the weight measurement of the empty pycnometer and the pycnometer with the soil specimen, distilled water was added to the specimen. A partial vacuum was also applied to the soil for 16 to 24 hours to remove the air bubbles. Then water was added to the pycnometer up to the desired level, and the weight was measured. Distilled water was then added to the clean pycnometer, and the weight was re-measured.

3.3.4 Moisture Density Relation

The Standard Proctor compaction test was conducted on the collected soil samples, following the ASTM 698 standard method. Soil samples collected from different lysimeters were oven dried for 24 hours. After drying, the samples were crushed and

pulverized. The pulverized samples were then used for the proctor test to determine the optimum moisture content (OMC) and maximum dry density (MDD), and to evaluate the dry side and wet side of the compaction curve.

3.3.5 Hydraulic Conductivity

Saturated hydraulic conductivity was determined, using the falling head method on six soil samples and following the procedure in ASTM D 5084. Specimens were compacted to 95% of MDD at dry side of the compaction curve to simulate the field condition. A relationship was also developed between the coefficient of permeability and the compaction water content with one soil sample. The compaction water contents were selected so that they covered a wide range of moisture contents from the dry side to the wet side of the compaction curve. This test was conducted in a compaction permeameter.

3.4 Soil Suction Studies

Hydrologic properties of soil in the ET cover system, or in the vadose zone in general, play the most significant role in the quantification of water movement. The most useful properties are saturated hydraulic conductivity, hydraulic conductivity and moisture content function, and suction-moisture relationship or the soil water characteristic curve (SWCC).

3.4.1 Suction Measurement Technique

There are different methods to determine the SWCC for a soil specimen. The selection method depends on the desired suction level. The most common methods are the filter paper method, pressure plate extractor, hanging column, vapor pressure equilibrium method, dew point potentiometer (WP4C), psychrometers, and conductivity sensors. In the present study, two methods have been extensively used for the determination of the SWCC of the ET cover soil. They are presented in the following sections.

3.4.1.1 Pressure Cell Apparatus: The Fredlund SWCC Device

The Fredlund SWCC device is basically a pressure plate device that consists of three-inch diameter exchangeable ceramic disks (high-air-entry disks). The device contains a pressure cell assemblage and a pressure panel. The schematic of the Fredlund SWCC device is shown in Figure 3.8.

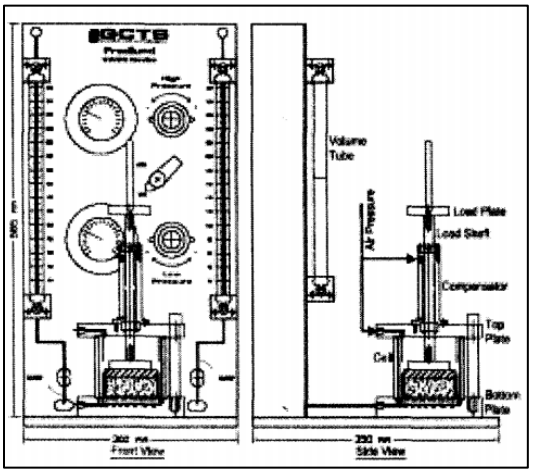

Figure 3.8 Schematic of the Fredlund SWCC device (D.G. Fredlund 2005)

Several features that are built into the Fredlund SWCC device have made the experiment method simple, precise, and consistent. This apparatus is capable of determining moisture content without being dismantled during the test. Two volume indicator tubes on the pressure panel can measure the absorbed or released water from the specimen. The soil specimen that is placed on a saturated ceramic disk is surrounded by a recess filled with water below the bottom plate of the apparatus. The connection between the recess and the two volume indicator tubes on the pressure panel is made with plastic tubing. The graduated volume indicator tubes take the readings of water released or absorbed during the test.

In this research, soil samples collected from each of the lysimeters were compacted at 95% of MDD moisture content, using the standard proctor method (ASTM

D-698) to bear a resemblance to the field relative compaction. Figure 3.9 presents the pressure cell apparatus (Fredlund SWCC device) utilized in the present study.

Figure 3.9 Pressure cell apparatus (Fredlund SWCC Device)

3.4.1.2 WP4C Dew Point Potentiometer

The working principle of this equipment is based on the measurement of the relative humidity of the air inside a small sealed chamber. At equilibrium, the relative humidity of the air in the chamber is the same as the relative humidity of the soil. The relative humidity of the soil is in direct relation to the soil water potential. A picture of the equipment used in this research is presented in Figure 3.10.

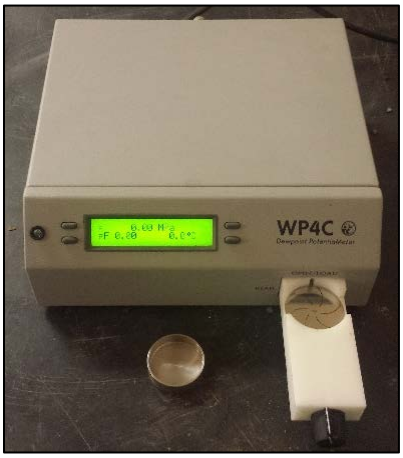

Figure 3.10 WP4C dew point potentiometer

The soil sample was cut into thin sections and placed in the container. The container was cleaned on the top to make sure that no soil particles came in contact with the relative humidity sensor. After the steel cup was positioned in the device, the sensor locked the top of the cup to measure the relative humidity of the air present at the top of the soil specimen. After equilibrium was attained, the total matric suction of the soil specimen was displayed on the device. This device has been used in this study only to determine the total suction for soil specimens at high suction ranges.

3.4.2 Soil Water Characteristic Curve (SWCC)

The soil water characteristic curve (SWCC) is one of the fundamental properties of soil. It is the mathematical relationship between the matric suction of a soil and either the gravimetric moisture content (GMC) and volumetric moisture content (VMC) or the degree or saturation (S) (Fredlund and Rahardjo 1993). VMC is most commonly used to describe the SWCC. It represents the water storage capacity of a given material and allows for the determination of changes in the matric suction with respect to changes in water content or degree of saturation. Figure 3.11 presents a typical SWCC for both drying (desorption) and wetting (sorption) phases.

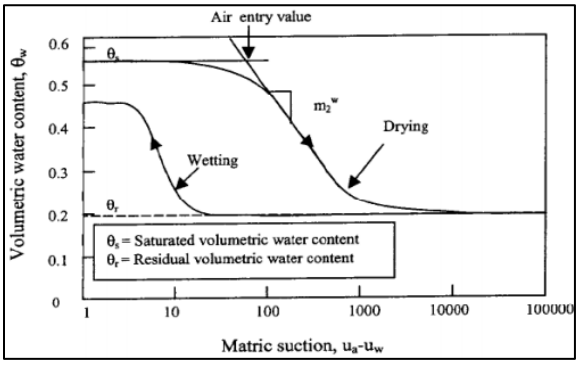

Figure 3.11 Typical soil water charateristic curve (Aung and Rahardjo 2001)

The drying and wetting methods yield a continuous curve, but the curves will not generally be identical. The moisture content at a given suction head is greater in drying

(desorption) than in wetting (sorption). The state of soil water upon the direction of process is referred to as the hysteresis effect, and it makes the suction-moisture relationship rather complex. In practice, the desorption method is most commonly used, and it has been used in this study.

3.4.2.1 Van Genuchten Model

A variety of equations can be used to describe the SWCCs parametrically (Leong and Rahardjo 1997). The most common and widely-used function to define the SWCC is the sigmoidal Van Genuchten (VG) equation (Van Genuchten 1980):

$$\frac{\theta - \theta_r}{\theta_s - \theta_r} = \left\{\frac{1}{1 + (\alpha\psi)^n}\right\}^m$$

Where, ψ = suction, Θ = volumetric water content, Θ_s = volumetric water content at saturation, Θ_r = residual volumetric water content. α, n and m are fitting parameters. m is defined as $m = 1 - n^{-1}$. The VG fitting parameters (α, n and m) were directly obtained from the RETC code, using the experimental data.

3.4.2.2. RETC Code (Retention Curve)

RETC (Van Genuchten et al. 1991) used a nonlinear least-square optimization process to determine the unknown model parameters from an observed retention data obtained from the experiment. The unsaturated soil hydraulic properties were obtained from laboratory testing of soils, using pressure cell apparatus and WP4C. The moisture characteristic curve data was then used as input for the RETC code, to analyze van Genuchten parameters (α, n and m). The Maulem conductivity function was assumed to describe the unsaturated hydraulic conductivity of the soils. The van Genuchten m parameter for this function was assumed to be 1-1/n. The van Genuchten curve fitting parameters obtained from the RETC code were then directly utilized to derive the mathematical model to describe the soil water characteristic curve.

3.5 Sensors Installation

To closely monitor the soil moisture and suction status in the field, 48 moisture and temperature sensors (Decagon 5TM soil moisture and temperature sensors, Decagon Devices, Pullman, WA) and 12 tensiometers (Decagon Devices, MPS-2, Pullman, WA) (Figure 3.12) were installed in the ET cover. Eight moisture and temperature sensors were installed in each lysimeter. Each lysimeter was divided into two nests: east nest and west nest, with four sensors in each nest. In the east nest, a hole was bored with a motorized augur to a depth of almost 39 inches. Then sensors were put in the hole at 9-inch intervals. The section of the installed moisture and temperature sensors is shown in Figure 3.13. The last sensor was positioned at the bottom of the vegetative layer, 12 inches below the surface, or at the top of the storage layer. A similar procedure was followed in the west nest. The wires of the sensors were connected to a data logger located just outside of the lysimeter.

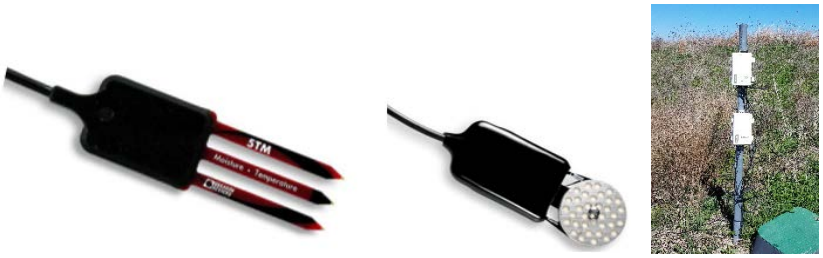

(a) (b) (c)

Figure 3.12 (a) Moisture and temperature sensors (b) tensiometers (c) data logger

Twelve tensiometers were installed in all of the lysimeters, two in each lysimeter. Tensiometers were installed in the east nest of all of the test sections. Similar approaches were made to install the tensiometers in all of the lysimeters. One tensiometer was put at a 12-inch depth, and the other one was at a 30-inch depth from the surface. The wires of the tensiometers were connected to the corresponding data loggers.

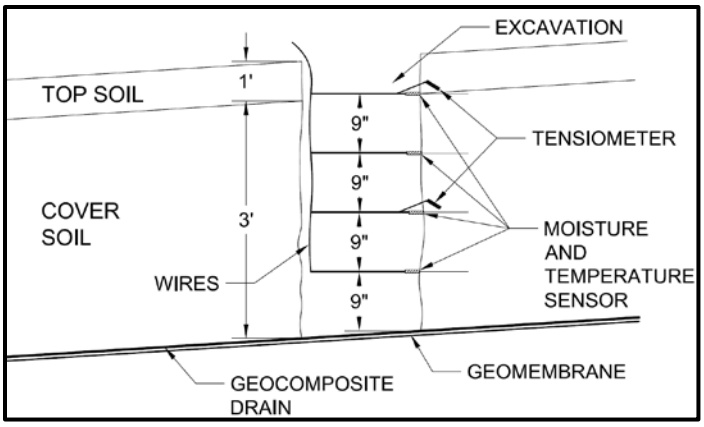

Figure 3.13 Section of moisture and temperature sensors (Devries, 2016)

3.6 Vegetation Study

Performance monitoring was conducted of different types of vegetation for all six lysimeters, both in-situ and in the laboratory. The detailed procedure for the vegetation study is given in the following section.

3.6.1 Field Monitoring of ET Cover Vegetation

The objective of field monitoring of the vegetation was to evaluate the in-situ performance of different kinds of vegetation seeded in different lysimeters. The field monitoring of vegetation included determination of time-dependent root depths of different vegetation, quantification of the distribution of root and root dynamics. Electrical resistivity was also conducted in the lysimeters, in an effort to verify the root depth and to determine the potential depth of evapotranspiration.

3.6.1.1 Installation of Acrylic Tube: Minirhizotrons

A transparent, hollow, cylindrical tube (Figure 3.14) was first introduced by Bates (1937) to observe in-situ plant roots behind the tube. This is a simple technique for root study. A hole is bored into the soil, then a tight-fitting acrylic plastic tube is forced into the hole to observe the root intrusion behind the glass interface. Later, Waddington (1971) used a similar method in a greenhouse experiment, but used a fiber optic rather than a

glass wall for observing the roots. Inspired by this idea, Bohm (1974) conducted a large-scale field study using this technique.

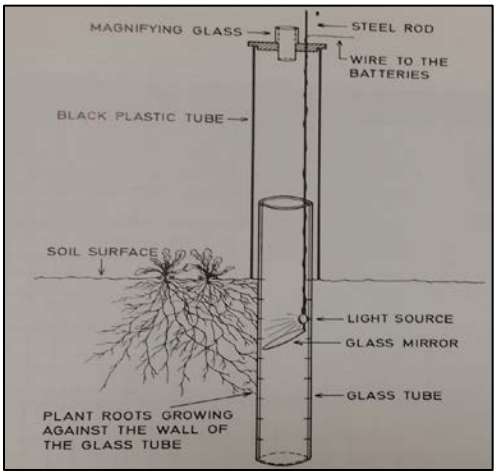

Figure 3.14 Block diagram with the principle of observing root through glass tube (Bohm, 1974)

The glass wall method allows for a continuous study of the roots for one or more plants during its entire life span. Certainly, the roots are not growing in completely natural surroundings when they hit the glass tube and grow along it, but this does not seem to be as serious as might be thought. A glass panel can be like a large, smooth, flint stone or a grain of sand (Rogers, 1939).

The acrylic hollow tube method is cheaper for root observation and root depth determination than the glass wall method at vertical trenches because it causes less soil damage in the field. The installation of enough tubes also satisfies statistical needs (Bohm 1977). It is obvious from various field observations that roots concentrate behind the wall tube. In accordance with the detailed study made by Kopke (1979), the root concentration in a 2-mm soil layer directly behind the tubes can be up to threefold that of the rooting density in the surrounding bulk soil. For solving research problems, this method is satisfactory, and researchers have begun to use this method effectively. Bohm (1974)

termed the tubes, which serve for root observations in natural soil profiles, minirhizotrons. The major benefits of the minirhizotron is that it maintains consistency in the measurement of the roots, as it allows same-point measurement. It is non-destructive method for determining the root depth and distribution; the only destructive activity is during the installation of the minirhizotron. This was the first-ever application of this method (minirhizotron) for a root system study for the evaluation of the performance of ET cover.

A 4-foot long, hollow, acrylic plastic tube, with an inside diameter of 6 inches was used for this research (Figure 3.15). The wall thickness of the pipe, which is an important factor in this study, was 1/8 inch, which is the optimum thickness for clear visibility root observation and is strong enough to resist buckling of the tube.

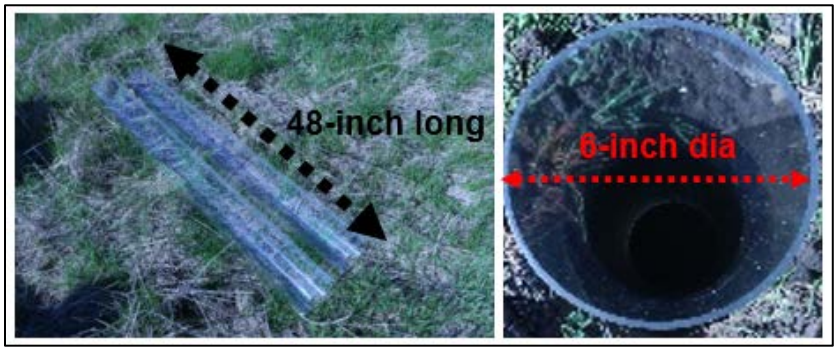

Figure 3.15 Acrylic plastic tube (4' long, 6" inside Dia, 1/8" wall thickness)

The lysimeters were constructed with a 3-ft. compacted soil layer, overlain by a 1-ft. vegetated layer. Geomembranes and a geocomposite drain were placed at the bottom of each of the lysimeters. Moisture and temperature sensors and tensiometers were installed in the east and west nest of each of the lysimeters. The minirhizotrons were installed, considering the placement of the geomembrane and geocomposite drain, and the location of the installed sensors. They were driven 30 inches into the cover soil, with 18 inches kept above the soil surface. Figure 3.16 shows the schematic of the minirhizotrons installed in the field.

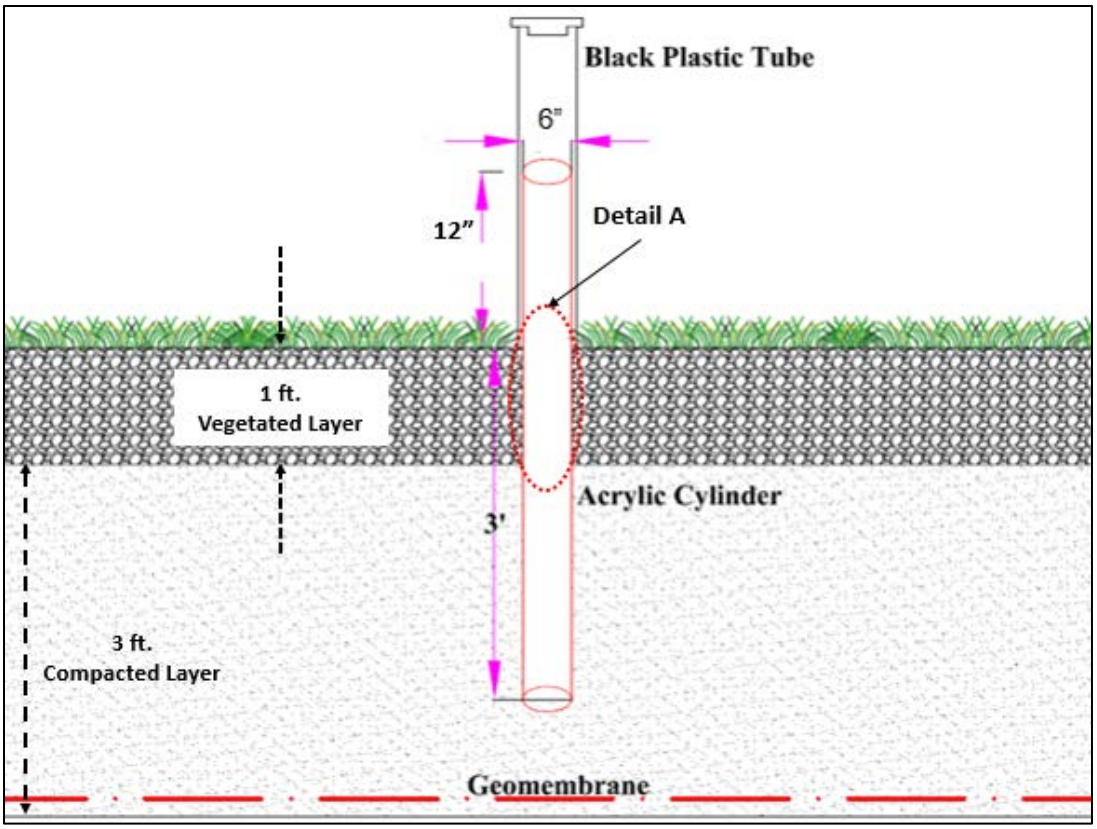

(a)

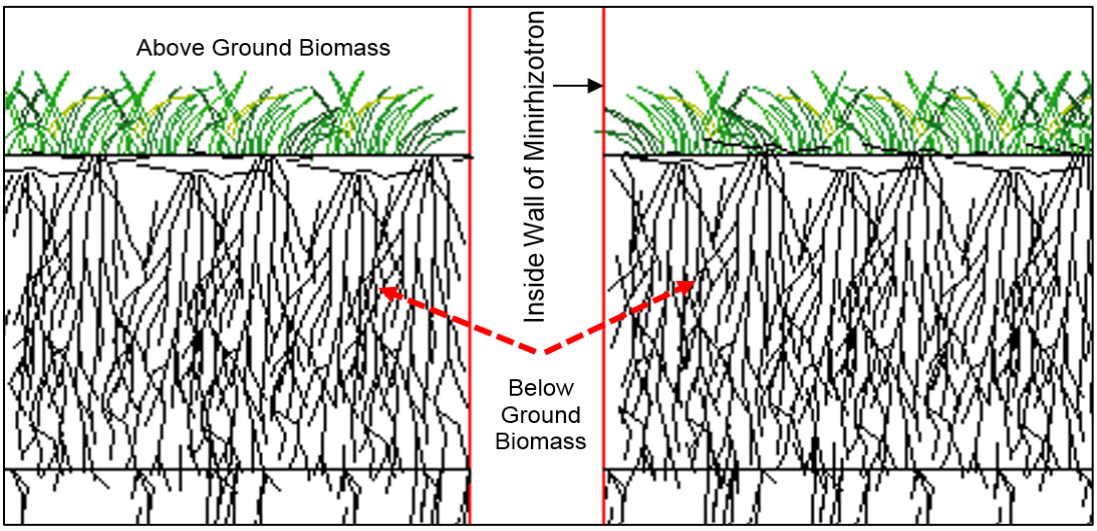

(b-Detail A)

Figure 3.16 (a) Schematic of the installed minirhizotron (b) Section of minirhizotron

The minirhizotrons were installed on February 27, 2016. Eight acrylic Plexiglas (minirhizotrons) were installed in the ET cover. For ease of identification, the minirhizotrons were designated in accordance with the lysimeter number, as presented in Table 3.5. One minirhizotron was installed in each lysimeter, except for numbers 3 and 6. Lysimeters 3 and 6 were seeded with Bermuda grass and Hulled Common Bermuda grass (Grade 80/90); therefore, two minirhizotrons were installed in each of these lysimeters. Figure 3.17 shows the locations of the minirhizotrons installed in the ET cover.

Table 3.5 Designation of Minirhizotron

Lysimeter	Plant ID	Minirhizotron ID
1	NT	M-1
2	SG	M-2
3	BG	M-3B
	HBG	M-3HB
4	NT	M-4
5	SG	M-5
6	BG	M-6B
	HBG	M-6HB

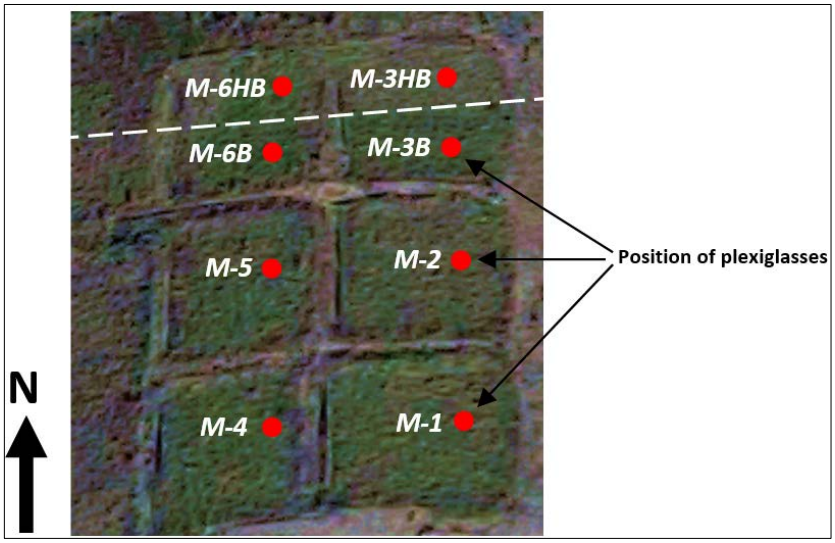

Figure 3.17 Position of minirhizotrons in lysimeters

A motorized spiral augur was used to bore holes of approximately 6-inch diameter vertically to a depth of 2.5 foot (30 inches). To limit the smear, a steel brush was pushed up and down several times after the holes were bored. The minirhizotron (48 inches) was then inserted into the holes, all the way to the bottom of the holes. The holes were bored in such a way that the diameters of the holes were slightly higher than the diameters of the minirhizotrons. The parts of the minirhizotrons extending above the soil surface (18 inches) were capped to prevent the entry of light and water. To obtain good contact between the outside wall and the soil, in-situ bored soil was used to fill the gap between the hole and the outside wall of the minirhizotron. During the installation of the minirhizotron, the existing root depth was measured and marked in the minirhizotron. Almost two weeks after the natural consolidation of the soil, roots were visible inside the minirhizotron. A step-by-step minirhizotron installation procedure is shown in Figure 3.18.

Figure 3.18 (a) Boring with spiral augur (b) measuring depth of hole (c) inserting plexiglass (d) top 18-inch of plexiglass (e) gap filling with soil between hole and outer wall of plexiglass and compaction (f) in-place plexiglass (g) temporary wrappedup plexiglass

3.6.1.1.1 Roots and Root Zone Observation

The roots were observed throughout the monitoring period. Initially, root observation (e.g. root depth inside the lysimeters, density of roots) was accomplished by collecting soil samples, along with root samples, at the different locations of the lysimeters, and then investigating them in the laboratory. Collecting root samples and quantification were time consuming and laborious. After the installation of the minirhizotrons, root observation could be made at the same point, and photographing the roots and subsequent image analysis of the root system and quantification made the process less time consuming and more accurate. However, some root samples were collected even after the installation of the minirhizotrons to compare the effectiveness of the image-based root density measurement. Few days (1-2 weeks) after the installation of the minirhizotrons, roots were not visible due to the disturbance around the minirhizotrons (Figure 3.19 a). However, almost two weeks after the natural consolidation of the soil, roots started to concentrate behind the minirhizotron wall (Figure 3.19 b). Root depth measurements into the cover were made using a LED telescope investigation mirror and scale that were inserted inside the minirhizotrons (Figure 3.20). The image acquisition and analysis processes are described in the following section.

(a) (b)

Figure 3.19 (a) Soil disturbance around the minirhizotron (b) root concentration behind minirhizotron wall

Figure 3.20 Root observation using telescopi inspection mirror

3.6.1.1.2 Image Acquisition System

Advanced technology has made the process of image collection, storage, and analysis much easier. Root observation, photographing the minirhizotron surface, and subsequent image analysis to quantify root dynamics have progressed over time (Taylor et al. 1990), making the whole process much easier. Bates (1937) used a mirror and electric light bulb, Waddington (1971) used fiber optic scope, Sanders and Brown (1978) used a 35-mm camera, and Upchurch and Ritchie (1984) operated a color video camera. In recent years, researchers have used digital color video images on computer and digital scanners to quantify root dynamics, depending on the required outputs from the images. In the current study, a high-resolution minirhizotron camera (mini camera) (Figure 3.21) was utilized to view the roots, capture and store the digital images, and then transfer them to the computer. The advantage of the mini camera is that it can be rotated 360^{o} in the minirhizotron tube, at any depth. However, because of the curved surface of the minirhizotron, obtaining uniform lighting was difficult. Nonetheless, the lighting effect in the images were removed through several image enhancement procedures. The step-by-step image acquisition system is shown in Figure 3.22.

Figure 3.21 Minirhizotron camera

Image calibration is an important task to perform before analysis and quantification can occur. Images were captured from inside the minirhizotron, with the camera set at a fixed depth. The focal distance (distance of the camera and photographing area inside the tube) of the camera was set at 5 inches (Figure 3.23), and the 4.5 × 4.5 in^2 root area inside the tube was photographed. Therefore, four images were captured at a fixed depth at every 90^o angle, covering the 360^o viewing area.

(a) (b)

(c)

(d)

Figure 3.22 In -situ image acquisition from minirhizotron: (a) setting up camera (b) plug-in with computer (c) fixing depth (d) image acquisition

The height of the captured images was cropped to 3 inches in order to compare the image analysis-based root measurements and traditional root measurements. The timing and frequency of image collection from the minirhizotrons depended on the interest of analysis. Most of the time during monitoring, images were collected monthly from all the minirhizotrons; however, images were collected twice or thrice during some of the months to provide additional data for analysis. Frequency of image collection further increased when images with clearly visible roots were not obtained. Attempts were made to collect images at every site visit between 10 am and 2 pm to maintain consistency. However, this timing was not always possible because of site conditions and other interruptions (e.g. rainfall and site accessibility).

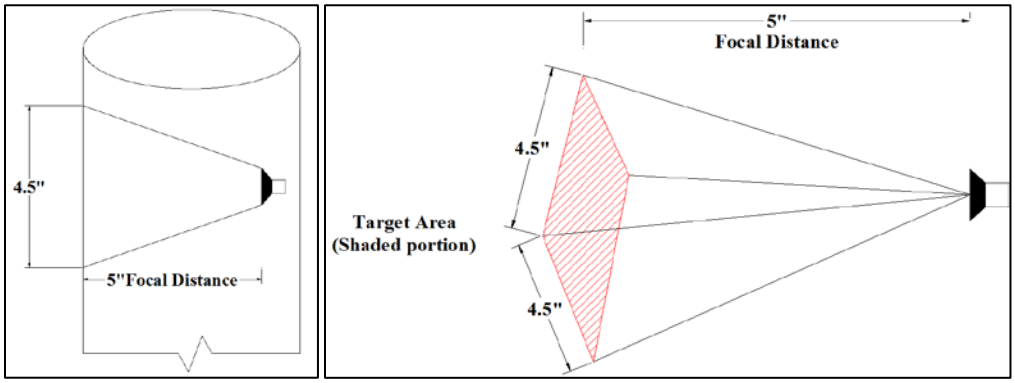

Figure 3.23 Focal distance of camera

3.6.1.1.3 Image analysis using ImageJ software

There are many software available for minirhizotron-based image analysis. In this study, the ImageJ program was selected for root image analysis and quantification. Additionally, SmartRoot software was also used to compare the results obtained from ImageJ. ImageJ is a public domain Java image-processing software which can measure distance, area of objects, angle between objects, etc. It also provides intensity distribution, statistical data of pixel value, and histograms. The main window of ImageJ software is

presented in Figure 3.24. The overall flow diagram of minirhizotron-based image analysis is presented in Figure 3.25.

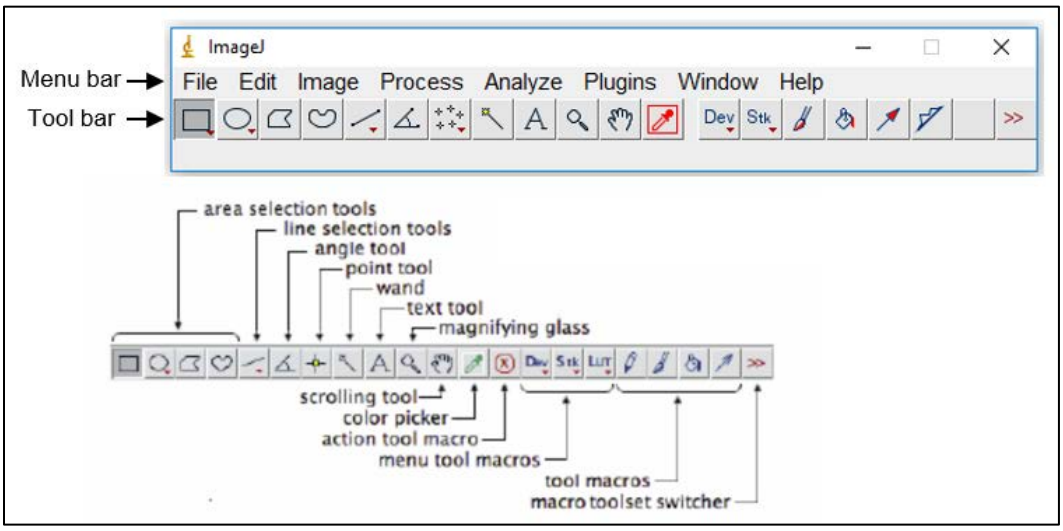

Figure 3.24 Window of main menu of ImageJ program

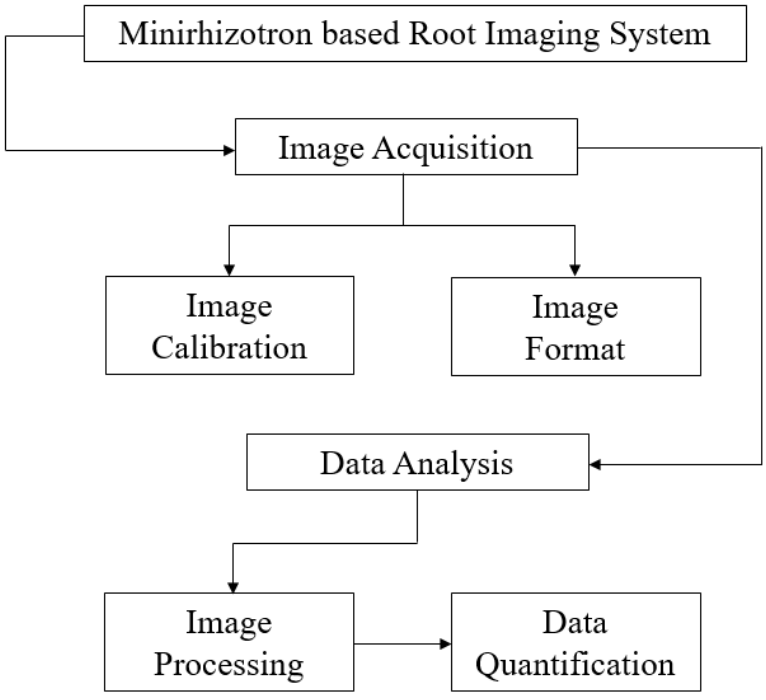

Figure 3.25 Flow diagram for minirhizotron-based root imaging

3.6.1.2 Resistivity Imaging (RI)

The objective of performing resistivity imaging in the lysimeters was to verify the measurements of the root depth through the minirhizotrons, determine the potential depth of evapotranspiration of the cover soil for different types of vegetation, and detect in-situ below-ground root biomass for different types of vegetation. Since, to determine the important vegetation parameters (RLD, RMD), destructive samples were collected, the RI technique was thought to be a promising, non-destructive way of quantifying the root biomass in the ET cover system. The results obtained through the RI method yielded a clear indication of a significant relationship between resistivity value and root biomass.

Electrical resistivity measurements were performed on the top-section lysimeters (1, 2 and 3). Similar vegetation types and patterns were present in the slope-section lysimeters (4, 5 and 6). Therefore, only top-section lysimeters were selected for the RI method. A SuperSting R8/IP resistivity meter was utilized during the field investigation (Figure 3.26).

(a) (b) (c)

Figure 3.26 (a) Electrical resistivity equipment (R8/IP resistivity meter) (b) field setup with resistivity meter (c) execution of RI test

The multi-channel resistivity equipment can perform an RI test with a maximum of 56 electrodes. However, 28 electrodes were utilized to perform resistivity imaging for this study, based on the area of the test sections. The cover soil depth for each lysimeter was 4 ft., and the geomembrane was placed at the bottom of the lysimeter. Therefore, the

spacing between the electrodes was fixed at 0.5 ft. intervals, considering the cover soil depth and the geomembrane position. A 14 ft. transect was fixed in each lysimeter, and RI was performed along that transect every time. The measured resistivity data sets were analyzed using Earthimager-2D software. Figure 3.27 presents the RI line in the lysimeters.

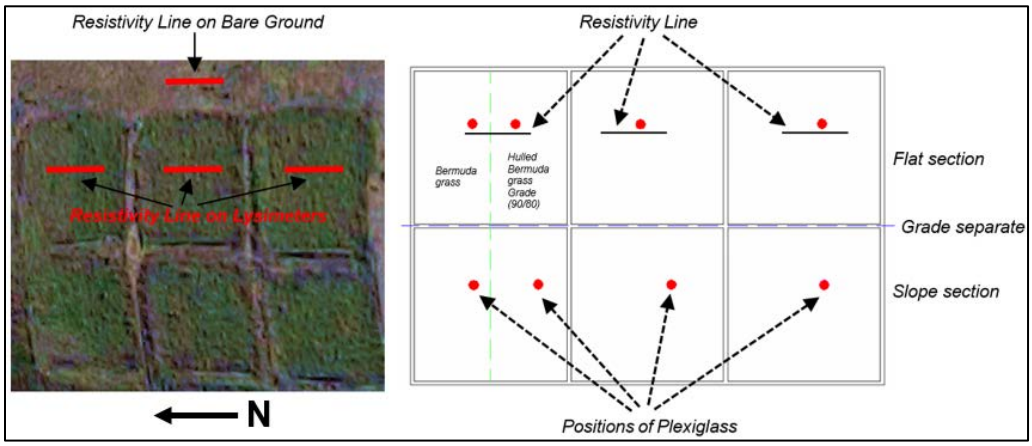

Figure 3.27 Layout of electrical resistivity line

Additional RI measurements were conducted in the bare soil (no vegetation), just outside the lysimeters (Figure 3.27). This was done to compare the RI profile with and without vegetation and to distinguish the electrical resistivity (ρ) due to the presence and absence of plant roots.

For the quantification of below-ground biomass using electrical resistivity (ρ), root samples were collected from the lysimeters from a position along the transect line. Locations of contrasting resistivity were chosen from which to collect samples. The procedures for sample collection and determination of RMD are described in Section 3.6.2.1. To keep the maximum integrity and cause the least destruction to the cover, samples were collected from two locations along the transect of the top three lysimeters. Figure 3.28 depicts the electrodes' line positions along the transect and points of root sampling.

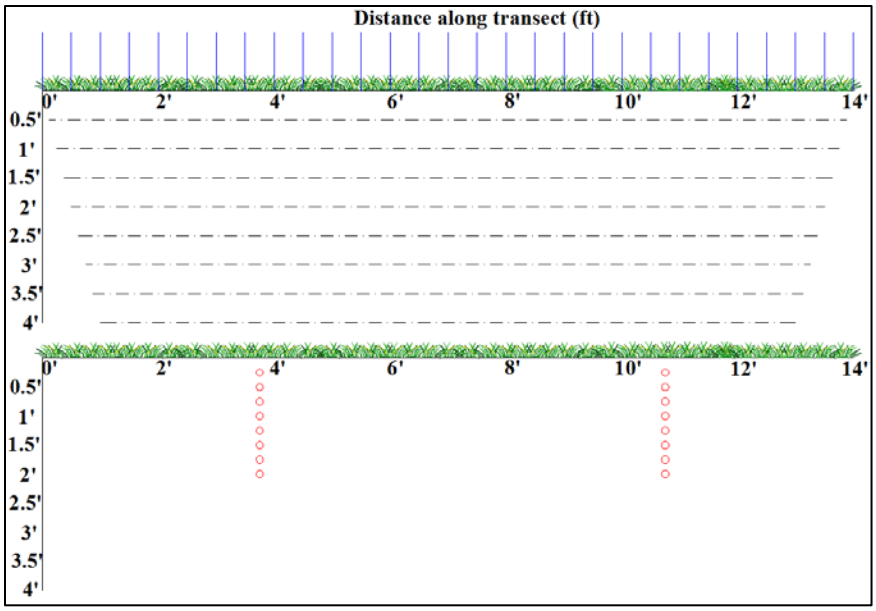

Figure 3.28 Positions of root sampling along the RI line

3.6.2 Laboratory Investigation of Vegetation

Laboratory investigation of vegetation includes determination of root length density (RLD) and root mass density (RMD). Determination of RLD and RMD was sensitive and as it was destructive to the lysimeters, root samples were collected three times a year (fall, spring, and summer) to evaluate the root distribution below the cover soil at different seasons of the year.

3.6.2.1 Root Mass Density (RMD)

Root mass density (RMD) was measured following the procedure described in Amato et al. (2010). To determine the RMD of different vegetation, root samples were collected from each of the lysimeters at different seasons of the monitoring period. Destructive samples were taken, using a 3-inch sample corer to a depth of 18 to 20 inches at 3-inch intervals (Figure 3.29). These samples were shipped to the laboratory and weighed, and the soil water content was measured on a 20 to 25 g subsample by weighing before and after drying at 110^{o}C to constant mass, obtaining soil dry mass (DM_s) in grams.

Figure 3.29 Destructive sample collection for RMD test

The remaining sample was weighed and washed over a 0.2 mm sieve after clay dispersion with 85% w/w sodium hexametaphosphate solution. Non-root materials and other soil debris were separated manually, and the washed roots were dried in the oven at 70^{o} C constant mass to obtain root dry mass (DM_r) in grams. DM_r was then divided by DM_s for each sample and multiplied by the soil dry bulk density (BD) to give root dry mass per unit soil volume (RMD) in g/cm^3.

$$RMD = \frac{DM_r}{DM_s} \times BD$$

To determine the dry bulk density, undisturbed samples were collected very carefully in Shelby tubes. The samples were trimmed to a known volume, weighed, dried in an oven, and weighed again. Dry bulk density was calculated as the dried mass divided by the volume of the sample.

3.6.2.2 Root Length Density (RLD)

Root length (RL) was mostly measured with an mm-scaled tape, but in some cases, the line intersect method developed by Newman (1966) was used to verify the manual measurements of the root length. Root length density (RLD) was calculated using the following equation in cm.cm^{-3} units.

$$RLD = \frac{RL}{DM_S} \times BD$$

DM_s is the soil dry mass and BD is dry bulk density. These two parameters were calculated as per the process for RMD. RLD of different plants was measured from the samples collected during summer 2016.

3.7 In-situ Hydraulic Conductivity Test

3.7.1 Guelph Permeameter

A Model 2800K Guelph Permeameter (GP) (Figure 3.30a) from Soil Moisture Equipment Corp was used to measure the in-situ hydraulic conductivity of different lysimeters. The GP measures saturated hydraulic conductivity. It determines the steady state infiltration rate necessary to maintain a constant depth of water in a cylindrical augured hole. The time required for the GP to reach steady state flow is a function of the permeability of the soil.

(a) (b)

Figure 3.30 (a) Guelph Permeameter, GP (b) Schematic of Guelph test

A GP is comparatively easy to operate and is less time consuming and less destructive than other in-situ hydraulic conductivity testing methods (e.g. SDRI, tension infiltrometer). A hole of approximately 3 inches diameter is augured into the cover soil to the desired depth (6 inches and 12 inches), and the walls of the hole are then scarified to limit the smearing effect. The GP is placed into the hole, and the hole is filled with water

(Figure 3.31). The height of water in GP is recorded at regular time intervals until the infiltration rate reaches the steady state condition. Two different sets of equations are used to estimate the saturated hydraulic conductivity: the single-height calculation and the dual-height calculation. In this study, the single-height calculation was used, as single-height equation is more appropriate for fine-grained soil (Elrick and Reynolds, 1992; Meiers 2002). The single-height equation is as follow:

$$K_{fs} = \frac{\mathrm{CQ}}{\left(2\pi H^2 + C\pi r^2 + 2\pi\left(\frac{H}{\alpha^*}\right)\right)}$$

where K_{fs} (L/T) is the field-saturated hydraulic conductivity, α* (/L) is the ratio of K_{fs} to the matric flux potential, H (L) is the constant height of ponded water in the well, r (L) is the radius of the well, C is a dimensionless shape factor, and Q (L^3/T) is the steady-state flow rate from the GP.

Figure 3.31 In-situ hydraulic conductiviy test using GP

3.7.2 Instantaneous Profile Method (IPM)

Co-located moisture content and suction sensors were used to develop the FSWCC. The instantaneous profile method (IPM) (Watson 1966, Hillel et al. 1972, Khire et al. 1995, Meerdink et al. 1996) suggested by Benson and Gribb (1997) was used to determine the field unsaturated hydraulic conductivity. Mathematical fitting functions were estimated for the unsaturated hydraulic properties.

3.8 Numerical Modeling

3.8.1 Water Balance Model (UNSAT-H)

The UNSAT-H code was used for the numerical modeling of the ET cover system. The following section describes the methodology applied to the UNSAT-H for water balance modeling.

3.8.1.1 Selection Criteria

The purpose of a water balance model is to simplify and predict the real-world phenomena by explaining the appropriate constitutive principles that govern the problem (Hillel 1977). The critical requirement of a water balance model is the accurate representation of the constitutive relationship between isothermal and non-isothermal evaporation (Fayer and Gee 1997), the relationship for unsaturated soil water flow, soil water storage, soil texture effect, infiltration, runoff, preferential flow, a comprehensive root water uptake concept, suction-based hydraulic conductivity, and field verification. UNSAT-H was selected for this study, as it meets most of the required criteria.

3.8.1.2 Verification of UNSAT-H

Fayer and Jones (1990) made several comparisons of UNSAT-H predictions with known analytic and numerical solutions to definite problems, and they effectively solved water balance for several soil types. They covered the theory documentation and user manual for UNSAT- H. Verifications and benchmark tests of UNSAT-H were conducted by

Baca and Magnuson (1990). Fayer and Jones (1990) also conducted further tests on horizontal infiltration, imposition of a constant heat flux at the surface, infiltration of a stratified vadose zone, and coupled heat and water flow in a field test plot. Baca and Magnuson reported that UNSAT-H was operationally verified both for humid and arid regions.

3.8.2 Input Parameter for UNSAT-H

Climate data, soil data, vegetation data, simulation control variables, and boundary conditions are the input parameters for UNSAT-H.

3.8.2.1 Meteorological Input

The meteorological input for UNSAT-H includes the daily precipitation, daily maximum and minimum air temperatures, daily solar radiation, average dew point temperature, average daily wind speed, and daily cloud cover. All of this data was gathered from the on-site weather station and applied to the simulation in UNSAT-H. UNSAT-H does not cover the snowmelt algorithm, and during the monitoring period of the site, snow fall was not observed. Therefore, the simulation was conducted based on the on-site precipitation data.

3.8.2.2 Soil Data

The required soil data for UNSAT-H is saturated hydraulic conductivity, saturated (Θ_s) and residual (Θ_r) volumetric water content, and unsaturated hydraulic characteristics. The unsaturated hydraulic properties consist of the parameters from the soil water characteristic curve (ψ-Θ) and the unsaturated permeability function (K_ψ). The VG function and the Maulem model for K_ψ were used for the UNSAT-H simulations. Θ_s and Θ_r were obtained from the experimental data subsequently fitted in the VG model (RETC). Saturated hydraulic conductivity was used from the laboratory results and in-situ measurements (GP).

3.8.2.3 Vegetation Data

The leaf area index (LAI), length of growing season, percent of bare area (PBA), rooting depth (RD), and root length density (RLD) functions are the main vegetation input parameters for UNSAT-H. RLD coefficients (a, b, and c) were obtained based on the laboratory RLD measurements and curve fitting. RD was measured directly from the on-site minirhizotrons installed at different lysimeters. PBA and LAI data used in the simulation was obtained from previous literature and ground coverage monitoring results.

3.8.2.4 Model Geometry and Boundary Conditions

Model geometry was based on the top soil and compacted soil depth. The nodal spacing was set at 1 cm, based on expert opinion (Fayer 2002, Webb 2002, and Dwyer 2005). Water flow across the surface and the lower boundary was determined by specified boundary condition. The initial head for each node for the first year of simulation was set at the wilting point.

3.9 Parametric Study

Numerical study was further extended, using a parametric evaluation. The parametric study was performed to determine the significance of the sensitive parameters for the optimum ET cover performance. The parametric analysis was performed to assess the effect of precipitation, vegetation, hydraulic properties, and the depth of cover on the most critical water balance performance indicator, percolation. In this current research, 4 feet of cover soil was placed in all of the lysimeters, and the extent of root into the cover was from 14 to 20 inches, based on the field monitoring results. During the monitoring period, substantial changes were observed in the soil hydraulic properties. Therefore, how the ET cover will react under further increases in root depth, changes of root density and hydraulic properties, and varying cover depths were analyzed. The sensitivity of these input

parameters was assessed by evaluating the annual percolation. The model matrix for the parametric simulation is listed in Table 3.6

Table 3.6 Model matrix for parametric study

Cover Depth	Meteorological parameter	Vegetation Parameter		Soil parameter		
	Rainfall	Root Distribution (RLD)	Root Zone Depth	α	n	Saturated Hydraulic Conductivity
(ft.)	mm/year		(ft.)	1/kPa		cm/sec
1 to 7	300 to 1500	Shallow, steep, very steep	0.5 to 3.5	0.001 - 0.3	1.1 - 2.5	10^{-3} to 10^{-8}

Chapter 4

Soil Characterization

4.1 Introduction

The objective of soil characterization is to evaluate the behavior of the evapotranspiration cover (ET cover) soil. Therefore, an extensive experimental program was developed to determine both the saturated and unsaturated characteristics (SWCC) of the soil. The detailed soil characterization results are inclusive of a) physical properties, b) hydraulic properties, and c) unsaturated soil properties are presented in this chapter. The in-situ SWCC of the soil is more representative of the actual conditions than the SWCC developed in the laboratory. Consequently, the field soil water characteristic curve (FSWCC) was also evaluated, based on the instrumentation results in this chapter.

4.2 Geotechnical Properties

4.2.1 Grain Size Distribution

Grain size distribution of the soil samples is presented in Figure 4.1. The results are shown for the vegetative-layer soil only. It was observed that the percent passing through a No.200 sieve ranged from 82% to 96% in the soil samples. The soil samples for all of the lysimeters were characterized as highly fine grained, with more than 82% passing through the No. 200 sieve.

From hydrometer analysis, it was found that all of the silt and clay in the soil were very close to each other. In all of the soil samples collected from different lysimeters and at different depths, the silt fraction was found to be approximately 35% to 56%, and the clay fraction was found to be 36% to 43%. The percent of silt and clay fraction for soils at different depths are listed in Table 4.1.

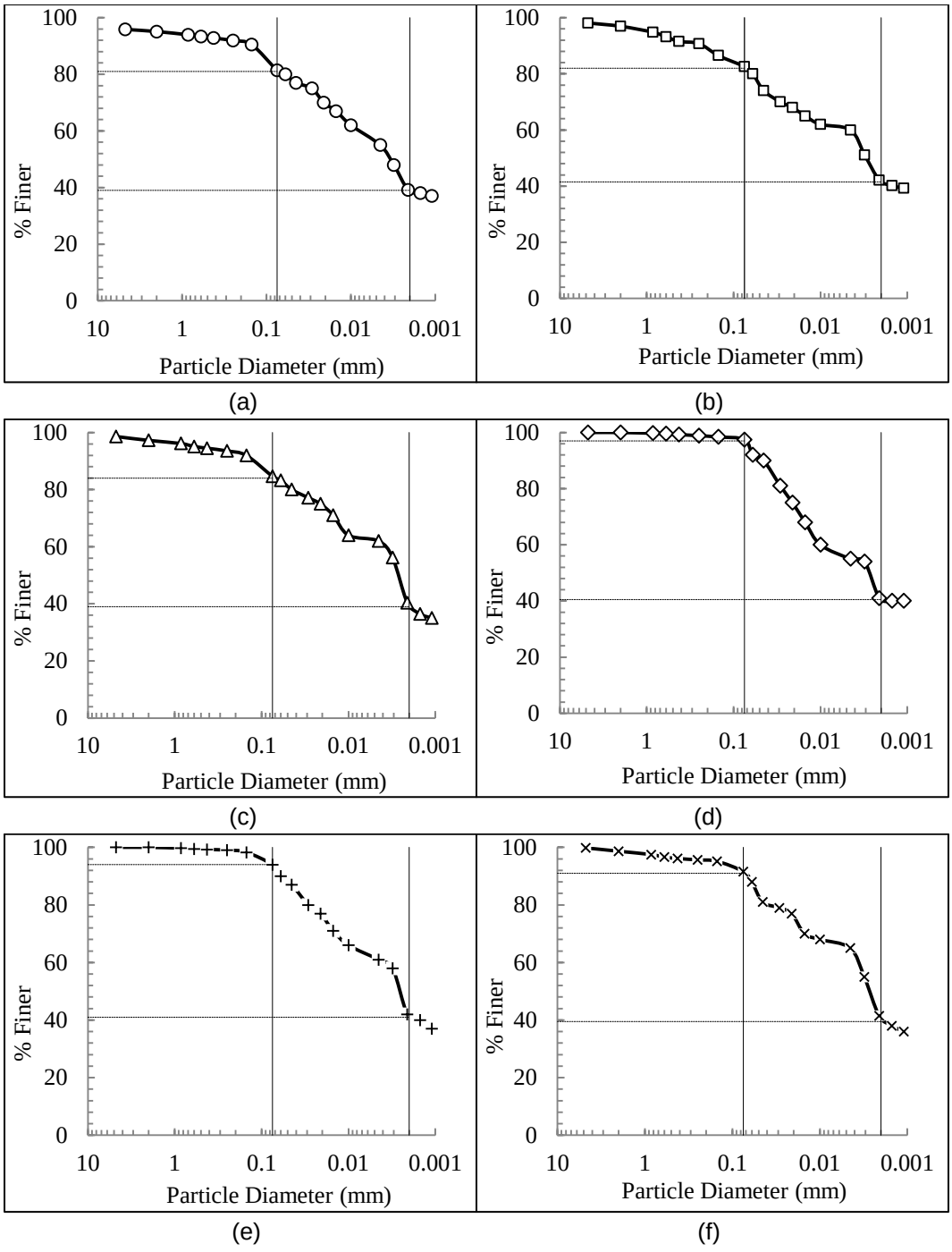

Figure 4.1 Grain size distribution curve for six lysimeters soil (a) L1-top, (b) L2-top, (c) L3-top, (d) L4-top, (e) L5-top, (f) L6-top

4.2.2 Atterberg Limits

The observed liquid limits and plasticity indices of the soil samples collected from the lysimeters were between 51 to 60 and 26 to 33, respectively. The plasticity chart for the investigated soils is shown in Figure 4.2. Based on the sieve analysis and Atterberg limit test results, soils from different lysimeters were classified as high plastic clay (CH) per the Unified Soil Classification System (USCS). A summary of Atterberg limit test results of the soil specimens is presented in Table 4.1.

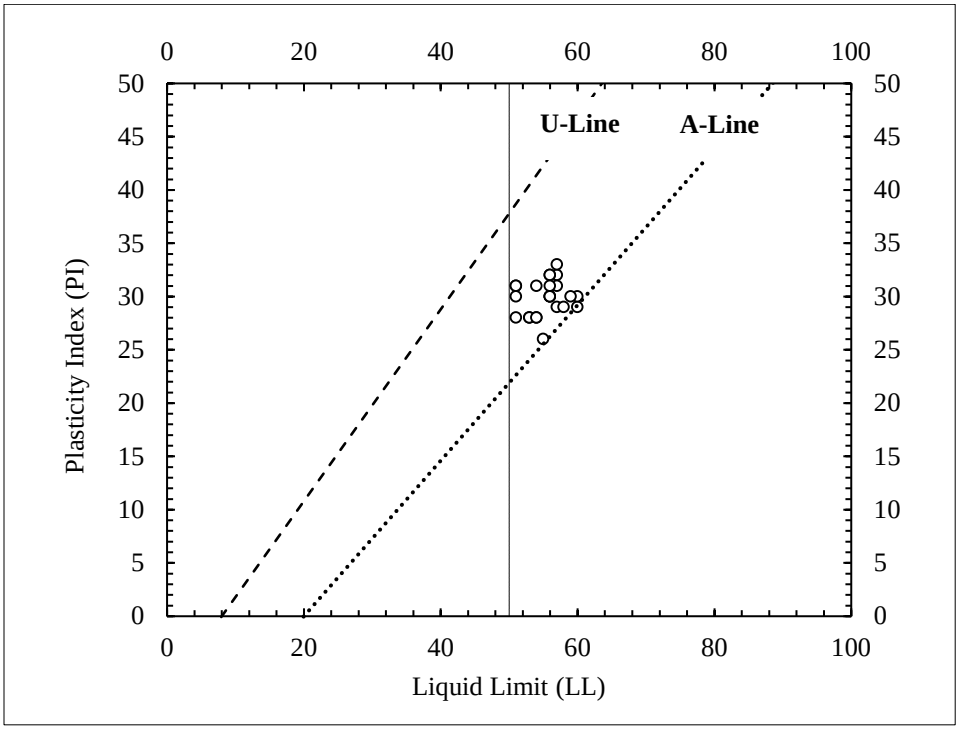

Figure 4.2 Plasticity chart for ET cover soil

4.2.3 Specific Gravity

Specific gravity of the collected soil samples was determined in accordance with the ASTM standards. It was found that the soils are, on average, 2.77 times heavier than water. The specific gravity of the test specimens is summarized in Table 4.1.

Table 4.1 Index properties of ET cover soil

Lysimeter	Designation	% Gravel	% Sand	% Silt	% Clay	Liquid Limit (LL)	Plasticity Index (PI)	USCS Classification	Specific Gravity (G_s)
		(%)	(%)	(%)	(%)	(%)	(%)		
Lysimeter 1	L1-Top	0	19	42	39	51	30	CH	2.78
	L1-1	0	16	43	41	57	29		2.72
	L1-2	0	17	41	42	54	28		2.71
	L1-3	0	18	43	39	60	29		2.79
Lysimeter 2	L2-Top	0	18	40	42	57	32	CH	2.74
	L2-1	0	17	43	40	56	32		2.77
	L2-2	0	19	43	38	51	31		2.78
	L2-3	0	16	43	41	58	29		2.69
Lysimeter 3	L3-Top	0	16	45	39	51	28	CH	2.74
	L3-1	0	22	35	43	54	31		2.80
	L3-2	0	17	43	40	57	31		2.74
	L3-3	0	15	47	38	51	31		2.79
Lysimeter 4	L4-Top	0	3	56	41	56	32	CH	2.79
	L4-1	0	7	51	42	60	30		2.74
	L4-2	0	14	43	43	53	28		2.75
	L4-3	0	8	54	38	56	31		2.77
Lysimeter 5	L5-Top	0	6	53	41	53	28	CH	2.75
	L5-1	0	9	55	36	56	30		2.74
	L5-2	0	11	52	37	54	28		2.79
	L5-3	0	10	48	42	56	30		2.75
Lysimeter 6	L6-Top	0	9	51	40	55	26	CH	2.78
	L6-1	0	14	46	40	56	30		2.79
	L6-2	0	12	52	36	59	30		2.70
	L6-3	0	11	51	38	57	33		2.73

4.2.4 Moisture Density Relation

Standard Proctor compaction tests were conducted on the collected soil specimens from different lysimeters. The compaction curves for the top soil of six lysimeters are shown in Figure 4.3. The maximum dry density (MDD) was found in the range of 16.75 KN/m^3 (108.8 pcf) to 17 KN/m^3 (111 pcf) at an optimum moisture content (OMC) of 17% to 18%. 95% of MDD was found in the range between 15.9 KN/m^3 to 16.15 KN/m^3. The average OMC at 95% MDD at the dry side and wet side was found to be 16.7% and 18.6%, respectively, for different lysimeter soils. Table 4.2 shows the OMC and MDD of the top layer of the soil.

Table 4.2 Standard Proctor compaction test results

Lysimeter	Designation	Optimum Moisture Content (OMC)	Maximum Dry Density(MDD)
		(%)	KN/m^3 (pcf)
Lysimeter 1	L1-Top	17.8	16.90 (109.2)
Lysimeter 2	L2-Top	17.2	17.00 (111.0)
Lysimeter 3	L3-Top	17.0	16.85 (109.0)
Lysimeter 4	L4-Top	18.0	16.86 (109.5)
Lysimeter 5	L5-Top	18.7	16.75 (108.8)
Lysimeter 6	L6-Top	17.4	16.85 (109.0)

4.2.5 Hydraulic Conductivity

Soil samples collected from different lysimeters were subjected to a hydraulic conductivity test in a flexible wall permeameter. The samples were compacted to 95% MDD at the dry side. The hydraulic conductivity results for all of the lysimeters soil were similar since the soils were from the same borrow pit. The results obtained from the tests ranged from 1.2 ×10^{-7} cm/sec to 1.5 × 10^{-6} cm/sec with a geometric mean of 5.85 × 10^{-7} cm/sec. The test results are summarized in Table 4.3.

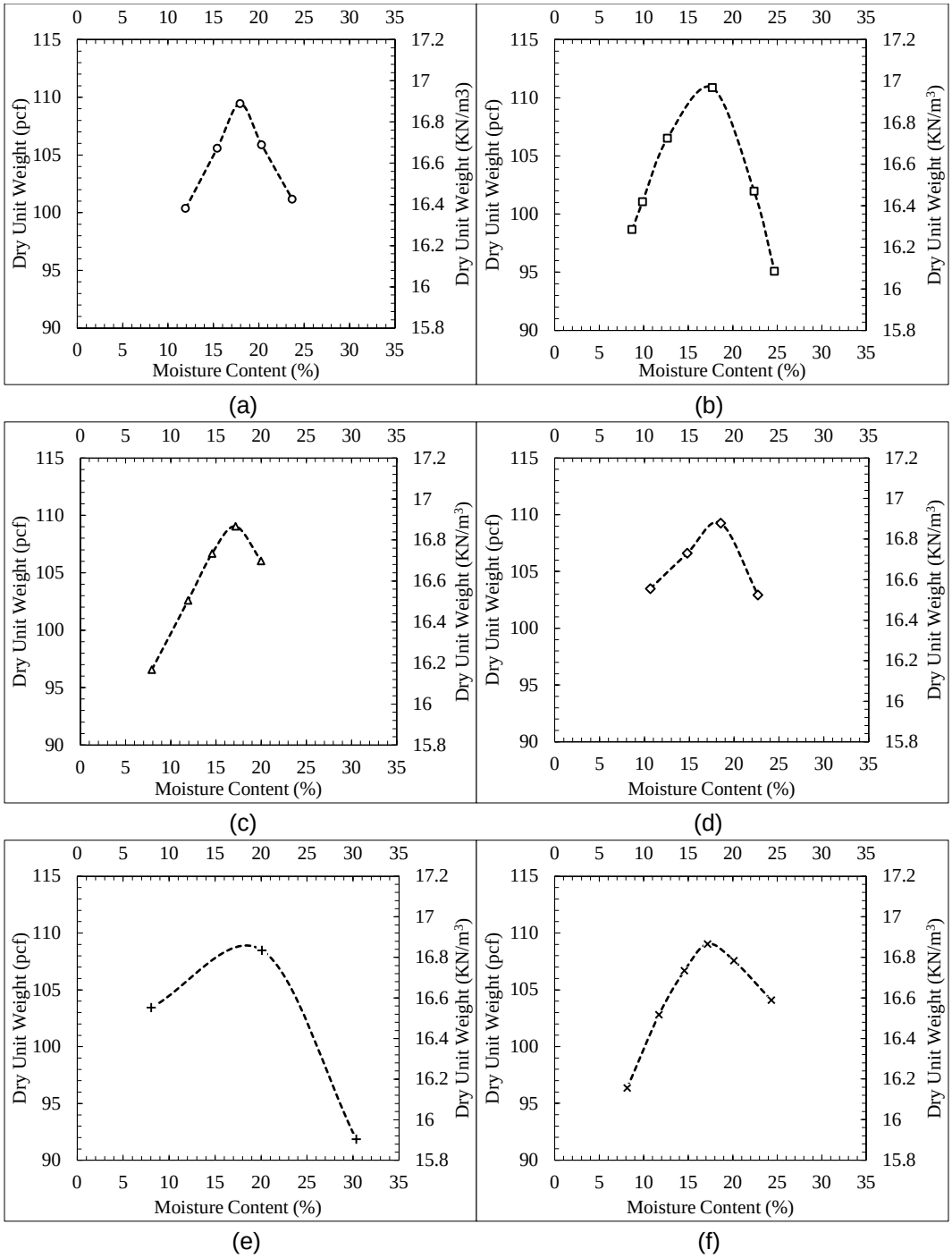

Figure 4.3 Compaction curve of different lysimeter soils (a) L1-top, (b) L2-top, (c) L3-top, (d) L4-top, (e) L5-top, (f) L6-top

Table 4.3 Hydraulic conductivity test results

Lysimeter	Permeability (cm/sec)
L-1	5.23E-07
L-2	3.65E-07
L-3	1.20E-07
L-4	1.22E-06
L-5	1.50E-06
L-6	9.60E-07

An attempt was made to develop a relationship between the saturated coefficient of permeability (K_s) and the compaction water content, using a rigid wall compaction permeameter. The soil compacted, using the standard Proctor method at different water contents, was subjected to the compaction permeameter. The water content was kept at a range from the dry side of OMC to the wet side of OMC during the compaction effort. The results indicated that K_s decreased significantly beyond the OMC at the wet side. Figure 4.4 shows the test results conducted on the soil specimen from L3-3. It is to be noted that only one specimen from the collected soil specimen was subjected to this test.

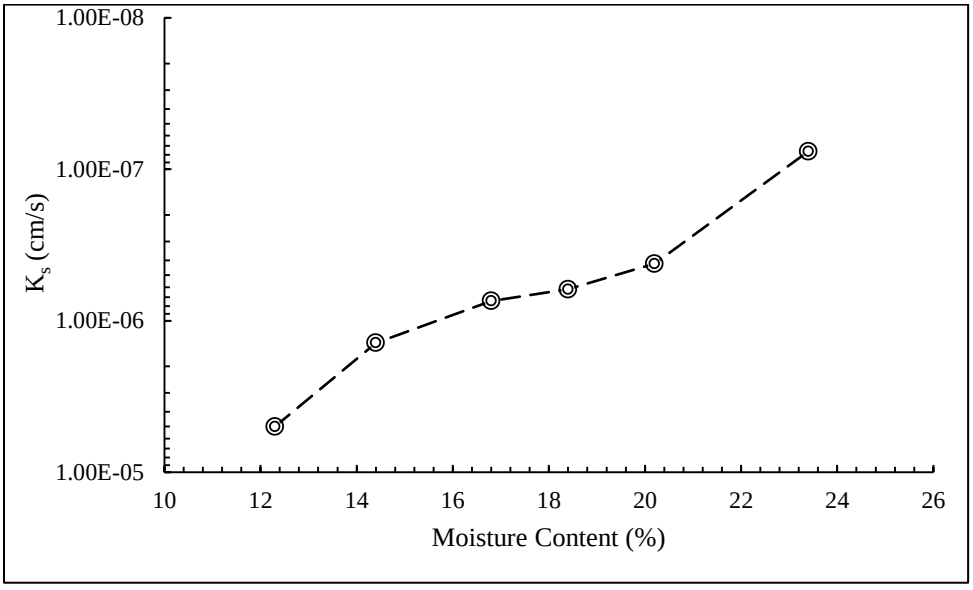

Figure 4.4 K_s at different water contents

4.3 Soil Suction Test Results

Several laboratory measurement techniques can be used to determine the soil water characteristic curve (SWCC). The moisture variation of the soil with corresponding changes in the matric suction is logged as SWCC. In this study, the soil specimen was subjected to SWCC measurement at 95% of the maximum dry density (MDD) condition, as the relative compaction in the field (six lysimeters) was almost 95%. The Van Genuchten (VG) curve fitting approach was used to analyze and model the SWCC behavior of different lysimeters' soil. The Retention Curve Program (RETC), (Van Genuchten, 1980) was used for the curve fitting of the laboratory results of the SWCC. It is possible to determine the unsaturated hydraulic conductivity, as well as some other parameters (e.g. field capacity, wilting point, and available water), from the SWCC. The detailed results of the SWCC study are shown in the following section.

4.3.1 SWCC of Different Lysimeters' Soil

All of the lysimeters were covered with soil from the same borrow pit, but the SWCC results of the different lysimeter soils will be presented separately. Sections 4.3.1.1 through 4.3.1.6 describe the detailed SWCC results.

4.3.1.1 SWCC of Lysimeter-1 Soil

Compacted soil from lysimeter-1 (L1-2) was subjected to SWCC at 95% MDD condition. The experimental data was then plugged into the RETC code to determine the Van Genuchten (VG) curve-fitting parameters. The variation of the volumetric moisture content with the matric suction for the L1-2 specimen is shown in Figure 4.5

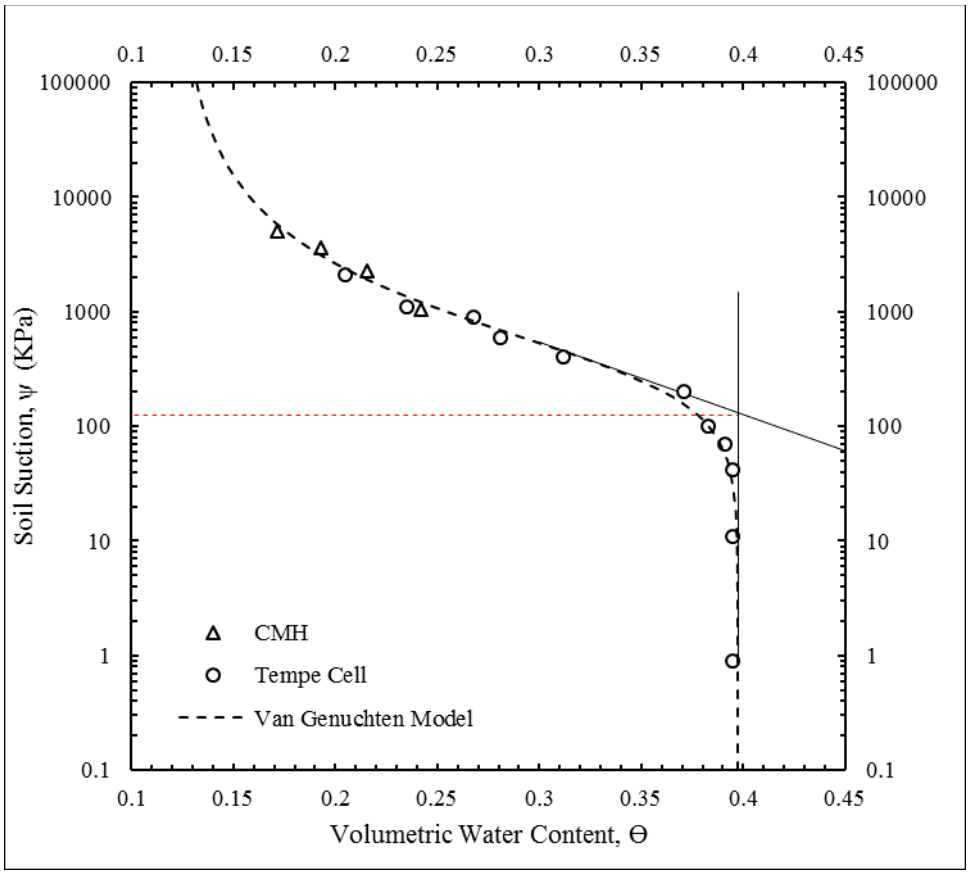

Figure 4.5 Soil water characteristic curve of Lysimeter - 1 soil (VG Model)

The soil (L1-2) was characterized as high plastic clay and exhibited the fundamental features in the SWCC, as shown in Table 4.4.

Table 4.4 Fundamental Features of L1-2 Soil SWCC

Salient features in the SWCC of L1-2 at 95% MDD	
Saturated Volumetric Water content, (Θ_s), %	39.74
Air entry value, AEV (ψ_a), KPa	125
Residual water content (Θ_r), %	12.30

Van Genuchten's curve-fitting model parameters for the SWCC, based on the RETC code of L1-2 soil, are presented in Table 4.5.

Table 4.5 Van Genuchten curve-fitting parameter of L1-2 Soil

Parameter	Value
α	0.0031
n	1.6
m	0.375

4.3.1.2 SWCC of Lysimeter-2 Soil

Compacted soil from lysimeter-2 (L2-1) was subjected to SWCC at 95% MDD condition. The experimental data was then plugged into the RETC code to determine the Van Genuchten (VG) curve-fitting parameters. The variation of volumetric moisture content with matric suction for the L2-1 specimen is shown in Figure 4.6.

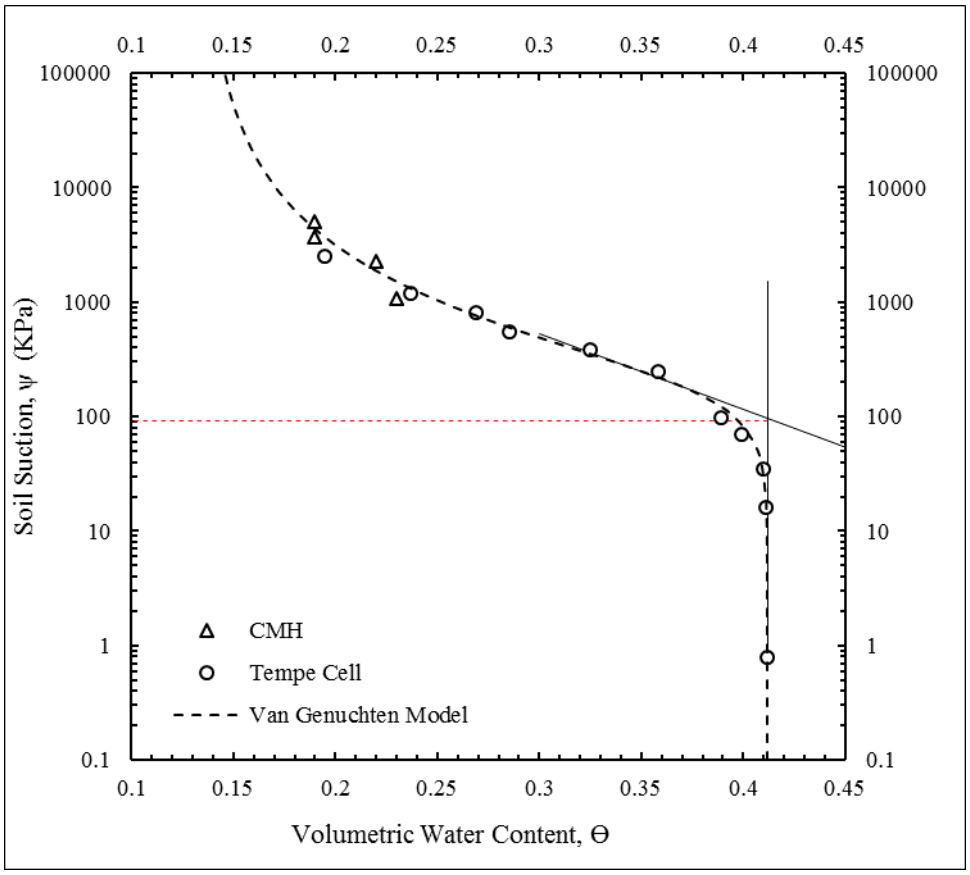

Figure 4.6 Soil water characteristic curve of Lysimeter–2 soil (VG Model)

The soil (L2-1) was characterized as high plastic clay and revealed the fundamental features in the SWCC, as shown in Table 4.6.

Table 4.6 Fundamental Features of L2-1 Soil SWCC

Salient features in the SWCC of L2-1 at 95% MDD	
Saturated Volumetric Water content, (Θ_s), %	41.2
Air entry value, AEV (ψ_a), KPa	91.0
Residual water content (Θ_r), %	13.5

Van Genuchten curve-fitting model parameters for the SWCC, based on the RETC code of L2-1 soil, are presented in Table 4.7.

Table 4.7 Van Genuchten curve-fitting parameter of L2-1 Soil

Parameter	Value
α	0.00514
n	1.53
m	0.26

4.3.1.3 SWCC of Lysimeter-3 Soil

Compacted soil from lysimeter-3 (L3-3) was subjected to SWCC at 95% MDD condition. The experimental data was then plugged into the RETC code to determine the Van Genuchten (VG) curve-fitting parameters. The variation of volumetric moisture content with matric suction for the L3-3 specimen is shown in Figure 4.7.

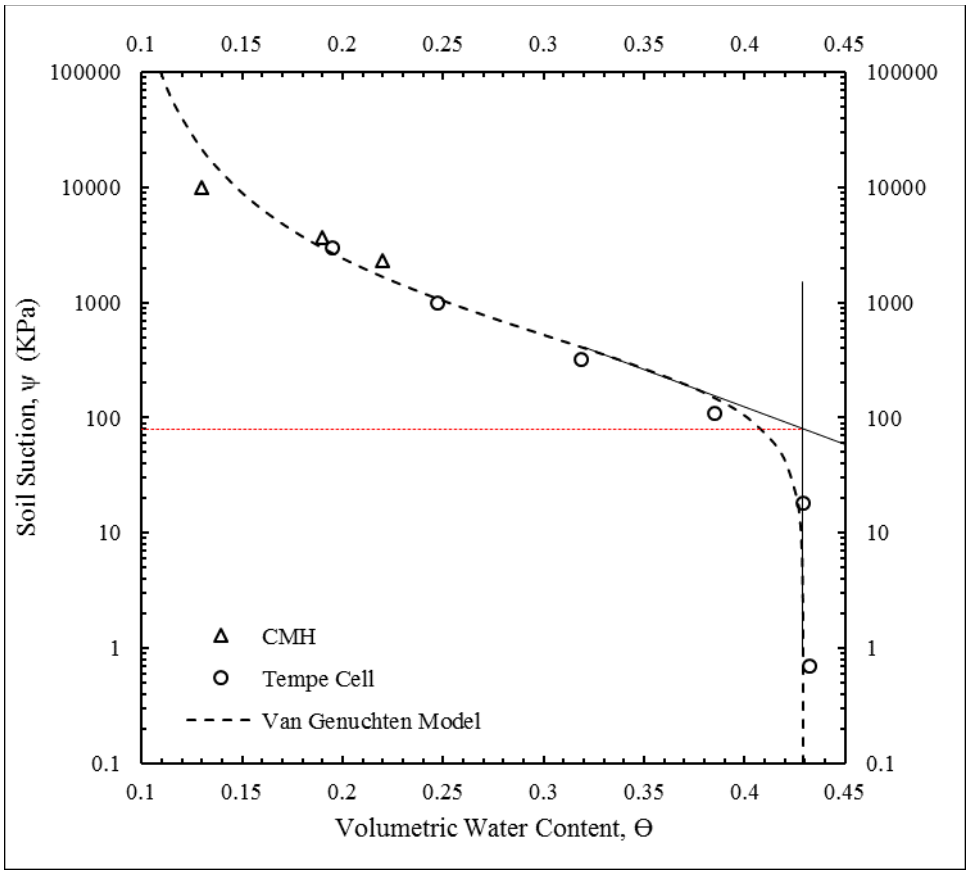

Figure 4.7 Soil water characteristic curve of Lysimeter–3 soil (VG Model)

The soil (L3-3) was characterized as high plastic clay and revealed the fundamental features in the SWCC, as shown in Table 4.8.

Table 4.8 Fundamental features of L3-3 soil SWCC

Salient features in the SWCC of L3-3 at 95% MDD	
Saturated Volumetric Water content, (Θ_s), %	42.88
Air entry value, AEV (ψ_a), KPa	80.0
Residual water content (Θ_r), %	9.00

Van Genuchten curve-fitting model parameters for the SWCC, based on the RETC code of L3-3 soil, are presented in Table 4.9.

Table 4.9 Van Genuchten curve-fitting parameter L3-3 Soil

Parameter	Value
A	0.00445
N	1.47
m	0.319

4.3.1.4 SWCC of Lysimeter-4 Soil

Compacted soil from lysimeter-3 (L4-3) was subjected to SWCC at 95% MDD condition. The experimental data was then plugged into the RETC code to determine the Van Genuchten (VG) curve-fitting parameters. The variation of volumetric moisture content with matric suction for the L4-3 specimen is shown in Figure 4.8.

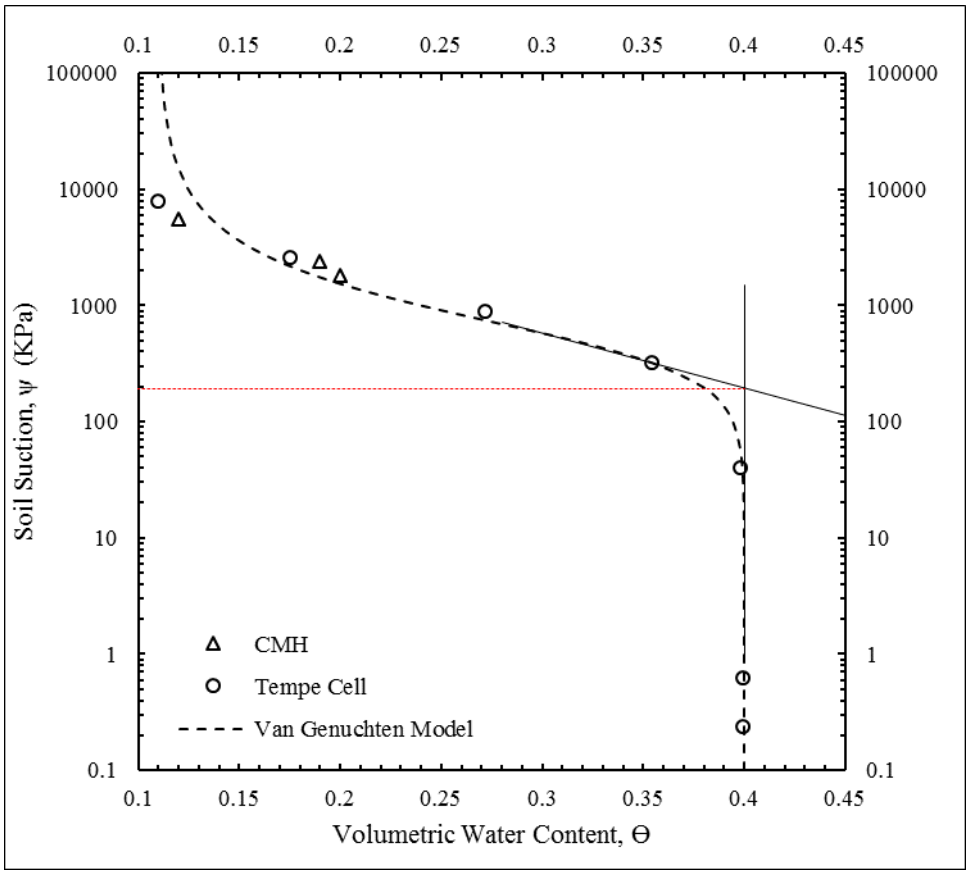

Figure 4.8 Soil water characteristic curve of Lysimeter - 4 soil (VG Model)

The soil (L4-3), being characterized as high plastic clay, revealed the fundamental features in the SWCC, as shown in Table 4.10.

Table 4.10 Fundamental features of L4-3 soil SWCC

Salient features in the SWCC of L4-3 at 95% MDD	
Saturated Volumetric Water content, (Θ_s), %	40.02
Air entry value, AEV (ψ_a), KPa	180
Residual water content (Θ_r), %	11.00

Van Genuchten curve-fitting model parameters for the SWCC, based on the RETC code of the L4-3 soil, are presented in Table 4.11.

Table 4.11 Van Genuchten curve-fitting parameter L4-3 soil

Parameter	Value
A	0.0037
n	1.96
m	0.50

4.3.1.5 SWCC of Lysimeter- 5 Soil

Compacted soil from lysimeter-5 (L5-1) was subjected to SWCC at 95% MDD condition. The experimental data was then plugged into the RETC code to determine the Van Genuchten (VG) curve-fitting parameters. The variation of volumetric moisture content with matric suction for the L5-1 specimen is shown in Figure 4.9.

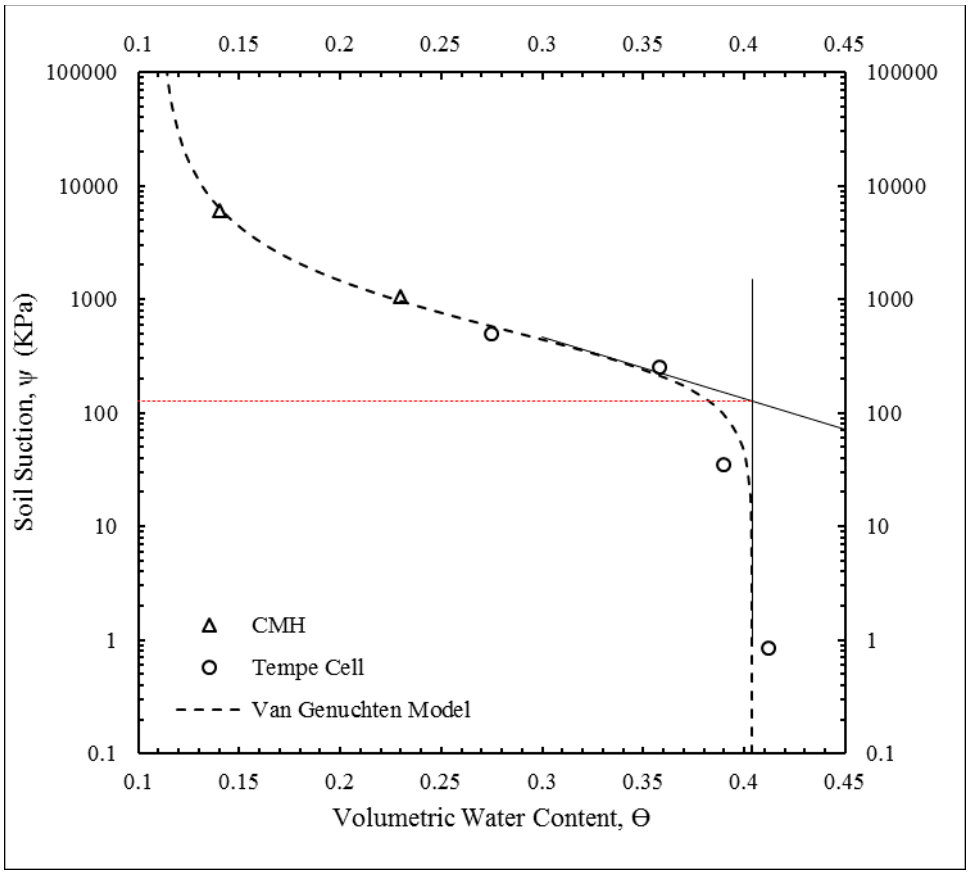

Figure 4.9 Soil water characteristic curve of Lysimeter - 5 soil (VG Model)

The soil (L5-1), being characterized as high plastic clay, revealed the fundamental features in the SWCC, as shown in Table 4.12.

Table 4.12 Fundamental features of L5-1 soil SWCC

Salient features in the SWCC of L5-1 at 95% MDD	
Saturated Volumetric Water content, (Θ_s), %	40.39
Air entry value, AEV (ψ_a), KPa	127
Residual water content (Θ_r), %	11.08

Van Genuchten curve-fitting model parameters for the SWCC, based on the RETC code of L5-1 soil, are presented in Table 4.13.

Table 4.13 Van Genuchten curve-fitting parameter L5-1 soil

Parameter	Value
α	0.0031
n	1.77
m	0.43

4.3.1.6 SWCC of Lysimeter-6 Soil

Compacted soil from lysimeter- 6 (L6-3) was subjected to SWCC at 95% MDD condition. The experimental data was then plugged into the RETC code to determine the Van Genuchten (VG) curve-fitting parameters. The variation of volumetric moisture content with matric suction for the L6-3 specimen is shown in Figure 4.10.

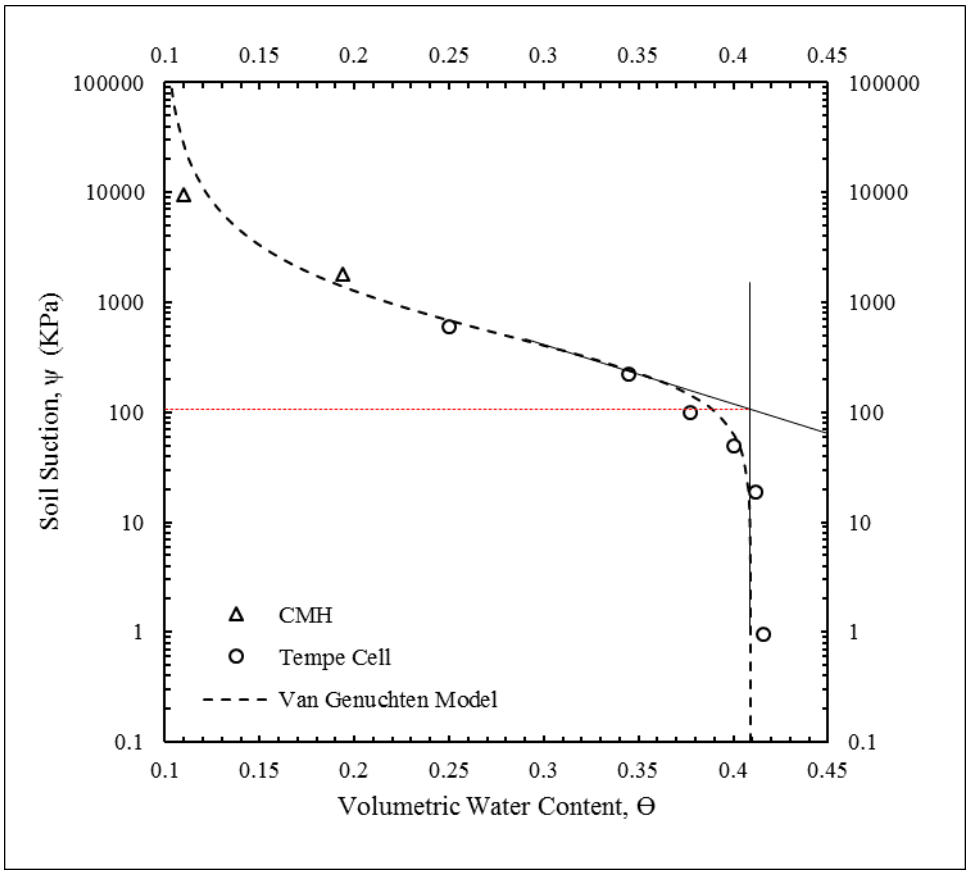

Figure 4.10 Soil water characteristic curve of Lysimeter - 6 soil (VG Model)

The soil (L6-3), being characterized as high plastic clay, revealed the fundamental features in the SWCC, as shown in Table 4.14.

Table 4.14 Fundamental features of L6-3 soil SWCC

Salient features in the SWCC of L6-3 at 95% MDD	
Saturated Volumetric Water content, (Θ_s), %	40.89
Air entry value, AEV (ψ_a), KPa	105
Residual water content (Θ_r), %	9.90

Van Genuchten curve-fitting model parameters for the SWCC, based on the RETC code of L6-3 soil, are presented in Table 4.15.

Table 4.15 Van Genuchten curve-fitting parameter L6-3 soil

Parameter	Value
α	0.00345
n	1.74
m	0.42

4.3.2 Unsaturated Hydraulic Conductivity Function of ET Cover Soil

The desorption SWCCs of the compacted soil specimens were evaluated in the laboratory using the procedures mentioned in Chapter 3. The compaction of the soil specimen was ensured at the bulk densities representative of the field condition. The saturated hydraulic conductivity of the compacted clay (remolded to the as-built condition) was determined in the laboratory. The in-situ hydraulic conductivities of the cover soil were measured, using the Guelph permeameter installed in shallow depths (6-inch depth and 12-inch depth). It is to be noted that the Guelph permeameter was used one year after the construction of the lysimeters. Therefore, in this dissertation, laboratory-measured hydraulic conductivities were selected as representative of the Van Genuchten-Mualem unsaturated hydraulic conductivity function development. Since SWCC is the relationship

between the matric suction and the volumetric moisture content, the hydraulic conductivity functions were developed, relating permeability with matric suction and volumetric water content.

Van Genuchten-Mualem's unsaturated hydraulic conductivity functions for different lysimeter soils are presented in Figure 4.11. At lower suction levels (up to 100-180 kPa for different lysimeter soils), the hydraulic conductivity remains constant, and the permeability decreases considerably with an increase in the matric suction. The sharp changes in the curves occur basically at the air entry suction. Therefore, flow of water in the ET cover soil should be expected at a rate of saturated hydraulic conductivity until the soil overcomes the air-entry suction.

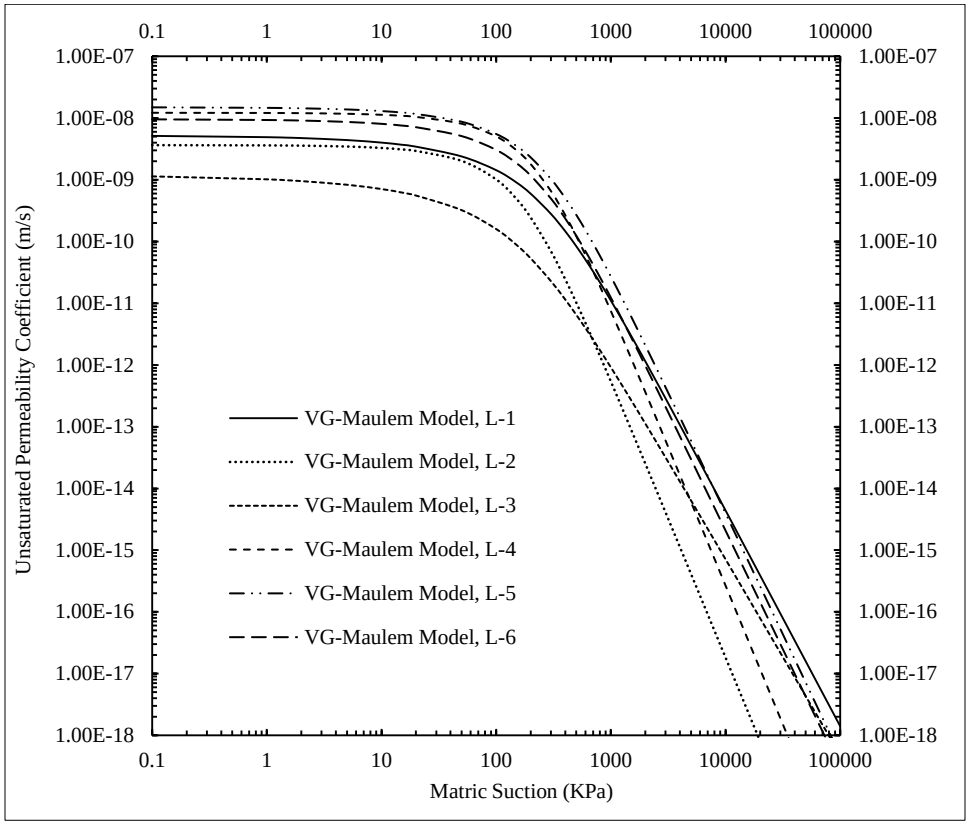

(a)

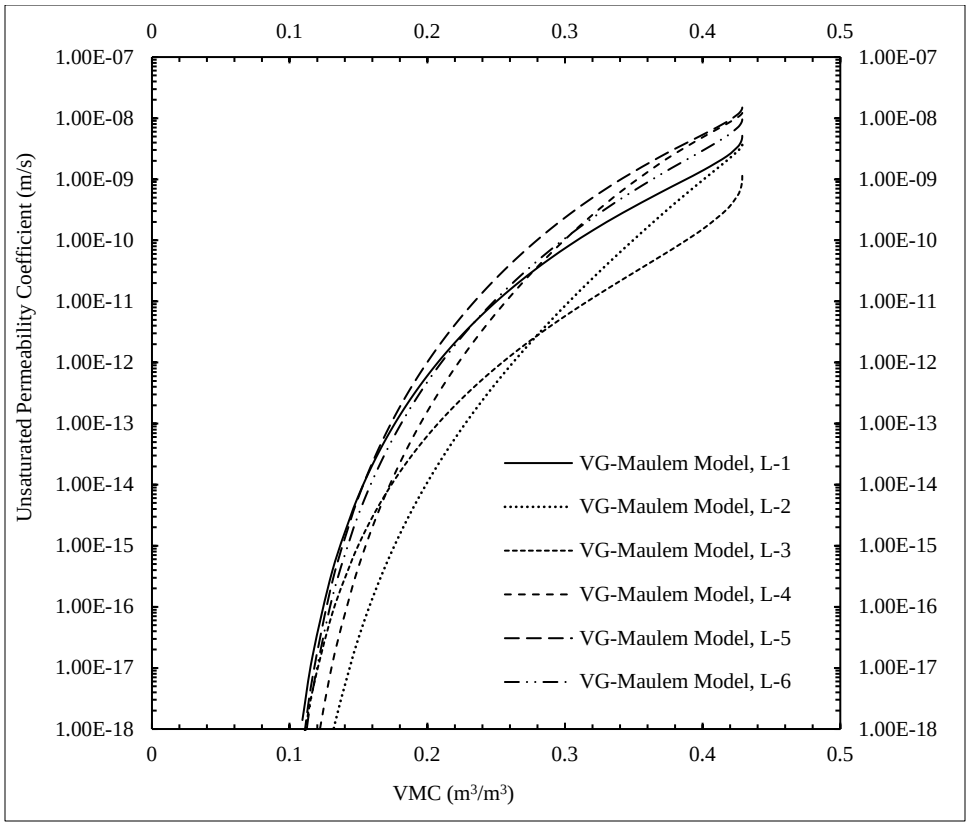

(b)

Figure 4.11 Van Genuchten-Maulem hydraulic conductivity function for different lysimeter cover soils, (a) hydraulic conductivity (K_ψ) Vs matric suction (ψ) (b) hydraulic conductivity (K_ψ) Vs volumetric moisture content(Θ)

4.3.3 Field Capacity (Θ_{FC}) and Wilting Point (Θ_{WP}) Water Content

Field capacity of soil is the water content (Θ_{FC}) at which a single drop of water from the top of the cover will allow a drop of percolation from the bottom of the cover. Conventionally, the field capacity is assumed to be the water content at a suction of 33 KPa. The water content at which the plants are unable to draw water from the soil is referred to as the wilting point (Θ_{WP}), which corresponds to the suction value of 1500 KPa.

The field capacity (Θ_{FC}) and wilting point (Θ_{WP}) were computed from the SWCC and corresponded to the suction at 33 KPa and 1500 KPa (Figure 4.12). Since the soil for

all of the cover soil was from the same borrow pit, Θ_{FC} and Θ_{WP} were similar. The Θ_{FC} ranged from 39.5% to 42.2%, and Θ_{WP} varied from 18.8% to 25.8%. The average Θ_{FC} is 40.5%, and the average Θ_{WP} is 21.9%. It is to be noted that due to a higher air entry value, the water content at field capacity was almost equal to the saturated volumetric moisture content (Figure 4.12). The Θ_{FC} and Θ_{WP} for different lysimeter soils are listed in Table 4.16.

Table 4.16 FC and WP water content for different lysimeter soils (Compacted layer)

Lysimeter	Field capacity water content, (Θ_{FC})	Wilting point water content, (Θ_{WP})
L1-2	0.395057888	0.240633149
L2-2	0.407181660	0.258467346
L3-3	0.422585850	0.226200627
L4-3	0.399530089	0.201756649
L5-1	0.401668547	0.198203203
L6-3	0.405967271	0.188493438

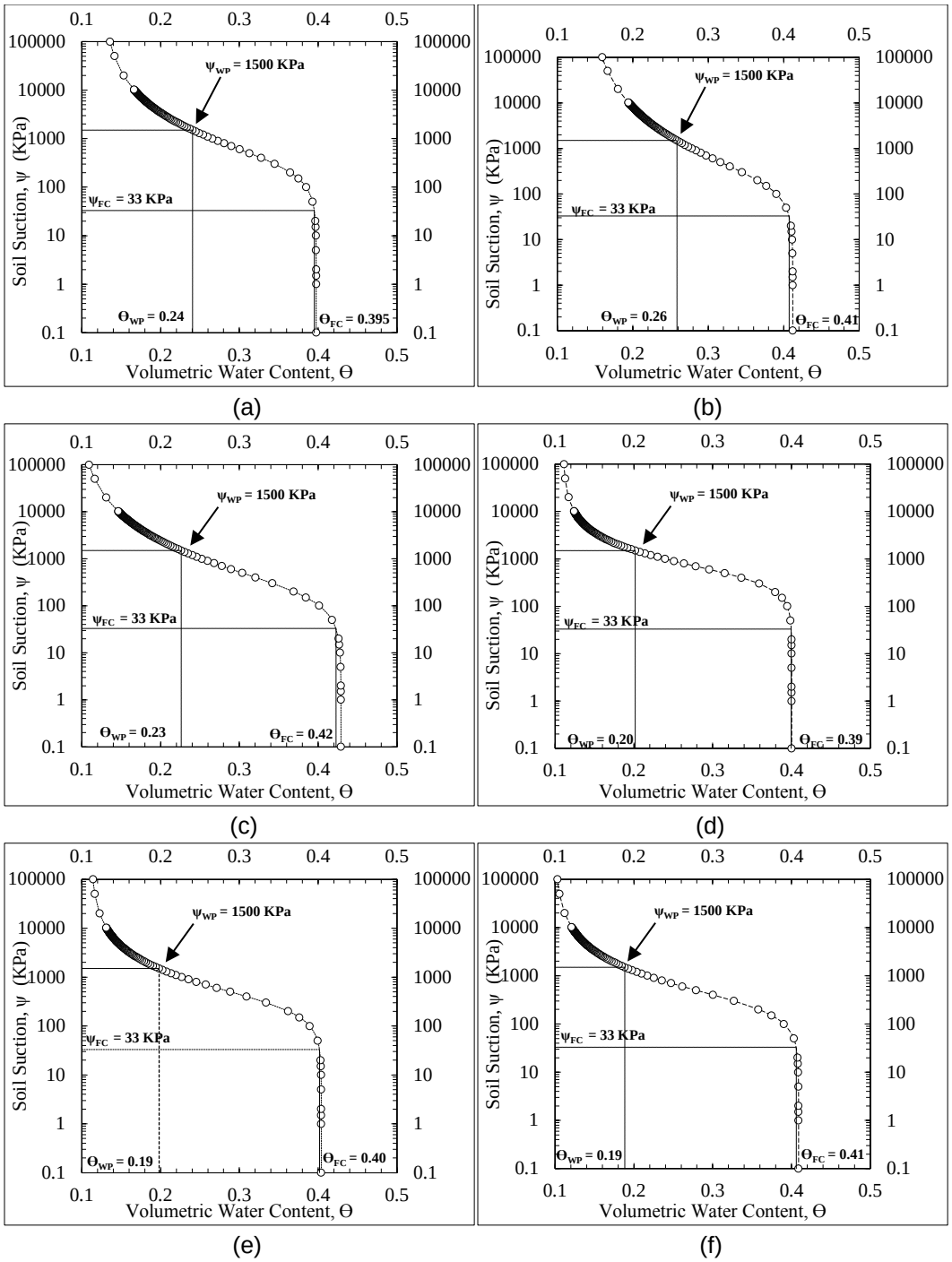

Figure 4.12 Field capacity and wilting point of different lysimeter soils from SWCC. L1-2 (a), L2-2 (b), L3-3 (c), L4-3 (d), L5-1 (e), L6-3 (f)

4.3.4 Water Storage Capacity (S_c) and Available Water Storage (S_a)

Total storage capacity (S_c) of the soil represents the fully saturated condition of the ET cover. When the soil water storage exceeds the capacity, percolation starts from the bottom of the cover. S_c was determined from measured Θ_{FC} from SWCC and the cover thickness. Plant available water storage (S_a) was also determined, based on the laboratory SWCC. S_a is the stored water in the soil between the Θ_{FC} and Θ_{WP}. Based on the SWCC and the field cover soil thickness, the water storage capacity of the ET cover soil from the same borrow pit was 8.96 inches (481.65 mm) to 20.28 inches (515.22 mm), with an average value of 19.45 inches (494.14 mm). Unit available storage, or the plant available water storage capacity, was 7.43 inches to 10.47 inches for different lysimeter soils. The S_c and S_a of different lysimeter soils are listed in Table 4.17.

Table 4.17 Water storage capacity and unit available storage for different lysimeter soils

Lysimeter	Unit Available Storage, (Θ_u), mm/ m cover thickness	Unit Available Storage, (Θ_u), inch/ 4 ft. cover thickness	Field Capacity (inch)	Field Capacity (mm)
L1-2	154.4247	7.4318	18.9627	481.6545
L2-2	148.7143	7.1570	19.5447	496.4358
L3-3	196.3852	9.4512	20.2841	515.2166
L4-3	197.7734	9.5180	19.1774	487.1070
L5-1	203.4653	9.7919	19.2800	489.7142
L6-3	217.4738	10.466	19.4864	494.9552

4.4 Field Soil Water Characteristic Curve (FSWCC)

The response of soil water at different suction levels in the field was observed during the study period. The field soil water characteristic curve (FSWCC) was different from the laboratory-measured SWCC during the monitoring period. This difference can be addressed due to the change in the soil structure, pedogenesis effect, root growth,

hysteresis effect, etc. Figure 4.13 shows the FSWCC obtained from the co-located sensors at different lysimeters in the ET cover.

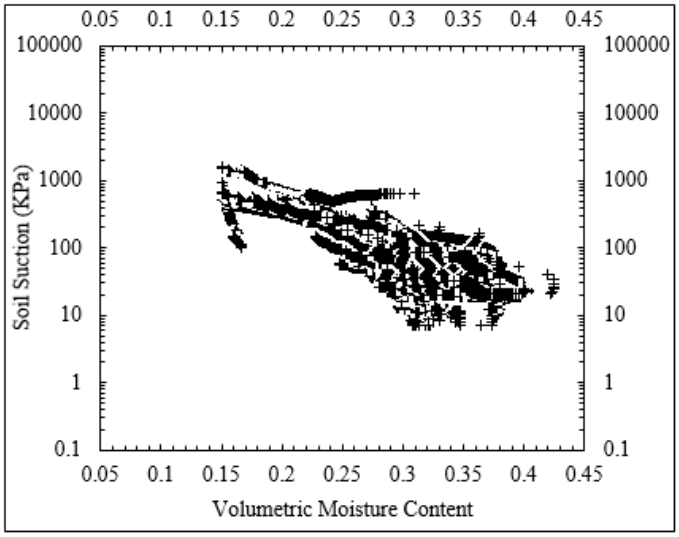

Figure 4.13 Field response of soil water at different suction levels(data from co-located sensors in the ET cover)

The actual soil water response under different suction levels in the field was different from the laboratory-measured SWCC. Therefore, based on the actual field response, the field-measured SWCC was developed for each of the lysimeter soils. The FSWCCs for all six lysimeters are shown in Figure 4.14. The upper-bound and lower-bound curves in Figure 4.14 are the maximum and minimum range between which the field data exists. The curve in the middle represents the average field condition of soil moisture and suction. A significant change can be observed in the FSWCC, when compared to the SWCC measured in the laboratory. Therefore, from the field response of the SWCC, it is obvious that the water storage capacity of the cover soil changes with time. The hydraulic parameters α, n and m also change with time, due to changes in the shapes of the SWCCs. Therefore, while designing an ET cover, laboratory-measured SWCC should be corrected, based on the FSWCC, to obtain accurate design parameters.

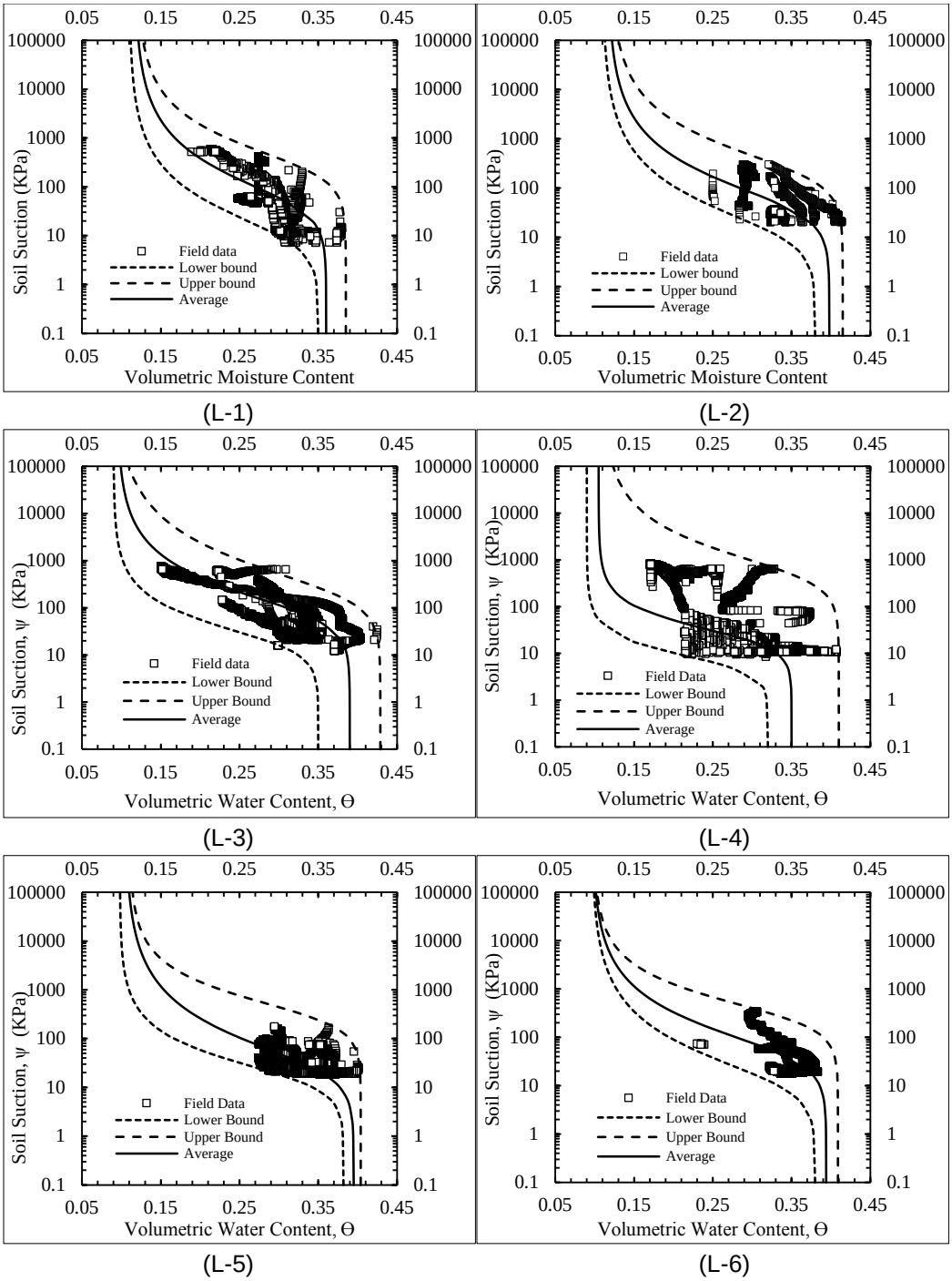

Figure 4.14 Field-measured SWCC with moisture content and suction data from sensors of six lysimeters.

4.4.1 Available Water Based on FSWCC:

The field capacity (Θ_{FC}) and wilting point (Θ_{WP}) were computed from the FSWCC corresponding to the suction at 33 KPa and 1500 KPa. SWCC curves, based on the field instrumentation results, are presented in Figure 4.15. A significant change was observed when comparing the Θ_{FC} with the Θ_{FC} values measured from SWCC. The Θ_{FC} ranged from 25% to 36%, and the Θ_{WP} varied from 10% to 15%. The major contributing factors to the changes in the Θ_{FC} are the wet-dry cycle in the field, the natural pedogensis process, a change in soil structure, etc. The ratio of the field-SWCC-based Θ_{FC} to the lab-SWCC-based Θ_{FC} is depicted in Table 4.18.

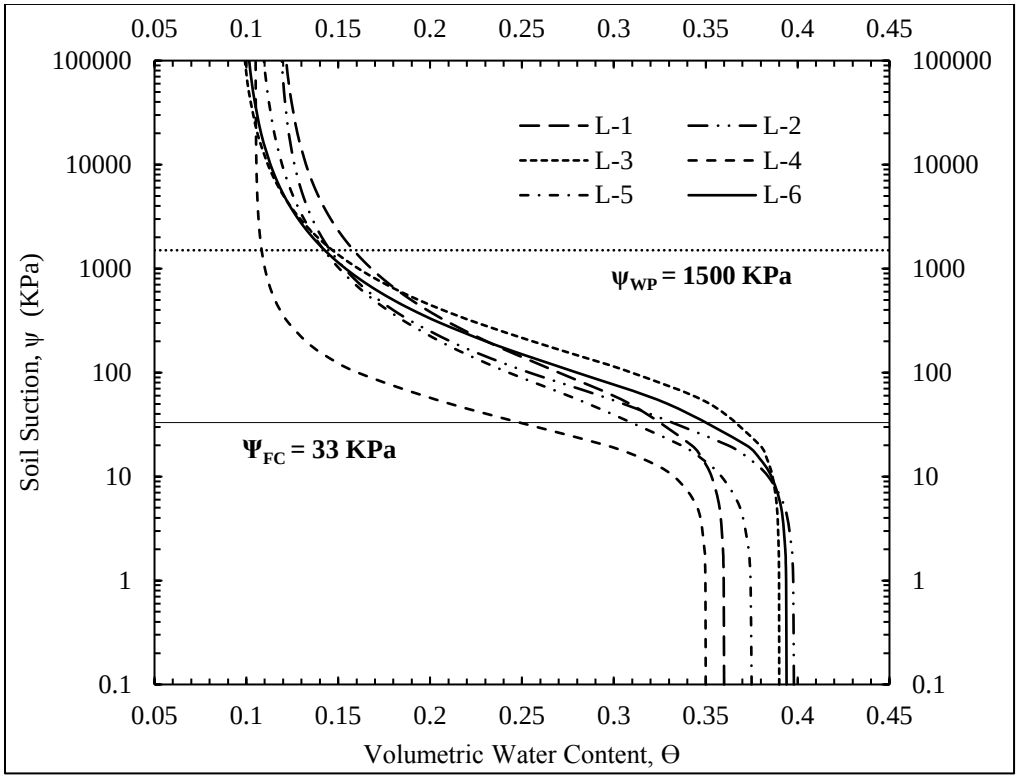

Figure 4.15 Field capacity and wilting point of different lysimeter soils from FSWCC

From Table 4.18, it is obvious that the Θ_{FC} reduced approximately 12.8% to 37% in the field, in different lysimeters. The cover soil in L-4 underwent the most changes (37%),

followed by the L-5 soil (23%). The rest of the four lysimeter soils experienced changes similar to each other. The consequences of the changes in Θ_{FC} were observed in the cumulative percolation of the different lysimeters. Lysimeters 4 and 5 had the highest cumulative percolation. It is obvious that the lower the field capacity of the soil is, the higher is the infiltration of water into the cover. Detailed results of cumulative percolation in the six lysimeters are presented in Chapter 6. Therefore, the ratio of Θ_{FC} is a good indicator to use in evaluating the performance of the ET cover.

Table 4.18 Ratio of field capacity moisture content

Lysimeter	$(\Theta_{FC})_{field}/(\Theta_{FC})_{lab}$
L-1	0.827767572
L-2	0.821088765
L-3	0.871309290
L-4	0.626926013
L-5	0.775054850
L-6	0.868757547

4.4.2 Change of Unsaturated Parameters (α and n)

The changes in α and n values were observed during the monitoring period. The α parameter for all of the lysimeter soils increased after three years of field exposure. The soils in lysimeters 4 and 5 had an increased value in α of two orders of magnitude. On the other hand, n parameter decreased in all of the regions. The changes in the n parameter were relatively small compared to those of the α parameter. Figure 4.16 shows the changes in the α and n parameters for all of the lysimeter soils, three years after construction. In all the cases, the n values were found below the 1:1 line. From the ACAP test plot, Benson, Albright and Apiwantragoon found a similar trend of post construction changes of α and n parameters.

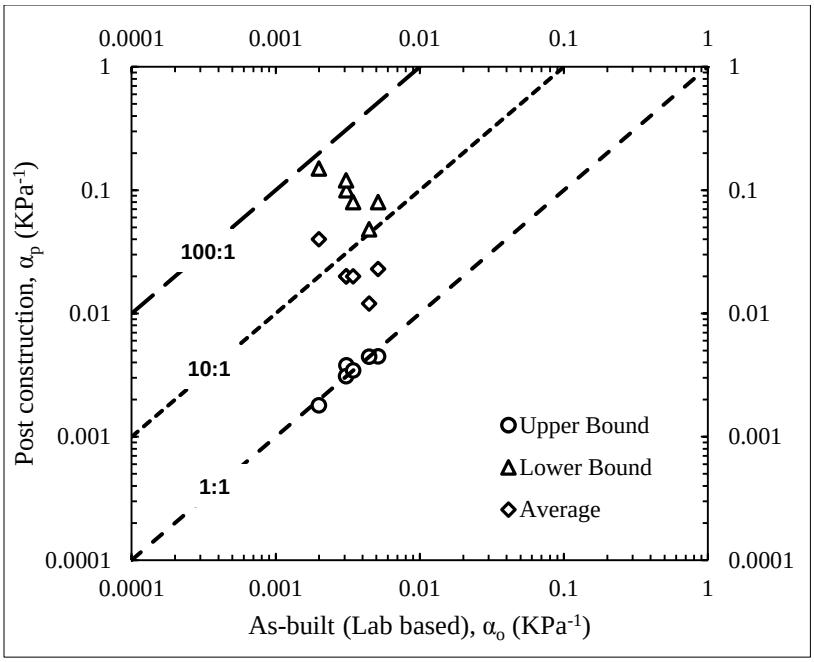

(a)

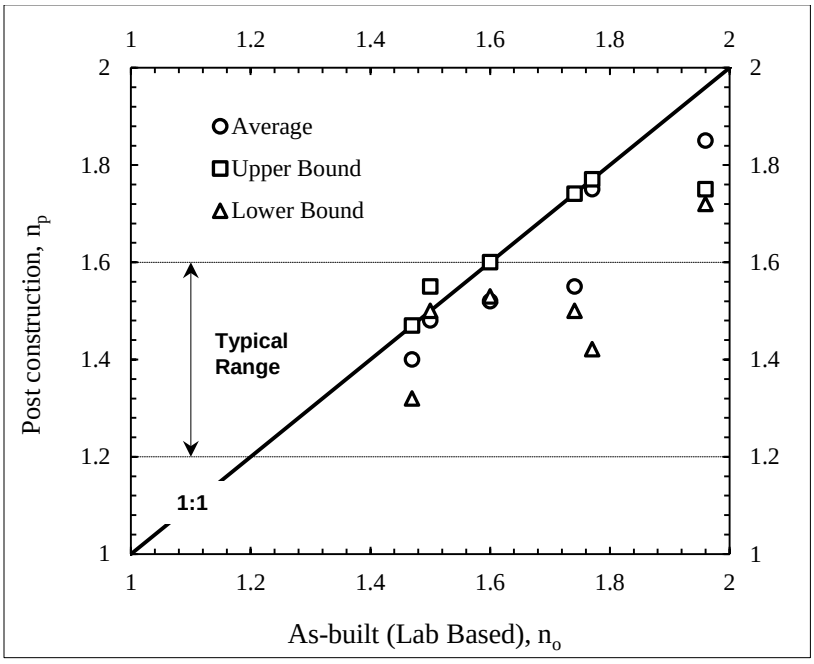

(b)

Figure 4.16 Post construction changes of α and n parameter

The field average of the α parameter for different lysimeter soils increased by a multiple of 2.69 to 20 from the lab-based results. It is to be noted that the largest increment was found in the soil which initially had a lower value of α. In lysimeter 4, the as-built α was 0.02, and increased to a value of 0.04. The changed values of the α and n parameters for the six lysimeters are listed in Table 4.19.

Table 4.19 Value of α, n and m parameter based on FSWCC

Lysimeter	Upper Bound			Lower Bound			Average		
	α	n	m	α	n	m	α	n	m
1	0.0038	1.60	0.375	0.10	1.53	0.346	0.02	1.52	0.342
2	0.0045	1.55	0.367	0.08	1.50	0.333	0.02	1.48	0.324
3	0.0045	1.47	0.319	0.05	1.32	0.242	0.01	1.40	0.286
4	0.0018	1.75	0.375	0.15	1.51	0.338	0.04	1.85	0.459
5	0.0031	1.77	0.435	0.12	1.42	0.296	0.02	1.75	0.429
6	0.0035	1.74	0.4257	0.08	1.50	0.333	0.02	1.55	0.355

4.4.3 Change of Θ_s and Θ_r

Changes in saturated (Θ_s) and residual (Θ_r) volumetric moisture content was computed based on FSWCC. FSWCC was divided into three regions: upper bound, lower bound, and average. The values of Θ_s and Θ_r obtained from the three regions are presented in Table 4.20. There is a significant difference in the Θ_s values between the upper bound and the lower bound. The Θ_s values in the lower bound were approximately 7% to 22% lower than the upper-bound values in the six lysimeters. Therefore, under the same meteorological condition, the soils from the different lysimeters experienced different Θ_s. Rainfall intensity, initial compaction of the cover soil, hysteresis effect, pedogenesis process, change in pore water pressure, change in soil structure, etc. could be potential reasons for these changes in the Θ_s values. Θ_r was also found to adopt changed values. The plant root system is a potential factor for Θ_r, as each plant has a unique adaptability to use the stored water in the cover.

Table 4.20 Saturated and residual volumetric moisture content based on FSWCC

Lysimeters	Upper Bound		Lower Bound		Average	
	(Θ_s)	(Θ_r)	(Θ_s)	(Θ_r)	(Θ_s)	(Θ_r)
L-1	0.385	0.120	0.350	0.11	0.360	0.117
L-2	0.415	0.120	0.380	0.11	0.398	0.117
L-3	0.429	0.090	0.350	0.09	0.390	0.095
L-4	0.410	0.110	0.320	0.09	0.350	0.105
L-5	0.404	0.111	0.330	0.09	0.375	0.105
L-6	0.409	0.099	0.380	0.09	0.394	0.097

The change in Θ_s from FSWCC, compared to the as-built (laboratory based Θ_s) condition, was evaluated. The ratio (SWCC/FSWCC) of the Θ_s values are listed in Table 4.21. The Θ_s was slightly lower than the lower-bound and average values. However, the ratio of Θ_s with the upper bound values was close to one. On the other hand, the change in Θ_r was very negligible. As can be seen from Figure 4.17, the values lie on the 45^o straight line.

Table 4.21 Ratio of saturated volumetric moisture content Θ_s (SWCC/FSWCC)

Lysimeters	(Θ_s)		
	lab/upper bound	lab/lower bound	lab/average
L-1	1.032	1.135	1.103
L-2	0.992	1.084	1.035
L-3	1.000	1.225	1.099
L-4	0.976	1.250	1.143
L-5	1.000	1.223	1.077
L-6	0.999	1.076	1.037

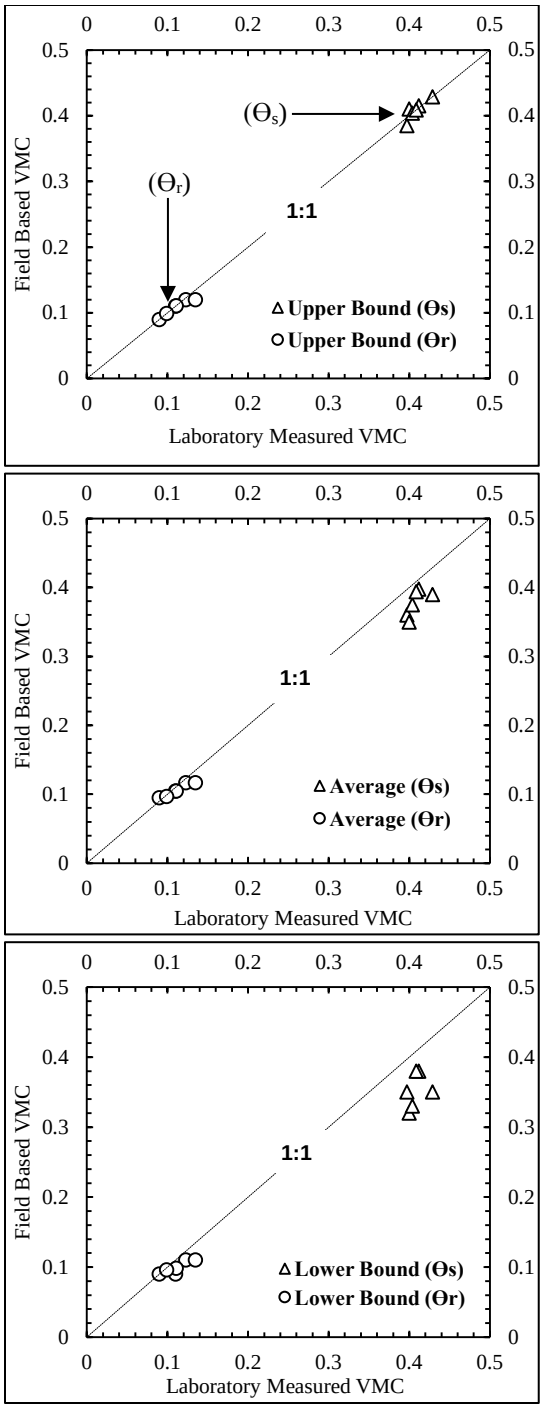

Figure 4.17 Post-construction changes in Θ_s and Θ_r

Chapter 5

Investigation of Plant Root

5.1 Introduction

The objectives of this chapter are to investigate the behavior of the evapotranspiration cover (ET cover) plant root. Vertical root growth, lateral elongation of root, and quantification of root length, based on the minirhizotron technique, are presented in this chapter. Image analysis was conducted using ImageJ software and has been extensively used for the quantification of roots. Root investigation results from destructive testing is also presented, and the effect of soil bulk density on root growth has been evaluated. A comparison study, between the minirhizotron-based root density and destructive sampling, was also conducted. A geophysical investigation was included to characterize the ET cover plant root. The investigated parameters, using different methods, are summarized in Table 5.1.

Table 5.1 Influential plant parameters on optimum ET cover performance

Method	Investigated Parameter
Minirhizotron	Vertical root growth
Minirhizotron (Image analysis)	Root length, root density
Shelby tube	Root density
Geophysical method (ERI)	Detecting root zone

5.2 Typical Characteristic of In-situ ET Cover Vegetation

The vegetation used in the different lysimeters is typically summer grass that has a high growth rate. All of the vegetation has a longer life span to effectively serve the purpose of the ET cover. The pH range for the vegetation to adapt efficiently to the soil is typically from 4 to 8. The grass can adjust its growth during winter, even during freezing temperatures. Bermuda grass has the highest moisture use among all of the vegetation

types. It uses more moisture and releases the highest amount of water to the environment through the transpiration process. The important characteristics of the vegetation are listed in Table 5.1.

Table 5.2 Typical characteristics of in-situ vegetation

Characteristics	Native Trail Mix	Switch Grass	Bermuda Grass
Active Growth Period	Summer	Summer	Summer, Fall
Growth Rate	Rapid	Rapid	Rapid
Height, Mature (feet)	4	5	2
Lifespan	Long	Long	Long
Adapted to Fine Textured Soils	Yes	Yes	Yes
Drought Tolerance	Medium	Medium	Medium
Fertility Requirement	High	High	High
Fire Tolerance	High	High	High
Moisture Use	Medium	Medium	High
pH Range	4.5-8.0	4.5-8.0	5.0-8.0
Root Depth, Minimum (inches)	12	12	14
Temperature, Minimum (°F)	-30	-43	-8
Bloom Period	Mid-Summer	Mid-Summer	Late Spring

5.3 Root Investigation Using Acrylic Tube (Minirhizotron)

The main objective was to develop and connect a methodological framework to efficiently examine the plant root dynamics in an ET cover system through the installed minirhizotron technology. Several root dynamics were investigated, using the non-destructive method. The following subsections describe the results obtained from the minirhizotron study.

5.3.1 Root Penetration Depth into ET Cover

The root depth for each of the grass types in each lysimeter was measured through the minirhizotrons. Initially, before the installation of the minirhizotrons, root depth into the cover soil was obtained by direct excavation of small pits at random locations in the lysimeters. Later, the root depth measurements were made by observation through the

minirhizotrons. The minirhizotron technique offers two major advantages in the measurements of root depth and distribution. The first one is that the destructive sampling used to measure root depth is no longer required. The second one is that the technique allows the evaluation of the dynamics of root growth at the same point of the same plant. This section describes the root penetration depth into the soil and evaluates the root growth function.

The three grass types in the six lysimeters were Native Trail grass (NT) in Lysimeters 1 and 4; Switch grass (SG) in lysimeters 2 and 5; Bermuda grass (BG) and Hulled Common Bermuda grass (HB) in lysimeters 3 and 6, covering 50% in each of the lysimeters. The measured root depth into the lysimeter soils ranged from 13 inches (33 cm) to 20 inches (50.8 cm) till April 2017. The measured root depths of different plants are listed in Table 5.3. Based on the field observation, the Bermuda root type, mainly the HB root system, penetrates the deepest (20 inches). NT and SG have almost equal root depth at different lysimeters, ranging from 13 to 15 inches. Time-dependent vertical root penetration depths (time series analysis) for different plants are presented in Figure 5.1. It is to be noted that all of the root systems extended beyond their typical minimum root depth, and it took approximately 500 days to reach that point under the field climatic conditions.

Table 5.3 Measured root depths of different grass (Till April 2017)

Grass Type	Mix of Native Trail, Perennial Wildflower Mix, and Caliche (NT)		Mix of Upland Switchgrass, Perennial Wildflower Mix, and Caliche (SG)		Common Bermuda Grass (BG)		Hulled Common Bermuda Grass (Grade 90/80) (HB)	
Lysimeters	L-1	L-4	L-2	L-5	L-3	L-6	L-3	L-6
Root Depth (inch)	14	15	14	13	15	17	18	20

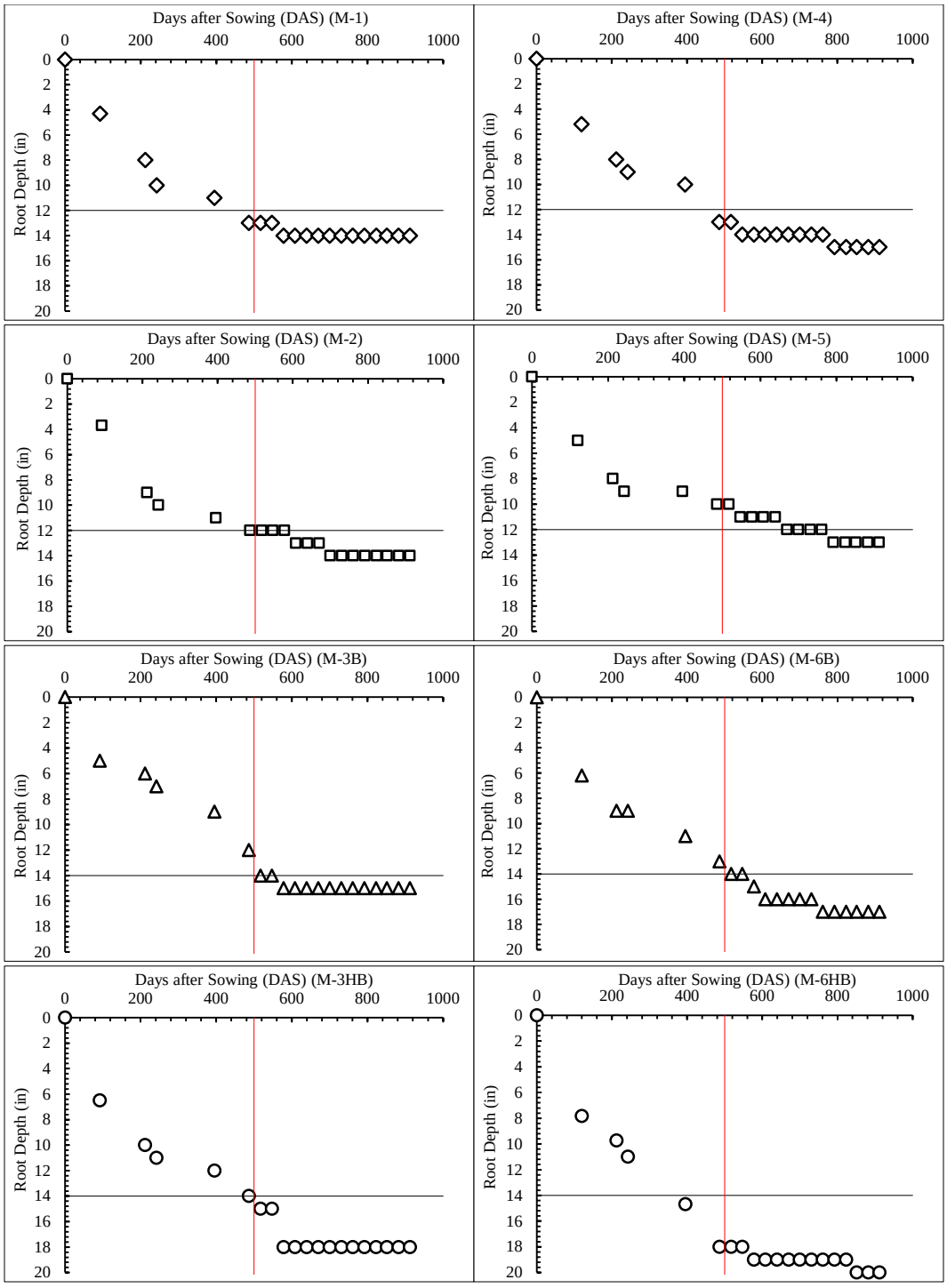

Figure 5.1 Measured root depths at different times of the year

The vertical root growth rate for all of the grasses was faster for the first 100 to 200 days. A 9 to 11-inch root depth was recorded in first 200 days. Based on field observation, the root growth rate was 0.01 inch/day to 0.065 inch/day during the rapid root growth period. But the growth rate slowed down after 200 days, and this relatively slower rate of root growth continued. After almost 500 days, the root growth almost ceased in all of the monitoring minirhizotrons. It was observed that the ceasing of vertical root development occurred when the root structure penetrated around 12 to 15 inches into the soil. Among all the grass types in the lysimeters, the HB root system had the highest root penetration depth (18 to 20 inches). A root growth rate below 12 to 15 inches can be attributed due to the existence of a denser soil layer, formed during construction and subsequently induced by pedogenetic compaction in the soil profile. This highly compacted soil results in a dense concentration of roots in the upper part of the ET cover soil and reduced rooting in the deeper layers.

Different curve-fitting functions (polynomial, power, exponential) were executed in an attempt to develop a root growth function, based upon observing root growth in the field. Eventually, root growth into the ET cover was found to follow the simplest parabolic function which best suited the field observation points (Figure 5.2). The following equation represents the field-fitted root growth function.

$$y^2 = Rx$$

x = Time in days

y = Root depth in inches

R = Field-fit coefficient of vertical root extension or root growth with unit (inch^2/day)

Different root growth coefficient (R) values were attained for the various lysimeter plants during the generation of the functions. Grass roots of several types were fitted with ‘R’ values. A higher coefficient value indicated higher growth rate. The Hulled Bermuda

grass root was found to have the highest growth rate coefficient in both lysimeters 3 and 6, based on the curve fitting of different grass roots in different lysimeters. The root growth coefficients for different plants in different lysimeters are listed in Table 5.4.

Table 5.4 Coefficient of root growth for different grass

Lysimeter	Grass Type	Field Fit Coefficient (R)
1	NT	0.357143
4		0.370370
2	SG	0.333333
5		0.270270
3	BG	0.384615
6		0.416667
3	HB	0.555556
6		0.666667

It is obvious from Figure 5.2 that the root growth functions were in good agreement with the field-measured data until it reached the denser soil layers, where the root depths followed an almost-flat path. Therefore, the generated functions represent the continuous path of vertical root penetration into the ET cover under favorable growing conditions.

Based on the field observation of vertical root growth, Bermuda grass, mainly the Hulled Bermuda (Grade 90/80) grass, had the highest rooting depth. The rooting depths differed during the monitoring period according to plant types, even though they were under the same meteorological conditions. Therefore, it was concluded that the plant's intrinsic characteristics drive the plants to adapt to environmental conditions. Thus, based on the rooting depth characteristics only, it can be concluded that Bermuda grass is more suitable for the ET cover system than other plants, as it's root system is adaptable to changes in climatic conditions.

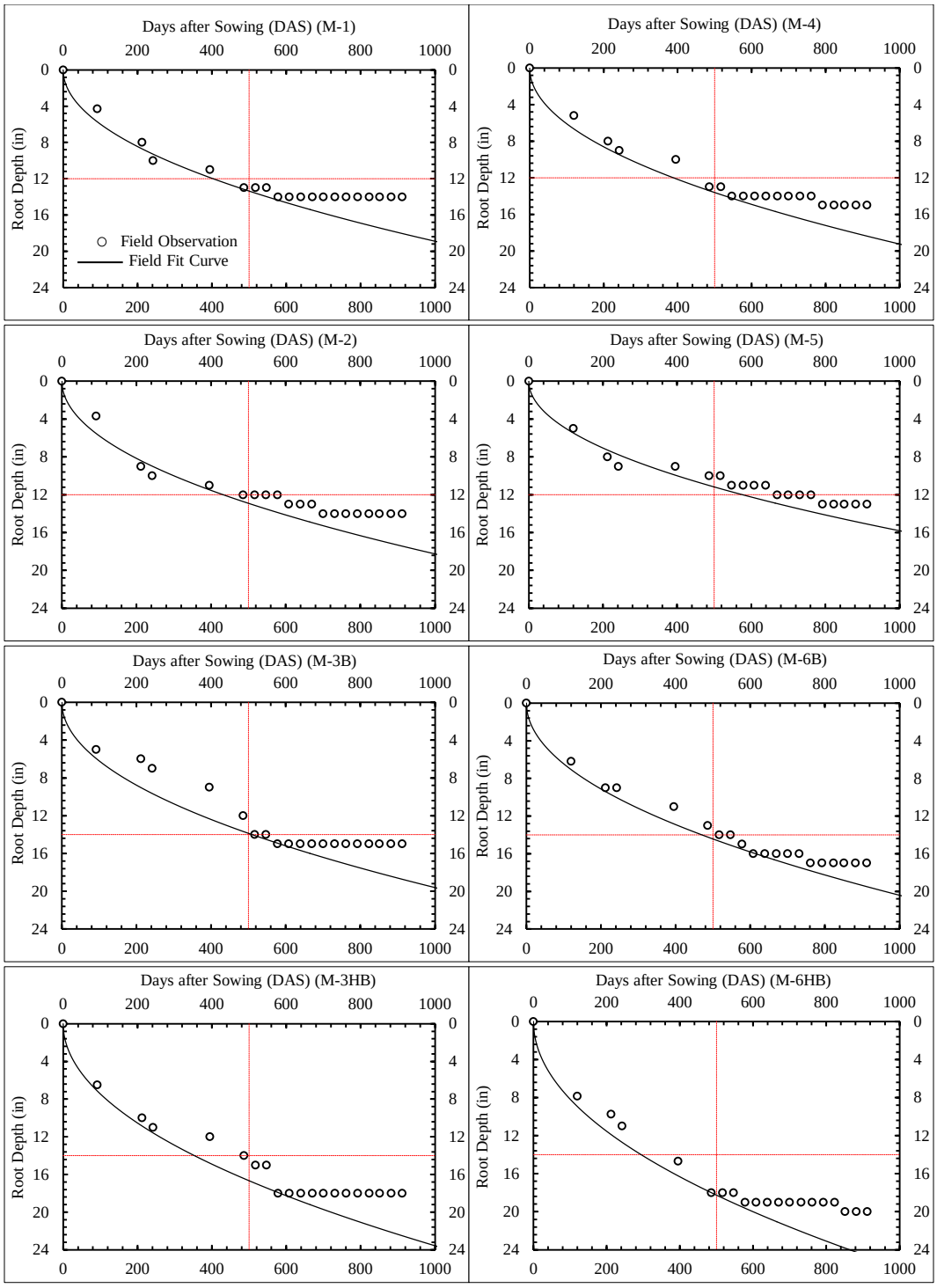

Figure 5.2 Field-fit root depth function

5.3.2 Image Processing

Images obtained through the minirhizotrons were subjected to processing before quantification. Several steps, described in the following sections, were implemented before the actual root measurement.

5.3.2.1 Defining Image Area and Pixel

The first step in the image processing was to set the perimeter of the image in pixel units. Based on the calibration process during the image acquisition from the minirhizotron, the size of the image was 4.5 inches (W) × 3.0-inches (H). The image was then opened with the ImageJ program, and based on the known dimensions of the image, ImageJ automatically found the distance in pixel units. The width of the image was 4.5 inches, which is equivalent to 3,024 pixels (Figure 5.3 a), and the height of the image (3 inches) corresponded to 2,041 pixels (Figure 5.3 b). Thus, the size of the image in pixel units was (W) 3,024 × (H) 2,041, with every 1 inch of distance representing 672 pixels (Figure 5.3). During the image acquisition, due to human error, the dimensions of the images were not always 4.5 inches (W) × 3.0 inches (H). The calculated maximum error was approximately 3%. To maintain consistency in the measurements, 672 pixels were considered the standard for all of the images.

Attempts were made to capture images inside the minirhizotron, at various depths and sections, to fulfill different objectives of the analysis. The most challenging and difficult part of obtaining the images was retrieving an image with an all-inclusive area at a fixed depth. The perimeter of the minirhizotron was 18.8 inches (478 mm). The width of each image was 4.5 inches (114.3 mm). Therefore, images taken at every 90^{o} angle, at a fixed depth all around the minirhizotron, covered 18 inches (457.2 mm) of the actual perimeter. So, approximately 4% of the area at every depth interval of the minirhizotron was not included in the root quantification.

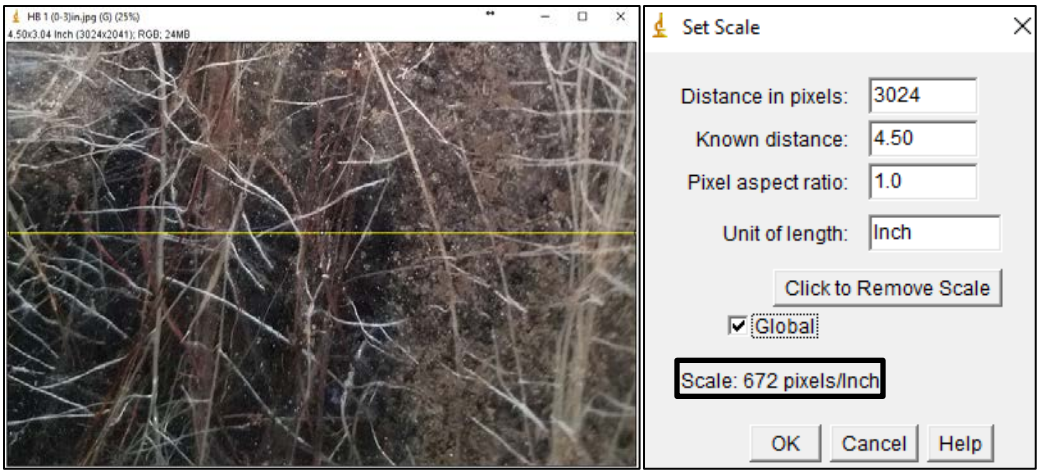

(a)

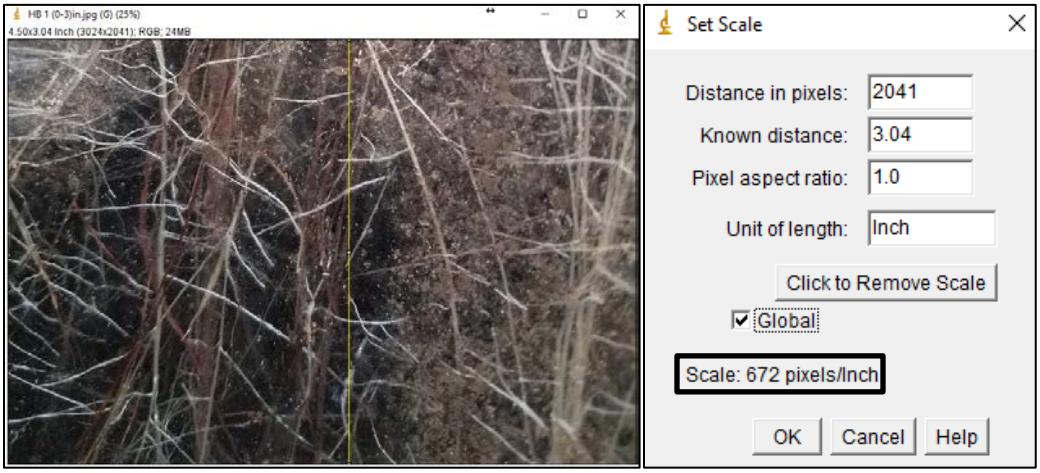

(b)

Figure 5.3 Image scale factor in ImageJ

Figure 5.4 represents the images captured at the top 3-inch depth interval in minirhizotron M-1 (NT), M-2 (SG) and M-3HB (HB). The images taken at the first 3-inch depth were cropped approximately 0.1 inch from the top to avoid portraying surface-dead fescue in the image. The images revealed that the root skeleton of M-3HB was denser than the other two types of roots (Figure 5.4). The images in Figure 5.4 were captured during late summer of 2016, but they were not all taken on the same day.

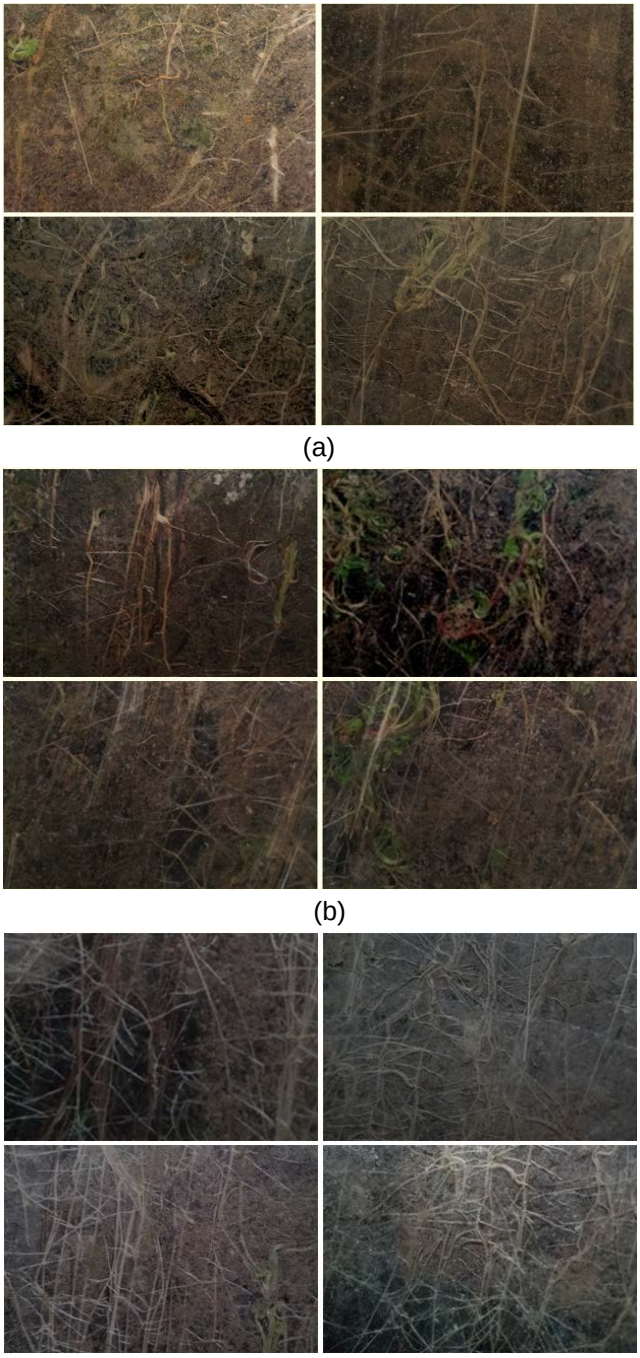

Figure 5.4 Sections of root profile images at top 3-inch segment at every 90^{o} angle (a) Native trail grass, (b) Switch grass, (c) Hulled Common Bermuda grass

The areas of the images photographed at different sections of the minirhizotrons were defined in ImageJ. Through the visual inspection of the raw images, it was obvious that different types of vegetation had different root structures. Differences in color contrast were also observed. Initially, the raw images were transformed into binary images for root quantification and showed a substantial amount of background noise (Figures 5.5, 5.6 and 5.7). Soil particles, water droplets, accumulation of above-ground biomass (grass leaves), and contrasting brightness in the image-viewing area caused the development of the background noise, which hindered identification of the root structure. Therefore, it was essential to improve the image quality to avoid misleading quantification.

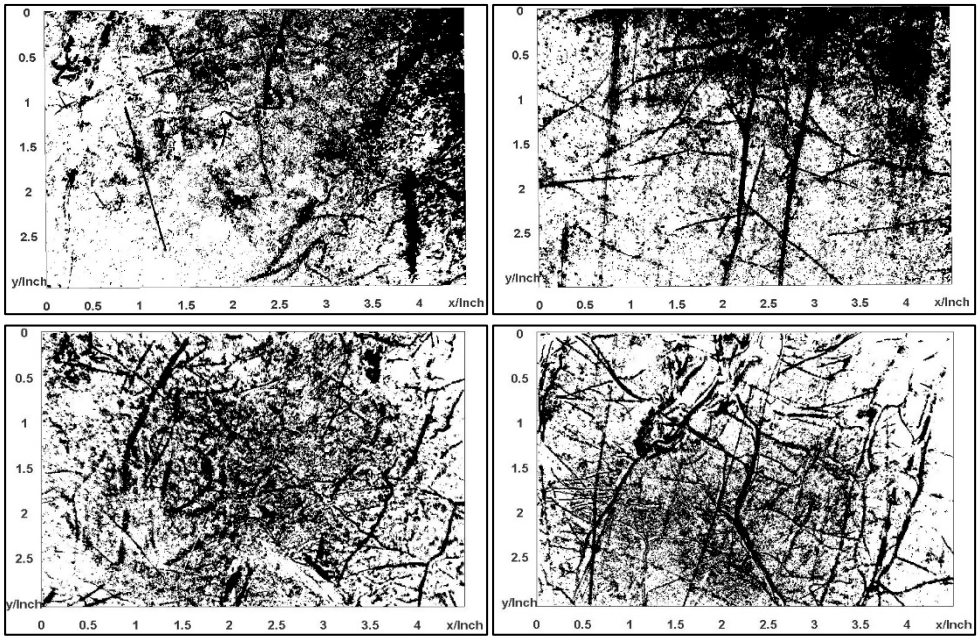

Figure 5.5 Image area demarcated by ImageJ program (Image from M-1)

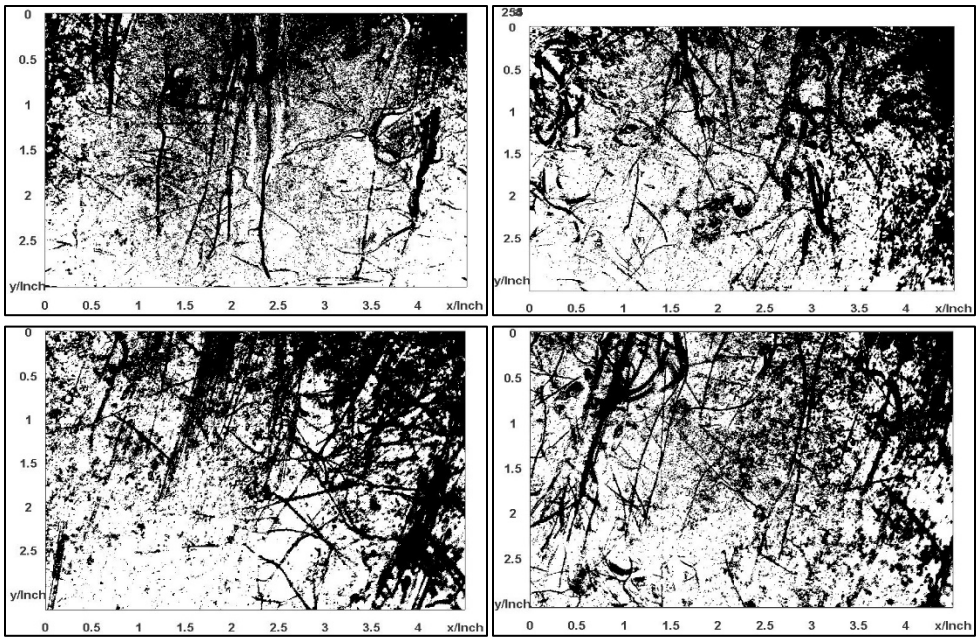

Figure 5.6 Image area demarcated by ImageJ program (Image from M-2)

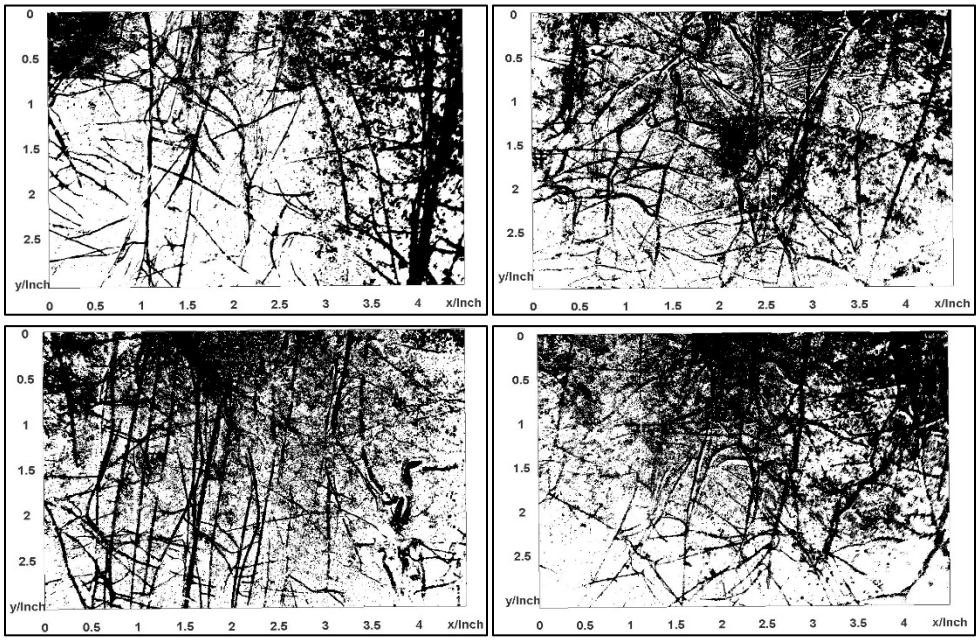

Figure 5.7 Image area demarcated by ImageJ program (Image from M-3HB)

5.3.2.2 Image Enhancement Process

Digital images contain grids of pixels, and each image has a defined bit depth. Typically, in an 8-bit image, pixel values range between 0 (black) to 255 (white). This implies that the gray scale of the image has $2^8 = 256$ steps in dividing the grayness of the image between black and white. In a 16-bit image, the grayness of the image is divided into 2^{16} (65536) steps. Therefore, a 16-bit image can take any integer value between 0 (black) to 65535 (white) (Megahed, 2012). Root skeletons in the images captured from different minirhizotrons in the study area were not always directly readable by the software. The presence of water molecules and buildup of soil particles and other obstacles in the image-viewing area were frequently found in the images. These factors are considered noise in the image, and may lead to misleading quantification. During the study period, images were captured from the minirhizotrons at different times of the day on different dates, often causing variability in image brightness and contrast. The root skeleton was less visible in some of the images. Additionally, there was less light in the images captured from the deeper depths of the minirhizotron. Therefore, to quantify the root structure, the quality of the images had to be improved by reducing artifacts and removing noise to the extent possible.

Several steps were executed to enhance the images by correcting the noise and defects in the images. The images originally captured from the minirhizotron were in the RGB format and were converted to 8-bit greyscale images. The 8-bit images were then processed for noise and defects removal. Two types of stains were observed in the images: water droplets after rainfall and an accumulation of soil particles. Corrective procedures were applied, based on the degree of noise that existed. Small variations in pixel distribution, due to water molecules and insignificant soil accrual within the images, were minimized by filtering the image. Median filtering was executed in such cases. Median

filtering is considered a suitable image corrective method, as it doesn't generate any new impractical pixel values within the images (Marion, 1991). Image filtering in the ImageJ program works by calculating the median value of the pixel intensity of the neighboring pixel values. The median pixel value then replaces the initial pixel value. Figure 5.8 illustrates a general median filtering matrix. The central pixel value of 138 is larger than the other 8 neighboring pixel values; 116 is representative in this case. In this dissertation, a consistent value of 5 pixels was applied for the median filtering of all of the images.

100	117	118	125	128
107	115	104	116	129
114	105	138	109	122
106	108	112	119	110
118	99	111	123	120

Figure 5.8 Median filtering matrix

A wide variation of pixel intensity is mainly prevalent when a large area in the image is occupied by soil clustering and/or daylight effect (image brightness and contrast). It may exist even after the median-filtering process. This wide variation of pixel distribution was amended by a background subtraction (BS) algorithm. The BS process calculates the mean pixel intensity over the neighboring pixels. The mean value is then subtracted from the initial pixel value. A constant rolling ball radius of 20 pixels was applied to all of the BS processes, for all of the images analyzed through the ImageJ program. In some of the images, after the BS application, a Gaussian filtering was applied to obtain a smooth root skeleton for more precision. Figure 5.9 shows the state of images after the application of different image-enhancement processes. In Figure 5.9 (e), the binary image was obtained from the further image improvement, through the segmentation process.

(a) (b) (c) (d) (e)

Figure 5.9 Image processing steps: (a) original RGB Image (b) 8-bit image (c) processed after median filtering (d) image after BS process (e) transformed binary image

The next step of image enhancement was to execute the segmentation process. Image segmentation is the process of disintegrating the image into different pixels (Barrow and Tenenbaum, 1978; Haralick and Shapiro, 1992). In this process, the image is differentiated or segmented by local intensity, neighboring pixels, or spatial position.

In the current research, automated thresholding was applied for the image segmentation by the ImageJ program. The image-thresholding technique transformed the images into black and white images, which are called binary images. ImageJ contains sixteen thresholding algorithms, and initially, all of them were evaluated. Based on several automatic thresholding algorithms on different images, five algorithms were finally selected for quantification and were applied for the evaluation of the images. The five algorithms are: Isodata (Ridler and Calvard, 1978), Li (Li and Lee, 1993; Li and Tam, 1998), Moments (Tsai, 1985), Otsu (Otsu, 1979), and Triangle algorithms (Zack et al. 1977). Adu (2014) found that the same five algorithms worked satisfactorily for segmentation of the root systems. Figure 5.10 depicts the sixteen images evaluated by the automated segmentation process on a HB root system whose image was obtained from M-3HB. Figure 5.10 clearly demonstrates the suitability of the selected five algorithms.

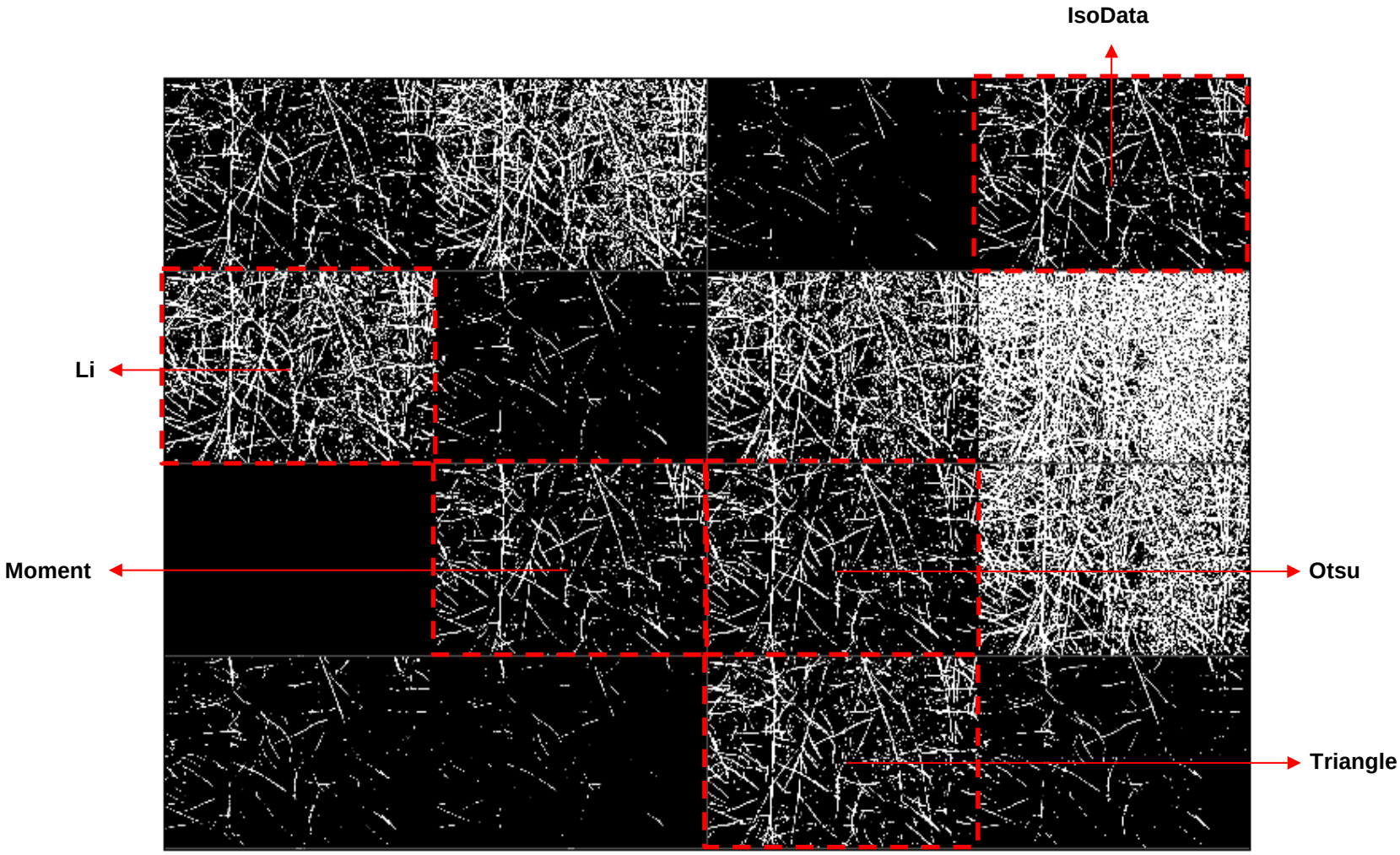

Figure 5.10 Auto thresholding of Hulled Bermuda root system for different algorithms

All of the root images exhibited a considerable amount of background noise, but the noise-reduction process removed the majority of the noises from most of the images captured through the minirhizotron. A small amount of noise was still found in the images after the corrective measurements, through the reflection from the small soil particles which were visible in the image as scattered black dots (Figure 5.11 b). Figure 5.11 shows the differences of the images before and after the corrective actions. Nonetheless, the revised images are representative enough for root quantification.

Figure 5.11 Noise distribution (a) before corrective measures (b) after corrective measures

All of the images captured from different minirhizotrons were subjected to corrective measurements before root quantification. Enhanced images from M-1, M-2 and M-3HB are presented in Figure 5.12. 3D distribution of gray values (pixels) of the corrected images (M-3HB) are also presented in Figure 5.13. Where, x axis and y axis represent the length and width of the image and z axis represents the distribution of the image pixel. The 3D distribution of pixels is presented for the images captured from M-3HB (four images surrounding 360^{o} of the minirhizotron at 3-inch depth) in summer 2016.

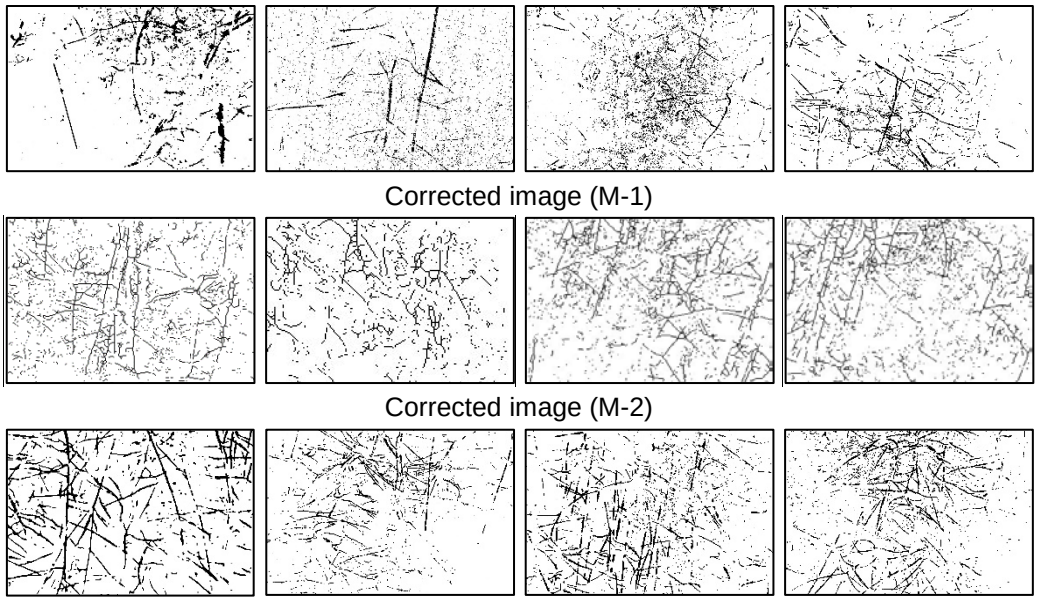

Figure 5.12 Processed image after corrective measures

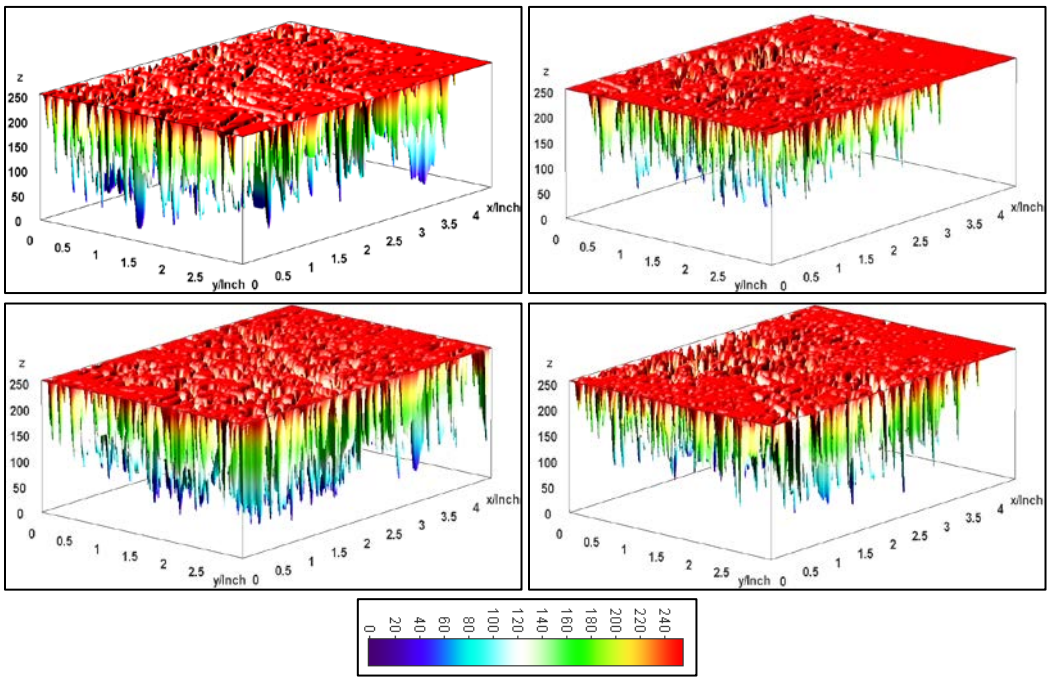

Figure 5.13 3D imagining of root distribuion for each individual image section of HB root at top 3-inch segment of the minirhizotron (M-3HB)

5.3.3 Root Intensity Detection Using Image Analysis

ImageJ is an image-processing program that is suitable for determining distances and angles, calculating area and pixel value statistics, and providing density histograms and line profile plots. Using this software, attempts were made to perform profile plots of the entire ET cover root zone to detect the root distribution. Profile plots display a 2-dimensional diagram of pixel intensities of an image along a line within the image. Images captured from the minirhizotron throughout the root zone depth at different segments were subjected to plot profiling. The intensity plots for the images captured from M-3HB are presented in this section. The images were acquired along the length of the minirhizotron, from 0 to 15-inch depth at 3-inch intervals. Based on the calibration of the minirhizotron camera, the images were 4.5 inches (w) × 3 inches (h). The images were obtained along a fixed section throughout the depth on the same day (August 20, 2016).

The line plot in the ImageJ program shows the intensity profile of pixels along a section. Figure 5.14 presents the original RGB image of HB roots in the top 3-inch depth. To determine the pixel intensity, a linear region of interest (ROI) was selected at the middle of the image to output the graph of pixel intensities along the line. The plot profile of pixel intensity of the RGB image of the top 3-inch segment is presented in Figure 5.15. High peaks of the gray value in the figure illustrate the detection of roots, and the lower gray values or the medium ranged gray values indicate pixel intensity of the soil.

Figure 5.14 Original RGB image of HB roots (top 3 inch segment)

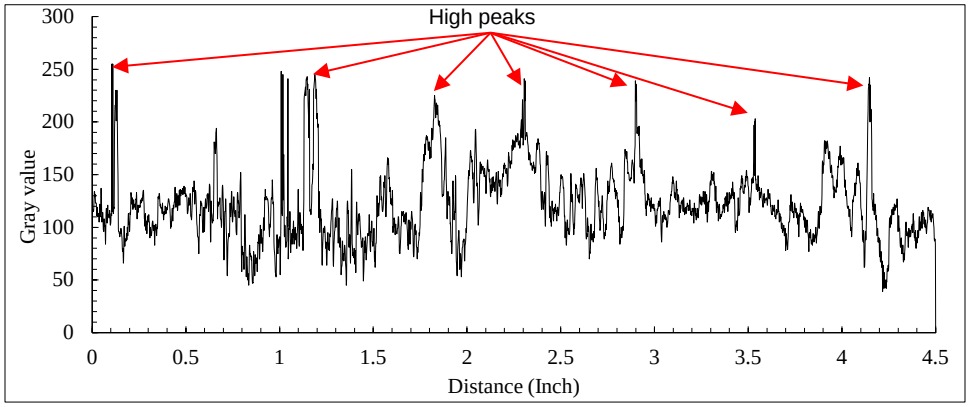

Figure 5.15 ImageJ profile plot of RGB image of HB roots (M-3HB) (segment top 3 inch)

The ImageJ program can also plot the profile intensity of binary images. In an 8-bit binary image, the number is stored as an integer, with a gray value of 0 and 255. Usually, 0 is taken as black, and 255 as white. Figure 5.16 shows the line profile plot of root images in different sections in the binary mode. The root skeleton in the binary image is depicted by the red lines on the black background. The line profile tool in ImageJ clearly distinguishes the roots from the background. In all of the pictures in Figure 5.16, where there is root, there is a peak value of 255 throughout the section; otherwise, it shows a 0 gray value.

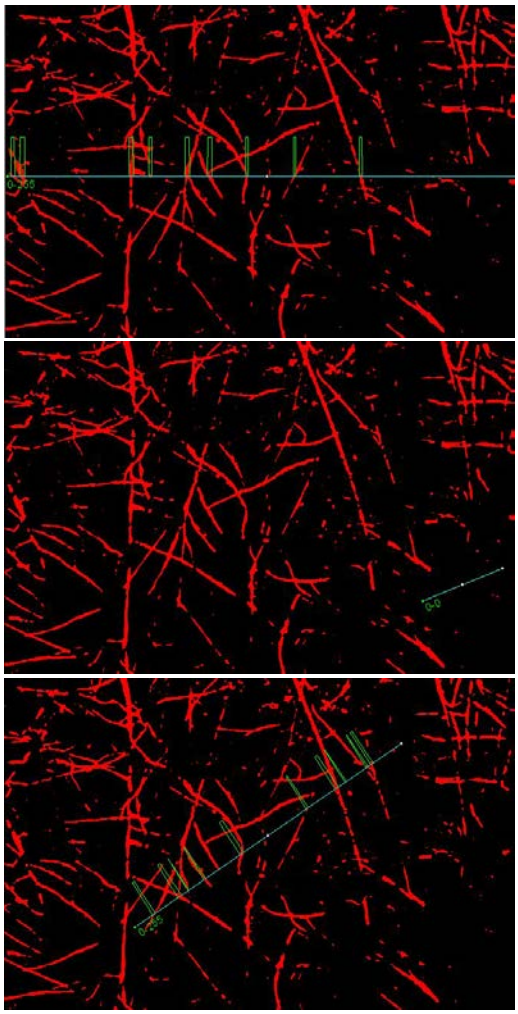

Figure 5.16 Line profile plot to differentiate roots from other objects in binary image

Figure 5.17 represents the processed binary image of the original RGB image of Figure 5.14. The RGB image was defined as a 16-bit image and converted to a binary image. Before processing the image to binary mode, background subtraction was applied to remove the possible noise. The black lines on the white background are the roots of the fixed area (4.5-inch width and 3-inch height). The ROI was set at the middle of the image, along the width at 1.5-inch depth. The plot profile of pixel intensity of the binary image is presented in Figure 5.18.

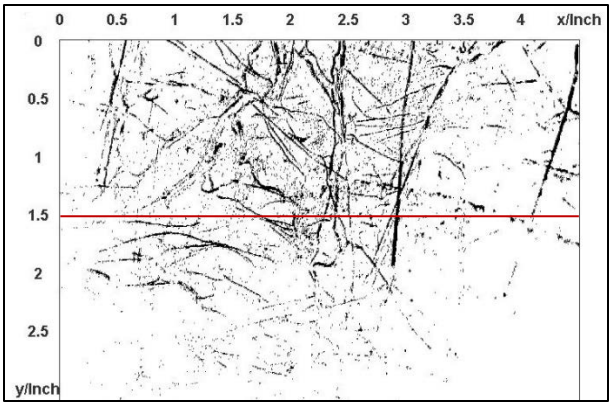

Figure 5.17 Root area defined by ImageJ after binary process (HB)

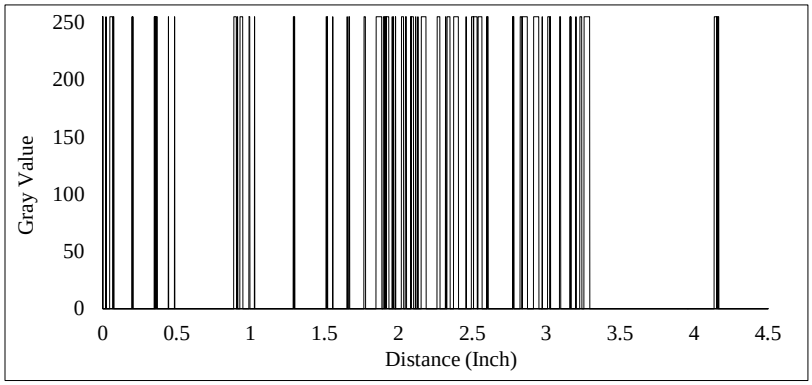

Figure 5.18 ImageJ profile plot of binary image of HB roots (segment top 3 inch)

The plot profile in Figure 5.18 shows only two gray values, 0 (white) and 255 (black). The peak values along the ROI epitomize the detection of roots, whereas the voids in the figure represent the soil.

For the root zone detection of lysimeter 3, all of the images captured throughout the depth from minirhizotron (M-3HB) were subjected to background subtraction for noise removal. The images were then converted to binary image. ROI was set at the middle of the images. The plot profiles for the images are presented in Figure 5.19. The figures clearly differentiate the root intensity of different images. The plot profiles for the 0 to 3-inch and 3 to 6-inch segments are almost similar. This indicates that the root density at the

first 6-inch depth of HB grass in lysimeter-3 is almost parallel. A drastic decline in the root density was observed below 6-inch depth, as the plot profiles show gradual reduction in the black gray value (255) as it moves to the deeper depths. In 12 to 15-inch image segments, the 8-bit and binary images clearly outline the penetration of three root branches beyond twelve-inch cover depth. This was clearly identified by the pixel distribution in the profile plot. The intensity profile, through image analysis, concludes that the root density of HB grass type in lysimeter-3 decreases with depth. Results obtained from destructive sampling support this conclusion and are presented in Section 5.4. Further, the ERI method validates the conclusion drawn from the intensity profile method. An intensity profile could be a potential method to use to identify the root density throughout the root zone depth; however, background noise in the images could be a potential source of error in the root zone detection process.

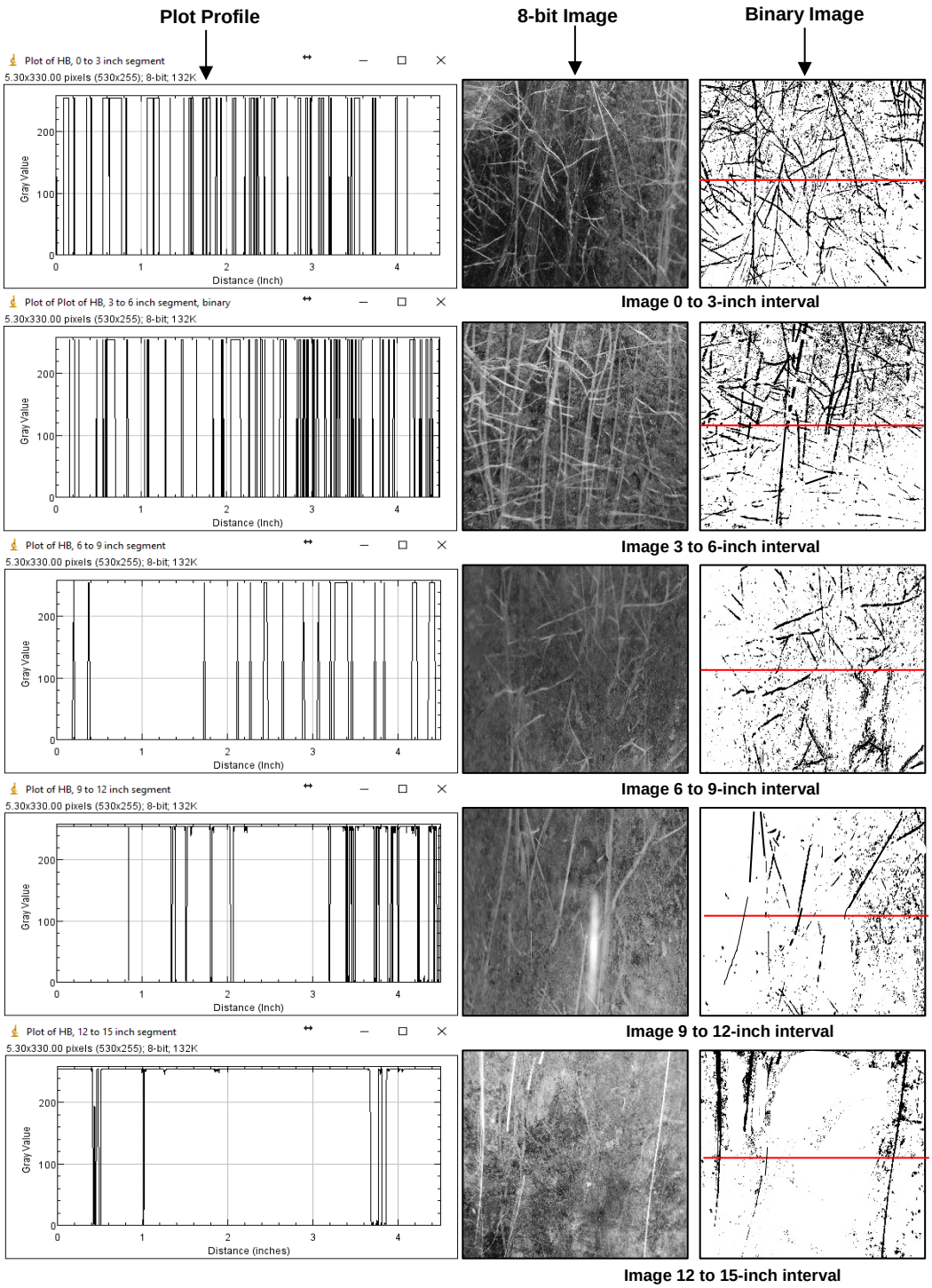

Figure 5.19 Profile of root distribution for Hulled Common Bermuda grass (pictures photographed during early fall 2016)

5.3.4 Determination of Root Length

Images taken from inside the minirhizotron at a fixed depth were used to compute the root length of various vegetation types with the ImageJ program. The length of the root skeleton in the images was obtained by measuring the pixel distance of the roots and then converting the pixels to cm/inch units. Some of these results were further compared with the root lengths measured with the root analyzing program, SmartRoot (Lobet et al. 2011). It was found that the SmartRoot program overestimated the root lengths; however, the results from these two methods showed similar root length magnitudes. Root images obtained from M-1 (NT, photographed in one direction inside the minirhizotron and segmented by automated thresholding, are presented in Figure 5.20. The five most suitable thresholding segmented images are presented.

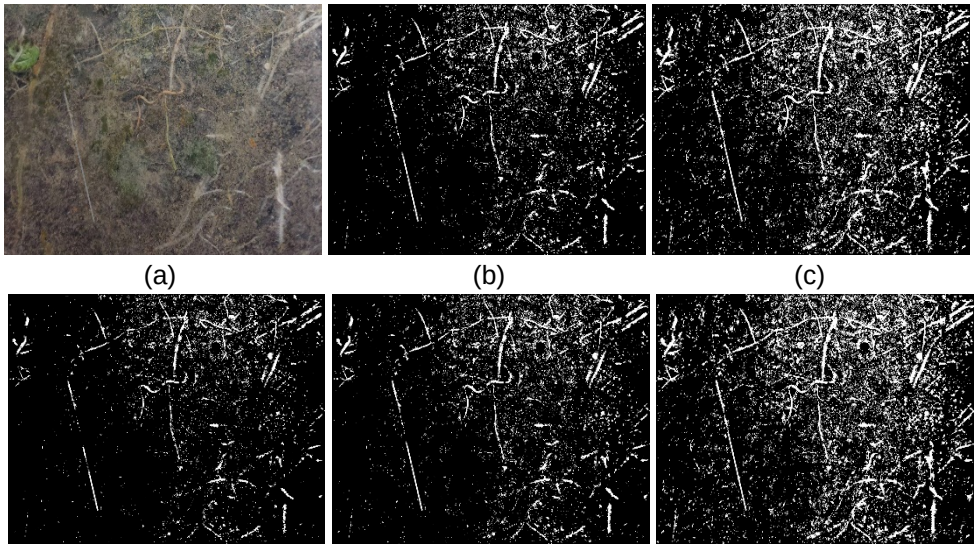

Figure 5.20 RGB image of a Native Trail grass (Image-1) root system segmented with ImageJ automated threshold-based algorithms. (a) Original RGB image, segmented with (b) Isodata, (c) Li, (d) Moment, (e) Otsu, (f) Triangle algorithms

Root lengths measured, using the ImageJ program, are presented in Table 5.5. Results are presented for two sets at 0"-3" depth intervals. Each set is comprised of four images, which includes the 360^{o} view of roots inside the minirhizotron taken at the first 3-inch depth interval. The images were captured on different dates during the monitoring period. Root lengths varied between different algorithms, but the change in root length data was insignificant. Root lengths varied from 75 to 96 cm in different thresholding processes for Set-1, and 68 to 89 cm for Set-2. The average length of roots in different algorithms at the top 3-inch depth ranged from 79.32 cm to 91.2 cm. The maximum average root length value was obtained by the Triangle algorithm; the most conservative algorithm was Moment. A table reflecting all of the statistical data is given in Appendix B.

Table 5.5 Root Length of Native Trail grass from different segmentation algorithms

	Image Side	Threshold Algorithm				
		Isodata	Li	Moments	Otsu	Triangle
	Depth 0"-3"	Root Length (cm)				
Set-1	Image 1	89.527	92.341	83.693	85.124	96.223
	Image 2	84.121	87.124	79.124	81.232	90.659
	Image 3	81.652	85.325	75.365	78.325	88.659
	Image 4	83.214	88.121	79.124	80.998	89.652
	Average	84.628	88.228	79.326	81.420	91.298
Set-2	Image 1	82.403	85.2183	76.569	78.001	89.099
	Image 2	76.998	80.0011	72.001	74.109	83.536
	Image 3	74.529	78.2022	68.242	71.202	81.536
	Image 4	76.091	80.998	72.001	73.874	82.52
	Average	77.505	81.1049	72.203	74.296	84.175

The measured data of root length is also shown in a graph in Figure 5.21. The root length in all of the images was maximum in the Triangle algorithm and minimum in the Moment algorithm. The total root length at the fixed depth of 0-3 inches is also presented in Figure 5.22. The total root length varied between 317.3 cm and 365.2 cm for Set-1, and 288.8 cm and 336.7 cm for Set-2, indicating the root growth or dieback under the in-situ

meteorological condition. The total root lengths were maximum and minimum in the Triangle and Moment algorithms, respectively.

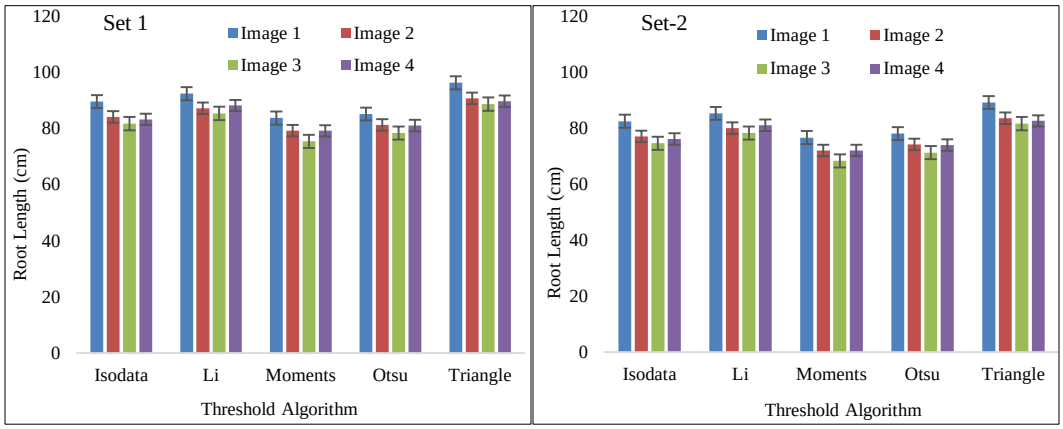

Figure 5.21 Root length of Native Trail grass measured from different algorithms

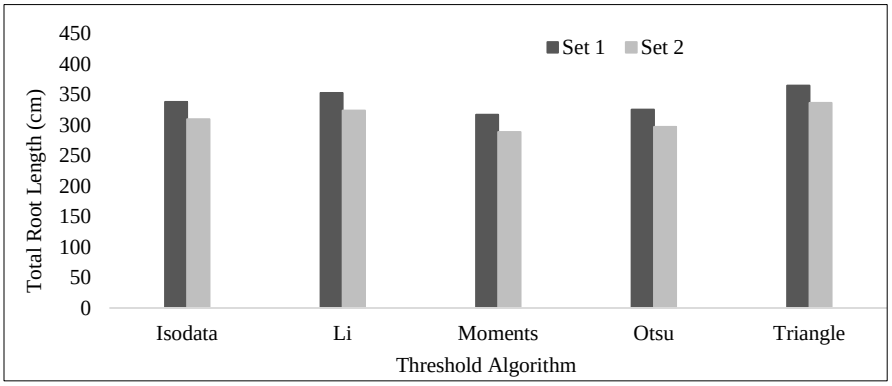

Figure 5.22 Total root length of Native Trail grass estimated from root images captured from four directions in the minirhizotron at depth 0-3 inches and processed with different automated threshold-based algorithms in ImageJ program

One segmented root image of SG, obtained from M-2 at 0 to 3-inch depth based on automated thresholding, is presented in Figure 5.23. The figure shows considerable differences in the white objects (roots) on the black background. Li and Triangle algorithms have greater noise than other algorithms.

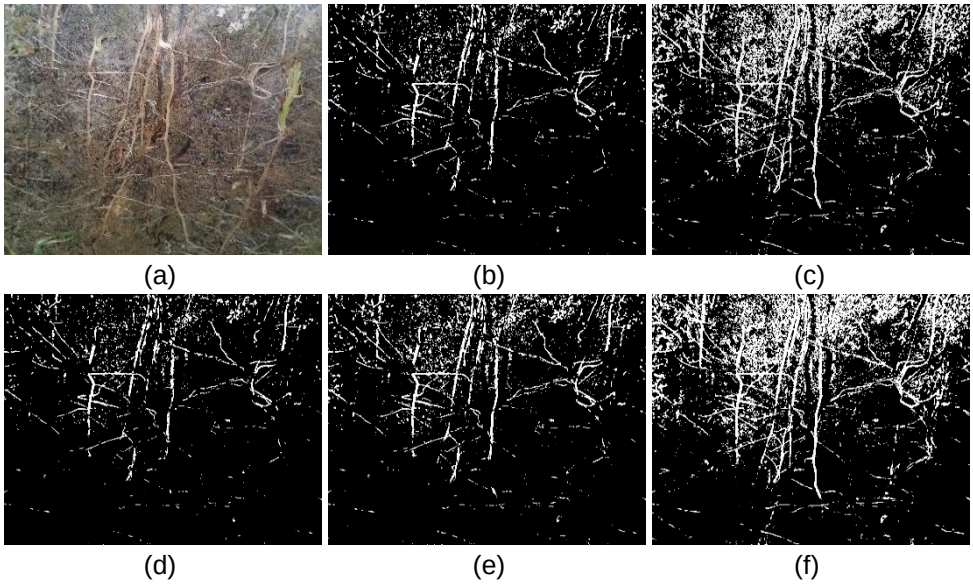

Figure 5.23 RGB image of a Switch grass root system segmented with ImageJ automated threshold-based algorithms. (a) Original RGB image, segmented with (b) Isodata, (c) Li, (d) Moment, (e) Otsu, (f) Triangle algorithms

The root lengths measured with the ImageJ program by different segmentation processes are presented in Figure 5.24. Similar to NT, two sets of data are shown in the figure. Root lengths from individual images were lower in magnitude than NT. The total root length at 0-3-inch depth intervals also differed from NT. Total root length at the fixed depth of 0-3 inches is presented in Figure 5.25. The total root length varied from 281.3 cm to 326.2 cm in Set-1 and from 258.7 cm to 303.5 cm in Set-2. Appendix B shows a detailed data set of root lengths for SG (M-2), with statistical significance.

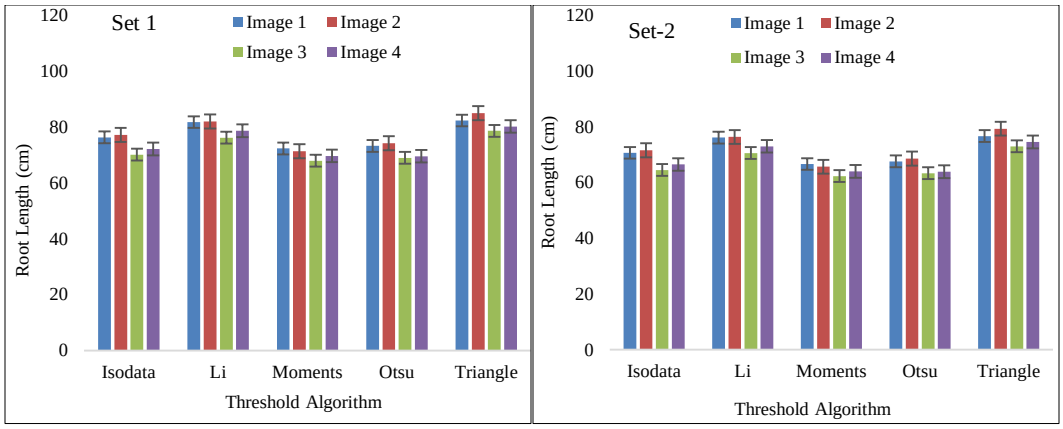

Figure 5.24 Root length of Switch grass measured from different algoriths

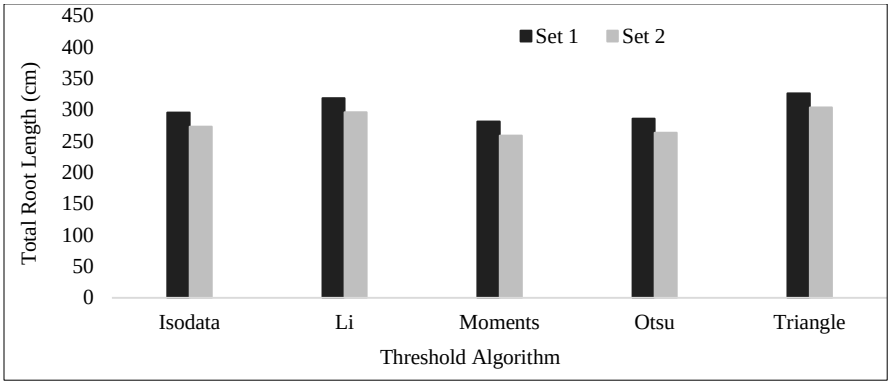

Figure 5.25 Total root length of Switch grass estimated from root images captured from four directions in the minirhizotron at 0-3 inch depth and processed with different automated threshold-based algorithms in ImageJ program

Figure 5.26 shows an image of a Hulled Bermuda root system obtained from M-3HB at 0 to 3-inch depth intervals and segmented with ImageJ's automated threshold-based algorithms. There was very little difference among the algorithms, except for Li, where a considerable amount of noise was visible.

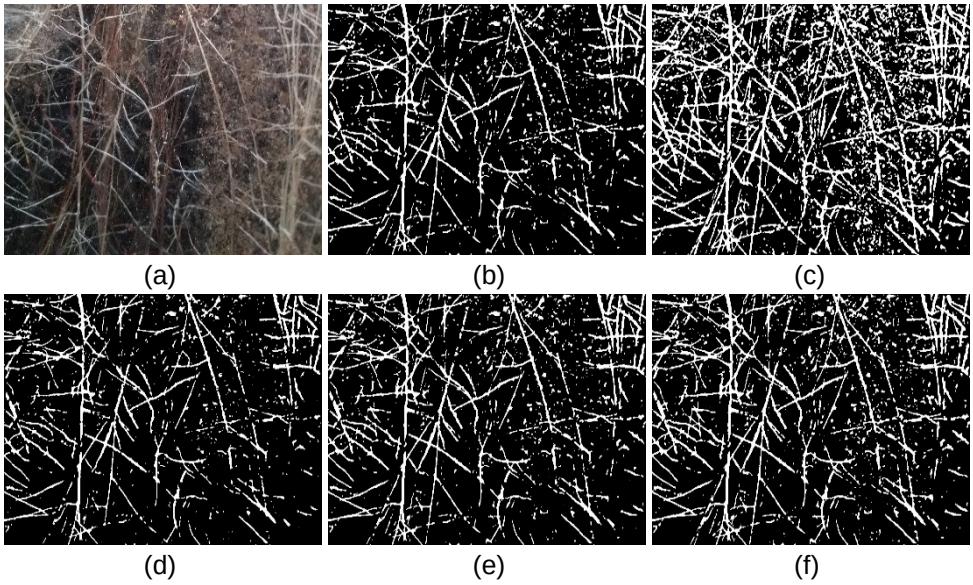

Figure 5.26 RGB image of a Hulled Bermuda root system segmented with ImageJ automated threshold-based algorithms. (a) Original RGB image, segmented with (b) Isodata, (c) Li, (d) Moment, (e) Otsu, (f) Triangle algorithms

Figure 5.27 depicts the measured root length of HB grass. Four sets of data are presented at the first three-inch depth, which means that the results are of images photographed four times at 0 to 3-inch depth and encompassing a 360^{o} inside viewing area. The maximum root length was found for Hulled Bermuda grass and was compared to the other two types of grass. A table including all of the measured root length data is presented in Appendix B. The average root length from individual images varied from 77 cm to 105 cm among the different algorithms. The maximum root length from an individual image was 110 cm in the Li algorithm. It should be noted that the Moment algorithm was conservative in all of the measurements (all grass root types). The total root length at the top 3-inch depth is shown in Figure 5.28. Hulled Bermuda grass roots were the longest, with a maximum length of 422 cm.

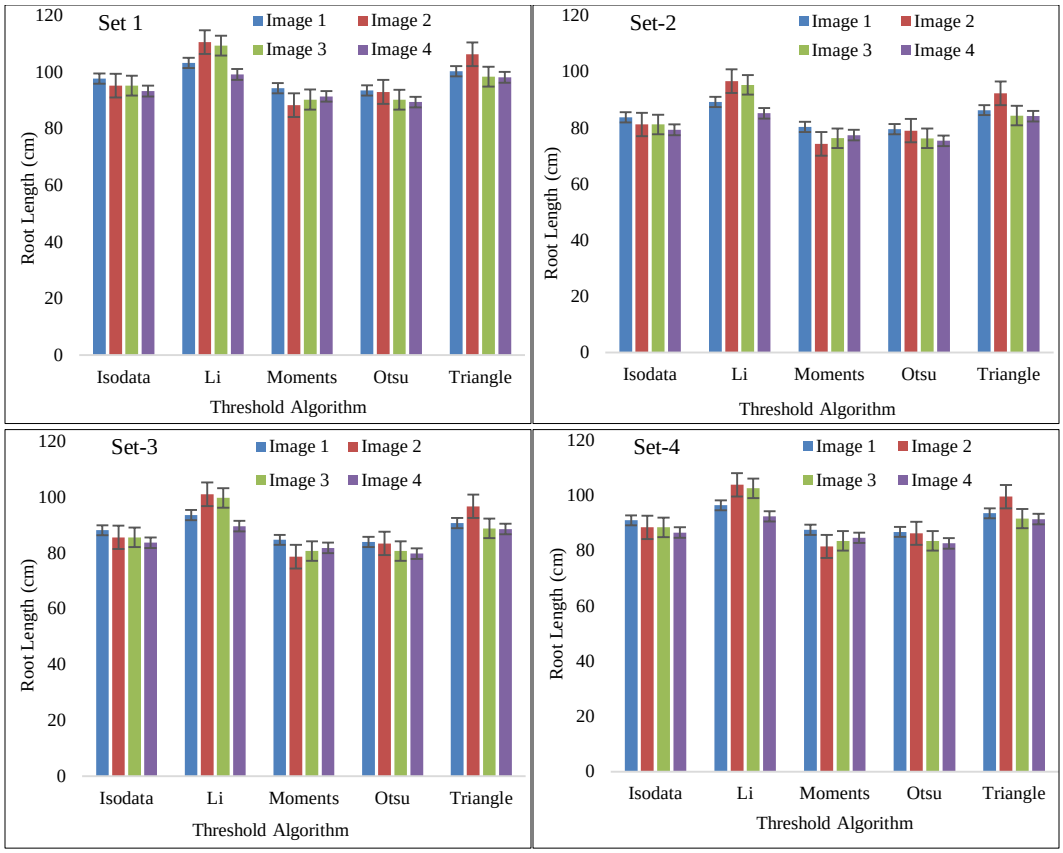

Figure 5.27 Root length of Bermuda grass measured from different algorithms

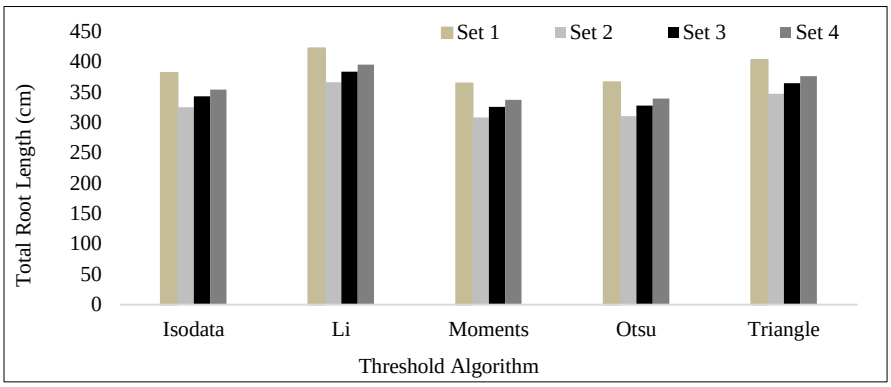

Figure 5.28 Total root length of Hulled Bermuda grass (Grade 90/80) estimated from root images captured from four directions in the minirhizotron at depths of 0-3 inch and processed with different automated threshold-based algorithms in ImageJ program

5.3.5 Evaluation of Root Dynamics

Root images collected from the installed minirhizotrons at certain depths and locations during the study period were subjected to analysis, to develop a spatial and temporal relationship of root dynamics. The term “root dynamics” refers to the root growth and mortality, change in root length, root elongation characteristics, lateral branching, etc.

Images were captured inside the minirhizotrons at every 90^{o} angle to cover the surrounding 360^{o} viewing area. Images were collected and stored along the length of the minirhizotrons to the bottom of the pipe. Images were usually collected once a month throughout the depth of the acrylic tube; however, they were sometimes collected three or four times a month, depending on the in-situ visibility of the roots. In most of the images, roots were visible up to a depth of 15 inches; however, in some of the acrylic tubes, the root skeleton was observed beyond that depth. To maintain consistency in the evaluation, analyses were made from the surface (top 3-inch segment) to a 15-inch depth.

The different grass types from all the six lysimeters had a well-developed and laterally branched root system. The greatest concentration of roots was in the top 4 to 6 inches of the soil profile (Figure 5.29). The roots remained in a dense reticulate pattern at the top 8 to 10-inch depth, and the pattern of root density decreased with an increase in depth. The root penetration depth was found to be limited to 12 to 15 inches. Below this depth, roots were very scarce and minute. Based on field observation, the vertical extension of Hulled Bermuda grass was 18 to 20 inches, and the roots were barely visible.

Differences in root lengths were observed at different depths. Lateral spreading of fine roots from the primary tap root was observed frequently. Roots were found to change the direction of spreading both laterally and vertically in response to the dense soil layer or possibly to the existence of some other hindrance in their growing path. All of the root systems grew in shallow soils, and most of their roots extended laterally were above the

interface of the dense and low-compacted soil layer. Based on the analyses of 100 different images, the major root elongation and lateral spreading was found at the top 10 inches of the root zone. In statistical language, the range of the data set (root length) measured at different depths was from 73 to 261 cm. The range of the data set is shown in Table 5.6.

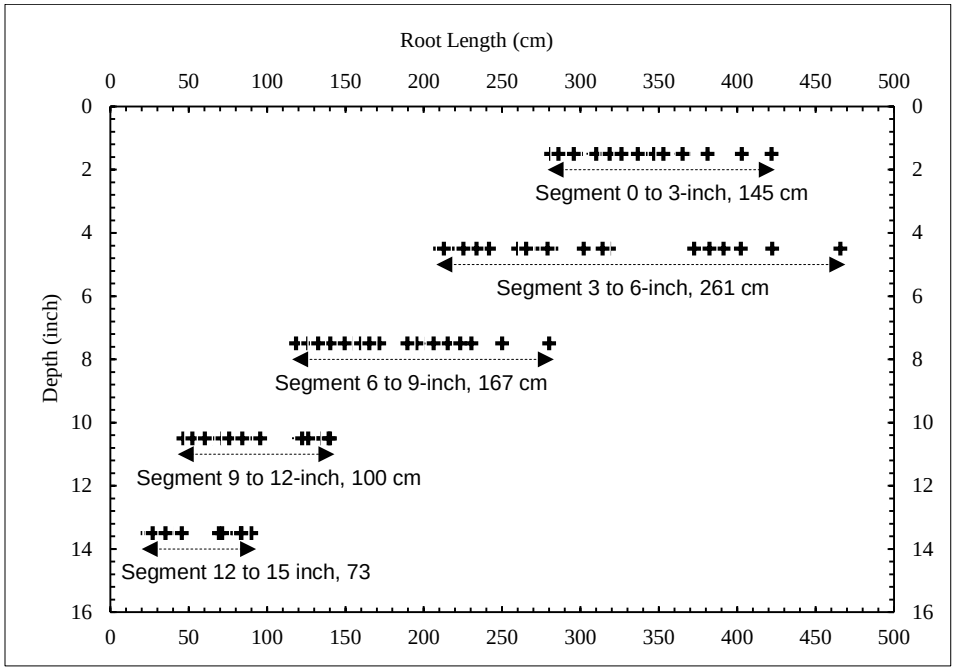

Figure 5.29 Plant root distribution at different depths evaluated through image analysis

Table 5.6 Range of root length at different depth segments

Depth Segment	Range
(inch)	(cm)
0 to 3	145
3 to 6	261
6 to 9	167
9 to 12	100
12 to 15	73

The highest range was found in the 3 to 6-inch image segment, with a value of 261. The range at the 0 to 3-inch segment and the 6 to 9-inch segment was 145 and 167, respectively. The ranges at deeper depths were relatively low, indicating that frequent root growth and elongation (lateral), root dieback, and distribution mainly occurred in the top 10 inches of the root zone. Therefore, based on the image analysis, it can be concluded that the structural changes in roots occur in a favorable soil condition where the roots have a smooth growing path. In the current study, the top 10 inches of relatively low-compacted soil showed more changes in the root dynamics. Environmental parameters, such as rainfall and temperature, also contribute to the dynamic behavior of plant root. Root dieback or decrease in length and density was observed due to the extended drought and high temperature and is indicative of the transpiration process. Again, the rainfall supplied sufficient water for effective root growth and eventual increase in density; however, the high intensity rainfall caused an excess of water to accumulate in the root zone and created an anaerobic condition. Consequently, the plant roots had more water than they could transpire. The excess water was eventually removed from the ET cover through downward drainage and increased the amount of percolation. Therefore, it can be concluded that rainfall intensity and frequency, duration of drought, and soil conditions jointly affect the dynamic characteristics of roots and ultimately control the performance of the ET cover system.

A comparative assessment of the different in-situ plants' root distribution is presented in Figure 5.30, based on the image analysis results. For ease of differentiating, comparison graphs were plotted in log scale. The image analysis results from the four minirhizotrons in lysimeters 3 and 6 are presented as Bermuda grass (BG) instead of presenting as BG and HB (Hulled Bermuda). The data in the figures clearly defines how roots distribute in different patterns. Native Trail (NT) and Switch Grass (SG) roots are

lower in density through the depth profile than the BG root, which was found to be a maximum of 1.7 times greater than NT in the top few inches of the root zone depth, and a maximum of 3.75 times greater in the lower depths of the root zone (Figure 5.30 a). A parallel trend was found in the comparison between SG and BG. SG root density at the upper part of the root zone was at maximum 2 folds lower than BG roots in density and almost 3.25 times lower in the deeper root zone depth (Figure 5.30 b). The comparison of the root distribution of NT and SG grasses is shown in Figure 5.30 (c). Nearly identical distribution patterns were observed, as almost all of the data points were uniformly distributed along the 45^{o} equivalent line.

To summarize, soil profiles have different patterns and numbers of roots for different plant types. Hence, the dataset suggests that differences in root growth and distribution occurred due to the differences in the genetic influence on different root types. Moreover, soil environment and plant physiology are also responsible for efficient root growth. Roots find the optimum way into the soil and use all of the benefits of the soil profile where physical, chemical, and biological activities favor growth and survival.

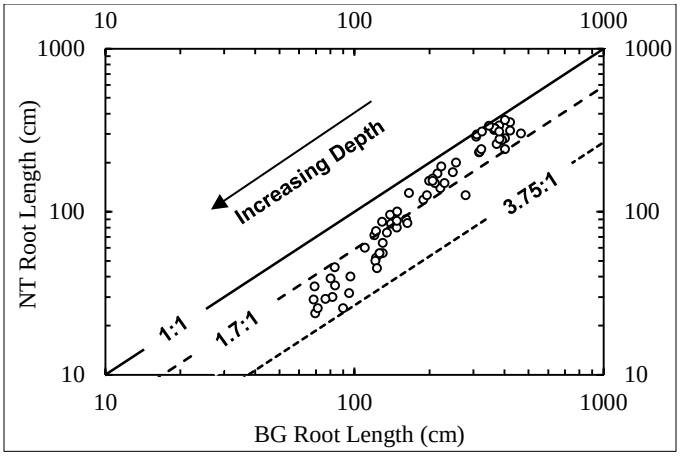

(a)

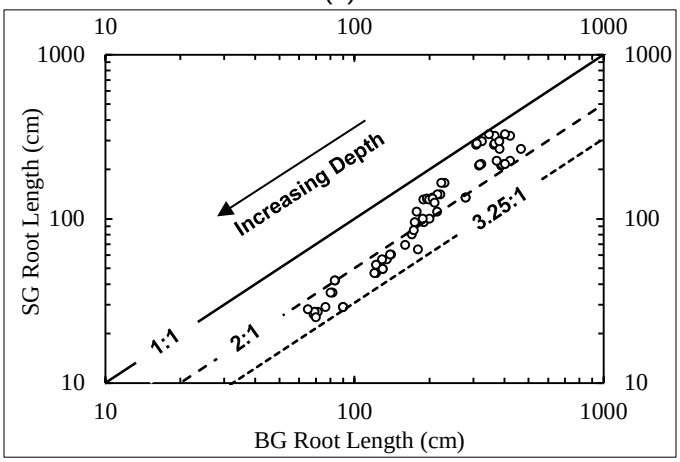

(b)

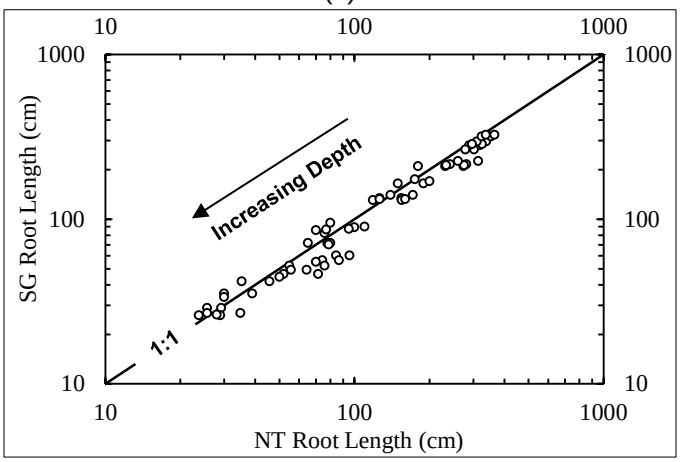

(c)

Figure 5.30 Comparison of root length (based on image analysis) for different vegetation

5.3.6 Evaluation of Plant Transpiration in Response to Root Dynamics

Root elongation and lateral and vertical root branching were evaluated by profiling two-dimensional images of field-grown ET cover plant root systems. Images captured from the minirhizotron were used to determine the vertical and lateral root elongation. The images were analyzed, using the ImageJ program. An area inside the minirhizotron was fixed to capture the images at different times of the year. The analysis was mainly focused during the growing season, when the roots are expected to grow. The images captured throughout the growing season, from March 2016 to December 2016, were used to analyze the root elongation. The calibrated images were 4.5 inches in width and 3 inches in height. Therefore, the area of interest of the root zone was 13.5 inches^2 (87 cm^2). Root lengths per unit in the minirhizotron viewing area for each sampling time were designated as the root elongation frequency (REF). Detailed procedures for root length measurement are presented in Section 5.3.4. REF was calculated based on the following equation.

$$REF = \frac{L_2 - L_1}{T_2 - T_1}$$

Where, REF = Root Elongation Frequency

L_1 = root length at time T_1,

L_2 = root length at time T_2

In the current study, REF was measured for all the plant roots pictured from all the minirhizotrons at different depth segments and different times of the year. Due to accumulation of soil and water inside the viewing areas after the rainfall, some images were not clear enough to analyze (Figure 5.31). However, with the passage of time, reformation of soil and roots occurred and roots were visible from inside the minirhizotron, where it was previously hazy.

Figure 5.31 Blurred image (soil accumulation at the interface of the outside minirhizotron wall and soil cover)

The first image captured for this analysis was on March 17, 2016, 20 days after the installation of the minirhizotron. During the installation of the minirhizotron, the soil and roots were disturbed. However, after the natural consolidation process, the roots started to grow along the wall of the minirhizotron (Figure 5.32). During the next 22 days, more roots were visible in the captured images (Figure 5.32, April 08, 2015). During the next 50 days, Bermuda grass produced extensive new roots with new root hair at the shallow soil depth (3 inches to 6 inches). The amount of precipitation was 303 mm in May 2015, and was one of the factors for the extensive root growth during that period. Some water droplets were visible in the image captured on May 27, 2015. A multiaxial grouping of Bermuda roots through the same soil channel was observed (Figure 5.33). The calculated root density, based on the image analysis, was almost 24 mm/cm^2, and the highest REF was 0.271 $mm/cm^2/day$. The calculated REF for the images at a fixed depth segment of M-3B is presented in Table 5.7.

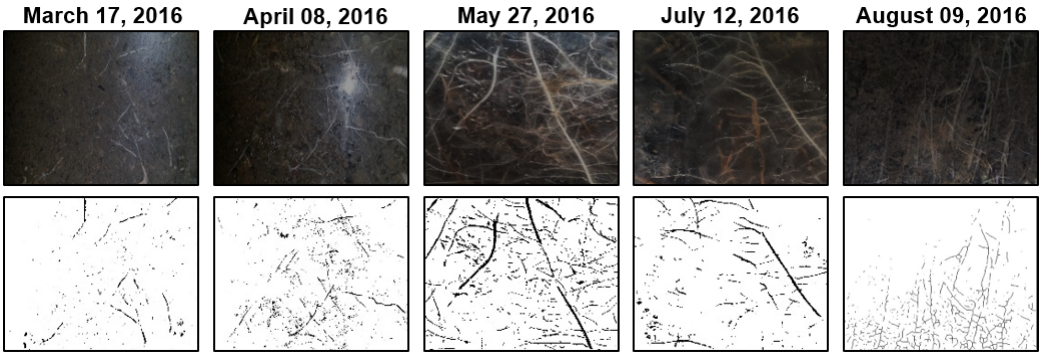

Figure 5.32 Illustration of root growth of Bermuda grass (3”-6” depth)

During July 2016, when high temperatures were prevailing and rainfall was minimal, the Bermuda roots started to decline and negative REF, which is a sign of dieback of a root system due to a lack of water, was observed (Table 5.7). This implies that the Bermuda root system used the available water, which was the moisture removed from the ET cover through transpiration, for growing. Negative REF was observed until the end of the growing season, which was an indication of the active evapotranspiration process.

Figure 5.33 Section of root image of Bermuda grass captured during the growing season (May 27, 2015) at 3 to 6 inches, image presented in actual size to demonstrate lateral branching and multiaxial grouping of roots in the same soil profile

Table 5.7 REF of Bermuda root

Days Interval	Root density	REF
day	mm/cm^2	mm/cm^2/day
0 - 22	7.77273	0.08934
22 - 49	23.5429	0.27061
49 - 95	6.73333	-0.07739
95 - 123	11.6429	-0.13383

Measured REF values based on the image analysis from all the lysimeters were then subjected to evaluate with the field evapotranspiration (ET). ET values computed from the field water balance measurements were converted to daily ET (mm/day). The daily ET values from March 2016 to December 2016 were considered only for the evaluation, since the REF computation were carried out during that period. The relationship between REF and daily ET is graphed in Figure 5.34. Figure 5.34 clearly demonstrate that higher ET rate is associated with negative REF (root dieback) and lower ET rate corresponds to the positive REF (root growth). Based on the trend of data points, a fitting curve was generated. A three-order polynomial function was found most appropriate for the data points (Figure 5.34). The polynomial function used in constructing the trend curve is as following:

$$y = ax^3 + bx^2 + cx + d$$

Where, y = ET (in mm/day), x = REF (mm/cm^2/day) and a, b, c and d are fitting coefficients. The values of a, b, c and d are -900, 1.00, -8.00 and 2.20 respectively. It is to be noted that, ET rate of approximately 2.25 mm/day divides REF zone, which implies that the change in root dynamics (growth and dieback) is explicitly related to the evapotranspiration process.

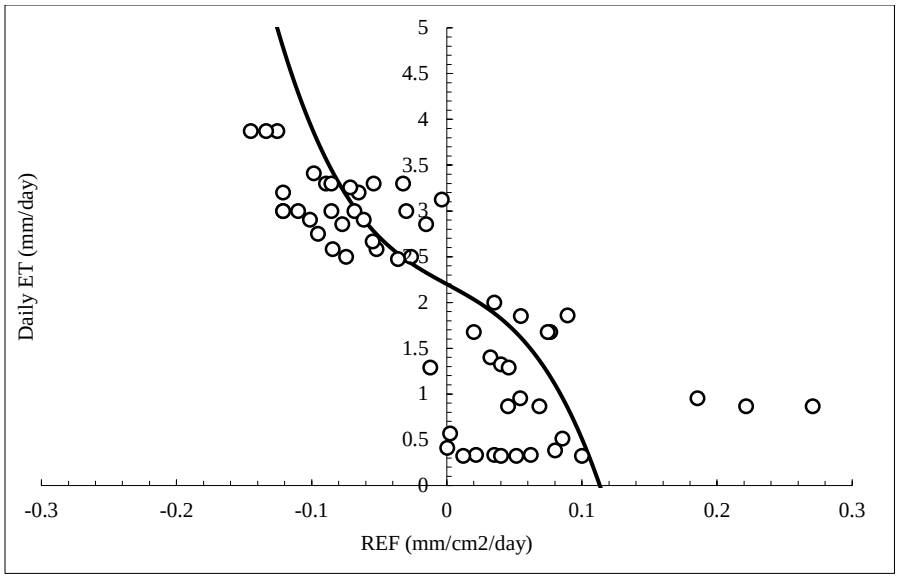

Figure 5.34 Effect of root elongation frequency on evapotranspiration (ET)

A preliminary investigation of image analysis showed that positive REF is an indication of root growth (laterally and vertically), and negative REF is indicative of the evapotranspiration process. Therefore, the measurement of REF, using image analysis, is a viable way of evaluating the ET cover performance. However, an analytical solution, using image analysis throughout the root zone segmented at different depths, is expected to deliver more precise results.

5.3.7 Evaluation of Image Analysis with Destructive Sampling

The data points measured, based on the image analysis of the six minirhizotrons, were evaluated to make a comparative assessment with the traditional root measurement method. The root distribution of the in-situ plants indicated a decreasing trend with depth from the traditional RLD measurements. For the traditional method of root measurement, 3-inch diameter samples (sample volume 21.21 in^2) were characterized at 3-inch depth intervals. For image analysis, 4 images (4.5 inches in width × 3 inches in height), captured at every 90^o angle, surrounding the minirhizotron at 3-inch depth represent a single depth

measurement. Hence, a larger volume of roots was characterized through the image analysis method than through the traditional destructive method at every depth interval. Therefore, these two methods were evaluated based on the normalized dataset. Data normalization was performed by following the procedure described by Benson et al. (2007). Normalization is the ratio of mass/length of roots in a specified increment to the total mass/length of roots in the depth profile.

The data points (125 normalized data) obtained from the image analysis of different grass roots plotted with depth are shown in Figure 5.35. A general RLD curve was developed, based on the following equation with the analyzed data points from image analysis.

$$RLD = a \times e^{(-bz)} + c$$

The parameters were set as a = 0.4, b = 1.6 and c = 0.0005. The fitted general RLD curve with the observed data points is represented in Figure 5.35, along with the RLD curves obtained by the traditional method for different grasses. The figure clearly illustrates the trend of decreasing root distribution with increasing depth. Therefore, the general RLD curve, based on the image analysis, followed the field trend of root distribution. Very few of the roots of any of the lysimeters penetrated more than 15 inches below the ET cover soil. The average rooting depth observed in all the minirhizotrons also suggests this result.

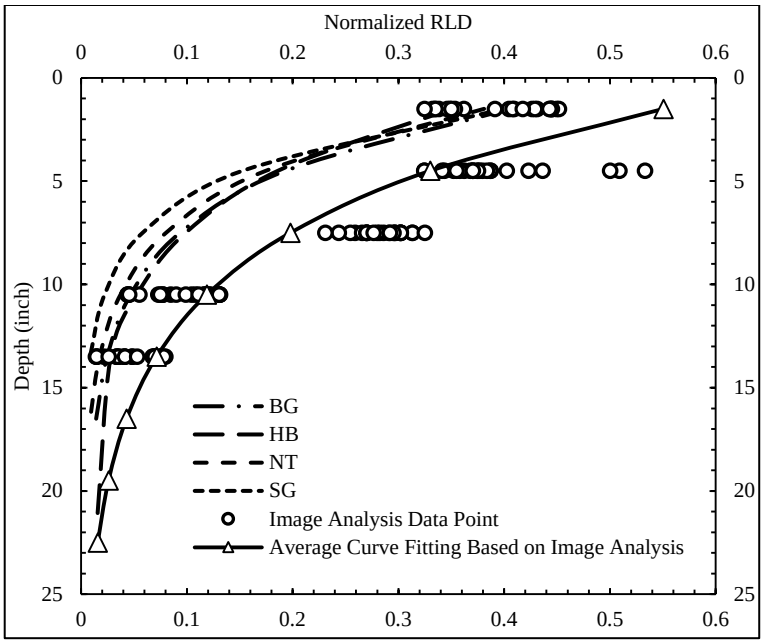

Figure 5.35 Comparison of RLD function based on image analysis and traditional method

The normalized data points obtained from the image analysis and destructive sampling were further plotted with a 45^{o} inclined straight line, as shown in Figure 5.36. The plotted trend followed a straight-line pattern. It was observed from the figure that at shallow depths, the data points were more scattered and far from the 1:1 line (Figure 5.36). At the deeper depths of the root zone, the data points were found relatively close to the 1:1 straight line (Figure 5.36). The normalized data points from the image analysis were as much as 1.6 times higher than the destructive sampling data points, especially in the shallow root zone (Figure 5.36). Background noise of the images was the primary reason for this. The major root dynamics occurred in the shallower root zone. Changes in root structure (root growth or dieback), moisture variations in the image viewing areas, and changes in soil structure around the minirhizotrons were often found in the images captured at shallower depths. The effect of daylight was prominent in the shallow root zone images from the minirhizotrons, whereas images captured in deeper root zones had a negligible

effect of light contrasting. So, the deeper the images are pictured into the Plexiglasses, the less probability of day light effect and other types of noise. Therefore, the processed images at the shallow root zone depths had some sort of background which was hard to remove. These background noises, other than the root skeleton, contributed to the increased image pixel values that eventually resulted in greater root length.

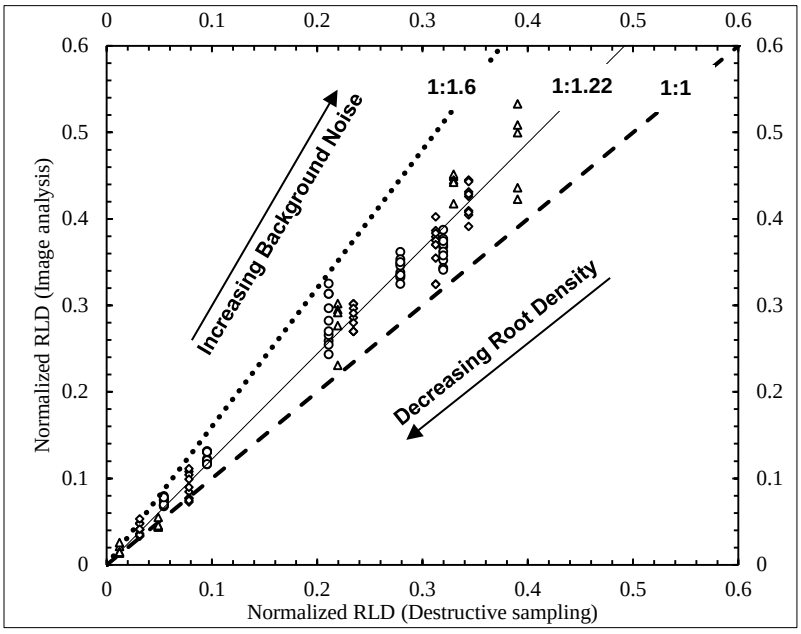

Figure 5.36 Comparison of normalized RLD obtained by traditional method and image analysis method

A transformation factor or noise reduction factor (F_{NR}) was multiplied with the normalized data obtained from image analysis to make the image analysis-based data set comparable with the data set obtained from traditional method. Based on the observation of the data set, $F_{NR} = 0.8197$ was found optimal for the image analysis-based data to match with the traditional data set, as can be seen from Figure 5.37. The data points stay close to the 45^o straight line. This factorization adjusted the results from these two methods by further reducing the noise from the image. Therefore, quantified data from the image

analysis method needs to be factored for more accuracy. In this study, 0.8197 was found to be the ideal transformation factor.

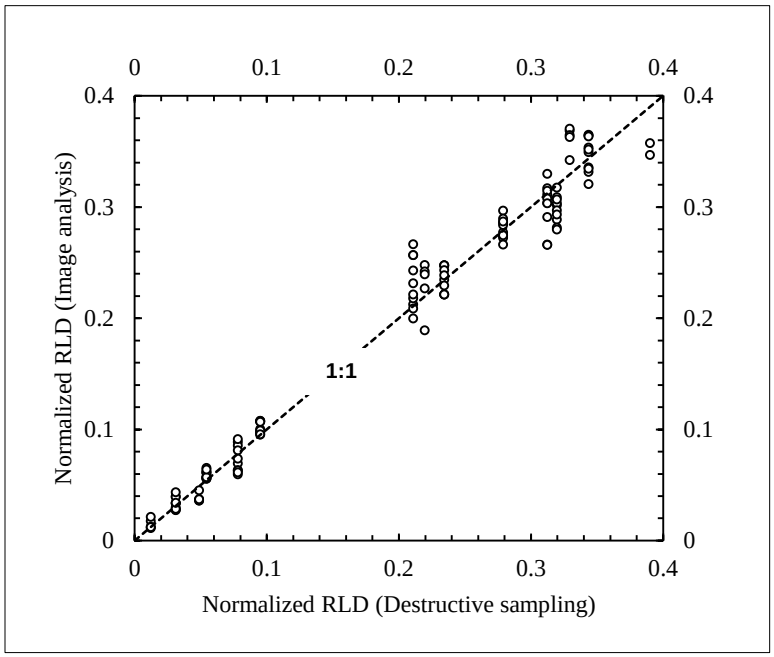

Figure 5.37 Comparison of normalized RLD obtained by traditional method and image analysis method after applying the transformation factor or the noise reduction factor (F_{NR}=0.8197)

Root depth and distribution are critical parameters for optimum ET cover response. Often, due to their complexity and time constraints, root parameters are not measured properly for long-term ET cover designs and performance assessments. Minirhizotron-based root analysis proved to be a powerful tool in this research for evaluating the root system of the ET cover. Minirhizotron technology has been proven to be advantageous to understanding the functions and dynamics of plant roots. Photographing inside the minirhizotron and subsequent image analysis have allowed the quantification and evaluation of the in-situ dynamics and characteristics of the roots in a continuous and non-destructive manner.

5.4 Laboratory Investigation Results of Root

Root length density (RLD) and root mass density (RMD) are important parameters in evaluating the ET cover system. RLD is a significant input parameter used to design the ET cover and predict its performance. The following two sections describe the results obtained from the laboratory investigation.

5.4.1 Root Length Density (RLD)

The major objective of determining RLD was to establish a relationship between root distribution and depth. It is to be noted that traditional RLD measurement is time consuming and precise. Therefore, only two sets of samples for each root type from the top section lysimeters were subjected to RLD measurement. The measured root length at each depth increment for the first set samples is shown in Table 5.8.

Table 5.8 Measured root length at different depth intervals (Spring 2016)

Depth Interval	NT	SG	BG	HB
	Length of roots			
inch	Cm			
0 to 3	44	27	24	41
3 to 6	40	32	21	47
6 to 9	30	18	8	31
9 to 12	10	4	4	14
12 to 15	4	1	3	8
15 to 18	0	0	0	4
18 to 21	0	0	0	2
Total	128	82	60	147

Calculated RLD is presented in the normalized form in Figure 5.38. Normalization is the ratio of length of roots in a specified depth increment to the total length of roots in the depth profile (Benson et al. 2007). The measured RLD was fitted with the following function.

$$RLD = a \times e^{-bz} + c$$

Where, a, b and c are fitting parameters and z = depth below surface. The fitting parameters for different grass roots are listed in Table 5.9. Figure 5.38 clearly indicates that root density decreases with depth. Hulled Bermuda grass was found to have a deeper root distribution than the other grass roots. Therefore, based on the RLD test results, the roots of all of the vegetation in the ET cover system can be considered as shallow roots. Soil bulk density is one of the major reasons behind the generation of shallow root systems in the lysimeters. Detailed results on soil bulk density are presented in Section 5.4.2.

Table 5.9 RLD curve fitting parameters

Grass Type	Parameter	Value
NT	a	0.38
	b	2.6
	c	0.001
SG	a	0.4
	b	3.2
	c	0.00001
BG	a	0.4
	b	2.5
	c	0.005

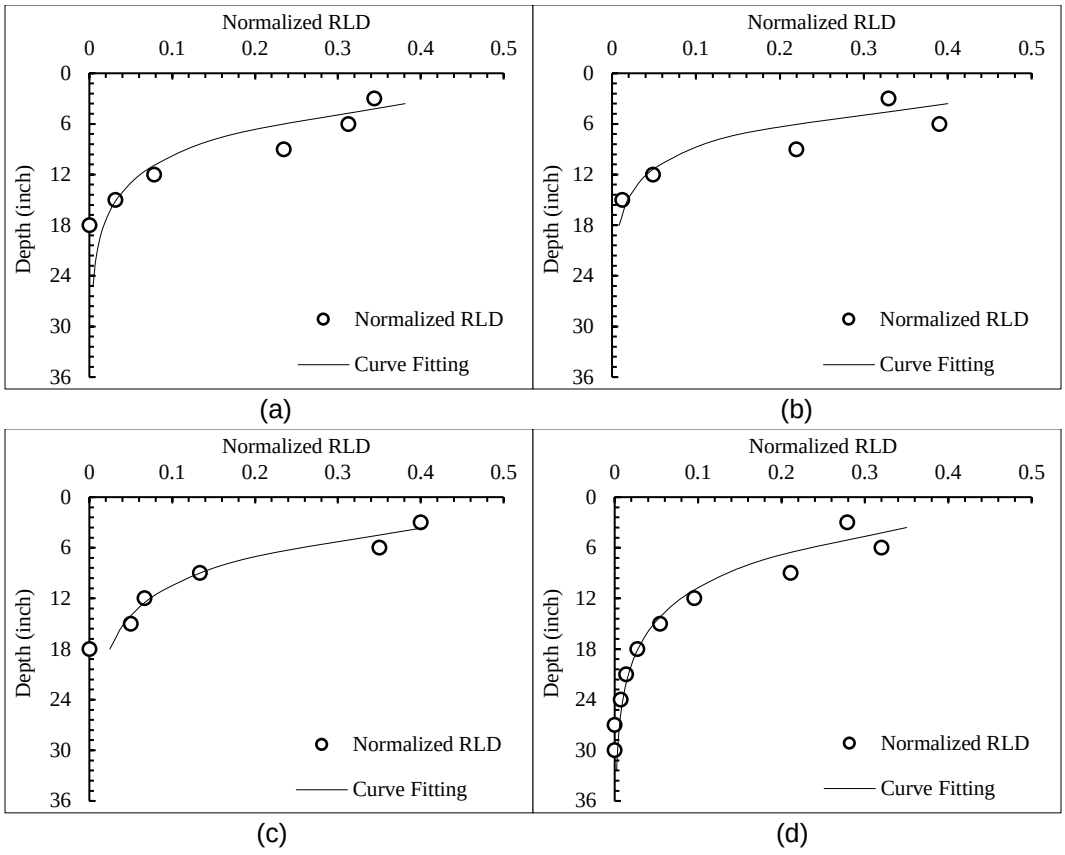

Figure 5.38 RLD test results of (a) Native trail grass, (b) Switch grass, (c) Bermuda Grass, (d) Hulled Common Bermuda grass

5.4.2 Root Mass Density (RMD)

Root samples and soil were collected with a Shelby tube three times a year to develop a relationship between the in-situ root density and depth. The key objective of this measurement was to determine the relative distribution of roots with depth and time. It should be noted that root samples were collected and analyzed for the top three section lysimeters (L-1, L-2 and L-3). Root samples were collected at random locations within the test section. Table 5.10 summarizes the findings of the root investigation conducted at different times of the year. N/A in the table indicates that no root materials were obtained at that depth.

Table 5.10 Root mass at different depths for different vegetation

Depth Interval	Root Mass (g)											
	Native Trail Grass				Switch Grass				Bermuda Grass			
inch	Spring 16	Summer 16	Fall 16	Spring 17	Spring 16	Summer 16	Fall 16	Spring 17	Spring 16	Summer 16	Fall 16	Spring 17
0 to 3	3.12	2.50	2.10	1.80	2.10	1.95	1.72	1.92	2.57	2.45	1.42	3.14
3 to 6	2.94	2.10	1.90	1.70	1.41	1.90	1.0	2.00	2.82	2.40	1.11	2.92
6 to 9	0.84	1.50	1.84	1.49	1.21	1.68	0.52	1.72	2.01	1.62	1.00	1.60
9 to 12	0.24	0.51	0.15	0.48	0.14	0.71	0.14	0.41	0.67	1.42	0.14	0.42
12 to 15	0.04	0.08	0.10	0.12	0.07	0.08	0.11	0.03	0.10	0.30	0.04	0.11
15 to 18	0.01	N/A	0.02	0.01	0.02	0.02	0.02	0.01	0.04	0.10	N/A	0.06
18 to 21	N/A	N/A	N/A	N/A	N/A	N/A	N/A	N/A	0.02	N/A	N/A	0.01

N/A = No root was found at that depth

5.4.2.1 RMD Results of Native Trail Grass

The RMD of Native trail grass is presented in Figure 5.39 (a). The figure highlights the distribution of roots with depths. It was observed that the root distribution diminishes with increasing depth, and the roots tapered off at a depth of nearly 12 inches. The measured bulk density was also found beyond the restricting value at depths near 8 to 10 inches (Figure 5.39 b). A change in root mass of approximately 44% change was observed at the top 6 inches of the soil profile, in a range of soil density below the restricting value (1.6 g/cm^3). The average soil porosity ranged from 0.39 to 0.42. The calculated porosity of the soil is presented in Appendix C.

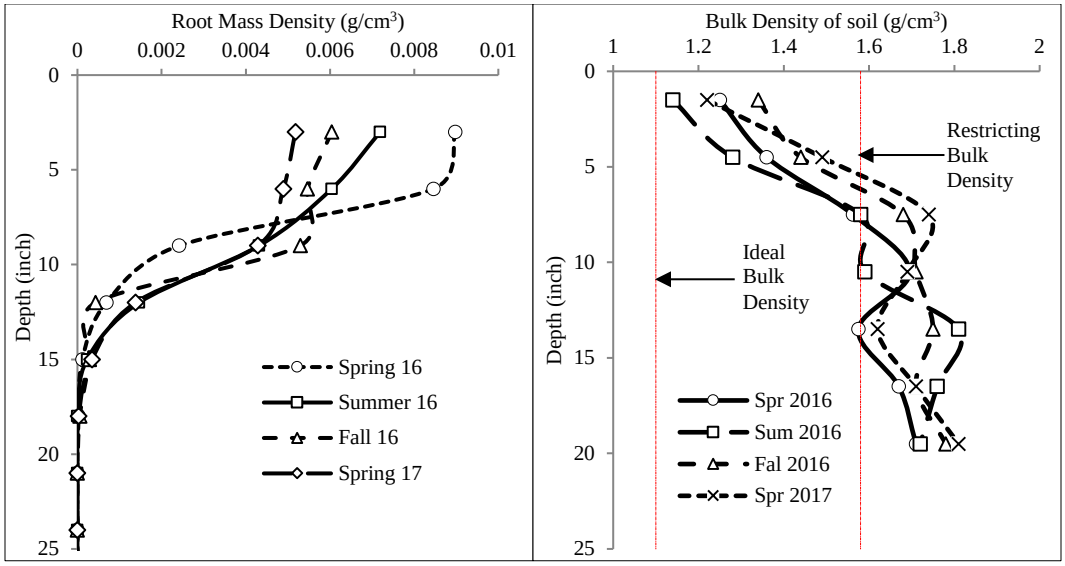

(a) (b)

Figure 5.39 (a) Root mass distribution of Native Trail grass (b) Bulk density measured from the undisturbed sample

5.4.2.2 RMD Results of Switch Grass

The RMD test results for Switch grass are shown in Figure 5.40 (a) and were similar to those of the Native Trail roots. Root density reduced with depth. The measured soil density was found higher than the restricting value near 10-inch depth (Figure 5.40 b).

The change in root mass at the top 6-inch soil layer was lower than that of the Native Trail root system. The range of average soil porosity was 0.40 to 0.43. Calculated porosity of the soil during different investigations is summarized in Appendix C.

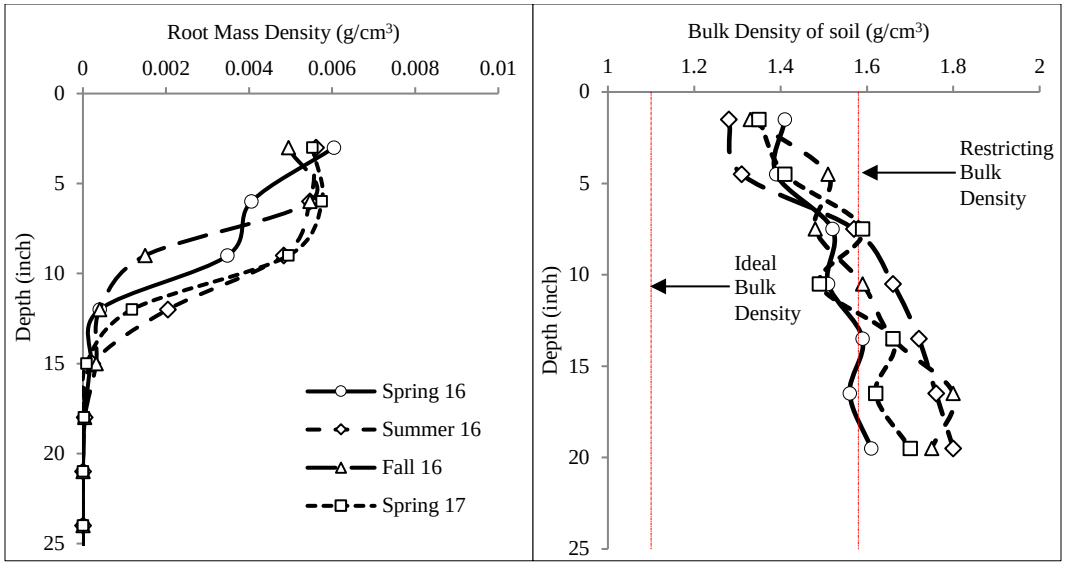

Figure 5.40 (a) Root mass distribution of Switch grass (b) Bulk density measured from the undisturbed sample

5.4.2.3 RMD Results of Bermuda grass

RMD test results for Bermuda grass are highlighted in Figure 5.41 (a). The root distribution trend was comparable to those of the Native Trail and Switch grass roots. However, the Bermuda grass root samples penetrated to deeper depths (20 inches). A root mass change of approximately 56% was observed at the top 6 inches of the cover soil. Soil bulk density was in the suitable range (1.1 g/cm^3 to 1.6 g/cm^3) for effective root growth at the top 10-inch of the cover soil. Average soil porosity ranged from 0.38 to 0.43. Measured soil porosity is listed in Appendix C and was calculated during different soil investigations.

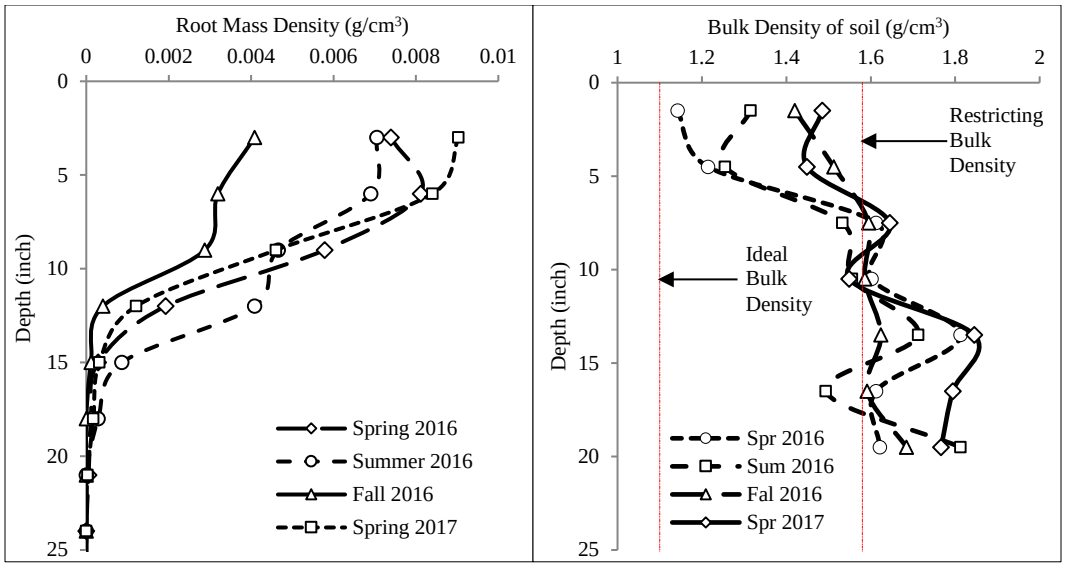

Figure 5.41 (a) Root mass distribution of Bermuda grass (b) Bulk density measured from the undisturbed sample

5.4.2.4 Summary of RMD Test Results

The results obtained from the RMD test indicated that the roots of all of the vegetation types had a higher density (RMD) at the top one foot of the cover soil. There was a drastic reduction in root density below a 12-inch depth of the cover profile, except for Bermuda root, which was found to penetrate deeper into the soil, up to 20 inches. The root system was concentrated near the surface of the cover, as shown in the Figures 5.39 (a), 5.40 (a) and 5.41 (a). Bermuda root was found to have a tap root - a long primary root with fine roots branching from it. Native Trail and Switch grass were found to have a fibrous root system with thin branching.

Placement of soil density (95% of MDD, dry side) during construction, based on the NDG measurement, was almost 16.15 KN/m^3 (105 pcf), which is equivalent to 1.68 g/cm^3. The MDD of the soil was 17 KN/m^3 (111 pcf) or 1.76 g/cm^3. Therefore, the soil layers in the lysimeters were initially considered to be highly compacted. The restrictive bulk

density of clayey soil for limiting root growth is 1.6 g/cm^3. The higher soil density at deeper depths was an obstacle for establishing a deeper root system in the ET cover system. Therefore, a shallow root system was observed for all the grass roots in all the lysimeters.

In the practice of ET cover construction, landfill owners, operators, and regulatory agencies are reluctant to place the cover soil at a density suitable for root growth. Designers are more comfortable in designing the cover system as a structural member or hydraulic barrier which can serve to maintain a lower saturated hydraulic conductivity. Moreover, high soil density is recommended for cover systems constructed on slopes. Slope stability of the ET cover system constructed on the steep slopes depends on the soil density to a large extent.

5.5 Geophysical Investigation of Root Zone

5.5.1 Determination of Active Root Zone Depth

The electrical resistivity imaging (ERI) method was exploited in this study in an aim to measure the active root zone depth (potential evapotranspiration depth). The investigation was conducted throughout the summer of 2016, with the ERI test being implemented every week in the field. Additionally, one ERI test was carried out on the same day on non-vegetated ground, just outside the test section to compare the contrast between the vegetated and non-vegetated ERI profiles under identical environmental conditions. The hydrologic processes in the vadose zone are highlighted through the ERI profile in Figure 5.42. RI profiles for July 8, 2016 and August 2, 2016 are presented in the figure. Precipitation totaling 20 mm occurred two days before July 8, 2016 and 66 mm rainfall with low frequency was recorded from July 8 to August 2, 2016. Recorded temperatures on July 8th, 2016 and August 2nd, 2016 were 98^o F and 104^o F, respectively. The effects of different rooting depth among the vegetation types are clearly visible in Figure 5.42.

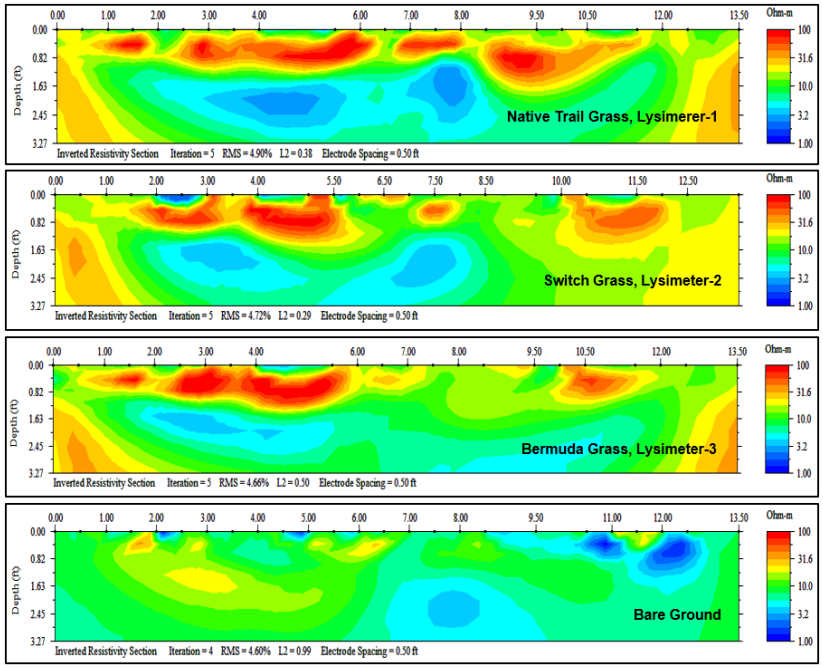

(a)

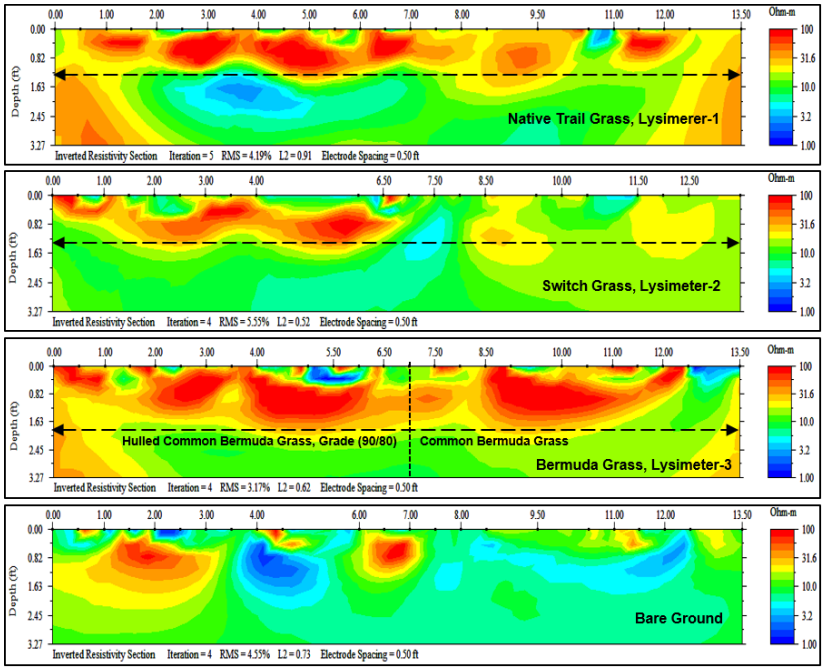

(b)

Figure 5.42 RI profile of vegetated lysimeters and non-vegetated ground (outside the constructed lysimeters), (a) July 8, 2016 (b) August 2, 2016

Due to high temperatures, shallow resistivity values rapidly declined for all of the vegetation types after the 20 mm rainfall which occurred two days before July 8th, 2016 (red contour at the root zone). However, lower resistivity values at similar depths (below 10 inches) in the three lysimeters indicated downward drainage of precipitated water (Figure 5.42). The bare ground ERI profile had no consistent contour. On August 2nd, the high rate of ET further reduced the root zone soil moisture, increasing the shallow depth resistivity value. L-3 with Bermuda grass underwent greater transpiration and thus increased the resistivity value up to approximately 1.67 ft. (20.4-inches) (Figure 5.42 a). L-1 (NT) and L-2 (SG) soil had similar resistivity contours with high resistivity value at the top 1.23 ft. (14.7 inches) (Figure 5.42 a). The ERI profile of the bare ground showed an irregular resistivity contour. Changes in resistivity were plotted against the depth for all of the lysimeter soils, 4 ft. from the origin (x = 4 ft.), as shown in Figure 5.43. The figure clearly distinguishes the active root zone depth since the top 1 to 1.5 ft. of soil had higher resistivity values measured throughout the summer 2016 than the deeper depth of the cover soil.

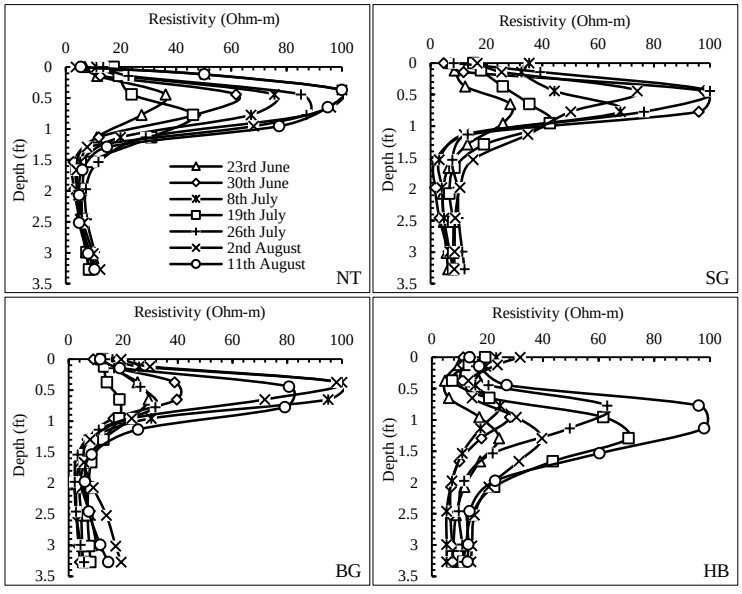

Figure 5.43 RI profile with depth at section x = 4 ft. (Summer 2016)

A plot of the resistivity distribution between the root zone depth or ET layer (top 15 inches) and the storage layer (bottom 30 inches) is shown in Figure 5.44. The distribution profile shows a higher resistivity value within the ET layer zone than within the non-rooted storage layer. The distribution profile for the bare ground is also presented in Figure 5.45. Almost-uniform distribution can be observed from the figure. Therefore, the presence of plant roots makes a significant difference in the resistivity values. Root depth measured through a minirhizotron was approximately18 to 20 inches for BG and 13 to 15 inches for NT and SG grasses. The ERI method indicated clear differences in the root zone moisture uptake, showing different contrasting images for the various vegetated lysimeters. Therefore, the ERI method noticeably indicates active root zone depth or potential evapotranspiration depth. Based on this investigation, the active root zone depth for BG, NT, and SG is 18 to 20 inches, 13 to 15 inches, and 13 to 15 inches, respectively.

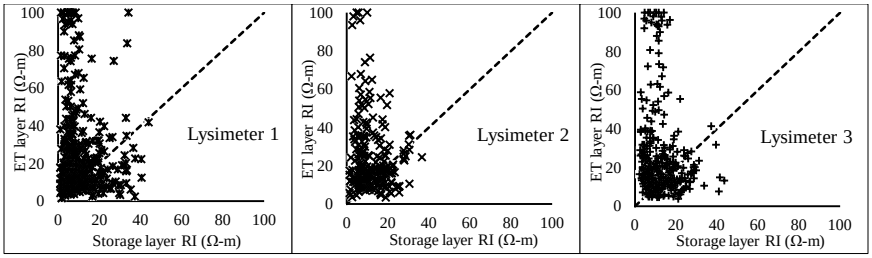

Figure 5.44 Distribution of Resistivity (Ω-m) in the ET cover (Summer 2016) between evapotranspiration layer (top 1.5 ft. rooted zone, and the storage layer (bottom 2.5 ft. non-rooted area) of different vegetated lysimeters

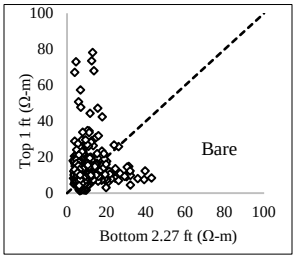

Figure 5.45 Distribution of Resistivity (Ω-m) in the bare ground

5.5.2 In-situ Detection of Root Distribution

The main objective was to use electrical resistivity (RI) as a non-destructive application for detecting and quantifying plant roots in response to dry and wet seasons. The resistivity value (ρ) was used to develop a relationship with the plant root. RMD characterization was conducted four times throughout the study period. During each RMD sampling, the RI test was performed in desired locations. The RMD sampling point was chosen along the transect of the RI line. The analyzed dataset consisted of 84 pairs of RMD-ρ data (n=84).

Resistivity values ranged from 0 to 100 Ω-m along the transect and the depth. Measured RMD ranged from 0 to 0.0089 g/cm^3. Initially, all of the measured RMD values for three different grass types corresponding to the ρ values were graphed in an arithmetic plot. An arbitrarily scattered plot was observed (Figure 5.46). It was noticed that at lower ρ value (0 to 40 Ω-m), the RMD was concentrated to almost 0 root mass. Whereas, at higher ρ value (ρ > 40 Ω-m), the RMD showed a scattered distribution (Figure 5.46). At deeper depths of the root zone (below 1 ft.), the RMD values were very low. The ρ values corresponding to the lower RMD values at the deeper root zone ranged from 0 to approximately 40 Ω-m. At shallow dense root zone (top 10 inches), which is considered the effective evapotranspiration depth, a wide range of RMD existed at corresponding ρ, and ranged between 40 and 100 Ω-m. However, at lower ρ value, some higher RMD was recorded. Since, changes in soil resistivity value are highly sensitive to the degree of saturation (Abu-Hassanein et al. 1996) or moisture content (McCarter 1984), higher RMD measured after heavy precipitation could not be contrasted by the RI contour. Moreover, organic content present in the soil (Ekwue and Bartholomew 2011), pore water composition (Kalinski and Kelly1993), and geologic formation of soil (Giao et al. 2003) also affect soil

electrical resistivity significantly. Therefore, a threshold point needs to be set to quantify the RMD through the resistivity imaging method.

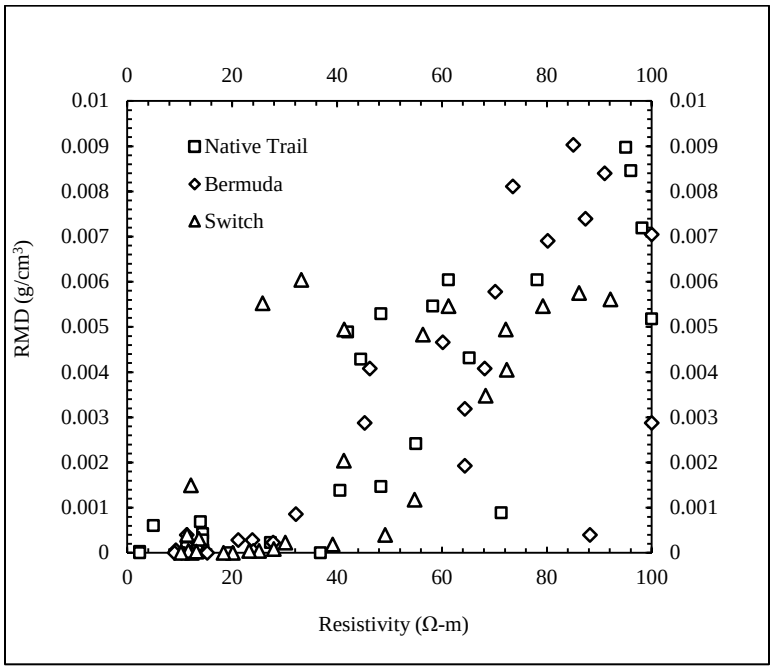

Figure 5.46 Scattered plot of RMD vs resistivity (RI)

The necessity of determining the threshold is illustrated through the geophysical imaging in Figure 5.47. The resistivity profiles (L-1) shown in Figure 5.47 illustrate the different soil moisture status on November 11th, 2016 and February 10th, 2017. Approximately 47 mm of precipitation was recorded in the in-situ weather station on Nov. 8, 2016. Based on the RI profile (Figure 5.47 a), it is obvious that the precipitated water infiltrated the entire cover depth and slowly transitioned to the field available water (AW) condition (able to be transpired). Immediately after the rainfall, the shallow root zone was found at saturated or near-saturated condition. Although the destructive sampling suggested the existence of fine roots, it could not be contrasted through the RI profile. During the active root growth period (Figure 5.47 b), plant roots started to use the soil

moisture. Therefore, the hypothesis is that at higher moisture content (lower ρ value), the response of soil resistivity to fine roots cannot be distinguished.

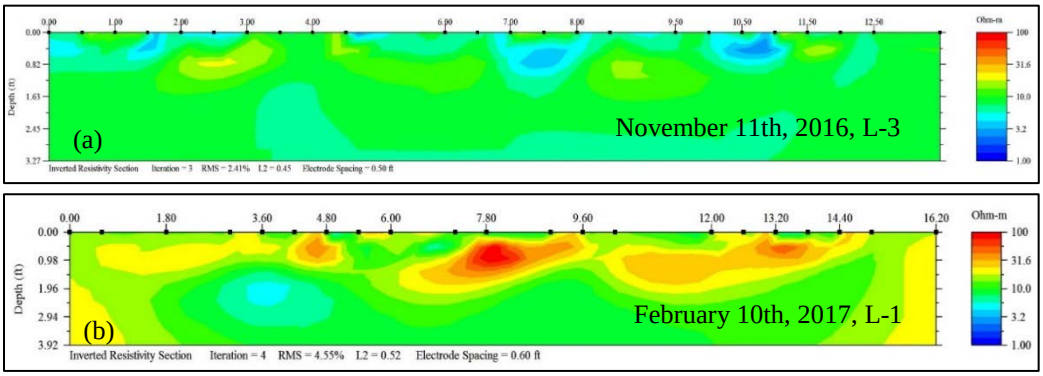

Figure 5.47 RI profile (a) 2 days after high intensity rainfall (b) no rainfall for last 20 days

Based on all the data pairs of RMD-ρ (n = 84) obtained from the three different lysimeters, statistical analysis was undertaken to develop a root density detection model (RDDM). A simple linear regression was introduced with all the observed data points. The properties of the initial RDDM are shown in Table 5.11.

Table 5.11 Properties of the initial regression statistics

Properties	Value
Multiple R	0.735278304
R^2	0.540634184
R^2 (adj.)	0.535032162
SE	0.001932971

$y = -0.000430918 + (7.20386 \times 10^{-5})x$; Where, x = resistivity value (Ω-m) and y = RMD (g/cm^3). In accordance with the initial RDDM, the R^2 value is 0.5406, which suggests that approximately 54% variability of the data set can be explained through the initial RDDM. To improve the accuracy of the RDDM, the RMD-ρ data pairs at lower ρ value were discarded. The data sets (n = 47) at which the ρ values ranged from 50 to 100 Ω-m

were regressed again. The first-degree polynomial (linear) model was reintroduced. The properties of the new RDDM are given in Table 5.12.

Table 5.12 Properties of the Final Prediction model

Properties	Value
Multiple R	0.930421246
R^2	0.865683695
R^2 (adj.)	0.858221678
SE	0.000630528

$y = -0.002395567 + (0.000106676)x$; Where, x = resistivity value (Ω-m) and y = RMD (g/cm^3). Based on the final RDDM equation, the R^2 raised to 0.8657 from the initial value of 0.5406. This rise in the R^2 value indicates the improvement of the RDDM. The intercept coefficient in the regressed equation was negative, which implies that there is a certain x (ρ) value below which the y parameter (RMD) becomes negative, which is not possible. Therefore, the final RDDM is valid at $x > 22.45653$ Ω-m.

For the verification of the developed RDDM, geophysical investigation was also further carried out in February 2016. RMD sampling was conducted at the corresponding transect line. The observed and predicted RMD is shown in Table 5.13. The predicted curve and the observed data points are plotted in Figure 5.48. The observed data points are scattered 15% from the prediction curve. Another point to be noticed from Figure 5.48 is that at higher ρ values, RMD is closer to the prediction curve than to the lower ρ values. It was also observed that the measured RMD at lower ρ value (0 to 50 Ω-m) does not follow the predicted curve at all. Therefore, the accuracy of the final RDDM is valid in the 50 to 100 Ω-m resistivity range. Additionally, the observed and predicted values were plotted at 45^o inclined straight line, as presented in Figure 5.49, indicating a good agreement between the observed and the predicted values.

Table 5.13 Observed and predicted RMD

Resistivity Value	Actual Value	Predicted Value
RI	RMD	
ohm-m	g/cm^3	
91.124	0.00739	0.00732
99.124	0.00811	0.00817
82.325	0.00578	0.00638
92.142	0.00704	0.00743
87.658	0.00690	0.00695
57.325	0.00420	0.00371
67.325	0.00408	0.00478
58.125	0.00310	0.00380

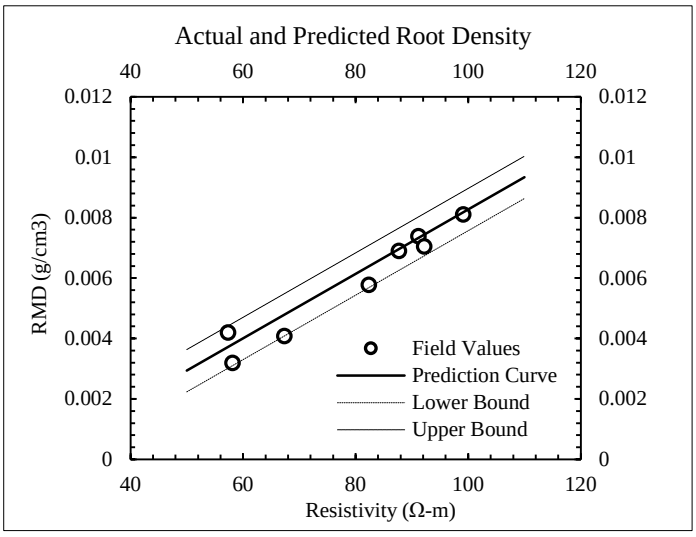

Figure 5.48 Prediction curve for RMD based on linear regression model with the field investigation values.

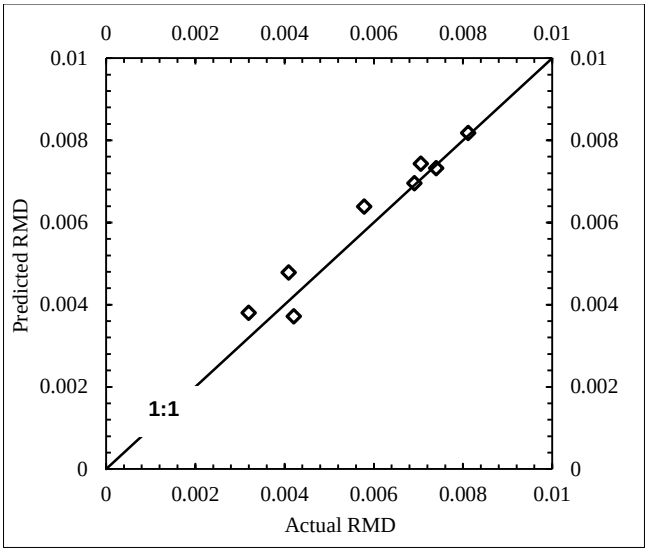

Figure 5.49 observed and predicted RMD value

The developed model showed that soil resistivity is quantitatively related to the below-ground biomass (root). This relationship provides a basis for the development of a quick, non-destructive approach to determine the distribution of plant roots in the ET cover system.

Chapter 6

Performance Monitoring and Evaluation

6.1 Introduction

This chapter includes the monitoring results obtained from the site and performance evaluation of the evapotranspiration cover (ET Cover). Climatological monitoring, seasonal changes in soil moisture, and in-situ hydraulic characteristics were monitored and are evaluated in this chapter. The water balance results of different vegetated lysimeters are presented. The performance of different types of vegetation was evaluated, based on the water balance results. Based on the field monitoring results, a field evaluation curve (FEC) was generated to assess the performance of the ET cover.

6.2 Meteorological Monitoring

The climatic condition is the major factor that contributes to the performance of the ET cover system. The most critical climatological factors are precipitation amount and intensity, temperature, relative humidity, wind speed, solar radiation, etc. All of the climatic data was obtained from the on-site weather station, and the monitoring results are described in the following sections.

6.2.1 Precipitation

Quantity and intensity of precipitation is one of the contributing factors for optimum ET cover performance. The location of an ET cover system decides the performance criteria to a large extent. Typically, arid and semi-arid regions are considered suitable for the ET cover, but some researchers have suggested that an ET cover can also be suitable for humid regions. Geographically, the City of Denton landfill is in a semi-humid region with an annual average precipitation of 36 to 50-inches. The geographical location of the study area with historical rainfall data is shown in Figure 6.1.

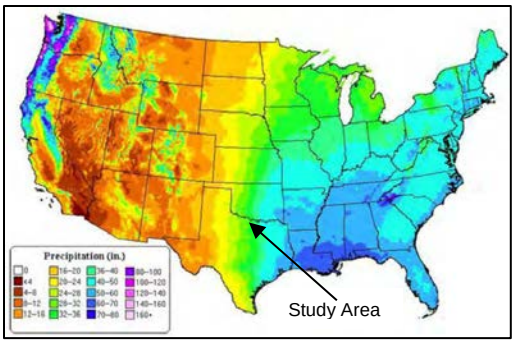

(a)

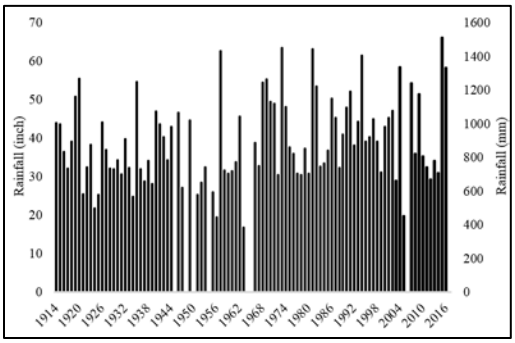

(b)

Figure 6.1 (a) Precipitation map of United States (b) Precipitation history of Denton,TX

Precipitation measured from the on-site weather station during the monitoring period is presented in Figure 6.2. The total amount of rainfall during the study period was 128.5 inches (3263.9 mm). Annual precipitation in the years 2015 and 2016 was 59.5 inches (1511.3 mm) and 52.5-inches (1333.5 mm), respectively. Annual precipitation in the study area is listed in Table 6.1. As shown in the figure, relatively large quantities of rainfall were recorded at the weather station. Several patterns of precipitation were observed at the site during the monitoring period. Large-quantity rainfall with both high and low frequency and small-quantity rainfall with high frequency were experienced at the site. Precipitation intensity was found as high as approximately 200 mm/hr. during the large-quantity rainfall with high frequency. Based on the field water balance measurement, a large pulse of percolation occurred during the large-quantity precipitation with high

frequency. Moreover, continuous precipitation with low frequency slowly added moisture to the deeper depths of the ET cover, which subsequently increased the amount of percolation. Several precipitation events at the site also showed the coincidence of high temperature and frequent rainfall.

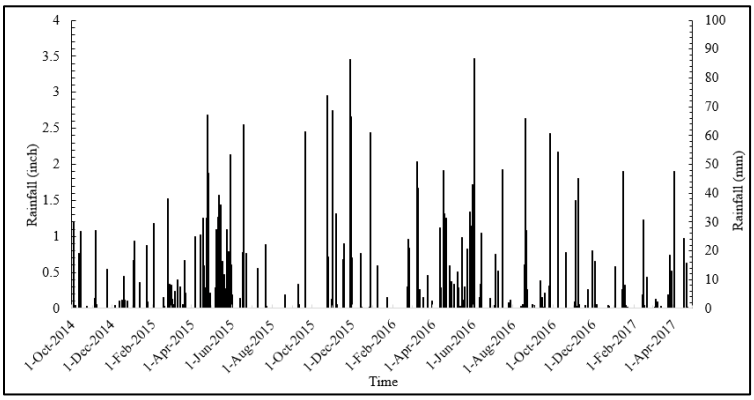

Figure 6.2 (a) Precipitation from the on-site weather station

Table 6.1 Annual Rainfall in the study area

Year	Total Rainfall (inch)	Total Rainfall (mm)
2014[a]	5.50	139.70
2015	59.5	1511.3
2016	52.5	1333.5
2017[b]	11.0	279.40

a = 2014 year includes October, November, December
b = 2017 year includes January, February, March, April

6.2.2 Atmospheric Temperature

Atmospheric temperature measured from the weather station throughout the monitoring period is presented in Figure 6.3. The results are shown in monthly maximum, minimum, and average temperatures. It is shown in the figure that fluctuation of temperature follows a sinusoidal pattern, with lower temperatures throughout the winter and higher temperatures during the summer. The average temperature in the summers of 2015 and 2016 was approximately 40^{o}C. During this summer period, there was a significant

decrease in soil water storage because of the high ET rate. However, there were few events during this period where high temperatures coincided with large-quantity rainfall, resulting in an increase in the amount of percolation that quickly changed the soil water storage. Changes in water storage occurred less frequently in the winter because of lower temperatures.

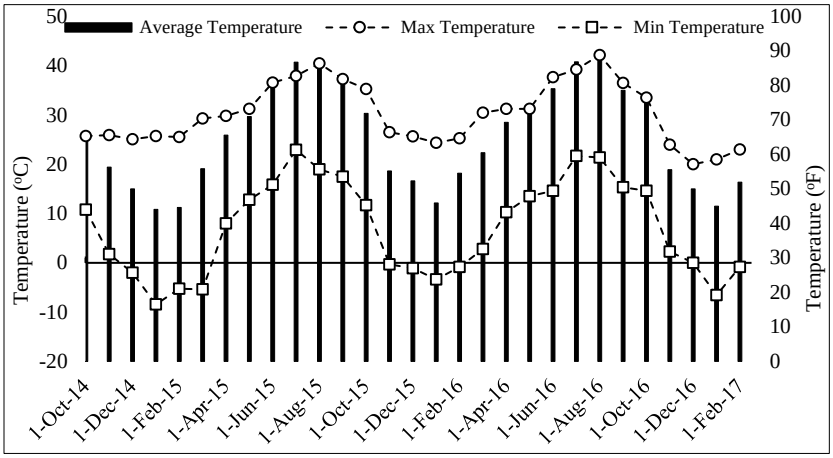

Figure 6.3 Atmospheric temperature at the site

6.2.3 Relative Humidity, Solar Radiation, and Wind Speed

Measured relative humidity, solar radiation, and wind speed data are shown in Figure 6.4. Relative humidity throughout the monitoring period didn't appear to be in a regular trend. A frequent ups and downs were observed in the relative humidity value. On an average, relative humidity was found in a range of 30 to 92%. Trend of relative humidity was found downward during the end of summer 2015 (Figure 6.4 a). Higher relative humidity is one of the conditions that lowers the rate of ET; consequently, water storage changes negligibly. Wind speed on top of the lysimeters throughout the monitoring period ranged between 0 and 30 mph (Figure 6.4 b), with an average of 7.5 mph. Higher wind speeds tend to enhance the ET process, thereby reducing the amount of stored water from the cover. Solar radiation at the site followed a sinusoidal pattern, increasing during the

summer and decreasing during the winter (Figure 6.4 c). The highest solar radiation was approximately 1100 W/m^2 in the summer, while it was near 600 W/m^2 during the winter period.

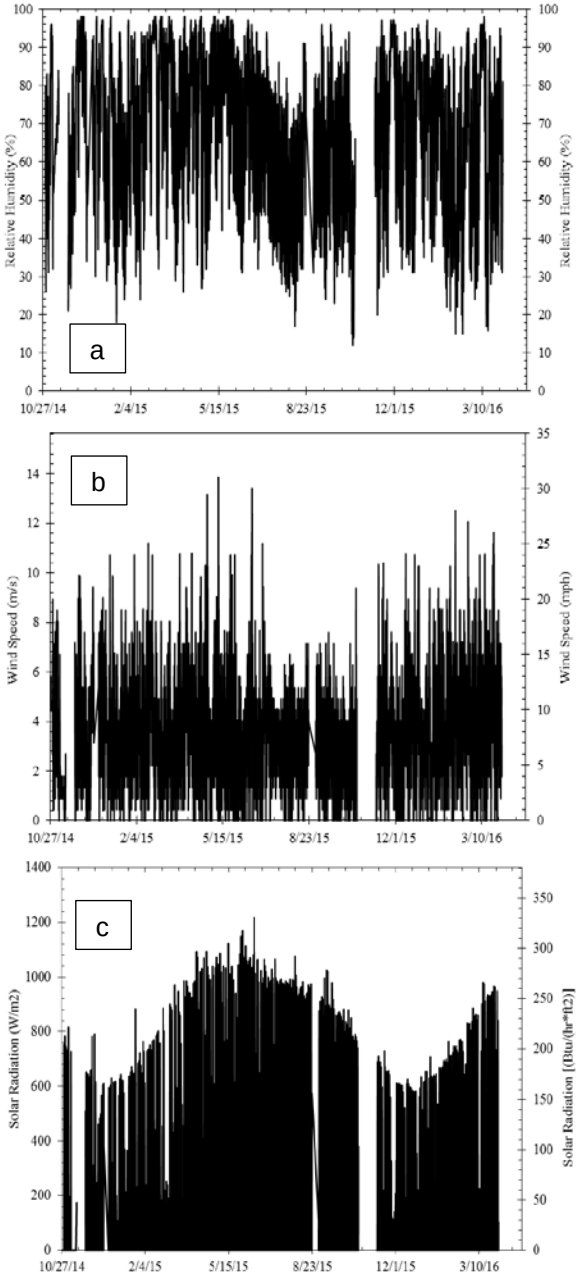

Figure 6.4 (a) Relative humidity; (b) wind speed and (c) solar radiation

6.3 Spatial and Temporal Variations of Soil Moisture

Soil moisture characteristics are the fundamental component of the hydrologic cycle of an ET cover system and are mainly influenced by processes, including infiltration, percolation, evapotranspiration, and root water uptake. Figures 6.5, 6.6 and 6.7 show the vertical distribution of soil moisture for three vegetation types. Soil moisture profiles for the flat-section lysimeters (L-1, L-2 and L-3) are presented, which consist of three different vegetation types. The entire year was divided into three different seasons: spring (January – April), summer (May – August), and fall (September – December). The moisture distribution for 2015 and 2016 is presented. All of the lysimeter soil with different grass types had a parallel seasonal variation of soil moisture. Soil moisture variations during the fall and spring periods were almost negligible at moderate intensity rainfall. However, except for lysimeter 2, the temporal and spatial variations of soil moisture, in response to heavy rainfall, were more rapid after the dry period than before the dry period (Figure 6.5 b, 6.7 b summer 2015) In lysimeter 2, the change in the soil moisture occurred in the top 20 inches (Figure 6.5 b). The precipitation event after the dry period resulted in an immediate increase in soil moisture content at all depths. The faster circulation of water after the dry period, due to heavy rainfall, suggests that permeability of the soil increased substantially after the dry period. Albright et al. (2006) reported similar temporal and spatial variations of soil moisture content after the drought season. The pattern of seasonal change in the soil moisture was comparable, as all of the lysimeter soil was constructed with clayey soil from the nearby borrow pit. Nonetheless, in this study, actual soil moisture varied between vegetation types in the lysimeters. Vegetation pattern was one of the controlling factors for the soil water dynamics and seasonal variations. Due to the combined effects of transpiration, soil evaporation, and water recharge (rainfall), the soil moisture change was minor in the early growing season (May to mid-June). This is because

of the low difference between the ET and precipitation. In July and August 2015, the average temperature was usually above 30°C, with a maximum temperature of 40.44°C in August and with almost no rainfall. During this period, evapotranspiration occurred at a high rate and soil moisture changed based on the corresponding vegetation root depth. In October 2015, a soil water recharge occurred due to heavy rainfall (a total of 9.72 inches, with a one-day maximum rainfall of 0.54 inch). Due to this precipitation and the subsequent dormant period of ET, when plant roots were inactive and temperatures were low, changes in soil moisture content remained almost constant throughout the depth. During high ET period, the greater water demand for transpiration in the vegetation dried the soil layers. In summary, the plant root system plays an important role in the seasonal variations of soil moisture.

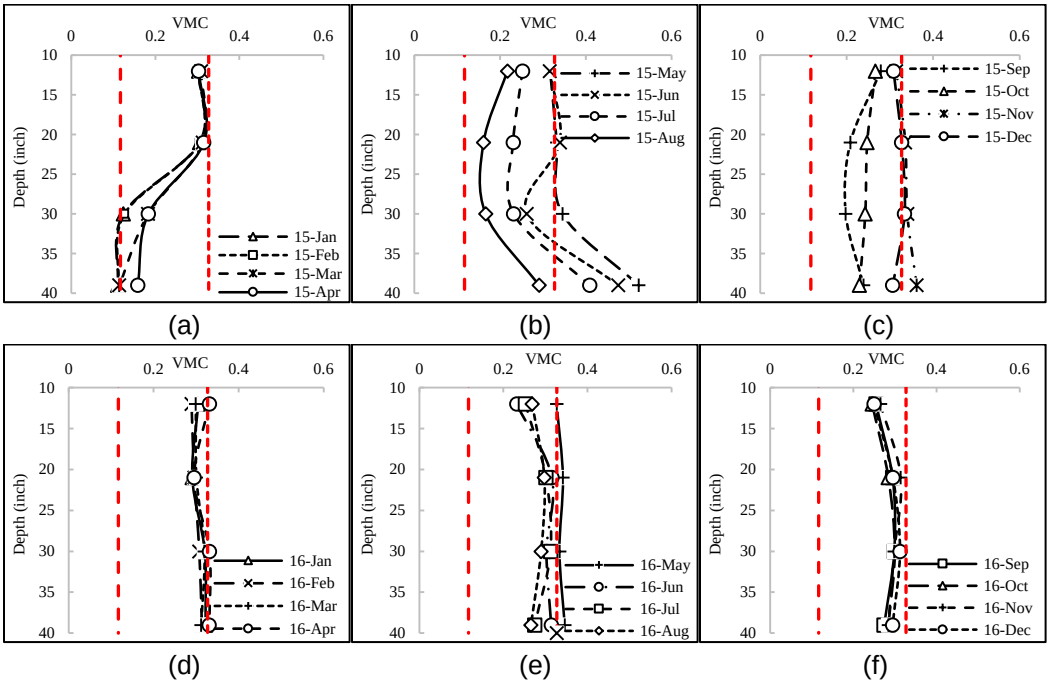

Figure 6.5 Profile distribution of average soil moisture content under NT (L-1)

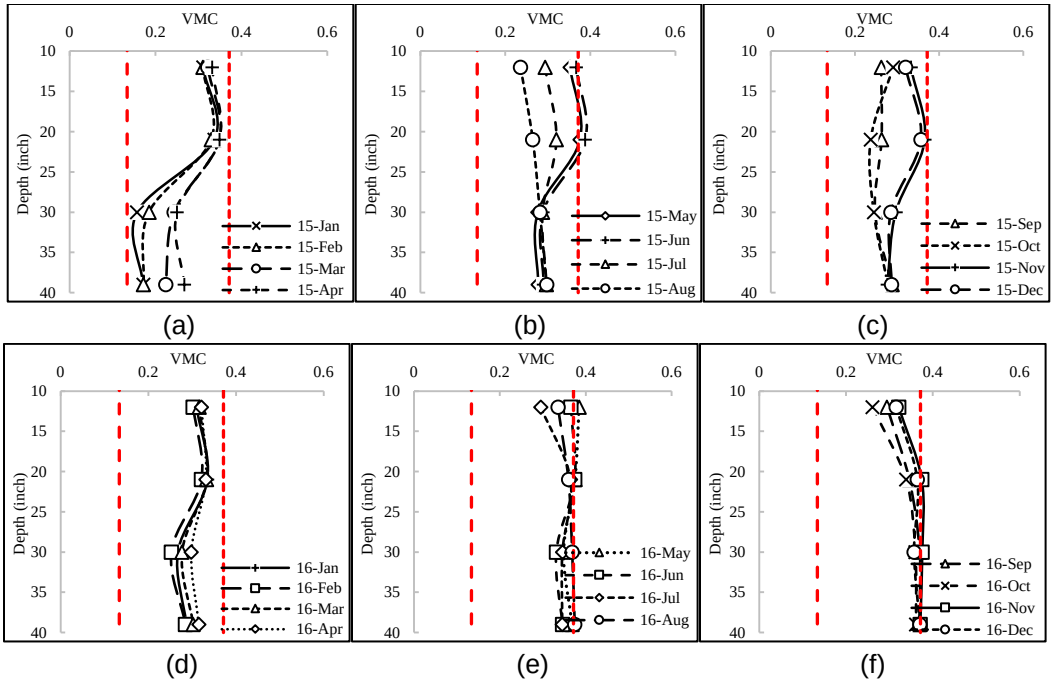

Figure 6.6 Profile distribution of average soil moisture content under SG (L-2)

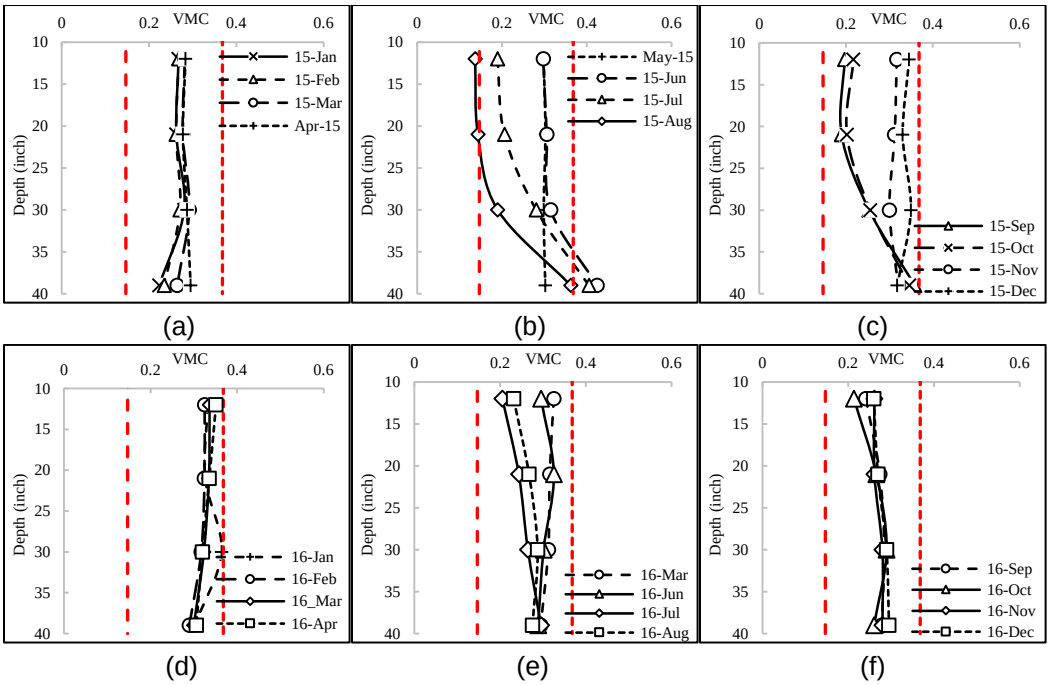

Figure 6.7 Profile distribution of average soil moisture content under BG (L-3)

6.4 In-situ Hydraulic Conductivity Test Results

The in-situ saturated hydraulic conductivity test results determined from the Guelph permeameter (GP) and unsaturated hydraulic conductivity results measured from the installed sensors are presented in the following section.

6.4.1 Saturated Hydraulic Conductivity (K_s)

GP was used to measure the in-situ hydraulic conductivity. Since GP is a slightly destructive test, measurements were made three times during the study period, in different lysimeters. The results obtained from the GP test (single-height method) are summarized in Table 6.2.

Table 6.2 Saturated hydraulic conductivity measured from GP

Lysimeter	14th June, 2016		19th Nov, 2016		8th April, 2017	
	Summer 2016		Fall 2016		Spring 2017	
	6-inch depth	12-inch depth	6-inch depth	12-inch depth	6-inch depth	12-inch depth
	cm/sec					
L-1	4.54E-07	6.11E-06	6.54E-05	3.47E-06	5.48E-05	3.57E-06
L-2	1.44E-06	5.14E-06	2.38E-05	8.79E-06	1.25E-05	5.15E-05
L-3	4.58E-06	2.67E-06	2.16E-06	3.88E-07	2.22E-06	4.85E-06
L-4	2.58E-04	9.10E-05				
L-5	6.01E-05	2.81E-05				
L-6	3.72E-05	1.85E-07				

The saturated hydraulic conductivity (K_s) of the cover soil at both 6-inch and 12-inch depths for different lysimeters varied by two orders of magnitude. The measured in-situ K_s also indicated one or two orders of magnitude increase in the values compared to the laboratory-measured K_s. The change in the saturated hydraulic conductivity was compared to the laboratory-measured value presented in Figure 6.8. The K_s changed 10 to 100 orders in magnitude compared to the value measured in the laboratory. In the field,

K_s mostly ranged between 1×10^{-4} to 1×10^{-6} cm/sec. Albright et al. (2004) reported, based on the extensive test results from ACAP, that the K_s of most soils ranges between 1×10^{-5} and 1×10^{-3} cm/sec after a few years of field exposure. Though the density measured at a different time was higher with increasing depth, no substantial variation was observed at 6-inch and 12-inch values of saturated hydraulic conductivity. Benson et al. (2007) reported that root intrusion is not a significant factor in causing a large increase in the hydraulic conductivity. Since the top 12 to 15 inches of the cover soil was occupied by dense roots, similar K_s values were observed. Based on the average (geometric mean) K_s value, it was concluded that approximately 0.1 to 0.42 mm of rainfall can infiltrate the cover soil per hour. Strunk (2009) reported similar results from a study on the Regina Fleet Street landfill, northeast of Regina, Saskatchewan.

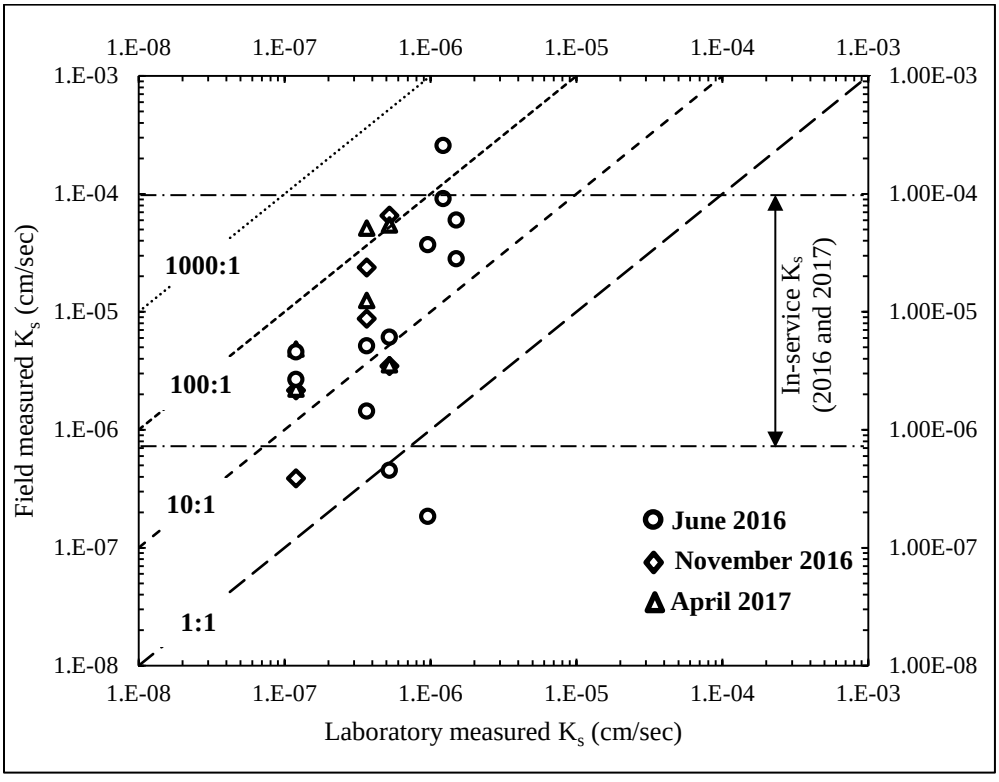

Figure 6.8 Post-construction changes in K_s (cm/sec)

6.4.2 Unsaturated Hydraulic Conductivity (K_ψ)

K_ψ was determined from the FSWCC, and the moisture flow in the cover was assessed based on the measured value of the conductivity. The instantaneous profile method (IPM) (Meerdink et al. 1996, Khire et al. 1995) was applied to determine K_ψ. The dataset used for the calculation of K_ψ was clustered into several groups. The clustering of the data set was done in such a way that it included a wide range of moisture and suction variations (e.g. one bunch of data selected after heavy precipitation, another group of data gathered during high temperatures with no or minimal precipitation). The main assumption in the IPM method is that the flow is one-dimensional and unidirectional. The average FSWCC was used to calculate the hydraulic gradient. K_ψ measured at the entire suction range for different lysimeters in the field is shown in Figure 6.9. All the data points clustered at approximately 1×10^{-4} to 1×10^{-10} cm/sec conductivity range. K_ψ was also predicted using the Van Genuchten-Maulem function (Van Genuchten 1980) for all of the lysimeter soils. The Van Genuchten-Maulem prediction model uses the following equation:

$$K_\psi = K_{sat} \times \frac{\left\{1-(\alpha\psi)^{(n-1)}[1+(\alpha\psi)^n]^{-m}\right\}^2}{[1+(\alpha\psi)^n]^{\frac{m}{2}}}$$

Where, K_{sat} is the saturated hydraulic conductivity of the soil, based on laboratory and in-situ (Guelph) measurement. α and n are the fitting parameters obtained from laboratory-based SWCC average FSWCC. A comparison of the predicted and calculated K_ψ is presented in Figure 6.9. The prediction curve of K_ψ was in good agreement with the measured K_ψ at higher suction levels (Figure 6.9). At lower suction levels (saturated or near saturated condition), the measured data points appeared scattered due to the continuous effect of wet-dry cycles (precipitation followed by ET and vice versa). IPM measured K_ψ as much as 10^{-4} cm/sec (in some cases 10^{-3} cm/sec, L-5 and L-6) at suction levels near 5 to 20 kPa. At this lower suction level, moisture is assumed to flow under

gravity (saturated condition). At greater suction levels (~1000 kPa), K_ψ was found approximately 10^{-10} cm/sec for all of the lysimeter soil. At this higher K_ψ value, moisture is assumed to reach the residual status when moisture flow requires higher energy. An interesting point was observed in L-3 and L-6. The soils in lysimeter 3 and 6, which were seeded with the identical vegetation (BG-sodded cover), were found with K_ψ values as low as 10^{-12} cm/sec (almost 100 order lower in magnitude than 10^{-10} cm/sec). Under the same meteorological condition, these two lysimeter's soils showed a further decrease in K_ψ. Therefore, it is a clear indication of the plant root effect. BG, with its higher moisture usage capacity, causes the soil to shrink more than the other grass roots during the dry season, and water flow becomes negligible at this unsaturated condition.

Percolation is the movement of water from the bottom of the cover soil, and is the performance indicator for an ET cover system. At saturated condition, water flows under unit hydraulic gradient (Albright et al. 2004). When moisture starts decreasing, suction develops in the soil that eventually inhibits the free flow of water. In the field, during the high intensity precipitation event, moisture content increased and reached the saturation point very fast, while suction of the soil decreased to 5 to 10 kPa (Figure 6.9), which corresponds to lower hydraulic conductivity (10^{-3} cm/sec to 10^{-4} cm/sec). In-situ measured (Guelph) saturated hydraulic conductivity results also showed similar findings (Figure 6.9). The major pulses of percolation of the lysimeters were logged in the percolation collection tank during the heavy rainfall event. Percolation predicted by UNSAT-H also suggests that large pulses of water movement from the bottom of the cover occurred during high intensity rainfall. UNSAT-H simulation results are presented in chapter 7. After the precipitation, the soil began drying out (desorption), the suction increased, and the hydraulic conductivity at the unsaturated condition changed accordingly.

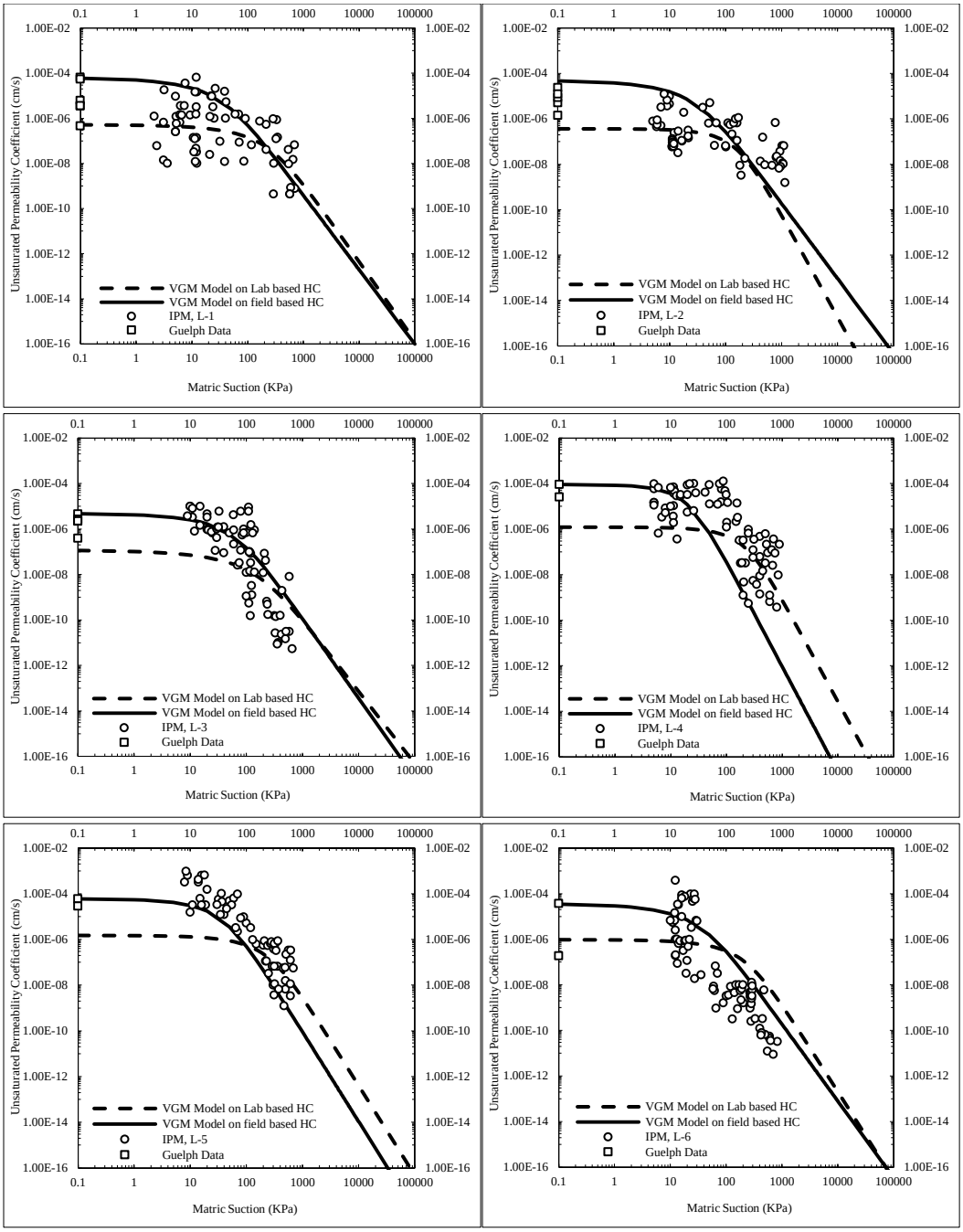

Figure 6.9 Unsaturated hydraulic conductivity of different cover soils

6.5 Evaluation of ET Cover Performance

6.5.1 Evaluation of Surface Runoff

Annual runoff figures for the entire data set obtained from the six lysimeters are shown in Figure 6.10 as a function of annual precipitation. In all six lysimeters, runoff ranged from 0 to 1088 mm/year with percent of precipitation as high as 72%. No general trend was observed between the annual precipitation and annual runoff. Larger quantities of annual precipitation produced a larger amount of annul runoff (Figure 6.10 a). The major increment in the surface runoff occurred with higher frequency during the greater intensity rainfall. Annual surface runoff is also shown as a function of the ratio of the mean precipitation intensity to the saturated hydraulic conductivity of the surface layer (I_p/K_s) in Figure 6.10 b. I_p and K_s are the geometric means of the non-zero hourly precipitation. The ratio I_p/K_s is an indicator of infiltration capacity (Apiwantragoon et al. 2014). Here, data is presented only for the years 2016 and 2017. Though, no specific trend exists between annual runoff and I_p/K_s, in general, higher I_p/K_s indicates higher annual runoff. The ratio I_p/K_s indicates that the intensity of precipitation exceeded the surface-saturated hydraulic conductivity in most of the cases. Therefore, a larger quantity precipitation with greater intensity is the major factor for more annual runoff.

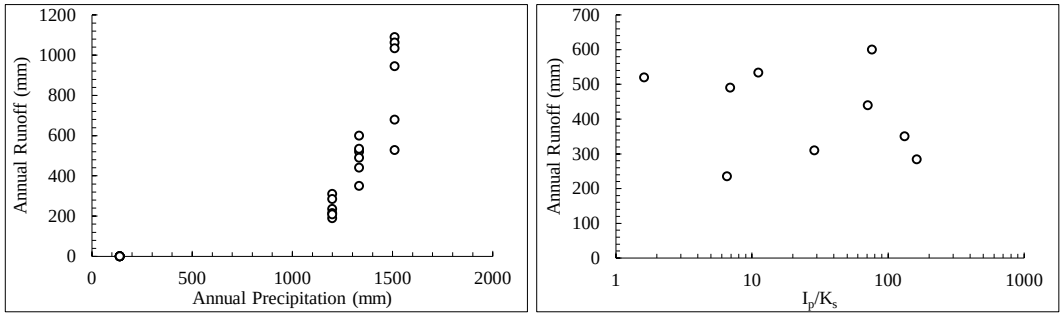

(a) (b)

Figure 6.10 (a) Annual runoff as a function of annual precipitation (b) Annual runoff as a function of precipitation intensity to saturated hydraulic conductivity

6.5.2 Evaluation of Percolation

Annual percolation of the six lysimeters is presented as a function of annual precipitation and time, and is shown in Figure 6.11. Annual percolation ranged from 42 to 75 mm/year for the different lysimeters. In general, Figure 6.11 (a) indicates that higher annual precipitation equates to a higher quantity of annual percolation. However, Figure 6.11 (b) shows that annual percolation decreased with time, even though the annual precipitation throughout the monitoring period was more than 1000 mm, with frequent high-intensity storms. This is an indication of lowering the annual percolation through enhanced ET by matured plant growth. Nonetheless, the decrease in annual percolation was not significant in amount (Figure 6.11 b). The ratio of annual precipitation to annual potential evapotranspiration, P/PET, was greater during the three years of the monitoring period. Therefore, the decrease in annual percolation was insignificant. The differences in the annual percolation values among the lysimeters under the on-site identical climatic conditions are the results of differences in the initial compaction level, initial soil moisture content and suction, different water holding capacity of plants, root growth, etc.

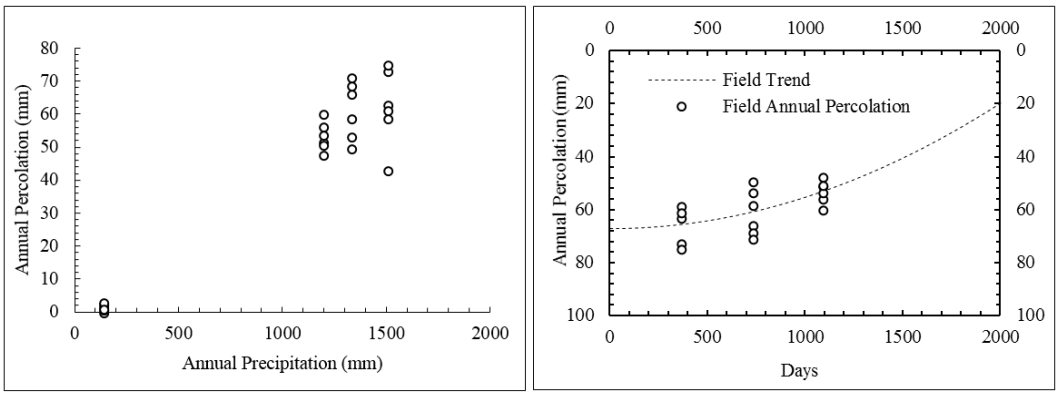

(a) (b)

Figure 6.11 Annual percolation as function of annual precipitation (b) Annual percolation as a function of time

6.5.3 Evaluation of Evapotranspiration

Evapotranspiration (ET) is the loss of water from the cover soil to the atmosphere by the combined process of evaporation from the soil and plant surface and transpiration through the plants. Accurate estimation of ET is one of the major hydrological components of water balance cover for optimum ET cover performance evaluation. Quantification of potential evapotranspiration (PET) for grass-type plants in the ET cover system is especially of great significance for the design and evaluation of the ET cover system, as it is an important design variable. Many approaches for quantifying ET have been developed and adapted for different applications. The most widely-used method is the Food and Agricultural Organization (FAO-56) Penman-Monteith (PM) method (Allen et al. 1998). This method is considered the standard method for quantifying ET. Another well-developed method is the modified Thornthwaite model (McKenney and Rosenberg, 1993). This method is one of the best-known methods for PET parameterization. The FAO-56 PM method and Thornthwaite method were applied in quantifying PET and evaluating ET of the lysimeters.

The FAO-56 PM method predicts ET based on many meteorological parameters. The following FAO-56 PM equation is used for estimating evapotranspiration (ET_0):

$$ET_0 = \frac{0.408\Delta(R_n - \mathrm{G}) + \gamma \frac{900}{T+273} \times u_2(e_s - e_a)}{\Delta + \gamma(1 + 0.34 \times u_2)}$$

Where, R_n is the net radiation at the cover surface ($MJm^{-2}day^{-1}$), G is the heat flux density ($MJm^{-2}day^{-1}$), T is the main daily temperature (^oC), e_s and e_a are the saturation and actual vapor pressure (KPa), Δ is slope vapor pressure curve (KPa $°C^{-1}$), and γ is psychrometric constant (KPa $°C^{-1}$). All of the meteorological input was collected from the weather station, and some of the data was based on literature.

The modified Thornthwaite model uses climatological and soil data to predict the PET. Climatological data includes only the average monthly temperature. Soil data is comprised of soil moisture content, field capacity (Θ_{FC}) and wilting point (Θ_{WP}), and moisture content. The model provides the PET and actual ET with these input parameters. The modified Thornthwaite model uses the following equation:

$$PET = 16 \times \left(\frac{10T_i}{I}\right)^{a} \times \left(\frac{N}{12}\right) \times \left(\frac{L}{30}\right)$$

Where, PET is potential evapotranspiration (mm/month), L is the monthly mean daytime duration (hours), N is the number of days in a month, T is the mean monthly temperature, and I is the heat index. I and a are expressed as follows:

$$\mathrm{I} = \sum_{i=1}^{12} \left(\frac{T_i}{5}\right)^{1.514}$$

$$a = 492390 + 17920I - 771I^2 + 0.675I^3) \times 10^{-6}$$

Actual evapotranspiration (ET) is a function of relative water content (Θ_{rel}). Actual ET can be computed using the following equations:

$$ET_{actual} = F\,(\Theta_{rel}) \times PET$$

$$\theta_{rel} = \frac{\theta - \theta_{WP}}{\theta_{FC} - \theta_{WP}}$$

Comparison of the results obtained from the FAO-56 PM and Thornthwaite model are presented in Figure 6.12. Both ET models propagate with a sinusoidal pattern. High ET was observed during the summer period, and a lower rate of ET was observed during the dormant period. However, none of the models showed the same results. The variations in the results reflect the differences in the input variables. Based on the estimation, the FAO-56 PM method has an annual PET ranging from 1080.97 mm/year to 1182.25 mm/year. The Thornthwaite method showed a relatively higher value of annual PET which ranged from 1149.15 mm/year to 1192.29 mm/year (Table 6.3).

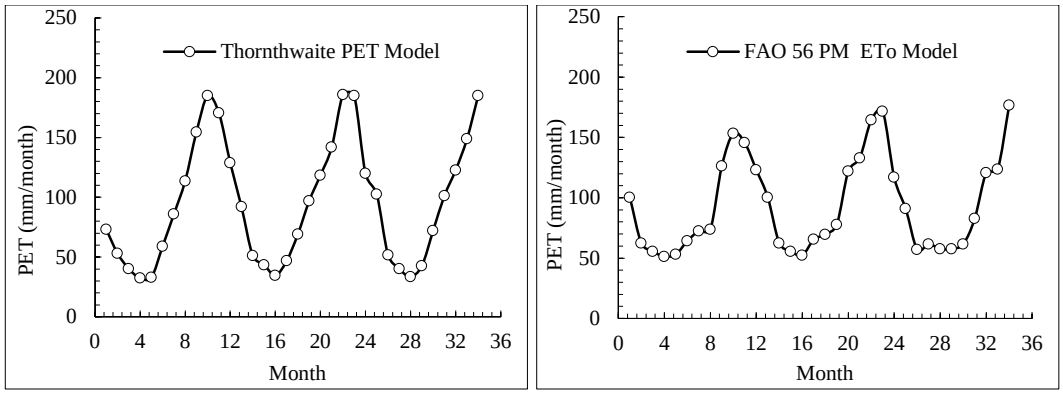

Figure 6.12 Estimated PET derived from different methods

Table 6.3 Annual PET from different models

Model	Year			
	2014	2015	2016	2017
FAO-56 PM	218.17	1080.974	1182.25	1166.47
Thornthwaite	166.3859	1149.147	1192.29	1209.98

Field-measured ET and actual ET based on the relative moisture content were further compared with the two derived models. Field-measured ET from the water balance equation was converted to monthly ET. PET calculated from the Thornthwaite model was converted to actual ET after multiplying with the relative moisture content. The comparison of the model-predicted ET and field-measured ET is presented in Figure 6.13. The trend of the field ET cycle followed the same sinusoidal propagation, with peak ET during the summer time at ambient high temperatures. However, a clear deficiency of ET was observed between the predicted and measured ET values (Figure 6.13). Based on the field-measure ET during the monitoring period, the annual ET was found to range between 616 mm/year to 795.5 mm/year the for different grass covers, representing a deficit of approximately 300 to 400 mm/year of ET. Comparisons of the monthly ET, obtained from the monitoring results and predicted values from the FAO-56 PM method, are presented in Figure 6.14. The data set lies within the model predicted PET zone, below the 45^{o} straight

line, while the actual ET and field-measure ET are in relatively good agreement. In the field, despite an abundance of available water, ET didn't occur in full demand due to the absence of a deeper root zone. Consequently, the surface layer underwent several wet-dry cycles by the combined effects of ET and rainfall. The deeper zone of the cover was recharged from inputs of precipitation, but water release was minimal from that zone. The maximum annual ET was from the cover planted with Bermuda grass (795.5 mm/year), which has a deeper root zone than other types. Therefore, it is the root system that maximizes the ET by removing moisture from the deeper depths of the ET cover.

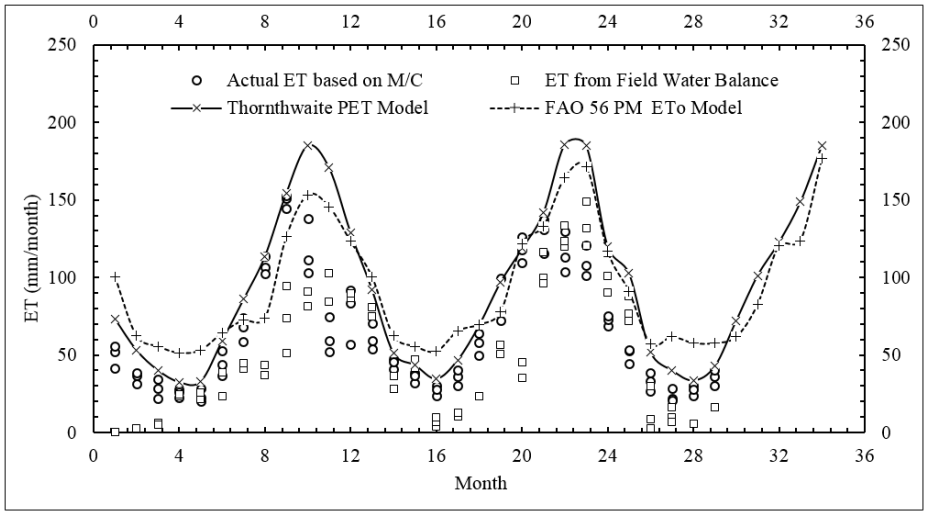

Figure 6.13 Comparison of field ET cycle with model prediction

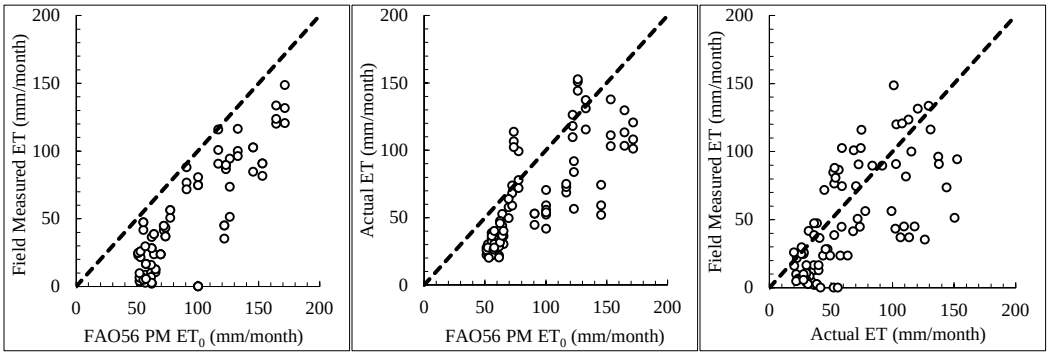

Figure 6.14 Distribution of field-measured and model-predicted monthly ET

The response of annual PET and ET as a function of annual precipitation is shown in Figure 6.15. The figure shows a non-linear relationship between ET and precipitation. As can be seen from the figure, annual ET increases as annual precipitation increases and is indicative of the availability of stored water within the cover soil to be removed by ET. Apiwantragoon et al. (2014) reported similar patterns of ET and precipitation response with an extensive data set from the ACAP sites. They found that the two curves of PET and ET initially extend linearly at a constant slope, and after a certain point, the slope of the curves reduces significantly. Therefore, regardless of the type of vegetation, the fraction of precipitated water released by ET reduces with increased precipitation after certain precipitation. This implies that having a surplus of water in the cover soil does not always mean that it will be removed by ET. There is a significant difference between the PET and ET curves, as can be seen from Figure 6.15. This large gap between the curves indicates the inadequacy of proper root depth. Despite available energy for ET at the site condition, due to the lack of a deeper root zone, the ET curve lies well below the PET curve. Therefore, greater annual precipitation tends to increase the annual ET. However, there is a precipitation transition above which the rate of ET diminishes. A deeper root zone is significant for converting annual ET to PET.

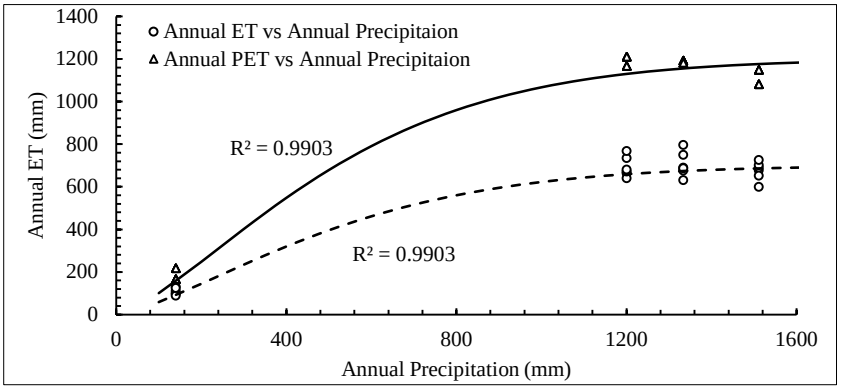

Figure 6.15 Annual PET and ET as a function of annual precipitation

The relationship of precipitation, PET, and ET is presented in Figure 6.16. Based on the calculated PET and field-measured ET from the water balance equation, the data points (ratio of ET to PET) cluster near 50 to 70% at PET/P of approximately one. This indicates that 50 to 70% of the stored water can be removed by ET, despite available energy (PET/P ~ 1) for the ET process. The 30 to 50% deficit of ET occurs due to the absence of an energizer to use the available energy to amplify the amount of ET. The energizer is the deeper root system which increases the amount of ET by extracting water from the deeper depth of the cover soil. The dataset obtained from the study was further compared with results from the ACAP sites. Apiwantragoon et al. (2014) developed a function to compare the relationship between ET/PET and PET/P, based on the extensive monitoring results of several ACAP sites. The form of the function is as follows:

$$\frac{ET}{PET} = 0.84 \times \left(\frac{P}{PET}\right)^{0.913}$$

The comparison of the results from the six lysimeters with the developed function is shown in Figure 6.16. The curve demonstrates that when PET/P>>1, ET will be negligible, as there is not available water to be removed. On the other hand, when PET/P is close to one, ET tends to be level with PET, as the energy available for ET becomes comparable to the water available.

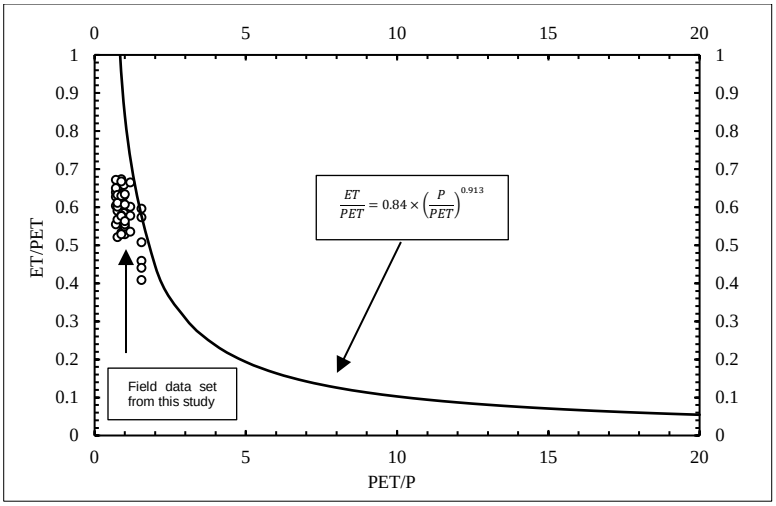

Figure 6.16 Ratio of annual ET to annual PET (ET/PET) as a function of ratio of annual PET to annual precipitation (PET/P)

6.5.4 Development of Generalized Field Evaluation Curve (FEC)

Based on the extensive field monitoring of the water balance components and the influential factors on the performance of the ET cover, a generalized field evaluation curve (FEC) was developed, using trend analysis. The significance of the FEC is that it can evaluate and predict the performance of the ET cover system based on the existing field results. Attempts were made to develop the FEC, relating the effect of root growth to the most important and optimization water balance parameter, evapotranspiration. The existing field data set was utilized to develop the FEC to present the actual field performance.

Field evapotranspiration (ET) was assessed with respect to plant root growth. To simplify analysis, field-measured ET was converted to an annual measurement. Time-dependent root measurements were made from the installed minirhizotrons. Based on the field-measured data points, curves were fitted with the best-suited function through least square analysis. Root growth function was developed based on the average field-

measured root depth for different grass types. The average rooting depth measured from all of the minirhizotrons was approximately 16-inches, based on the latest monitoring results. A proportional growth rate function (exponential) was found to best suit the field-measured data points. The following equation was used to produce the field fit root growth function:

$$y = -\left(\frac{h}{k}\right) \times \left(1 - e^{(-kx)}\right)$$

Where, y = root depth (inch), x = time in days, h and k are fitting parameters. The value of the fitting parameters h and k are -0.05662 and 0.003506, respectively. The field data points with the developed function are presented in Figure 6.17, in both arithmetic and logarithmic scale.

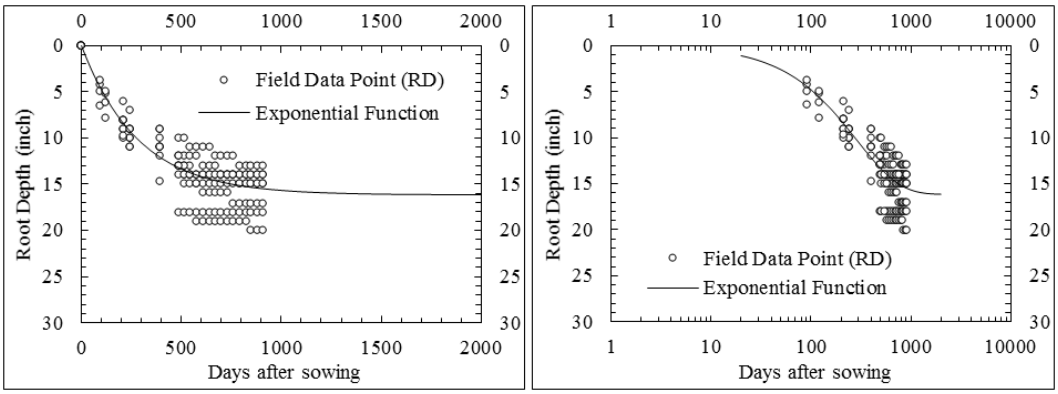

(a) (b)

Figure 6.17 Plot of fitted curve with field-measured data points of root growth (a) arithmetic scale (b) semi-logarithmic scale

The trend of annual ET at the field atmospheric condition and plant root status was evaluated and fitted with the appropriate function. The data set obtained from the annual measurement of ET showed no significant differences in all the six lysimeters. Based on the field-measured ET, using the water balance equation from the six lysimeters, an average of 690 mm annual ET occurred in the years 2015, 2016 and 2017. Just after the

construction (t = 0 days) of the lysimeters, ET was assumed to be zero. The total ET in the last three months of 2014 for all of the lysimeters was an average of approximately 96 mm. Based on the field results of the annual ET of the six constructed test sections, a 5-parameter logistic (5PL) sigmoid equation was found to closely fit the ET data points. The equation used in constructing the asymmetric sigmoidal curve is given below:

$$y = \left[d + \frac{a - d}{\left[1 + \left(\frac{x}{c}\right)^{n}\right]^{m}} \right]$$

Where, y = ET (mm), x = time in days, a = 0 (minimum asymptote), d = 690 mm (maximum value of the curve or maximum asymptote), c = 2907662 (inflection point), n = 1.43 (steepness/slope of the curve) and m = 860395 (asymmetry factor). The sigmoidal curve and the field data points are shown in Figure 6.18. ET increased significantly during the first 400 days, as shown in the figure with a steeper slope of the curve. There was a sharp change in the curvature after 400 days, which continued horizontally after approximately 500 days. However, the true characteristics of the 5PL function are clear in the semi-logarithmic scale (Figure 6.18 b). The function approaches two horizontal asymptotes, one to the infinity and the other to zero. The maximum asymptote is 690 (mm). The transition region is between the two asymptotic regions. There is a single point of inflection in the transition region. Lower asymptote in the curve signifies the lower rate of ET during the dormant period (first three months after construction of the ET cover). Just after the winter, as soon as growing period started, the rate of ET increased significantly until it reached the maximum asymptote.

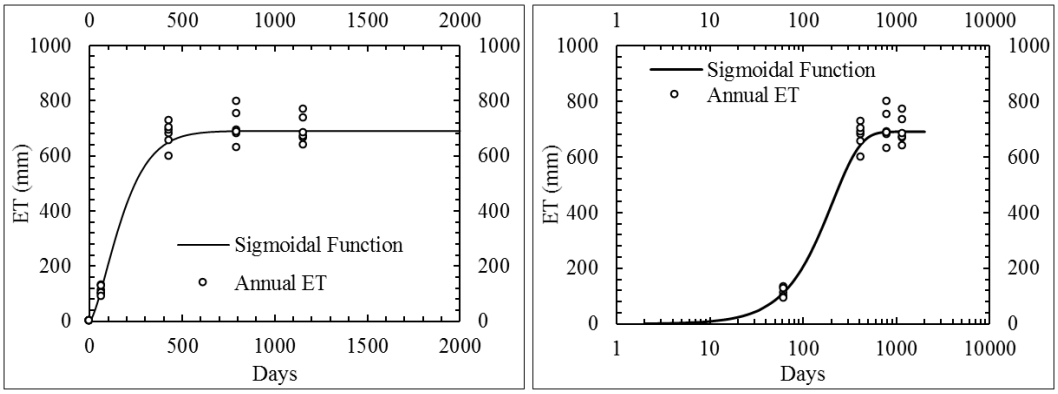

Figure 6.18 Plot of fitted curve with field-measured data points of annual ET (a) arithmetic scale (b) semi-logarithmic scale

The developed function on root growth and ET followed their respective patterns. Root growth became almost steady once the roots hit the highly compacted soil layer. The mean annual ET was practically constant after the first year in all of the lysimeters. An interesting trend was observed when the two functions were compared with respect to time (Figure 6.19 a). The root growth and ET function followed an almost-parallel path throughout the monitoring period. When root growth rate was faster, ET also occurred at a higher rate (Figure 6.19 a, steeper portion of the curve). As soon as root growth ceased, the annual ET reached the standstill condition. Therefore, it can be concluded that the rate of ET is highly dependent on the plant's deeper root system. A robust below-ground biomass can increase the ET significantly and optimize the ET cover performance. Based on this trend, the two constructed functions were combined, and the generalized FEC was developed. The FEC is shown in Figure 6.19 (b). The curve presents how ET performs in the field in response to RD, as can be observed in the figure. When the root depth is approximately 15 inches, almost 700 mm of ET will occur every year.

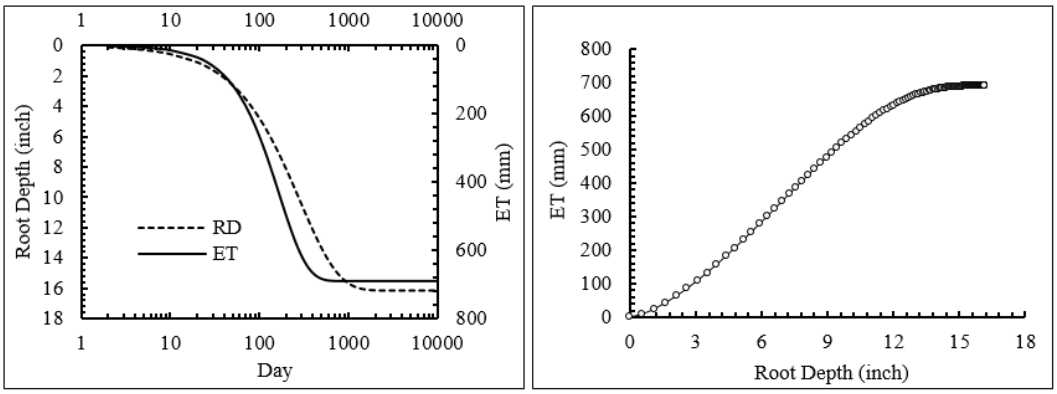

(a) (b)

Figure 6.19 (a) Comparison of the RD and ET functions (b) Generalized field evaluation curve (FEC)

6.6 Performance Comparison of Different Types of Vegetation

Ideal performance of the ET cover system largely depends on the presence of a robust and deep root system into the cover. Deep roots support the cover system's release of moisture from the deeper zone through the ET process. It is important to keep in mind that water usage, or the rate of ET, varies among different grass types. Therefore, the performance of the ET cover differs among vegetation types. Numerous studies have focused on measuring the rate of ET among different grass types. Green et al. 1990 used mini lysimeters to estimate the rate of ET for 12 cool-season grasses in a controlled environment. Green et al. (1990) reported that Kentucky bluegrasses showed the highest ET rate 0.48-inch d^{-1} (12.2 mm d^{-1}) among the 12 different grass species. Another study by Devitt et al. (1992) determined the rate of ET from lysimeters located on golf courses. Devitt et al. (1992) reported a two-year's average ET rate for Bermuda grass 0.16-inch d^{-1}(4.06 mm d^{-1}) and 0.11-inch d^{-1}(2.79 mm d^{-1}) for two different sites. Kneebone and Pepper (1984) evaluated the ET rate of Bermuda grass at different sand-soil mixes, using percolation lysimeters. Based on their analysis, they found that the ET rate from Bermuda grass was 0.2, 0.25 and 0.3-inch d^{-1} (5.08, 6.35 and 7.62 mm d^{-1}) in different soil mixes. Their dataset

showed that the rate of ET from Bermuda grass can exceed pan evaporation by a significant amount.

In this study, the ET rate was evaluated for three different vegetation types that were seeded in six lysimeters. The comparison of ET by different vegetation types is presented in Figure 6.20. It can be seen from the figure that the rate of ET from Bermuda grass is greater than from the other two types of grasses. Bermuda grass produced a maximum ET rate of 0.1887-inch d^{-1}(4.79 mm d^{-1}) during the summer. NT and SG produced a maximum ET rate of 0.1397-inch d^{-1}(3.55 mm d^{-1}) and 0.1569-inch d^{-1}(3.98 mm d^{-1}), respectively. Maximum, minimum, and average ET rates from three different types of vegetation are listed in Table 6.4. Figure 6.20 shows that most of the data lies above the 45^{o} straight line (within the Bermuda grass zone), especially when the ET rate exceeds approximately 3 mm d^{-1}. This indicates that during the high ET period, if there is available water, Bermuda grass can release a greater amount of water to the environment than the other two types of grasses. Therefore, based on the rate of ET from different vegetated lysimeters, it can be concluded that Bermuda grass performs better than Native Trail grass and Switch grass. It was also observed that vegetation in the slope-section lysimeters could produce higher amounts of ET than in the flat-section lysimeters.

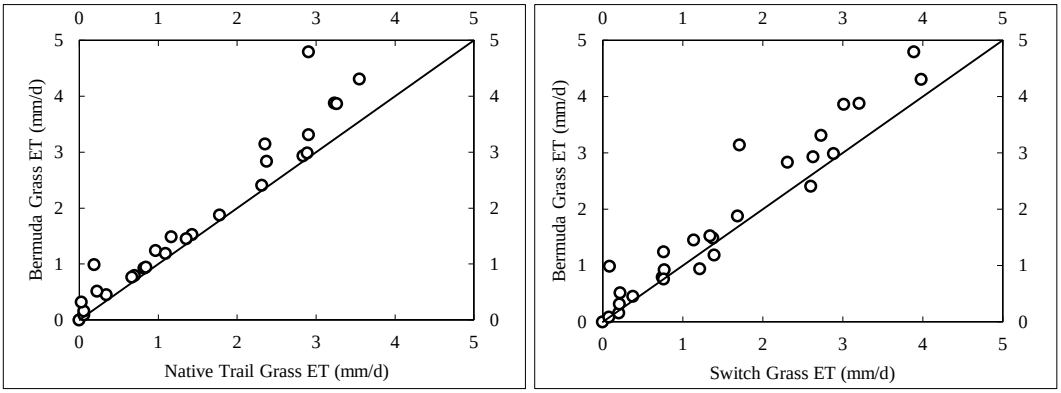

Figure 6.20 Comparison of ET rates between grasses

Table 6.4 Comparison of ET rates among different vegetation

Grass Type	Lysimeter	ET Rate		
		Inch d^{-1} (mm d^{-1})		
		Maximum	Minimum	Average
Native Trail Grass	1,4	0.1397(3.55)	0.0011(0.03)	0.0611(1.55)
Switch Grass	2,5	0.1569(3.98)	0.0031(0.07)	0.0626(1.59)
Bermuda Grass	3,6	0.1887(4.79)	0.0035(0.08)	0.0745(1.89)

The annual ET, calculated for the six lysimeters from the water balance equation, is shown in Figure 6.21. It is clear from the figure that L-3 and L-6 (Bermuda grass) has the maximum annual ET. It is to be noted that all six lysimeters received an equal amount of precipitation under the same climatic conditions (e.g. temperature, relative humidity, solar radiation). Hence, the soil water recharge was almost equal after heavy precipitation. Nonetheless, there were differences in the amount of ET among lysimeters. It can thus be concluded that it is the plant which makes the differences in the magnitude of ET. Bermuda grass, with its deeper root zone, removed a greater amount of water to the atmosphere compared to the other two grasses. Annual percolation was also found comparatively lower for the lysimeters seeded with Bermuda grass (Figure 6.21 b). Devries (2016) reported similar findings from his short-term hydraulic performance of ET cover in the City of Denton Landfill. However, annual percolation among the lysimeters does not make a significant difference, even though there is considerable variation in annual ET. This is because of the greater quantity precipitation with high frequency, which contributes to the large pulses of percolation and bumps up the annual percolation. Therefore, vegetation has a significant role in augmenting annual ET, but precipitation amounts and intensity impact annual percolation and the performance of the ET cover system.

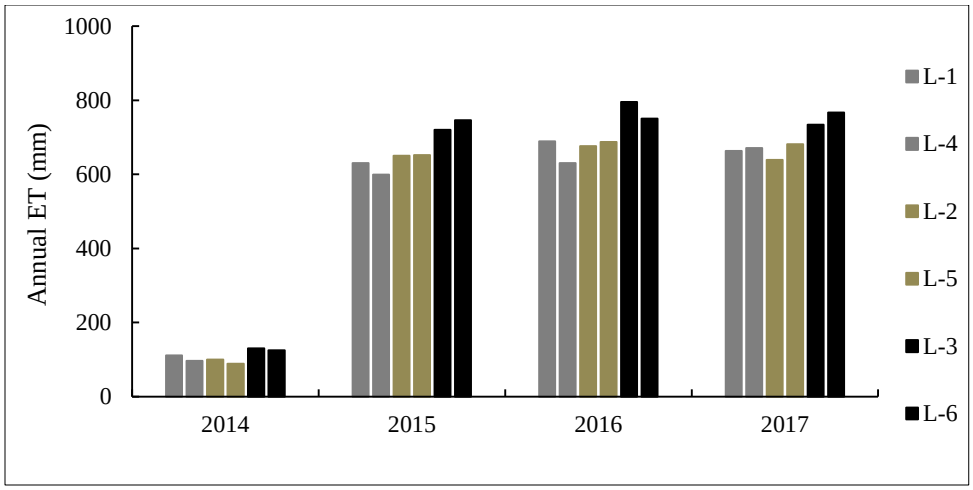

(a)

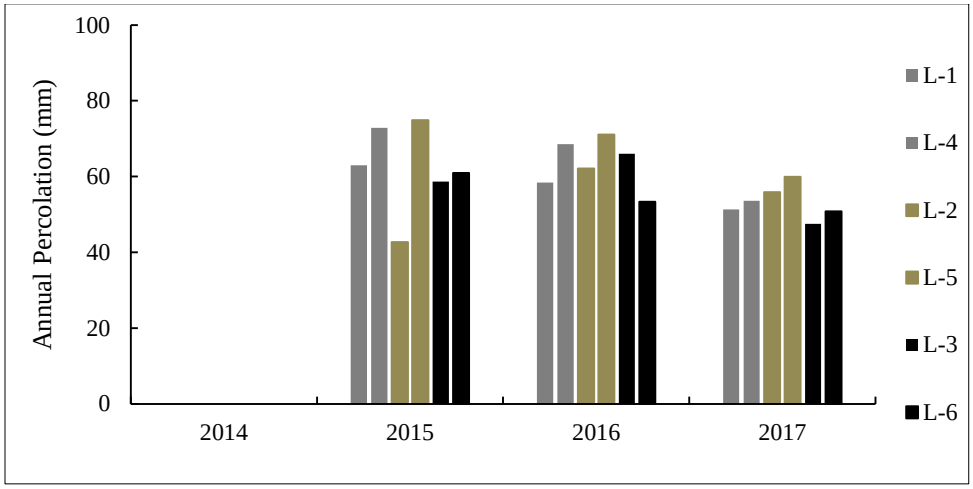

(b)

Figure 6.21 (a) Comparison of annual ET for different vegetation types (b) comparison of annual percolation for different vegetated lysimeters

Chapter 7

Numerical Modeling

7.1 Introduction

This chapter presents the numerical simulation results of the evapotranspiration cover (ET cover) system and parametric evaluation results of different parameters. Water balance simulation was approached in two ways: forward modeling (FM), which is the typical design approach, and field-fit (FF) water balance simulation. In FM, the input parameters used in the simulation were based on the laboratory test results of soil, conservative vegetation data, and on-site meteorological data. The input parameters for the FF approach were entirely based on the field monitoring results. The hydraulic properties of the soil, vegetation data, and the meteorological parameters collected during the study were directly used as input for the field-fit simulation. Both of these approaches of water balance simulation were compared to the field water balance results. The objective of the two-way approach for the water balance simulation was to find the optimum way for designing an ET cover.

A parametric study was conducted, using UNSAT-H to examine the sensitivity of different parameters. The term sensitivity refers to how changes in an input parameter result in significant changes to the output. The objective of the parametric study was to find the critical parameters for optimum ET cover performance and to determine the effect of different parameters on the water balance.

7.2 UNSAT-H Input Parameters

A set of parameters was developed for the water balance simulation in UNSAT-H to predict the hydrologic performance of the ET cover. The parameters were developed based on the field monitoring results and laboratory measurements of the soil and vegetation.

7.2.1 Model Geometry

The model geometry was based on the respective depths of the field cover soil. The total depth of the soil profile modeled was 4 ft. (1220 mm). For the parametric study, up to 7 ft. (2133 mm) of cover thickness was assessed. The nodal spacing was set at 1 cm (Dwyer, 2003, Fayer 2002; Webb 2002). This narrow spacing (1 cm) is supposed to accurately represent the modeled cover profile.

7.2.2 Boundary Condition

The water flow across the surface and lower boundary of the cover profile was set per the specifications set by Dwyer (2003). Precipitation intensity was applied from the default condition (10 mm/hr.) to the in-situ precipitation rate (up to 200 mm/hr.). Daily weather data was incorporated to model surface evaporation. The weather data used in the model was collected from the on-site weather station (Oct 2014 to Dec 2016). The daily precipitation data was recorded and the annual precipitation values were evaluated. The amount of average annual precipitation, derived from the on-site weather station and based on 2015 and 2016 data, was found to be 56-inches (1422.4 mm). The precipitation recorded during these years was above the historical average for Denton, TX. In 2015, recorded annual precipitation was approximately 60 inches (1511.3 mm). In UNSAT-H, potential evapotranspiration (PET) is divided into potential evaporation (E_p) and potential transpiration (T_p). E_p is estimated from daily weather, and the calculation of T_p is made based on the following equation. LAI was assigned in the equation, based on literature.

$$T_p = PET\ [a + b\ (LAI)^c]$$

7.2.3 Vegetation Properties

The vegetation parameters of UNSAT-H are the leaf area index (LAI), rooting depth and density, and root growth rate, as well as the suction head value that corresponds to the soil's field capacity and wilting point. The LAI value was assumed to be 1, based on

the geographical position of the study area (high precipitation in a semi-humid region). For comparison purposes, in West Texas, the typical LAI value is 0.1 to 0.15 (Scanlon et al. 2005) because it is geographically in the dry region, with a lack of precipitation. The growing season was assigned according to the visual observation of the vegetation, in-situ measurement of ground coverage, and percent of bare area (PBA). Based on the field measurements and visual observations, the growing season was defined as being from late March to early August (120 days). PBA was assigned based on the LPI method test results. The maximum rooting depth of 45-inches (1143 mm) was assigned for FM and for the FF modeling; rooting depth was assigned based on field measurements from the minirhizotrons. The root depth for each vegetation type measured from the minirhizotron is given in Chapter 5. The root length density (RLD) was assumed to follow the following exponential function:

$$RLD = a \times e^{(-bz)} + c$$

The parameters used in the FM were: a = 0.315, b=0.0073, and c = 0.076 (Fayer 2000). The parameters suggested by Fayer (2000) represent very steep RLD function, as can be seen in Figure 7.1, and represent deep-rooting grass. Fayer assumed that the roots grow from the surface to the bottom of the cover with the same density. Laboratory-measured RLD functions were used for the FF modeling. The curve-fitting parameters for FF modeling are given in Table 7.1. Suction values corresponding to the field capacity and wilting point were set at 1500 kPa and 330 kPa, respectively.

Table 7.1 Fitting parameters of RLD for field-fit modeling

NT			SG			BG		
a	b	c	a	b	c	A	b	c
0.38	2.6	0.001	0.4	3.2	0.00001	0.4	2.5	0.005

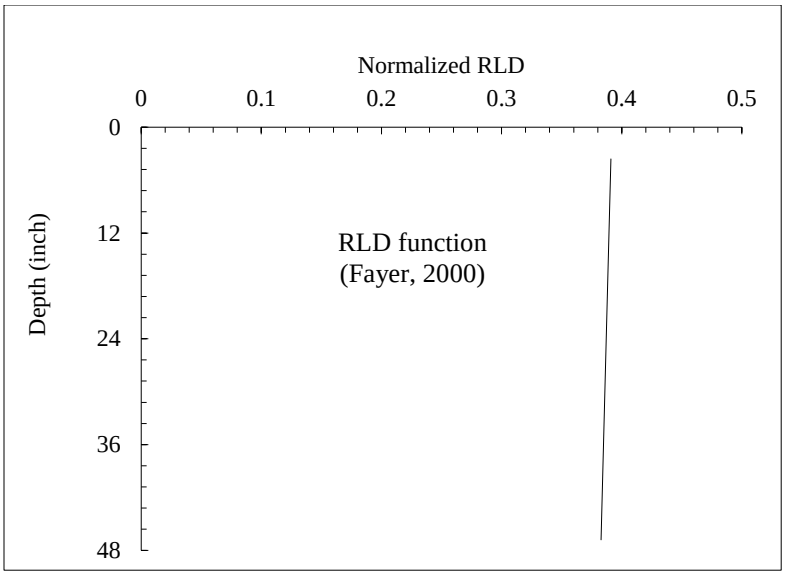

Figure 7.1 Shape of RLD function (Fayer 2000)

7.2.4 Soil Properties

The hydraulic properties of the soil for the simulation were selected based on the results of the laboratory investigation for the forward modeling (FM), and on the results of the field instrumentation for field fit (FF) simulation. The entire cover thickness was divided into two layers: top layer (surface layer) and storage layer. Saturated hydraulic conductivity and VG hydraulic parameters in FM for the storage layer were established based on the laboratory-measured test results. For FF simulation, saturated hydraulic conductivity data was set based on the in-situ hydraulic test results from the Guelph permeameter. In-situ hydraulic conductivities measured at 6-inch and 12-inch depth were assigned to the top layer and storage layer, respectively, in FF. The geometric mean of the measured conductivities was used as input. VG parameters for FF simulation were obtained from FSWCC. The upper-bound parameters were set at the storage layer, and lower-bound parameters at the storage layer. Hydraulic parameters used in the simulation are summarized in Table 7.2.

Table 7.2 UNSAT-H soil input parameters for different simulation approaches

Lysimeter	Model Approach	Soil Layer	Thickness	Saturated Hydraulic Conductivity	Van Genuchten Parameter			
					Θs	Θr	α	n
			inch (mm)	cm/sec	m^3/m^3	m^3/m^3	1/kPa	
L-1	FM	Top Soil	12 (304.8)	1.00E-06	0.420	0.09	0.0500	1.50
		Storage Layer	36 (914.4)	5.23E-07	0.397	0.12	0.0031	1.60
	FF	Top Soil	12 (304.8)	1.18E-05	0.385	0.12	0.0038	1.60
		Storage Layer	36 (914.4)	4.23E-06	0.350	0.11	0.1000	1.53
L-2	FM	Top Soil	12 (304.8)	1.00E-06	0.420	0.09	0.0500	1.50
		Storage Layer	36 (914.4)	3.65E-07	0.412	0.14	0.0051	1.53
	FF	Top Soil	12 (304.8)	7.54E-06	0.415	0.12	0.0045	1.55
		Storage Layer	36 (914.4)	1.33E-05	0.380	0.11	0.0800	1.50
L-3	FM	Top Soil	12 (304.8)	1.00E-06	0.420	0.09	0.0500	1.50
		Storage Layer	36 (914.4)	1.20E-07	0.429	0.09	0.0045	1.47
	FF	Top Soil	12 (304.8)	2.80E-06	0.429	0.09	0.0045	1.47
		Storage Layer	36 (914.4)	1.71E-06	0.350	0.09	0.0500	1.32

7.3 Forward Modeling Results

Simulations were conducted following the FM approach for the period between October 2014 and December 2017. Precipitation data for the period of June 2017 to December 2017 was considered identical to that which occurred from June 2016 to December 2016. Results of the water balance quantities predicted by UNSAT-H are shown in Figure 7.2. Cumulative precipitation during the simulation period was 4200 mm. ET was the largest component of the water balance quantities. Cumulative ET was 2,558 mm,

which was 60% of the total precipitation. The second largest component was surface runoff, which was approximately 47% of the total precipitation. Cumulative percolation simulated in the three-year period was 103 mm, which equated to 2.45% of the total precipitation, with an average of 34.3 mm each year. Several patterns were observed during the high intensity rainfall events (Figure 7.2). The effects of this high intensity rainfall were reflected in the high peak of soil water storage, runoff, and percolation. It is to be noted that there were several rainfall events which coincided with the growing season or high ET period. Nonetheless, in many of the cases, the amount of precipitation exceeded the rate of ET. Hence, under the on-site meteorological condition and the conservative soil and vegetation parameters, an average of 34.3 mm percolation is to be expected, based on the FM-based approach. The results obtained from the FF simulation are described, with field data, in Section 7.4.

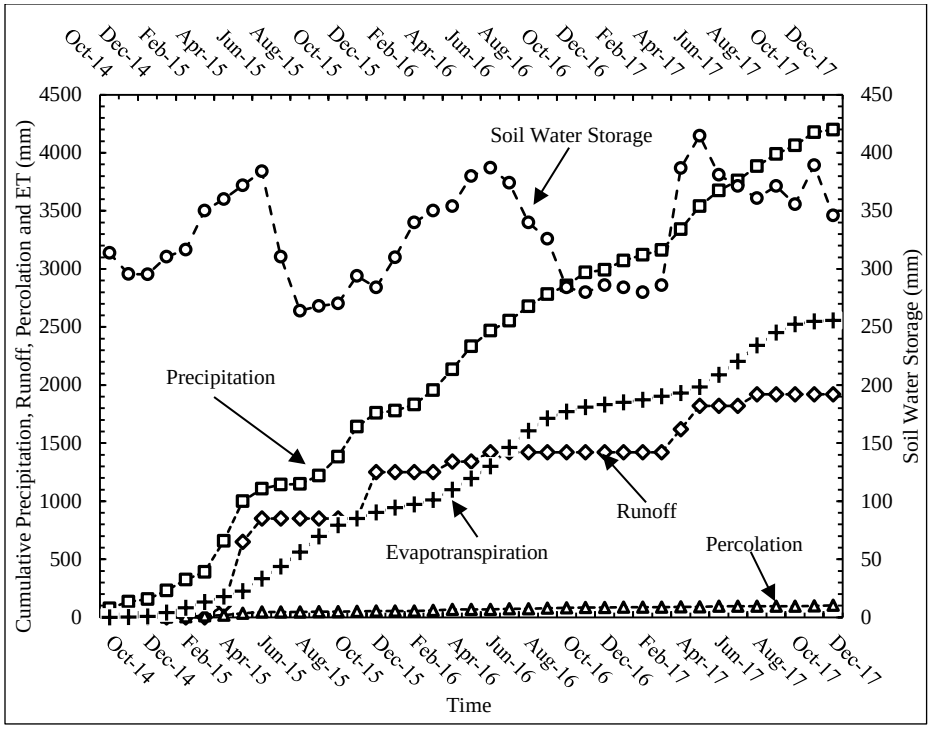

Figure 7.2 Water balance simulation results from UNSAT-H approaching FM

7.4 Comparison of Model Predictions and Field Data

A comparison of water balance components (e.g. soil water storage, percolation, runoff, and evapotranspiration) from model predictions both in FM and FF, will be presented in this section, along with the field water balance results. The simulation outcomes and comparison with the field-measured water balance results are presented for the top-section lysimeters (L-1, L-2 and L-3), which have three different kinds of vegetation.

7.4.1.1 Soil Water Storage

Field-measured and predicted soil water storage for the simulated lysimeters are shown in Figure 7.3. The field-measured data shows that water storage increased during the rainfall period and decreased during the summer. Changes in soil water storage were minimal during the winter period. A parallel trend was observed in water balance predictions of soil water storage, using both forward modeling and field-fit simulations. However, the seasonal variations in soil water storage measured by UNSAT-H were both under and over predicted. Underprediction occurred especially during high intensity precipitation events. One potential reason for the overprediction of soil water storage might be the overprediction of the overland flow or surface runoff. In addition, the hysteresis effect was not incorporated during the simulation, which might have resulted in over-and-under predictions of the soil water storage. Khire et al. (1997) reported the over-and-under predictions of simulated soil water storage while comparing the field soil water storage of the Live Oak landfill site in Atlanta, GA and the Greater Wenatchee Regional Landfill site in Washington. Fayer et al. (1992) also identified the effects of hysteresis as a significant factor in simulating water storage for greater accuracy.

The fluctuations in the soil water storage of the forward modeling and field-fit simulations were insignificant. However, during the dry period, forward modeling presented more-reduced soil water storage than the field-fit simulation (Figure 7.3). The reduced

storage got adjusted through the higher evapotranspiration rate, since the rooting depth was considered deeper than that of the field-fit modeling. This caused greater upward flow of water from the deeper soil layer to the dryer layer, through the root zone, by means of hydraulic lift.

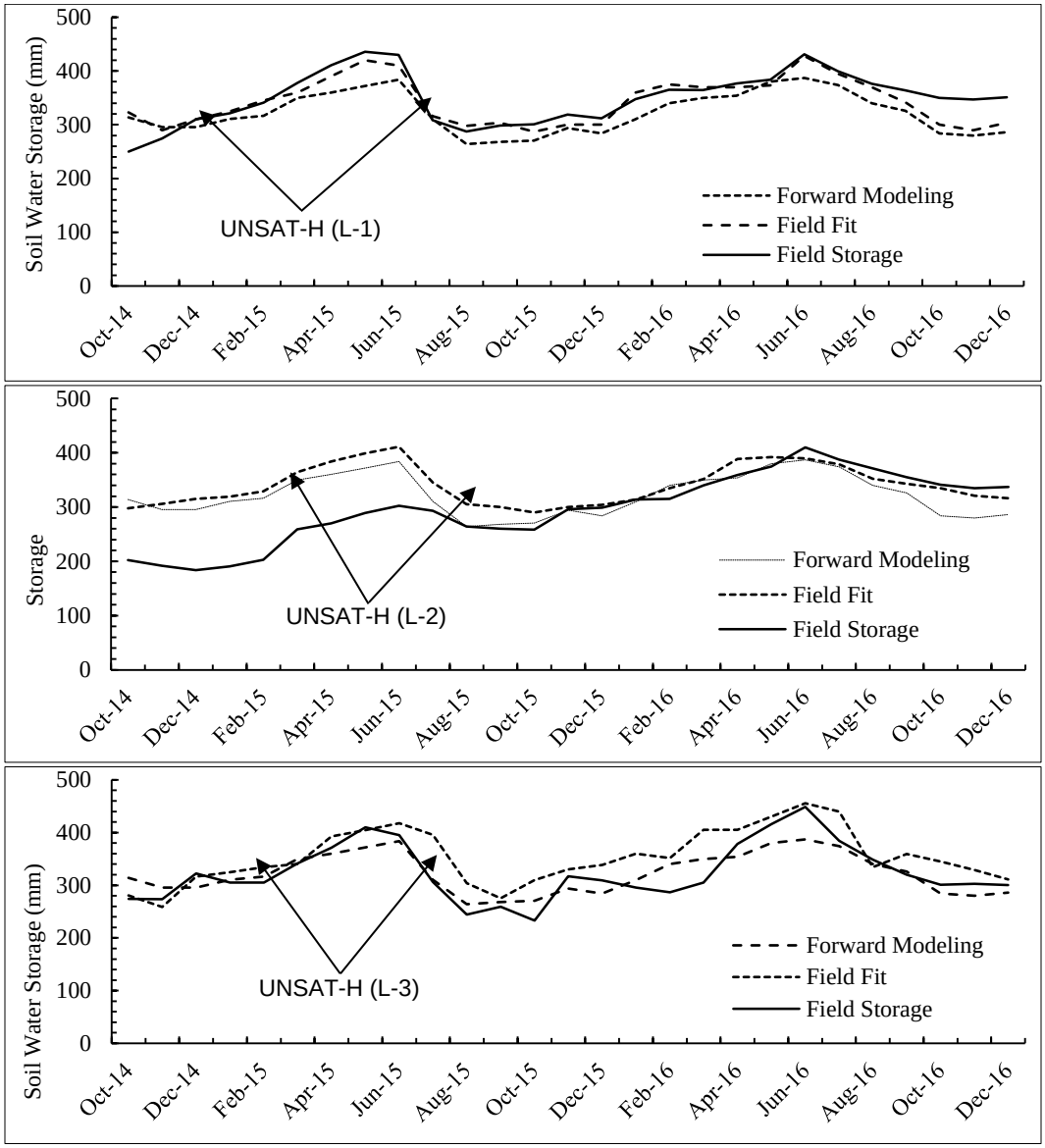

Figure 7.3 Measured and predicted soil water storage

7.4.1.2 Evapotranspiration

Field and simulation results of evapotranspiration (ET) are shown in Figure 7.4. The field ET was computed by subtracting the monthly surface runoff (R), percolation (Pr), and the change in soil water storage (ΔS) from monthly precipitation (P) data. The following equation was used to compute the field ET:

$$ET = P - R - P_r - \Delta S$$

The field data shows a higher rate of ET during late spring and summer and a lower rate during the winter season (Figure 7.4). These results are consistent with the site meteorology (seasonal changes in temperature, solar radiation, and humidity) and the growing season of the plants.

Good agreement was observed between the measured and predicted ET, as shown in Figure 7.4, particularly for the field-fit parameters. UNSAT-H predicted ET very accurately. In forward modeling, ET was over-estimated since runoff was under predicted. Therefore, water storage was higher, and there was available water for evaporation and transpiration. In field-fit simulation, UNSAT-H showed both over-and-under predictions. Slight over predictions of evapotranspiration occurred during late fall and winter seasons, and under predictions occurred mainly during the first few months of monitoring (Figure 7.4). Khire et al. (1997) had similar findings in the water balance simulation of the Live Oak landfill site in Atlanta and the Greater Wenatchee Regional Landfill site in Washington. Fayer et al. (1992) reported that ignoring the hysteresis effect is the primary reason for over-and-under predictions of ET. However, the field fit simulation results of ET were very close to those of the field ET. The percent of ET of annual precipitation in the field ranged from 40% to 59%. In forward modeling, nearly 76% of precipitation water was removed to the environment through the ET process (Table 7.3). Data obtained from the field-fit simulation was very close to that obtained from the field results. The percent of ET of

annual precipitation for three different vegetation is listed in Table 7.3. From the table, it can be clearly seen that Bermuda grass can remove the most water from the cover soil. According to Saxton (1982) and Federer (1975), in arid or semi-arid regions, plants typically can transpire 65% to 100% of annual precipitation. Based on the first three years' simulation results and field-measured results, the percent ET of annual precipitation is on an average nearly 50%. However, increased rooting depth can cause the size of the ET component to increase.

Table 7.3 Percent ET of annual precipitation

Lysimeter	Grass Types	Year	UNSAT-H Modeling		Field Measured
			Field Fit Simulation	Forward Modeling	
			(%)		
1	NT	2015	45.09257593	64.05715	44.841143
		2016	49.29242595	75.55426	51.68123
2	SG	2015	41.02428373	64.05715	40.756729
		2016	42.83247094	75.55426	47.907207
3	BG	2015	46.56569841	64.05715	46.210821
		2016	60.14113236	75.55426	59.652628

The modified soil and plant parameters in field fit-simulation captured the field ET. The measured and predicted ET was less than the PET. Based on the Thornthwaite PET model, the total ET for the 2 years' (2015 and 2016) simulation was approximately 2,300 mm. Based on the field measurement, the two years' cumulative ET was approximately 1,500 mm (for Bermuda grass, L-3, other two lysimeters had approximately 1250 mm). Field-fit simulation showed a cumulative ET value of 1,510 mm for the two years' simulation, while in forward modeling, the cumulative ET nearly 2,000 mm. So, field measured, and simulated ET didn't exceed the PET, and water stored in the storage layer

was available for transpiration through the existence of a deeper root zone. Hillel (1980) reported that the rate of evapotranspiration can get close to PET or can equal PET for cover soil having higher water content. Greater root depths exert the available energy to release more water from the storage layer to the environment. Therefore, deeper rooting depth is a significant factor for maximizing the amount of transpiration.

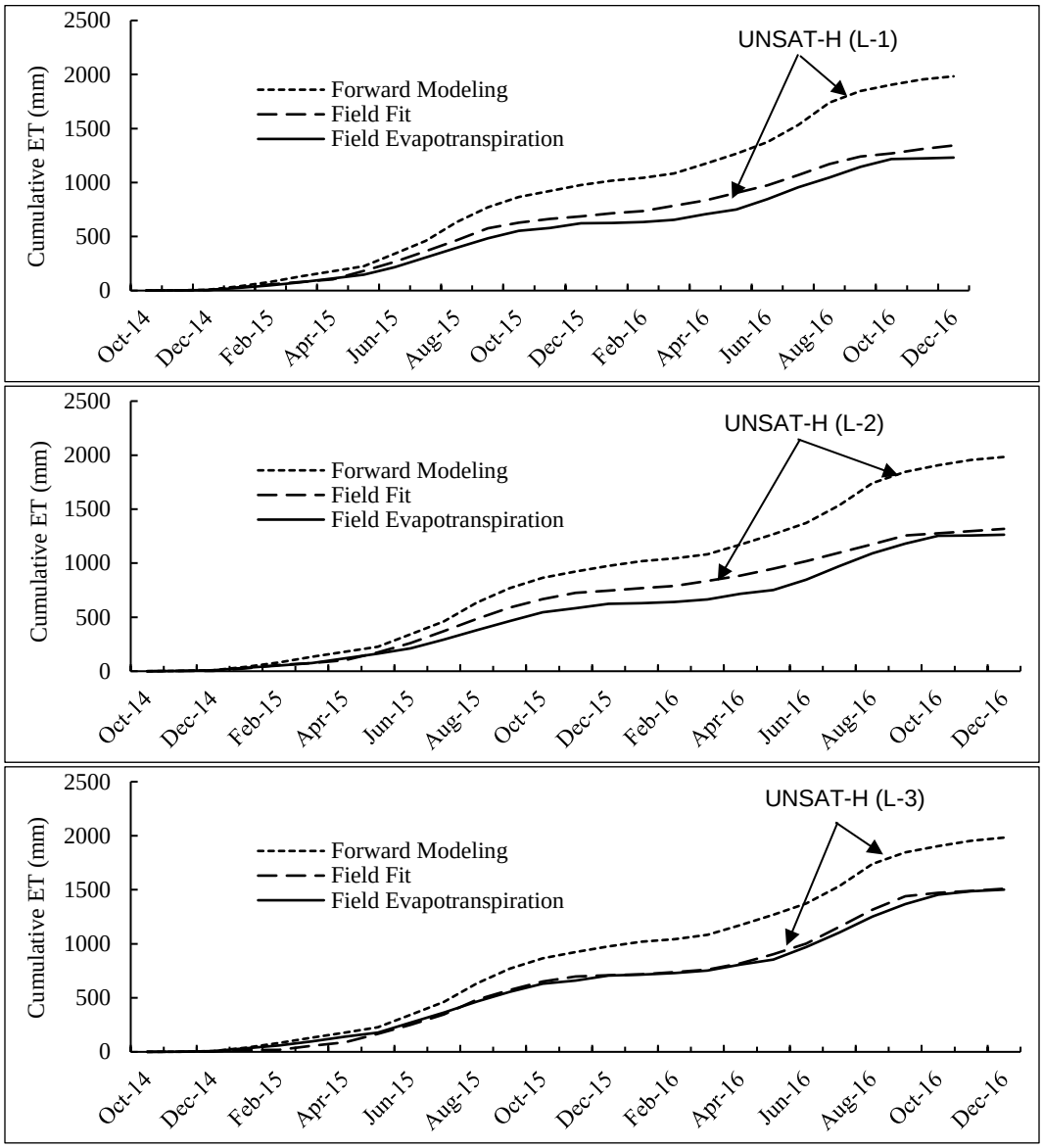

Figure 7.4 Measured and predicted evapotranspiration

7.4.1.3 Runoff

Accurate predictions of surface runoff are significant because the amount of water to be infiltrated is largely influenced by runoff. Simulation results of the runoff of the three lysimeters are shown in Figure 7.5. UNSAT-H under predicted surface runoff in the FF simulation. In the FM approach, UNSAT-H over predicted runoff, except in lysimeter 1 where runoff increased in the field at the end of the monitoring period. Based on the field-measured runoff from the runoff collection systems, approximately 1,550 mm, 1,420 mm and 1,250 mm of cumulative runoff were recorded in L-1, L-2, and L-3, respectively during the first three years of monitoring (Figure 7.5). Several large pulses of runoff were seen and are shown in Figure 7.5 during May and June 2015; November 2015; and June 2016. During this time, frequent rainfall with high intensity was recorded at the on-site weather station. Recorded precipitation intensity was 100 mm/hour to 230 mm/hour. Consequently, the infiltration capacity of the cover soil was exceeded during this rainfall event. This higher intensity rainfall caused the major pulses of runoff and contributed to the higher cumulative runoff. Field-measured percolation also showed the major increment of drainage during this time. UNSAT-H accurately captured the higher pulse of surface runoff. UNSAT-H was run at variable precipitation intensity, with the default value set to in-situ precipitation intensity. Forward modeling showed a higher value of runoff than the field-fit modeling, primarily because of the saturated hydraulic conductivity (K_s). In forward modeling, the lower value of K_s produced greater surface runoff. In field-fit simulation, based on field K_s measurements, higher K_s produced relatively lower amounts of runoff since the rate of infiltration was higher in the field-fit modeling than in the forward model. Roesler et al. (2002) reported a similar reason for the deviation of runoff due to a change in K_s. In their simulation, they found better prediction results by increasing the K_s of the surface layer.

Eventually, they suggested that K_s be utilized as a calibration parameter rather than as a soil property for accuracy of the design.

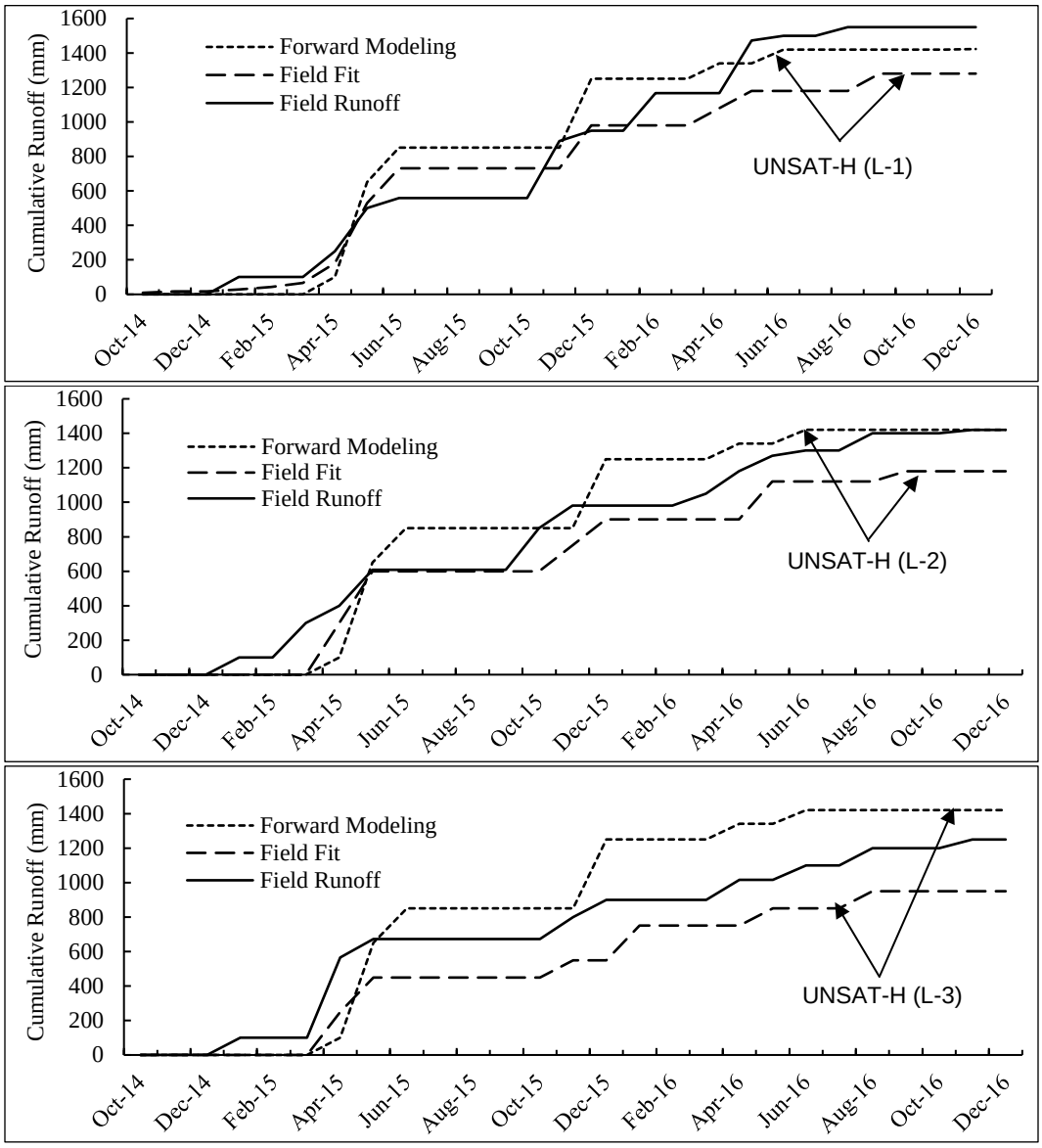

Figure 7.5 Measured and predicted runoff

7.4.1.4 Percolation

Measured and predicted percolation for the three lysimeters are shown in Figure 7.6. Two major pulses of percolation were observed in the field (one in early May 2015 and

the other in October 2015). During the major two pulses of percolation (due to higher intensity rainfall), soil water storage exceeded the storage capacity of the cover soil, resulting in drainage occurring at the saturated condition due to gravitational forces. Preferential flow could also be a reason for the higher value of cumulative percolation since, in some cases, a rapid rise in the percolation was observed before the soil water storage reached its peak. UNSAT-H also identified the two major pulses of percolation. However, the predicted percolation does not accurately match the rate of percolation that occurred in the field. A comparison of measured and predicted percolation, depicted in Figure 7.6, indicates that UNSAT-H under-and-over predicted percolation. In forward modeling, a lower K_s value and deeper root zone produced much lower percolation than field-fit simulation results. In field-fit modeling, in-situ measurement of K_s through the Guelph permeameter closely reflected the field pulse of percolation. However, an exception was observed in lysimeter 2, where the percolation trend nearly matched the forward modeling results for the first year. That can be attributed to the initial higher in-situ compaction level of the top layer of the lysimeter soil. Therefore, the amount of water that penetrated through the L-2 cover soil was less than that for the other lysimeters, resulting in less water being available for transpiration. The field ET results also showed a lower rate of ET than the field results for the other two lysimeter's field. Later, due to the bio intrusion effect, K_s increased, and water infiltration increased significantly at frequent rainfall with high intensity.

Another reason for the under-prediction of percolation in both forward modeling and field-fit simulation is the existence of minor fissures in the top surface layer during the summer. The small cracks in the soil layer created a preferential way for water to move deeper into the cover soil after a rainfall event. UNSAT-H does not account for flow of water through any cracks or any preferential paths in the soil.

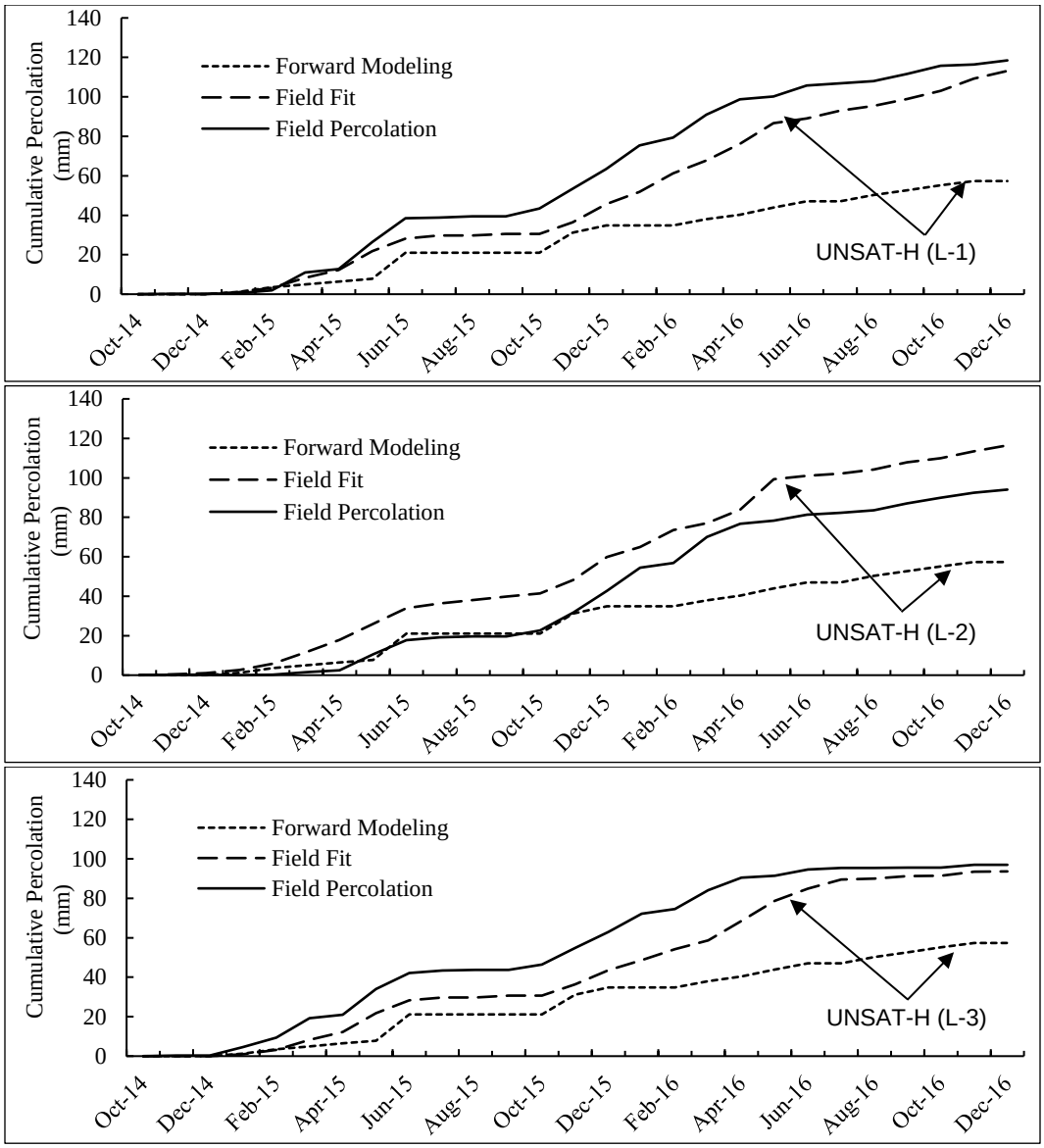

Figure 7.6 Measured and predicted percolation

7.5 Parametric Evaluation

The objective of parametric analysis is to investigate the critical parameters that have significant influence on the performance of an ET cover system. The influence of cover thickness, hydraulic properties, rooting characteristics, and intensity of precipitation were investigated. The following section elucidates the details of parametric analysis.

7.5.1 Effect of Cover Thickness on Annual Percolation

Plant root and soil water storage capacity play a significant role in reducing the annual percolation rate of an ET cover system. Plant roots transpire the soil water as it moves down through the root zone, thus reducing the percolation from the bottom of the cover. Increased storage capacity of the soil holds sufficient water and produces less percolation. The higher the cover thickness, the higher the water storage capacity. Therefore, a parametric study was conducted to illustrate the effects of an ET cover thickness on the annual percolation rate. Two climatic conditions were evaluated: typical arid region precipitation intensity (300 mm/year) and in-situ precipitation intensity (1511.3 mm/year). In both the cases, the cover thickness was varied to observe the annual percolation, keeping all of the input parameters at the in-situ condition. The soil parameters were set based on the laboratory investigation results, and vegetation parameters were set at in-situ condition. Cover thickness was varied from 1 ft. (304.8 mm) to 7 ft. (2134 mm) to evaluate the sensitivity of this parameter. The results from the parametric study are presented in Figure 7.7. A non-linear relationship was observed for both the cases. In the climatic zone where the precipitation intensity is 300 mm/year, a 1.97 ft. (600 mm) cover thickness is adequate to limit percolation $\leq$ 4 mm/year (TCEQ 2012). Under the in-situ precipitation condition (1511.3 mm/year), annual percolation decreases with the increased cover thickness, and beyond 6 ft. (1829 mm) of cover thickness, the change of annual percolation in insignificant. At this threshold point (6 ft.), annual percolation was approximately 15 mm/year. At 4 ft. cover thickness (field condition), annual percolation was observed almost 67 mm/year from the parametric simulation which was slightly underestimated from the field water balance percolation. Based on the parametric evaluation, it can be concluded that precipitation intensity significantly impacts the annual percolation. Increased soil cover thickness reduces the rate of annual percolation. The in-

situ annual precipitation indicates that, at a cover thickness of 6 ft. or more, annual percolation remains almost constant (approximately 15 mm/year), which suggests that increased cover thickness is not always an effective solution for minimizing percolation for ET covers in humid regions.

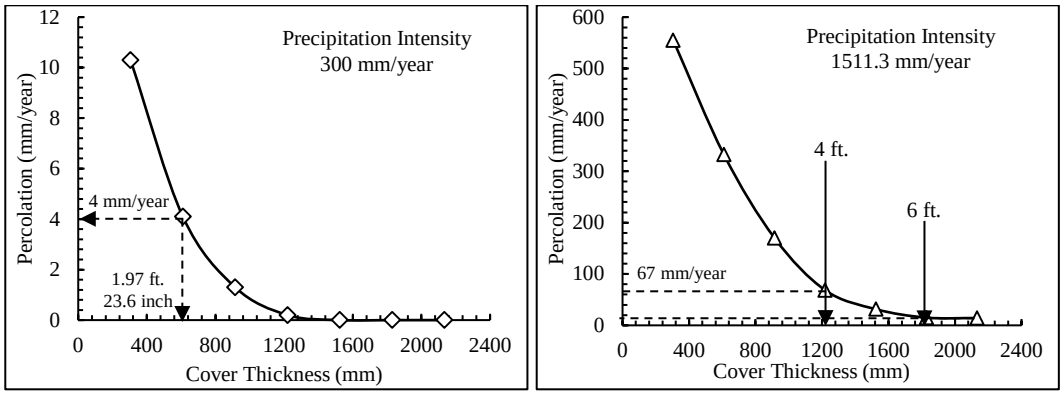

Figure 7.7 Parametric Evaluation of cover thickness

7.5.2 Effect of Saturated Hydraulic Conductivity on Percolation Rate

Saturated hydraulic conductivity was evaluated parametrically to simulate the annual percolation of the ET cover system. The range of saturated hydraulic conductivity considered was between 10^{-3} cm/sec to 10^{-8} cm/sec. All other parameters were set according to the in-situ condition. The simulation results are shown in Figure 7.8. A non-linear trend was observed, showing an expected decrease in the percolation rate with a decrease in the saturated hydraulic conductivity. It is to be noted that no significant decrease in estimated percolation was observed for saturated hydraulic conductivity values less than 10^{-7} cm/sec. Zornberg et al. (2003) also found similar results from their parametric evaluation, using the LEACHM program. The most critical range of conductivity values was found between 10^{-4} cm/sec. to 10^{-6} cm/sec., where one order increment of the hydraulic conductivity increased the annual percolation significantly (Figure 7.8). The in-situ measurement of saturated hydraulic conductivity at different lysimeters using GP showed

the range of saturated hydraulic conductivity values between 10^{-4} cm/sec. to 10^{-6} cm/sec. Therefore, a minimum of 35 mm/year percolation will be generated at 10^{-6} cm/sec hydraulic conductivity, based on the parametric simulation (Figure 7.8).

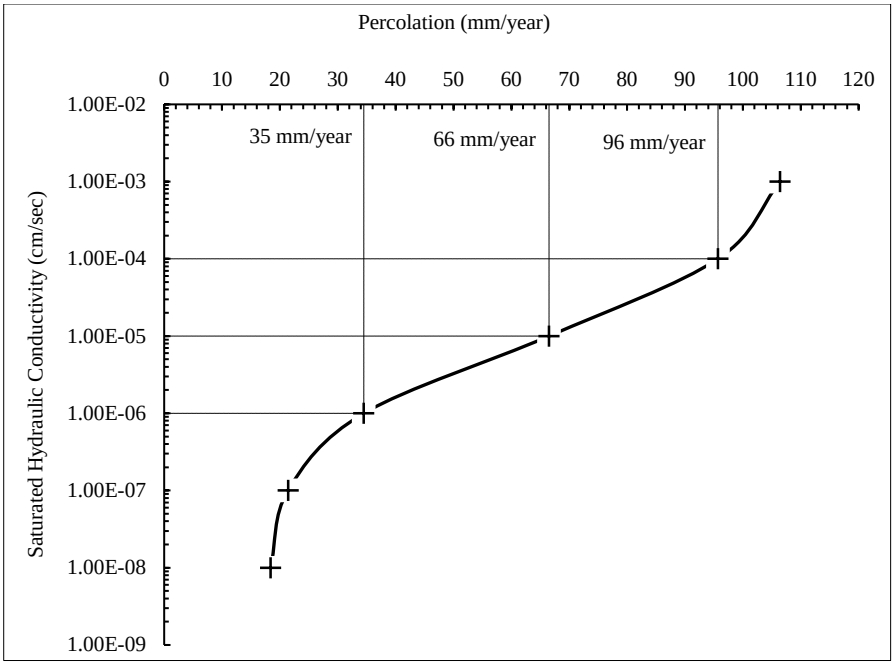

Figure 7.8 Parametric evaluation of saturated hydraulic conductivity

7.5.3 Effect of Water Retention Parameter (α and n)

To evaluate the sensitivity of unsaturated parameters (α and n), parametric simulation was conducted using UNSAT-H. UNSAT-H uses water retention parameters for water balance simulation. The n parameter basically represents the pore size distribution of the soil. A high value of n indicates larger pore size (sandy soil), and a low value of n indicates high pore size distribution (fine grained soil). The parametric analysis was conducted based on the data obtained from the FSWCC. For all six lysimeters soil, α lies in the lower end of 0.0018 kPa^{-1} to the higher end of 0.15 kPa^{-1} and n lies between 1.47 and 2.05. Both the parameters varied over their full range of field values: α varied from 0.15 to 0.0018 kPa^{-1} keeping n equal to 1.6 (field average), and n varied from 1.47 to 2.05,

setting α constant at 0.026 (Field average) kPa^{-1}. Additionally, n varied from the lowest possible value of 1.01 (n < 1 is unrealistic) to 4 to further investigate the effect of the change in pore size distribution. The K_s value was set at 10^{-5} cm/sec. Figures 7.9 and 7.10 represent the SWCC used in the parametric simulation. Θ_s and Θ_r were set based on the field average value. The vegetation parameters were set at in-situ condition.

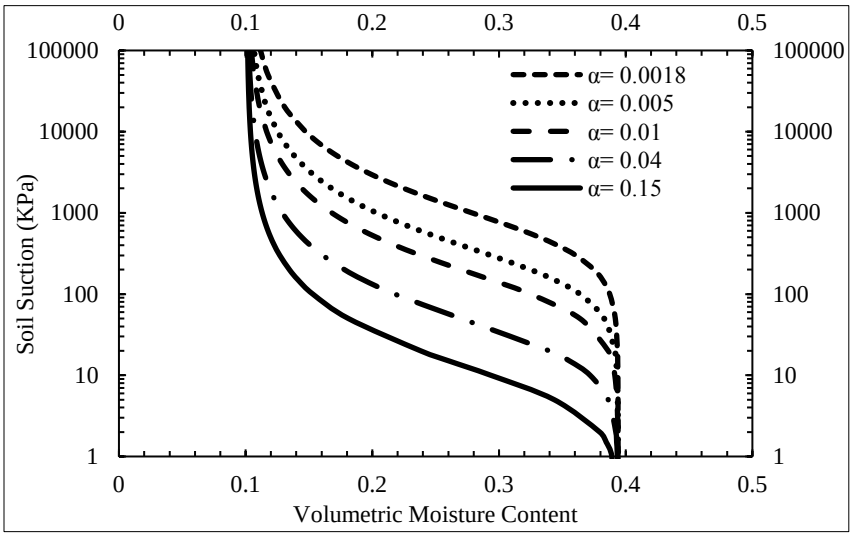

Figure 7.9 Shape of SWCC at varying α (n constant)

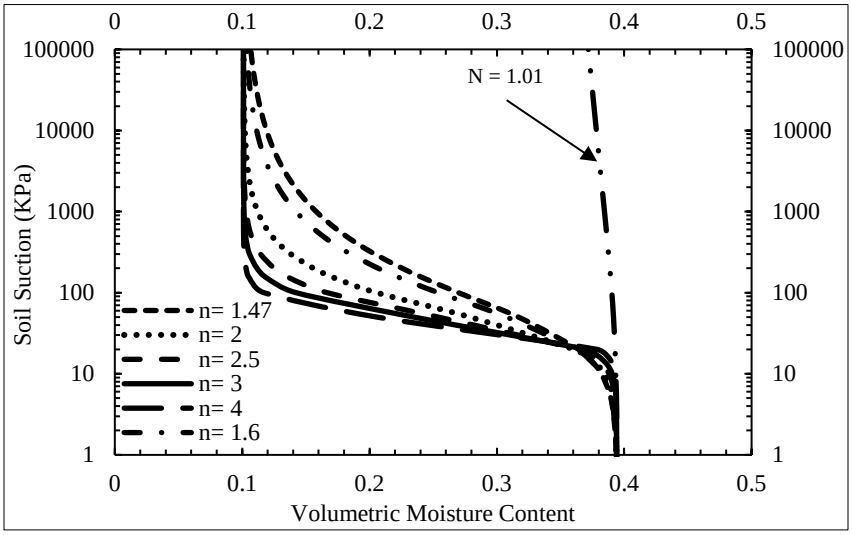

Figure 7.10 Shape of SWCC at varying n (α constant)

The response due to the change in the α parameter was more complicated than the change in the n parameter. Therefore, for the results for the parametric simulation, only the change in n value is presented. The slope (n) of the SWCC was found to influence the annual percolation more significantly than the α parameter. At the initial case (n=1.6, α=0.026), annual percolation was 61.25 mm/year. Decreasing n by a factor of 0.63125 (n=1.01) from the initial condition reduced the annual percolation by almost 10 mm/year (Figure 7.11), while a reduction factor of 0.9375 (n=1.5) reduced the annual percolation only slightly. In contrast, increasing the n by a factor of 1.25 (n=2) increased the annual percolation by approximately 11.25 mm/year. Figure 7.11 represents the effects of change in the n parameter, where the positive value indicates a decrease in the rate of percolation and the negative value indicates an increase in percolation. Increasing the n parameter further by a factor of 1.56 to 1.88 showed a slight increase in the annual percolation (approximately 14 mm/year), which is slightly higher (3 mm/year) than the annual percolation at the increased factor of 1.25. The change in annual percolation in UNSAT-H simulation showed that the change in the n value was balanced by adjusting the runoff. The ET and storage quantities were almost constant at different n values. Based on the parametric simulation, it can be concluded that the n parameter significantly affects annual percolation of ET cover. The n value between 1.5 and 2 is more sensitive since the major drainage or percolation mostly occurs at this range in the field (major drainage occurred at n=1.5 to n=2.0). In the field, n close to 1.01 was absent; therefore, no conclusion can be drawn from the simulation at n=1.01. The annual percolation at higher n value (3 or 4) makes no substantial changes in the simulation results. Therefore, n is considered as a significant design parameter for optimum ET cover performance, and hence the measurement of α and n from the FSWCC is of paramount importance.

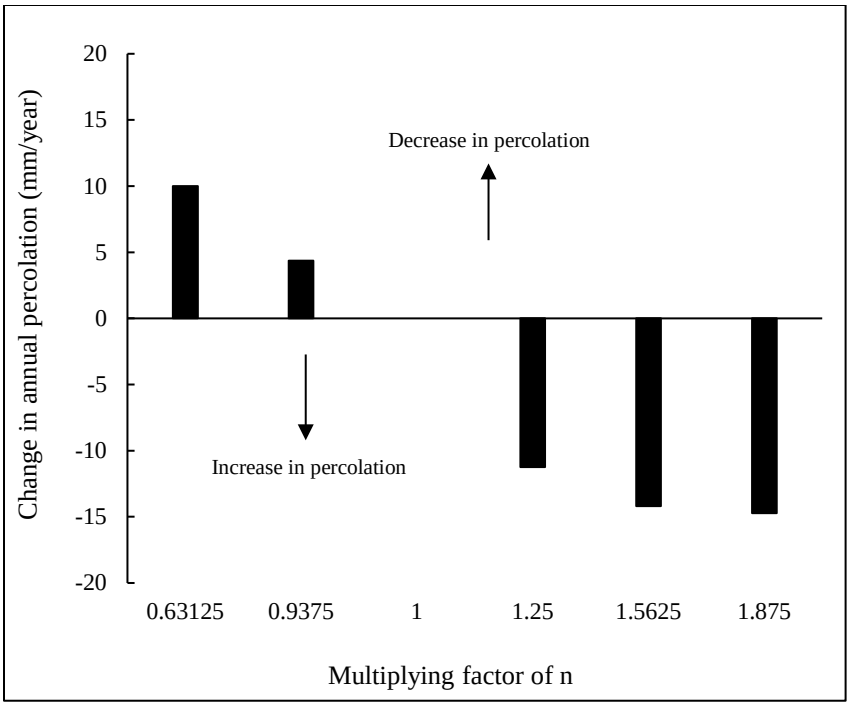

Figure 7.11 Response of annual percolation (mm/year) to varying n

7.5.4 Effect of RLD

The effect of RLD was evaluated parametrically to observe the distribution of potential transpiration (PT) and annual percolation. The RLD function for in-situ vegetation is shown in Chapter 5. Winkler (1999) described different RLD functions for shallow slopes, steep slopes, and very steep slopes. The in-situ RLD for all of the vegetation types in the ET cover closely resembles the shallow RLD function. For the parametric evaluation, three different RLDs were developed, based on the equation below:

$$RLD = a \times e^{(-bz)} + c$$

a, b and c are fitting parameters and z is the depth below surface. The RLD functions used in the parametric study are shown in Figure 7.12. The fitted parameters are listed in Table 7.4.

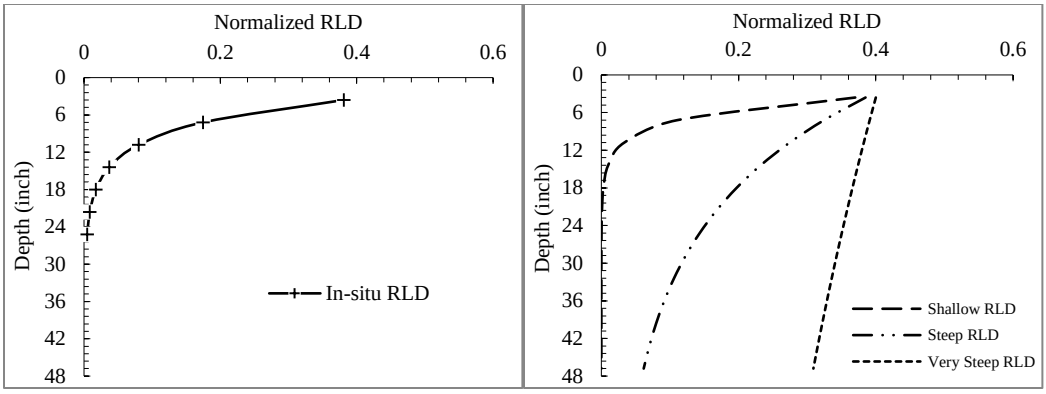

Figure 7.12 RLD function

Table 7.4 RLD curve fitting parameters

Parameters	Shallow RLD	Steep RLD	Very Steep RLD	Average In-situ RLD
a	0.37	0.365	0.3	0.4
b	4	0.6	0.1	2.5
c	0.0001	0.02	0.1	0.005

During the simulation, the percent of bare area (PBA), the leaf area index (LAI), and the growing season were kept constant to generate an equal amount of PT for each RLD simulation. The rooting depth (RD) was varied in two ways to evaluate the root distribution function (RLD). First, RD was varied up to a depth of 40 inches for each type of RLD. Then, RD was fixed at a constant depth, at varying RLD. RD was kept at 15 inches, based on the field average RD of all plant types. The soil parameters were set as input, based on the laboratory investigation results. Meteorological parameters were set according to the in-situ condition.

The effect of the RLD function on the annual percolation rate in the in-situ climate is shown in Figure 7.15. A curvilinear response was observed for all of the RLD functions, with a linear trend at the beginning and end of the curve. At shallow depth, a sharp change in annual percolation was observed due to the combined effects of evaporation and

transpiration for all of the RLD functions. At shallow depth, the water is removed by both evaporation from the surface and transpiration through the root zone. Therefore, the reduction in annual percolation is almost equal for all of the RLD functions at shallow depths (Figure 7.13 a). However, at deeper depth of the cover, the reduction in annual percolation shows significant changes for different RLDs when the rooting depth is considered 40 inches. The RLD function at shallow slopes has nearly bare transpiration, and thus reduces the annual percolation at a very steady rate, with increased rooting depth. The RLD function at steeper slopes provides relatively more transpiration than the shallow RLD function and continues to remove infiltrated water from the deeper zone of the cover. As Figure 7.13 (a) clearly demonstrates, the percolation curve of a shallow RLD function upholds a nearly vertical gradient at deeper depths, whereas the percolation curve of very steep RLD function shows a relatively steeper gradient. Therefore, the effect of root density on annual percolation is more significant at the deeper depth of the ET cover than at the shallow depth.

The results of an additional parametric analysis conducted on the RLD functions at a fixed rooting depth of 15 inches are shown in Figure 7.13 (b). Annual percolation reduced in a non-linear manner for all of the RLD functions. For the shallow RLD function, as root moves deeper into the soil, root density becomes sparser and provides little transpiration. Very steep RLD functions deliver more transpiration and eventually adjust the water balance by reducing the annual percolation. However, none of the RLD functions provide transpiration below the root zone depth. As is shown in Figure 7.13 (b), the curves below the root zone continue vertically. Based on the parametric simulation on the RLD curve, an annual percolation of almost 68 mm/year is expected for shallow RLD curves and 45 to 60 mm/year percolation for steep and very steep RLD curves at the fixed rooting depth of 15 inches under the on-site climatic condition. Therefore, it can be concluded that

an increased rooting depth is more significant than a dense root zone of shallow depth in the ET cover. The potential evapotranspiration (PET) can't reach its demand due to the lack of adequate rooting depth into the cover soil.

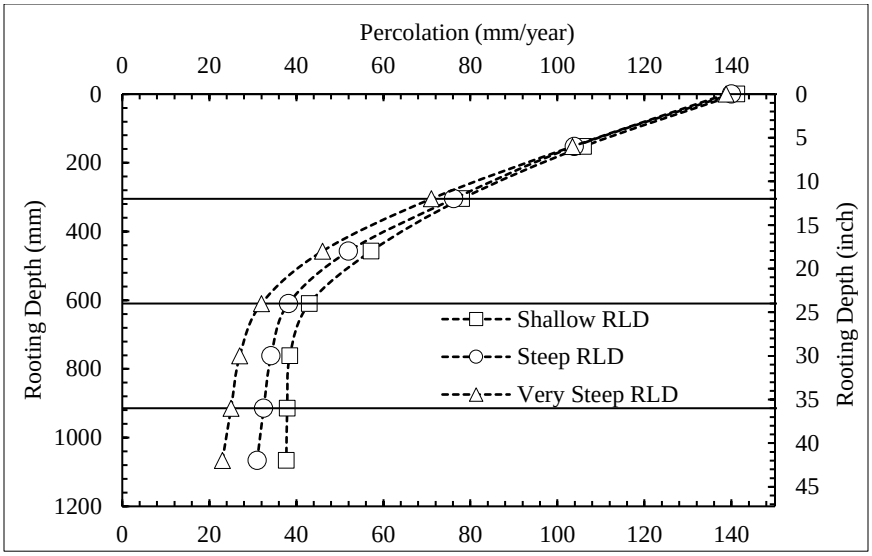

(a)

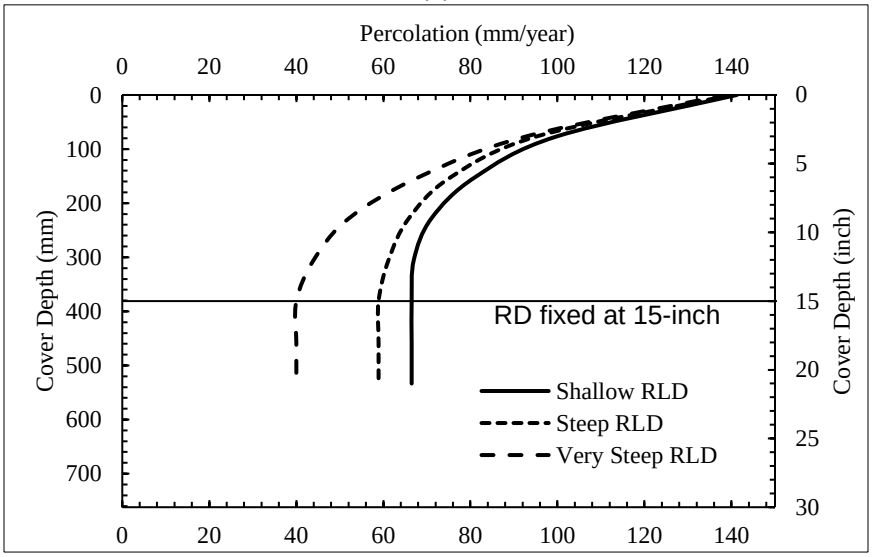

(b)

Figure 7.13 Parametric evaluation of root distribution (RLD functions) (a) at increased rooting depth (b) at fixed rooting depth

7.5.5 Effect of Root Depth (RD)

An investigation was performed to evaluate the sensitivity of vegetation rooting depth on the optimum performance of an ET cover. The average in-situ root depth in the ET cover for different vegetation is 15.45 inches (400 mm). To evaluate the sensitivity of rooting depth, no root condition (0 inch) to 40-inch (1066 mm) rooting depths were considered, based on the existing ET cover depth. The RLD was fixed at the in-situ condition, and all other soil properties were set based on the laboratory investigation results. In-situ rainfall intensity of 1,511.3 mm/year was used for the analysis. The response of the ET cover percolation at varying rooting depths is shown in Figure 7.14. An expected trend was observed from the analysis. The rate of percolation per year decreases as the rooting depths increases. The increased root depth supports removing more water through transpiration from the ET cover that may have infiltrated into the cover soil. It is to be noted that the response of the ET cover percolation at varying rooting depths is non-linear. At rooting depths larger than 24 inches (610 mm), the change of percolation is insignificant. The trend becomes almost linear at rooting depths larger than 30 inches (762 mm). Based on the analysis, under the meteorological conditions in Denton, TX, a minimum of 38 mm/year (2.87 % of annual precipitation) percolation is expected if the root depth of the vegetation is 30 inches or more. Therefore, it may be concluded that vegetation RD plays a significant role in reducing the annual percolation, and the performance of the ET cover is more sensitive to RD than RLD.

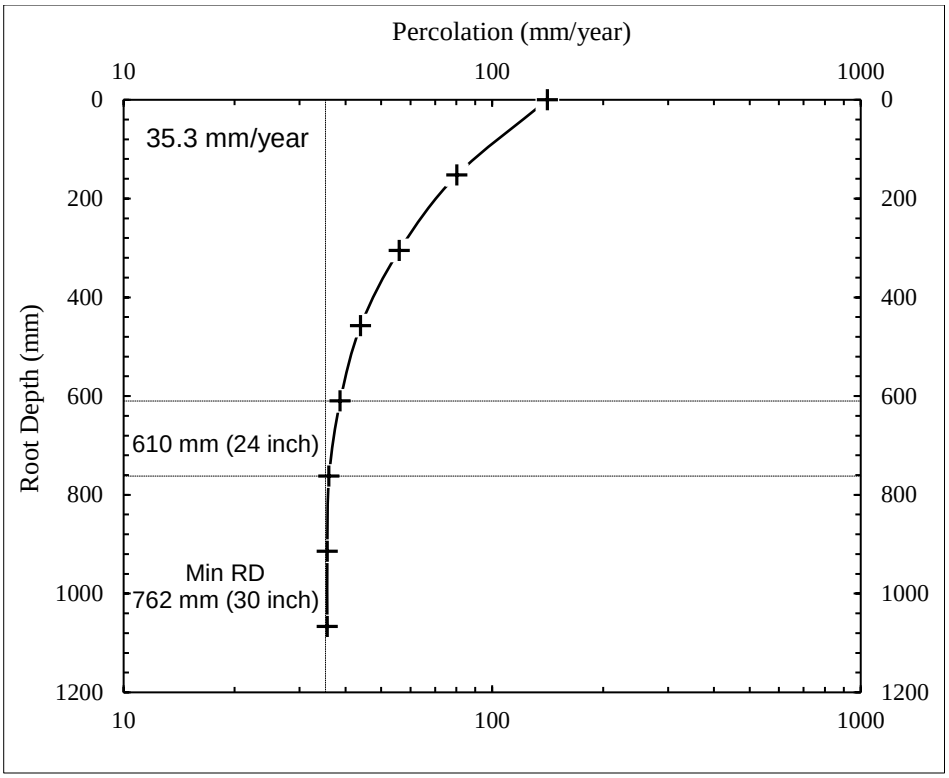

Figure 7.14 Parametric evaluation of root depth (RD)

The parametric simulation results on the effect of RD on annual percolation were further compared with the field-investigated annual percolation and RD. Time-to-time measurement of field percolation at the site was calculated and converted to annual percolation for all of the lysimeters. RD was measured from all the field-installed minirhizotrons, and the annual change in RD was calculated. A comparison was made of the UNSAT-H simulated annual percolation with the field annual percolation for 2015, 2016, and 2017. The comparison results are shown in Figure 7.15 and indicate good agreement between the field-measured percolation and simulation results for some of the data points. However, UNSAT-H under predicted the annual percolation in most of the cases. The major reasons for under prediction are the presence of a preferential flow path in the ET cover due to the desiccation of the soil, the natural pedogensis effect, and animal

burrowing. Brett (2016) reported the existence of several rodent burrows and cracking in the ET cover during the monitoring period. Annual percolation (an average 60 mm/year) in 2015 for all of the lysimeters was similar, except for that of L-2. Annual percolation in 2016 was reduced significantly compared to the previous year, even though the precipitation intensity was close to the 2015 precipitation. In 2017, annual percolation further reduced. This indicates that the matured and increased rooting depths adjust the reduced percolation by increasing the transpiration. Thus, it can be concluded that the performance (rate of percolation) of an ET cover improves with time, as the below-ground biomass grows and matures. Therefore, the field-measured percolation establishes a good agreement with the UNSAT-H parametric simulation responses of annual percolation on the RD, especially a few years after construction of the ET cover.

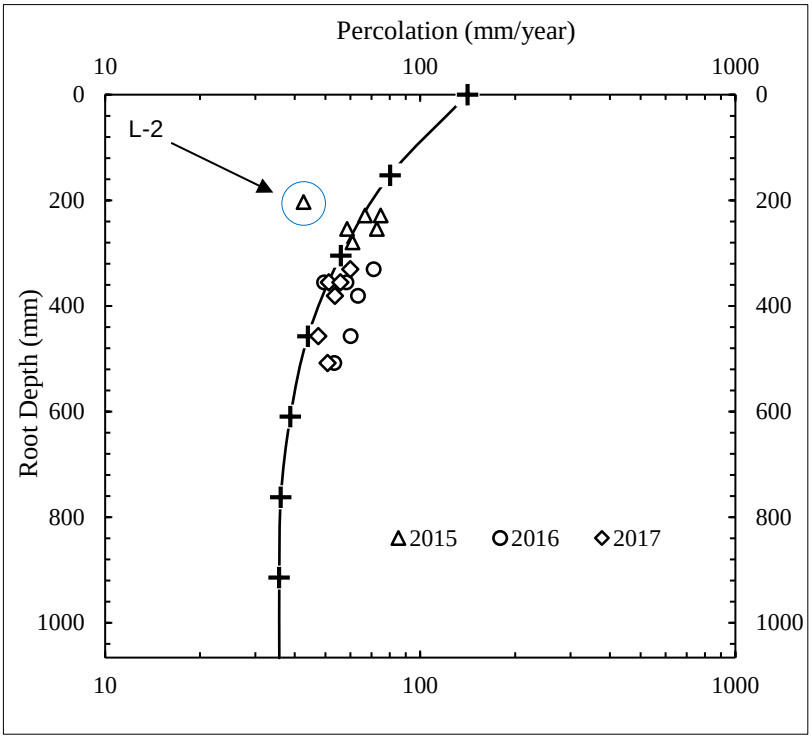

Figure 7.15 Comparison of field annual percolation and simulation-based percolation

Annual Percolation was also evaluated parametrically, using UNSAT-H at different precipitation distribution patterns and rooting depths. The precipitation pattern was selected in such a way that it included the typical precipitation from the arid region's annual precipitation to the in-situ's (semi-humid) annual precipitation. Average annual precipitation of 300 mm/year was selected for the arid and semi-arid regions, based on the ACAP arid region sites. Snowfall was not accounted for in the assumption. In-situ annual precipitation of 1500 mm/year in the year 2015 was considered as the maximum annual precipitation. Annual precipitation of 600, 900 and 1200 mm/year was assessed at different RDs. For the simulations with UNSAT-H, the intensity of precipitation was applied at the default condition (10 mm/hour) for the lower annual precipitation (300 mm/year, 600 mm/year) until the total precipitation amount was reached. However, for the greater amount of annual precipitation, the rate of rainfall was increased, based on on-site precipitation events and intensities.

The response of annual percolation at different precipitation patterns and at different RDs is shown in Figure 7.16. At no root condition (RD=0), a substantial amount of percolation was observed in all the precipitation patterns. The only way to remove water at this condition is by surface evaporation. As the RD increased, the annual percolation decreased significantly (Figure 7.16). At higher precipitation intensity, when water content exceeded the field capacity of the cover soil, noticeable percolation occurred, and the pulse of percolation contributed to the higher amount of annual percolation. At lower annual precipitation (300 to 600 mm/year), lower intensity of rainfall produced practically no percolation. RDs of 6 to 12 inches could transpire the stored water from the cover soil. Virtually no water was available for transpiration at this condition. On the other hand, at higher annual precipitation, a substantial amount of water was released from the cover soil with increased rooting depth. Nonetheless, water infiltrated from the bottom of the cover

soil mainly after the high pulse event of rainfall. Therefore, the amount of annual percolation largely depends on the precipitation pattern and annual precipitation.

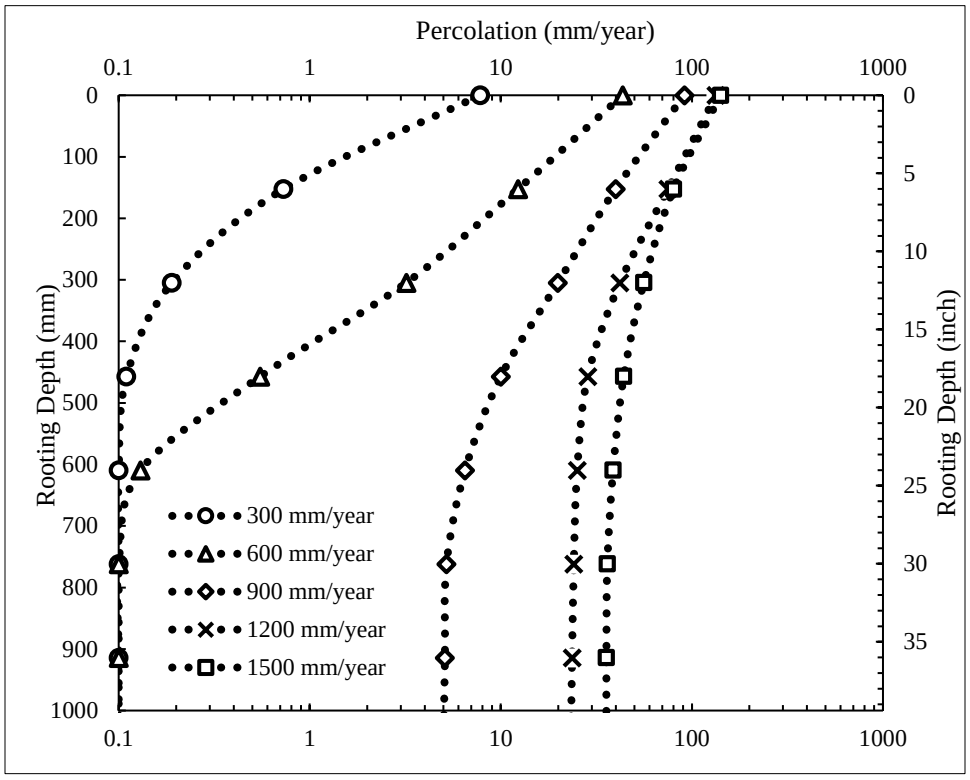

Figure 7.16 Effect of annual rainfall and root depth on annual percolation

The field annual percolation measured from the lysimeters and plotted with the simulated results are shown in Figure 7.17 in both logarithmic and arithmetic scales. Under the field climatological condition, approximately 45 to 70 mm/year of annual percolation occurred during the last three years of field observation at 8 to 20-inch rooting depths. The simulation results matched with good agreement the annual precipitation of 1,200 to 1,500 mm/year. Based on the parametric results, if the root depth can be increased to 30 inches (760 mm) or more, 23 to 38 mm/year of percolation will be generated every year under high intensity precipitation events (Figure 7.17). Therefore, it can be concluded that the meteorological condition has a great influence on the performance of ET covers. Increased

root depth into the cover plays the most significant role in removing the infiltrated water and optimizing the performance of the ET cover. However, precipitation distribution, and pattern contribute to the higher rate of percolation.

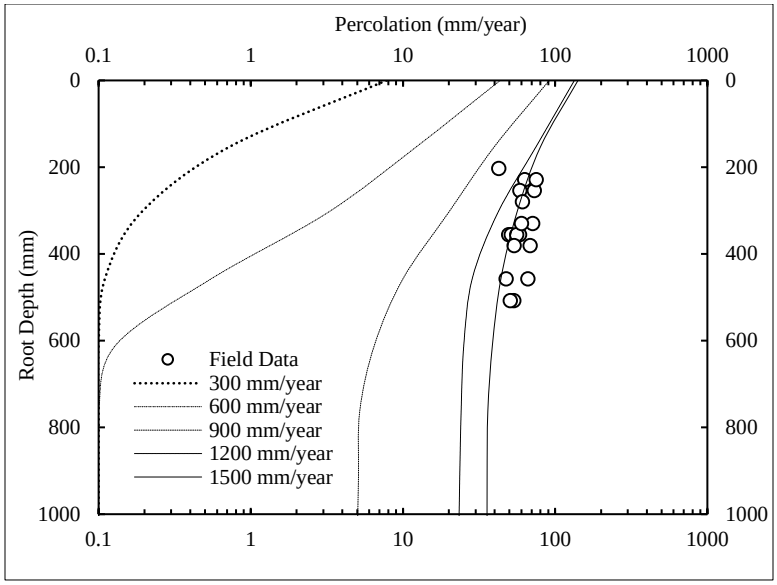

(a)

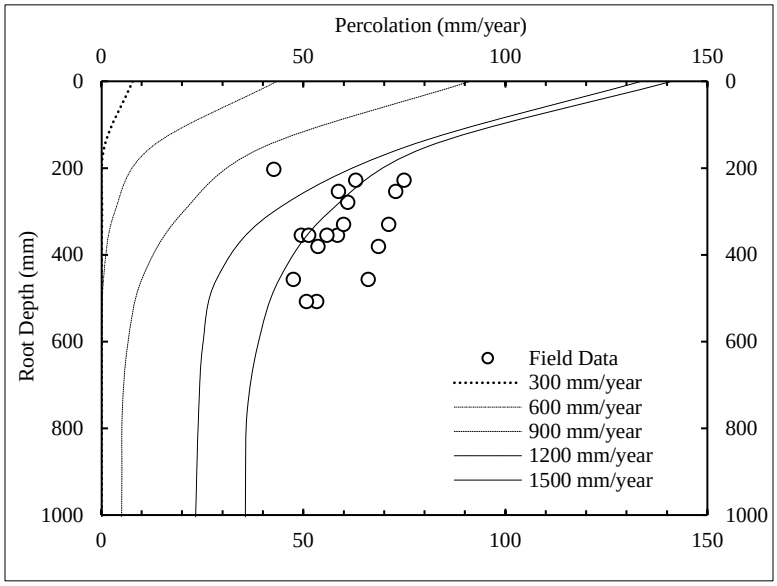

(b)

Figure 7.17 Effect of precipitation distribution (a) logarithmic scale (b) arithmetic scale

Chapter 8

Conclusions and Recommendations

8.1 Summary and Conclusion

A performance assessment of the ET cover system at the City of Denton Landfill was conducted for three years. Hydraulic performance and the effects of plant roots were evaluated for the six constructed lysimeters. A methodical approach to root study was developed. Soil hydraulic properties were assessed based on the laboratory and field investigation results. Water balance modeling was performed to simulate field hydrology of the ET cover system. General conclusions based on this study are provided in the subsequent section. Minirhizotron-based root analysis and quantification proved to be a useful tool. Based on the extensive root analysis and field water balance results, it was concluded that Bermuda grass produces the highest amount of annual transpiration, thereby the lowest annual percolation, than other types of grasses. A deep rooting depth has a significant influence on the removal of stored water from the cover. Precipitation intensity and frequency are influential factors in the amount of annual percolation. A general summary, discussion, and conclusions drawn from this study are provided below.

- Soil hydraulic characteristics changed with time due to the exposure of cover soil to the environment. Unsaturated hydraulic parameters α and n changed considerably during the monitoring period. The n parameter was less than the field-measured n value. Post-construction increments of the α value for all the lysimeter soil were as much as 100 times more than the initial lab-based α value. There were fewer changes in the n parameter than in the α parameter.
- Field capacity moisture content was reduced in different lysimeter soils after three years' field exposure. The reduction in the field capacity eventually increased the annual percolation. It is obvious that lower field capacity of the soil equates to higher

infiltration of water into the cover. Frequent wet-dry cycles in the field, the natural pedogenesis process, and changes in soil structure are the potential reasons for the reduction in field capacity.

- Saturated hydraulic conductivity (K_s) of the cover soil changed significantly at shallow depths (top 12 inches) in different lysimeters. A comparison of the laboratory-measured (as-built) K_s value and in-situ measurements in the field three years after field exposure indicated that saturated hydraulic conductivity increased as much as 100 times. Based on the field-measured results, in-service K_s values ranged between 1×10^{-4} to 1×10^{-6} cm/sec at shallow depths in all six lysimeters. The highest K_s value was found during the dry period (June 2016), indicating that the existence and formation of macropores and/or shrinkage cracks in the soil allowed a large flow of water after a precipitation event and eventually increased percolation.
- To determine the root depth into the ET cover, the minirhizotron method offered two major advantages. It allowed measurement of the root depth through a non-destructive procedure and provided a consistent measurement at the same point to evaluate root growth and dynamics.
- Based on the field observation of vertical root growth for lysimeter-6, Bermuda grass, specifically Hulled Bermuda (Grade 90/80) grass, had the highest rooting depth (20 inches). Native Trail and Switch grass had maximum rooting depths of 15 inches and 14 inches, respectively. The vertical root growth rate of all of the grasses was vigorous initially, but it began decelerating when the roots penetrated around 12 to 15 inches into the soil and touched the denser soil layer. Therefore, under the same meteorological conditions throughout the monitoring period, rooting depths differed according to plant types. Therefore, it can be concluded that the plant's intrinsic characteristics drive them to adapt to the existing environment. Bermuda grass is the

most suitable for the ET cover system, as its root system is very adaptable to changes in climatic conditions.

- The root system is concentrated at the shallow depth of the cover system. The restrictive bulk density of clayey soil for limiting root growth is 1.6 g/cm^3. Soil density was found beyond the restrictive density at deeper depths of the cover. The higher soil density at deeper depths was an obstacle for the growth of a deeper root system in the ET cover system. Therefore, shallow root systems were observed for all of the grass roots, in all of the lysimeters, and lateral branching was prominent because of high soil density.
- Minirhizotron-based root analysis proved to be a potential tool for evaluating the plant roots of ET covers. Minirhizotron technology is advantageous for understanding the functions and dynamics of plant roots. The ability to take photographs inside the minirhizotron and perform subsequent image analysis has allowed the quantification and evaluation of the in-situ dynamics and characteristics of the roots in a continuous and non-destructive manner. However, background noise in the images could be a potential source of error in the root analysis process.
- Dynamic behavior of roots explored through image analysis evaluated the response of roots under different atmospheric conditions. The term ‘root elongation frequency’ (REF) refers to root growth and dieback. Positive REF indicates root growth, and negative REF indicates the presence of the active evapotranspiration phenomenon.
- ERI is a useful tool for identifying the active root zone depth or potential evapotranspiration depth. The potential evapotranspiration depth is the depth at which plant roots can extract water effectively. The ERI method is also useful in detecting root density; however, at fully saturated condition, detection of roots is problematic.

- A greater quantity of precipitation at high intensity causes most of the annual surface runoff and percolation. Based on field-measured water balance results, large pulses of runoff and percolation occurred during heavy intensity rainfall.
- Annual precipitation (P) was higher than the potential demand for evapotranspiration (PET). The ratio of annual P/PET was higher than unit throughout the monitoring period, which is why no significant change in annual percolation was observed. A mild decreasing trend of annual percolation was observed, however. Differences in the annual percolation among the lysimeters occurred due to the differences in the initial compaction level, initial soil moisture content and suction, different water holding capacity of plants, root growth, etc.
- PET measured from two different models (FAO-56 PM model and Thornthwaite model) showed a slight difference in magnitude. The difference in the magnitude ensued due to the differences in input variables. The FAO-56 PM model showed a more conservative PET demand than did the Thornthwaite model. Estimated PET ranged between 1,080.97 mm/year to 1,192.29 mm/year during the three-year monitoring period. The annual ET, based on the field water balance measurements from different lysimeters, ranged from 616 mm/year to 795.5 mm/year. The deficit of the field ET didn't reach the PET due to the lack of a deeper root zone. Lysimeters 3 and 6, planted with Bermuda grass, showed a maximum annual ET of 795.5 mm/year, which was higher than that of the other lysimeters. Therefore, adequate root depth is a significant component of maximization of the annual ET.
- Annual ET, as a function of root depth (FEC), was developed based on the field-measured data. FEC showed a parallel trend of root growth and ET. Root growth and ET are significantly associated to each other. Therefore, efficient root growth and adequate root depth can increase the annual ET to its demand.

- The rate of ET estimated, based on field water balance measurements, was higher for Bermuda grass than for other types of grasses. Bermuda grass produced as much as 4.79 mm ET per day. Additionally, slope-section lysimeters were found to have a higher ET rate than the flat section. Therefore, with respect to evapotranspiration, Bermuda grass performed better than the other plants under identical environmental conditions.
- Several desiccation cracks in the soil and rodent burrows were observed during the monitoring period. Shortly after precipitation (especially during high intensity rainfall), a greater quantity of percolation was logged from the percolation collection system.
- Water balance modeling, using UNSAT-H, was compared with field-measured results. Field-fit simulation results were found closer to the field trends than forward modeling (conservative approach).
- Cumulative percolation was underpredicted by UNSAT-H, both in forward modeling and field-fit simulation. This underprediction of percolation may be connected to the input of K_s for the storage layer. In field-fit simulation, K_s, from the Guelph permeameter, was measured at shallow depths (6 inches and 12 inches). Measured K_s at 12-inch depth was set as storage-layer-saturated hydraulic conductivity.
- UNSAT-H can determine the large pulse of surface runoff after a heavy precipitation event; however, over/underprediction of runoff were also observed. The input of precipitation intensity was set to resemble the field condition. Therefore, it was concluded that field precipitation intensity is an important input factor for accurately predicting water balance. Saturated hydraulic conductivity is also a significant input parameter for precisely predicting water balance components.
- Simulated ET was found close to the field-cumulated ET. Modified plant and soil parameters were able to capture the field ET. Forward modeling overpredicted the cumulative ET, as rooting depth was considered deep enough for greater root water

uptake. Simulation of the three lysimeters, using the field-fit approach, showed that the ET was from 40 to 60% of the annual precipitation. Lysimeter-3, with greater rooting depth, had ET as high as 60% of annual precipitation. Soil water storage simulation showed available water in the lysimeters; however, due to the inadequate root depth, the annual ET, as a percent of annual precipitation, didn't increase.

- The hysteresis effect was not considered during simulation. However, in the field, the cover soil experienced continuous a hysteresis (wetting and drying) effect. Therefore, over/under predictions were observed from the water balance simulation. Nonetheless, the input parameters (meteorological, vegetation, and soil parameters) in the field-fit simulation captured the seasonal trend of water balance in the field. Therefore, actual on-site parameters need to be selected for designing and predicting the future performance of ET covers in the semi-humid regions of Texas.
- The parametric evaluation revealed that increased cover thickness reduces annual percolation. However, a greater quantity annual rainfall is a decisive factor in the amount of annual percolation. The typical annual precipitation of 300 mm/year for an arid region can restrict the annual percolation to below the value recommended by TCEQ (4 mm/year) at only 2 ft. of cover thickness. But under the in-situ annual precipitation and precipitation intensity, approximately 60 to 70 mm/year of percolation is expected at 4 ft. cover thickness.
- Based on the parametric simulation, annual percolation is highly sensitive to the saturated hydraulic conductivity values. An increase of one order in the conductivity value increases the annual percolation significantly. In this study, field-measured saturated hydraulic conductivity ranged between 10^{-4} cm/sec and 10^{-6} cm/sec after three years of field exposure. Therefore, annual percolation of 35 to 96 mm is predictable under the in-situ climatic condition.

- Van-Genuchten SWCC parameters (α and n) play significant roles in the quantity of annual percolation. While designing an ET cover, these parameters need to be corrected or adjusted, based on the field-evaluated SWCC.
- A deep rooting depth is more significant for minimizing annual percolation than a dense root zone at shallow depths of the ET cover. Under the in-situ precipitation characteristics, 38 mm of percolation will be generated every year at rooting depths of 30 inches or more.

8.2 Recommendations for Future Studies

In the progression of this study, several topics were identified for further study:

- Minirhizotron technology needs to be applied to investigate plant roots in the field, from the beginning of the monitoring period. Therefore, the installation of the minirhizotron needs to be completed immediately after the construction of the cover system, before seeding.
- Soil density was found to be a restrictive factor for efficient root growth into the cover soil. Therefore, a study is suggested to determine the optimum compaction of soil cover for efficient root growth and satisfactory hydraulic conductivity.
- The development of a statistical model would establish a relationship between root growth characteristics and water balance performance (ET).
- A study is suggested to monitor seasonal patterns of plant roots to determine the water distribution mechanism in an ET cover.
- Long-term monitoring of ET cover systems is needed in this semi-humid region (Denton, TX) to develop a better understanding of the processes of hydrology and phenology that affect the performance of ET covers over the required service life.
- Results from the field monitoring programs indicate that flow through macropores (preferential flow) may be a significant factor in contributing to the subsurface flow.

Therefore, to better understand the mechanism of preferential flow, a study needs to be conducted to evaluate the effect of flow through macropores.

- Desiccation cracking was observed in the ET cover during the monitoring period. There needs to be a better understanding of when desiccation cracks occur in a vegetated soil cover, how plants are related to the mechanism of desiccation, and how this issue can be rectified to improve ET cover performance. Therefore, a study on this topic would be valuable.
- Several computer programs can be used to simulate the field water balance of the ET cover system. Models such as HELP, LEACHM, VADOSE/W, HYDRUS may be used for the comparison of the simulation results from UNSAT-H and field monitoring results and to aid in the selection of a suitable model for designing an ET cover in this semi-humid region of Texas.
- A capillary-barrier ET cover needs to be tested in this region to compare the performances of the monolithic cover with the capillary barrier.

Appendix A

RETC

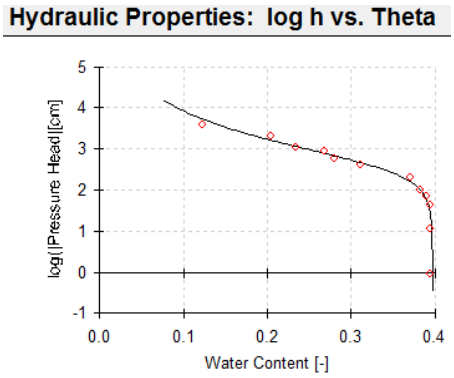

(L-1)

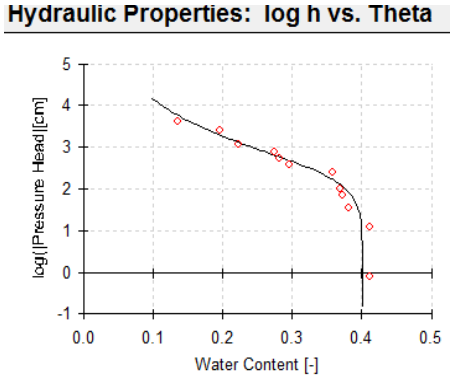

(L-2)

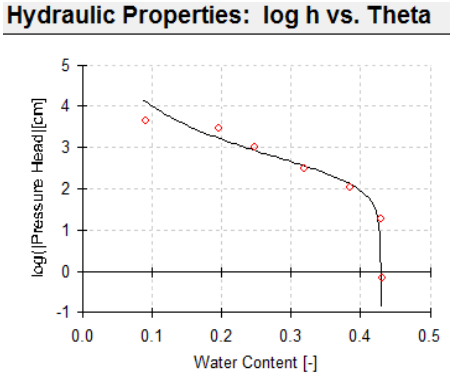

(L-3)

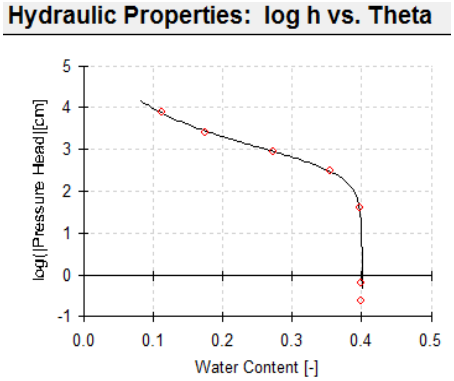

(L-4)

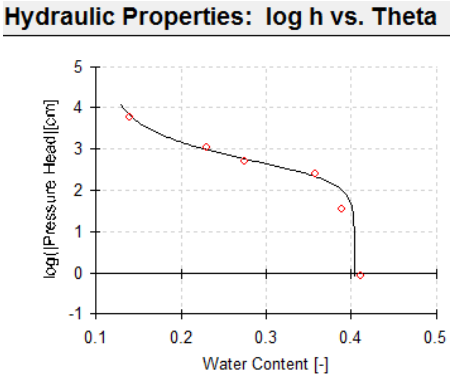

(L-5)

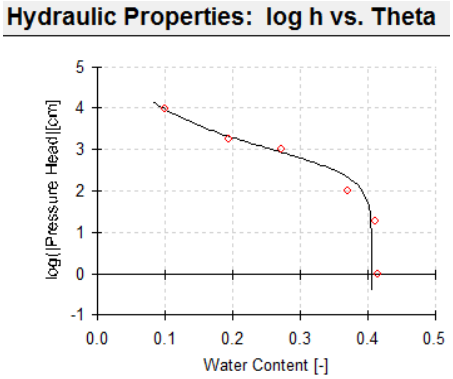

(L-6)

Figure A 1 SWCC from RETC Code

Appendix B

Root Length

Table B.1 Root Length of Native Trail grass from different segmentation algorithms

	Image Side	Threshold Algorithm									
		Isodata	Li	Moments	Otsu	Triangle	average	max	min	std dev	Sum
	Depth 0"-3"	Root Length (cm)									
Set-1	Image 1	89.52738	92.3417	83.693	85.1246	96.2231	89.38196	96.2231	83.693	5.149558	446.9098
	Image 2	84.1214	87.1245	79.1245	81.2325	90.6598	84.45254	90.6598	79.1245	4.597167	422.2627
	Image 3	81.6524	85.3256	75.3658	78.3256	88.6598	81.86584	88.6598	75.3658	5.314066	409.3292
	Image 4	83.2145	88.1214	79.1245	80.9981	89.6524	84.22218	89.6524	79.1245	4.530112	421.1109
	average	84.62892	88.2283	79.32695	81.4202	91.29878					
	max	89.52738	92.3417	83.693	85.1246	96.2231					
	min	81.6524	85.3256	75.3658	78.3256	88.6598					
	std dev	3.421147087	2.976325	3.407593	2.799555	3.382898					
	Sum	338.51568	352.9132	317.3078	325.6808	365.1951					
Set-2	Image 1	82.40398	85.2183	76.5696	78.0012	89.0997	82.25856	89.0997	76.5696	5.149558	411.2928
	Image 2	76.998	80.0011	72.0011	74.1091	83.5364	77.32914	83.5364	72.0011	4.597167	386.6457
	Image 3	74.529	78.2022	68.2424	71.2022	81.5364	74.74244	81.5364	68.2424	5.314066	373.7122
	Image 4	76.0911	80.998	72.0011	73.8747	82.529	77.09878	82.529	72.0011	4.530112	385.4939
	average	77.50552	81.1049	72.20355	74.2968	84.17538					
	max	82.40398	85.2183	76.5696	78.0012	89.0997					
	min	74.529	78.2022	68.2424	71.2022	81.5364					
	std dev	3.421147087	2.976325	3.407593	2.799555	3.382898					
	Sum	310.02208	324.4196	288.8142	297.1872	336.7015					

Table B.2 Root Length of Switch grass from different segmentation algorithms

	Image Side	Threshold Algorithm									
		Isodata	Li	Moments	Otsu	Triangle	average	max	min	std dev	Sum
	Depth 0"-3"	Root Length (cm)									
Set-1	Image 1	76.32954	81.78292	72.325	73.2655	82.3265	77.20589	82.3265	72.325	4.671392	386.0295
	Image 2	77.2154	82.0125	71.3256	74.2354	84.9585	77.94948	84.9585	71.3256	5.564251	389.7474
	Image 3	70.1235	76.2145	67.9568	68.9958	78.6589	72.3899	78.6589	67.9568	4.749652	361.9495
	Image 4	72.1254	78.6659	69.6658	69.5484	80.2154	74.04418	80.2154	69.5484	5.062317	370.2209
	average	73.94846	79.668955	70.3183	71.511275	81.539825					
	max	77.2154	82.0125	72.325	74.2354	84.9585					
	min	70.1235	76.2145	67.9568	68.9958	78.6589					
	std dev	3.381139	2.7628747	1.918675	2.6254304	2.730081					
	Sum	295.7938	318.67582	281.2732	286.0451	326.1593					
Set-2	Image 1	70.67484	76.12822	66.6703	67.6108	76.6718	71.55119	76.6718	66.6703	4.671392	357.756
	Image 2	71.5607	76.3578	65.6709	68.5807	79.3038	72.29478	79.3038	65.6709	5.564251	361.4739
	Image 3	64.4688	70.5598	62.3021	63.3411	73.0042	66.7352	73.0042	62.3021	4.749652	333.676
	Image 4	66.4707	73.0112	64.0111	63.8937	74.5607	68.38948	74.5607	63.8937	5.062317	341.9474
	average	68.29376	74.014255	64.6636	65.856575	75.885125					
	max	71.5607	76.3578	66.6703	68.5807	79.3038					
	min	64.4688	70.5598	62.3021	63.3411	73.0042					
	std dev	3.381139	2.7628747	1.918675	2.6254304	2.730081					
	Sum	273.175	296.05702	258.6544	263.4263	303.5405					

Table B.3 Root Length of Bermuda grass from different segmentation algorithms

	Image Side	Threshold Algorithm									
		Isodata	Li	Moments	Otsu	Triangle	average	max	min	std dev	Sum
	Depth 0"-3"	Root Length (cm)									
Set-1	Image 1	97.69602	103.1455	94.254	93.50019	100.2546	97.77005	103.1455	93.50019	4.051783	488.8503
	Image 2	95.1458	110.5484	88.23589	92.9584	106.2541	98.62852	110.5484	88.23589	9.38775	493.1426
	Image 3	95.1415	109.254	90.251	90.2354	98.3256	96.6415	109.254	90.2354	7.842799	483.2075
	Image 4	93.2541	99.1254	91.365	89.3658	98.1254	94.24714	99.1254	89.3658	4.241423	471.2357
	average	95.30936	105.5183	91.02647	91.51495	100.7399					
	max	97.69602	110.5484	94.254	93.50019	106.2541					
	min	93.2541	99.1254	88.23589	89.3658	98.1254					
	std dev	1.823474	5.346552	2.511324	2.023268	3.799403					
	Sum	381.2374	422.0733	364.1059	366.0598	402.9597					
Set-2	Image 1	83.69602	89.14547	80.254	79.50019	86.25458	83.77005	89.14547	79.50019	4.051783	418.8503
	Image 2	81.1458	96.5484	74.23589	78.9584	92.2541	84.62852	96.5484	74.23589	9.38775	423.1426
	Image 3	81.1415	95.254	76.251	76.2354	84.3256	82.6415	95.254	76.2354	7.842799	413.2075
	Image 4	79.2541	85.1254	77.365	75.3658	84.1254	80.24714	85.1254	75.3658	4.241423	401.2357
	average	81.30936	91.51832	77.02647	77.51495	86.73992					
	max	83.69602	96.5484	80.254	79.50019	92.2541					
	min	79.2541	85.1254	74.23589	75.3658	84.1254					
	std dev	1.823474	5.346552	2.511324	2.023268	3.799403					
	Sum	325.2374	366.0733	308.1059	310.0598	346.9597					

	Image Side	Threshold Algorithm									
		Isodata	Li	Moments	Otsu	Triangle	average	max	min	std dev	Sum
	Depth 0"-3"	Root Length (cm)									
Set-3	Image 1	88.05602	93.50547	84.614	83.86019	90.61458	88.13005	93.50547	83.86019	4.051783	440.6503
	Image 2	85.5058	100.9084	78.59589	83.3184	96.6141	88.98852	100.9084	78.59589	9.38775	444.9426
	Image 3	85.5015	99.614	80.611	80.5954	88.6856	87.0015	99.614	80.5954	7.842799	435.0075
	Image 4	83.6141	89.4854	81.725	79.7258	88.4854	84.60714	89.4854	79.7258	4.241423	423.0357
	average	85.66936	95.87832	81.38647	81.87495	91.09992					
	max	88.05602	100.9084	84.614	83.86019	96.6141					
	min	83.6141	89.4854	78.59589	79.7258	88.4854					
	std dev	1.823474	5.346552	2.511324	2.023268	3.799403					
	Sum	342.6774	383.5133	325.5459	327.4998	364.3997					
Set-4	Image 1	90.93052	96.37997	87.4885	86.73469	93.48908	91.00455	96.37997	86.73469	4.051783	455.0228
	Image 2	88.3803	103.7829	81.47039	86.1929	99.4886	91.86302	103.7829	81.47039	9.38775	459.3151
	Image 3	88.376	102.4885	83.4855	83.4699	91.5601	89.876	102.4885	83.4699	7.842799	449.38
	Image 4	86.4886	92.3599	84.5995	82.6003	91.3599	87.48164	92.3599	82.6003	4.241423	437.4082
	average	88.54386	98.75282	84.26097	84.74945	93.97442					
	max	90.93052	103.7829	87.4885	86.73469	99.4886					
	min	86.4886	92.3599	81.47039	82.6003	91.3599					
	std dev	1.823474	5.346552	2.511324	2.023268	3.799403					
	Sum	354.1754	395.0113	337.0439	338.9978	375.8977					

Appendix C

Soil Porosity

Table C.1 Calculated porosity for L-1 soil

		Spr 2016	Sum 2016	Fall 2016	Spr 2017
Depth (inch)	Depth (mm)	Porosity			
3	76.2	0.528302	0.569811	0.49434	0.539623
6	152.4	0.486792	0.516981	0.456604	0.437736
9	228.6	0.410377	0.403774	0.366038	0.343396
12	304.8	0.360226	0.400000	0.354717	0.362264
15	381	0.405736	0.316981	0.339623	0.388679
18	457.2	0.369887	0.335849	0.354717	0.354717
21	533.4	0.354717	0.350943	0.328302	0.316981
Average		0.416577	0.413477	0.384906	0.391914

Table C.2 Calculated porosity for L-2 soil

		Spr 2016	Sum 2016	Fall 2016	Spr 2017
Depth (inch)	Depth (mm)	Porosity			
3	76.2	0.467	0.490	0.498	0.516
6	152.4	0.475	0.467	0.4301	0.505
9	228.6	0.426	0.400	0.441	0.407
12	304.8	0.430	0.437	0.400	0.373
15	381	0.400	0.373	0.373	0.350
18	457.2	0.411	0.388	0.320	0.335
21	533.4	0.392	0.358	0.339	0.320
Average		0.429	0.416	0.400	0.401

Table C.3 Calculated porosity for L-3 soil

		Spr 2016	Sum 2016	Fall 2016	Spr 2017
Depth (inch)	Depth (mm)	Porosity			
3	76.20	0.569	0.503	0.464	0.439
6	152.4	0.541	0.526	0.429	0.453
9	228.6	0.391	0.421	0.398	0.379
12	304.8	0.395	0.413	0.401	0.415
15	381.0	0.316	0.353	0.387	0.303
18	457.2	0.391	0.436	0.399	0.322
21	533.4	0.388	0.316	0.364	0.333
Average		0.427	0.424	0.406	0.378

References

Alam, M. J., Hossain, M. S., Ahmed, A., and Khan, M. S. (2017). “Comparison of percolation of Flat and Slope Section Vegetated Lysimeters Using Field Soil Water Characteristic Curve.” Proc., Second Pan-American Conference on Unsaturated Soils, Geo-Institute of ASCE, Dallas, Texas.

Ahmed, A., Hossain, M.S., Alam, M.J., and Khan, M.S. (2017). “Moisture Distribution in unsaturated Subgrade through Field Instrumentation and Numerical Modeling”. Proc., Second Pan-American Conference on Unsaturated Soils, Geo-Institute of ASCE, Dallas, Texas.

Albright, W. H., and Benson, C. H. (2002). “Alternative cover assessment program, 2002 annual report.” Publication No. 41182. Division of Hydrological Sciences, Desert Research Institute, University and Community College System of Nevada, and Univ. of Wisconsin–Madison.

Albright, W. H., Gee, G. W., Wilson, G. V., & Fayer, M. J. (2002). “Alternative cover assessment project Phase I Report.” DRI-41183. Desert Res. Inst., Reno, NV.

Albright, W. H., Benson, C. H., Gee, G. W., Abichou, T., McDonald, E. V., Tyler, S. W., & Rock, S. A. (2006). “Field performance of a compacted clay landfill final cover at a humid site.” *J. Geotech. Geoenviron. Eng*., 132(11), 1393-1403.

Albright, W. H., Benson, C. H., Gee, G. W., Roesler, A. C., Abichou, T., Apiwantragoon, P., Lyles, B. and Rock, S. A. (2004). “Field water balance of landfill final covers.” Journal of environmental quality, 33(6), 2317-2332.

Albright, W. H., Benson, C. H., Gee, G. W., Abichou, T., Tyler, S. W., & Rock, S. A. (2006). “Field performance of three compacted clay landfill covers.” Vadose Zone Journal, 5(4), 1157-1171.

Albright, W.H., Benson, C. H., and Waugh, W. J. (2010). Water balance covers for waste containment: Principles and practice, ASCE, Reston, VA.

Albrecht, B. and Benson, C. (2001). “Effect of Desiccation on Compacted Natural Clays.” *J. Geotech. Geoenviron. Eng*., 127(1), 67-75.

Apiwantragoon, P., Benson, C. H., & Albright, W. H. (2014). “Field hydrology of water balance covers for waste containment.” *J. Geotech. Geoenviron. Eng*., 141(2), 04014101.

Abichou, T., Langoni, G., & Tawfiq, K. (2003). “Assessment of alternative earthen final covers for Florida landfills.” *Florida Center for Solid and Hazardous Waste Management, University of Florida, Report*, 03-05.

Abichou, T., Powelson, D., Aitchison, E., Benson, C. and Albright, W. (2005). “Water balances in vegetated lysimeters at a Georgia landfill.” *Soil Crop Sci. Soc. Florida Proc*. 64, 1-8.

Aung, K. K., Rahardjo, H., Leong, E. C., & Toll, D. G. (2001). “Relationship between porosimetry measurement and soil water characteristic curve for an unsaturated residual soil.” In Unsaturated Soil Concepts and Their Application in Geotechnical Practice (pp. 401-416). Springer Netherlands.

ASTM D698. (2007), “Standard Test Methods for Laboratory Compaction Characteristics of Soil Using Standard Effort,” West Conshohocken, Pennsylvania: ASTM International

ASTM D5084. (1990). Standard Test Method for Measurement of Hydraulic Conductivity of Saturated Porous Materials Using a Flexible Wall Permeameter. American Society for Testing and Materials, Philadelphia, PA.

Allen, G. R., Pereira, L. S., Raes, D and Smith, M. (1998). ‘‘Crop Evapotranspiration-Guidelines for computing crop water requirements.’’ *FAO Irrigation and Drainage Paper 56.* FAO, Rome, Italy, 78-86.

Adu, M. O. (2014). “Variations in root system architecture and root growth dynamics of Brassica rapa genotypes using a new scanner-based phenotyping system.” Ph.D. Dissertation, University of Nottingham.

Andrén, O., Elmquist, H., & Hansson, A. C. (1996). “Recording, processing and analysis of grass root images from a rhizotron.” *Plant and Soil*, *185*(2), 259-264.

Abu-Hassanein, Z. S., Benson, C. H., & Blotz, L. R. (1996). “Electrical resistivity of compacted clays.” *Journal of Geotechnical Engineering*, *122*(5), 397-406.

Abràmoff, M. D., Magalhães, P. J., & Ram, S. J. (2004). “Image processing with ImageJ.” *Biophotonics international*, *11*(7), 36-42.

Arsenault, J. L., Poulcur, S., Messier, C., & Guay, R. (1995). “WinRHlZO™, a root-measuring system with a unique overlap correction method.” *HortScience*, *30*(4), 906-906.

Amato, M., & Ritchie, J. T. (2002). “Spatial distribution of roots and water uptake of maize (L.) as affected by soil structure.” *Crop Science*, *42*(3), 773-780.

Attia al Hagrey, S. (2007). “Geophysical imaging of root-zone, trunk, and moisture heterogeneity.” *Journal of Experimental Botany*, *58*(4), 839-854.

Amato, M., Basso, B., Celano, G., Bitella, G., Morelli, G., & Rossi, R. (2008). “In situ detection of tree root distribution and biomass by multi-electrode resistivity imaging.” *Tree physiology*, *28*(10), 1441-1448.

Benson, C. H., Abichou, T., Albright, W., Gee, G., and Roesler, A. (2001). “Field Evaluation of Alternative Earthen Final Covers.” International Journal of Phytoremediation, Vol. 3, No. 1, pp. 105-127.

Benson, C. H. and Bareither, C. (2012). “Designing Water Balance Covers for Sustainable Waste Containment: Transitioning State of the Art to State of the Practice.” Geotechnical Engineering State of the Art and Practice: pp. 1-33.

Benson, C. H., Sawangsuriya, A., Trzebiatowski, B., & Albright, W. H. (2007). “Postconstruction changes in the hydraulic properties of water balance cover soils.” Journal of geotechnical and geoenvironmental engineering, 133(4), 349-359.

Benson, C. H., Abichou, T., Wang, X., Gee, G. W., and Albright, W. H. (1999a). “Test section installation instructions, Alternative Cover Assessment Program.” *Geo. Engineering Rep. No. 99–3*. Geo Engineering Program, Univ. of Wisconsin, Madison, Wis.

Benson, C. H., Daniel, D. E., and Boutwell, G. (1999b). “Field performance of compacted clay liners.” *J. Geotech. Geoenviron. Eng.*, 125(5), 390–403.

Benson, C. H., Hardianto, F. S., and Motan, E. S. (1994). “Representative specimen size for hydraulic conductivity assessment of compacted soil liners.” *Hydraulic conductivity and waste contaminant transport in soils: ASTM STP 1142*. S. Trautwein and D. Daniel, eds., ASTM, Philadelphia, 3–29.

Benson, C., and Khire, M. (1995). “Earthen covers for semi-arid and arid climates.” *Landfill Closures*, J. Dunn, and U. Singh, eds., ASCE, New York, 201–217.

Benson, C., and Khire, M. (1997). “Earthen materials in surface barriers.” *Barrier Technologies for Environmental Management: Summary of a Workshop*, National Academy Press, National Research Council, D79–D89.

Benson, C. H., and Othman, M. A. (1993). “Hydraulic conductivity of compacted clay frozen and thawed *in situ*.” *J. Geotech. Engrg.*, 119(2), 276–294.

Benson, C., and Wang, X. (1996). “Field hydraulic conductivity assessment of the NCASI final cover test plots.” *Environmental Geotechnics Rep. 96–9*, Dept. of Civil and Environmental Engineering, Univ. of Wisconsin, Madison, Wis.

Benson, C. H. and Khire, M. (1995). “Earthen Covers for Semi-Arid and Arid Climates.” *Landfill Closures*, ASCE, GSP No. 53, J. Dunn and U. Singh, eds., pp. 201-217.

Benson, C. H. (1997). “A review of alternative landfill cover demonstrations.” Department of Civil and Environmental Engineering, University of Wisconsin-Madison.

Benson, C. H., Albright, W. H., Roesler, A. C., & Abichou, T. (2002). “Evaluation of final cover performance: field data from the alternative cover assessment program (ACAP).” Proc. Waste Management, 2, 1-15.

Benson, C. H. and Gribb, M. M. (1997). “Measuring unsaturated hydraulic conductivity in the laboratory and field.” Proceedings of sessions on unsaturated soils at Geo-Logan 1997, July 15-19, Logan, Utah.

Benson, C. H., Bohnhoff, G. L., Ogorzalek, A. S., Shackelford, C. D., Apiwantragoon, P., and Albright, W. H. (2005). “Field Data and Model Predictions for a Monolithic Alternative Cover.” Waste Containment and Remediation: pp. 1-16.

Bohnhoff, C., Ogorzalek, A., Benson, C., Shackelford, C., and Apiwantragoon, P. (2009). “Field Data and Water-Balance Predictions for a Monolithic Cover in a Semiarid Climate.” *J. Geotech. Geoenviron. Eng*., 135(3), 333-348.

Barnswell, K. D. (2010). “Determining preliminary components for a landfill evapotranspiration cover.” Ph.D. Dissertation, University of Toledo, 2010.

Barnswell, K. D., & Dwyer, D. F. (2010). “Assessing the performance of evapotranspiration covers for municipal solid waste landfills in Northwestern Ohio.” Journal of Environmental Engineering, 137(4), 301-305.

Baecker, V. (2010). “Image processing and analysis with Image J and MRI Cell Image Analyzer.” *Montpellier RIO Imaging*, 1-93.

Barnett, D. P., Paul, J. L., Harris, R. W., & Henderson, D. W. (1983). Estimating root length densities around transplanted container-grown plants. *Journal of Arboriculture (USA)*.

Bates, G.H. 1937. A device for the observation of root growth in the soil. Nature. 139:966-967.

Böhm, W. (1979). Container methods. In *Methods of studying root systems* (pp. 95-114). Springer Berlin Heidelberg.

Barnett, D. P., Paul, J. L., Harris, R. W., & Henderson, D. W. (1983). “Estimating root length densities around transplanted container-grown plants.” *Journal of Arboriculture (USA)*.

Bucksch, A., Burridge, J., York, L. M., Das, A., Nord, E., Weitz, J. S., & Lynch, J. P. (2014). “Image-based high-throughput field phenotyping of crop roots.” *Plant Physiology*, *166*(2), 470-486.

Benjamin, J. G., & Nielsen, D. C. (2004). “A method to separate plant roots from soil and analyze root surface area.” *Plant and Soil*, *267*(1), 225-234.

Brown, D. P., Pratum, T. K., Bledsoe, C., Ford, E. D., Cothern, J. S., & Perry, D. (1991). “Noninvasive studies of conifer roots: nuclear magnetic resonance (NMR) imaging of Douglas-fir seedlings.” *Canadian Journal of Forest Research*, *21*(11), 1559-1566.

Bottema, M. J. (2000). “Circularity of objects in images.” In Acoustics, Speech, and Signal Processing, 2000. ICASSP'00. Proceedings. 2000 IEEE International Conference on (Vol. 4, pp. 2247-2250). IEEE.

Basu, P., & Pal, A. (2012). “A new tool for analysis of root growth in the spatio-temporal continuum.” *New Phytologist*, *195*(1), 264-274.

Beven, K., & Germann, P. (1982). “Macropores and water flow in soils.” *Water resources research*, *18*(5), 1311-1325.

Care, D., Nichols, S., & Woodfield, D. (1998). “Image analysis techniques to characterize white clover root morphology.” In *Proceedings of the New Zealand Grassland Association* (Vol. 60, pp. 187-191).

Cortina, J., & Maestre, F. T. (2005). “Plant effects on soils in drylands: implications for community dynamics and ecosystem restoration.” In *Tree species effects on soils: implications for global change* (pp. 85-118). Springer, Dordrecht.

Chen, L., Huang, Z., Gong, J., Fu, B., & Huang, Y. (2006). “The effect of land cover/vegetation on soil water dynamic in the hilly area of the loess plateau, China.” *Catena*, *70*(2), 200-208.

Chamberlain, E. J., & Gow, A. J. (1979). “Effect of freezing and thawing on the permeability and structure of soils.” *Engineering geology*, *13*(1-4), 73-92.

Dwyer, S. F., Rager, R. E., & Hopkins, J. (2007). “Cover system design guidance and requirements document.” EP2006-0667, Los Alamos National Laboratories, Los Alamos, New Mexico, USA.

DeVries, B. (2016). “Hydraulic Performance Evaluation of Evapotranspiration Cover Systems.” Ph.D. Dissertation, University of Texas at Arlington.

Dwyer, S. F. (2000). “Construction overview of six landfill cover designs.” Sandia Rep. SAND2000-2428, Sandia National Laboratories, Albuquerque, NM.

Dwyer, S. (2003). “Water Balance Measurements and Computer Simulations of Landfill Covers.” Ph.D. Dissertation, New Mexico State University.

Daniel, D. (1984). ‘‘Predicting hydraulic conductivity of clay liners.’’ J. Geotech. Engrg., ASCE, 110(2), 285–300.

Daniel, D. (1987). ‘‘Earthen liners for land disposal facilities.’’ Proc., Geotech. Pract. for Waste Disposal ’87, R. Woods, ed., ASCE, Reston, Va., 21–39.

Daniel, D. (1989). ‘‘In situ hydraulic conductivity tests for compacted clays.’’ J. Geotech. Engrg., ASCE, 115(9), 1205–1227.

Doorenbos, J., and Pruit, W. (1977). "Guidelines for predicting crop water requirements." FAO Irrigation Paper No. 24, 2"d ed., Food and Agricultural Organization of the United Nations, Rome, Italy.

Devitt, D. A., Morris, R. L., & Bowman, D. C. (1992). “Evapotranspiration, crop coefficients, and leaching fractions of irrigated desert turfgrass systems”. Agronomy Journal, 84(4), 717-723.

Daly, K. R., Mooney, S. J., Bennett, M. J., Crout, N. M., Roose, T., & Tracy, S. R. (2015). “Assessing the influence of the rhizosphere on soil hydraulic properties using X-ray computed tomography and numerical modelling.” *Journal of experimental botany*, *66*(8), 2305-2314.

Downie, H., Holden, N., Otten, W., Spiers, A. J., Valentine, T. A., & Dupuy, L. X. (2012). “Transparent soil for imaging the rhizosphere.” *PLoS One*, *7*(9), e44276.

Dannoura, M., Kominami, Y., Oguma, H., & Kanazawa, Y. (2008). “The development of an optical scanner method for observation of plant root dynamics.” *Plant Root*, *2*, 14-18.

Elrick, D.E., Reynolds, W.D., (1992). “Methods of analyzing constant head well permeameter data.” Soil Sci. Soc. Am. J. 56, 320–323.

Fayer, M. and Jones, T. (1990). “Unsaturated Soil-Water and Heat Flow Model, version 2.0.” Pacific Northwest Lab., Richland, Washington.

Fayer, M. J. (2000). “UNSAT-H version 3.0: Unsaturated soil water and heat flow model - Theory, User Manual and Examples.” PNNL-13249, Pacific Northwest National Laboratory, Richland, WA 99352.

Fayer, M.J., and G. Gee. (1992). "Predicted drainage at a semiarid site: sensitivity to hydraulic property description and vapor flow."

Fredlund, D. (1995). "Prediction of Unsaturated Soil Functions Using the Soil-Water Characteristic Curve." GEOTECHNICAL ENGINEERING, 13, 16.

Fredlund, D. G. and Rahardjo, H. (1993). "Soil Mechanics for Unsaturated Soils." John Wiley and Sons, New York, NY.

Foxx, S., G.D. Tierney, and J.M. Williams. (1984). "Rooting Depths of Plants on Low-Level Waste Disposal Sites." LA-10253-MS, Los Alamos National Laboratory, Los Alamos, NM.

Ferreira, T., & Rasband, W. (2012). "ImageJ user guide." *ImageJ/Fiji*, *1*.

Fang, S., Clark, R., & Liao, H. (2012). "3D quantification of plant root architecture in situ." In *Measuring Roots* (pp. 135-148). Springer Berlin Heidelberg.

Gurdal, T., Benson, C. H., and Albright, W. H. (2003). "Hydrologic properties of final cover soils from the alternative cover assessment program." Geo Engineering Rep. No. 03-02, Geo Engineering Program, Univ. of Wisconsin–Madison, Madison, WI.

Gross, B.A., R. Bonaparte, and J.P. Giroud. (2001). "Waste containment systems: problems and lessons learned." U.S. Environmental Protection Agency, National Risk Management Research Laboratory.

Green, R. L., Beard, J. B., & Casnoff, D. M. (1990). "Leaf blade stomatal characterizations and evapotranspiration rates of 12 cool-season perennial grasses". HortScience, 25(7), 760-761.

Green, R. L., Sifers, S. I., Atkins, C. E. and Beard, J. B. 1991. "Evapotranspiration rates of eleven Zoysia genotypes." HortScience 26(3):264-266.

Garbout, A., Munkholm, L. J., & Hansen, S. B. (2013). "Temporal dynamics for soil aggregates determined using X-ray CT scanning." *Geoderma*, *204*, 15-22.

Glinski, D. S., Karnok, K. J., & Carrow, R. N. (1993). “Comparison of reporting methods for root growth data from transparent-interface measurements.” *Crop science*, *33*(2), 310-314.

Hauser, V. L., & Gimon, D. M. (2004). “Evaluating evapotranspiration (ET) landfill cover performance using hydrologic models.” *Air Force Center for Environmental Excellence, San Antonio, Texas, USA*.

Hauser, V.L. (2009). “Evapotranspiration Covers for Landfills and Waste Sites.” CRC Press, Boca Raton, FL.

Hauser, V. L., and D. M. Gimon. 2001. “Vegetated Landfill Covers and Phytostabilization-The potential for Evapotranspiration-Based Remediation at Air Force Bases.” Air Force Center for Environmental Excellence (AFCEE), Brooks AFB, TX. Available at: http://www.afcee.brooks.af.mil/er/ert/landfill.htm

Hillel, D. (1998). “Environmental Soil Physics.” Academic Press, San Diego, CA.

Hillel, D. (1980). “Fundamentals of Soil Physics.” Academic Press, Inc., San Diego, CA.

Hakonson, T. E. (1986). “Evaluation of geologic materials to limit biological intrusion into low-level radioactive waste disposal sites (No. LA-10286-MS).” Los Alamos National Lab., NM (USA).

Hakonson, T.E., K.L. Maines, R.W. Warren, K.V. Bostick, G. Trujillo, J.S. Kent, and L.J. Lane. (1994). “Hydrologic evaluation of four landfill cover designs at Hill Air Force Base, Utah.” LAUR-93-4469, Los Alamos National Laboratory, Los Alamos, NM.

Huck, M. G., & Taylor, H. M. (1982). “The rhizotron as a tool for root research.” *Advances in agronomy*, *35*, 1-35.

Heeraman, D. A., Hopmans, J. W., & Clausnitzer, V. (1997). “Three-dimensional imaging of plant roots in situ with X-ray computed tomography.” *Plant and Soil*, *189*(2), 167-179.

Iversen, C. M., Murphy, M. T., Allen, M. F., Childs, J., Eissenstat, D. M., Lilleskov, E. A., Sarjala, T.M., Solan, V.L., & Sullivan, P. F. (2012). “Advancing the use of minirhizotrons in wetlands.” *Plant and Soil*, *352*(1-2), 23-39.

Ingram, K. T., & Leers, G. A. (2001). “Software for measuring root characters from digital images.” *Agronomy Journal*, *93*(4), 918-922.

Jackson, R. B., J. Canadell, J. R. Ehleringer, H. A. Mooney, O. E. Sala, and E.-D. Schulze, (1996). “A global analysis of root distributions for terrestrial biomes.” *Oecologia,* 108, 389–411.

Judd, L. A., Jackson, B. E., & Fonteno, W. C. (2015). “Advancements in root growth measurement technologies and observation capabilities for container-grown plants.” *Plants*, *4*(3), 369-392.

Khire, M. V., Meerdink, J., Benson, C. H. and Bosscher, P. (1995). ‘‘Unsaturated hydraulic conductivity and water balance predictions for earthen landfill final covers.’’ Soil Suction Applications in Geotechnical Engineering Practice, W. Wray and S. Houston, eds., ASCE, New York, 38–57.

Khire, M., Benson, C., and Bosscher, P. (1997). “Water Balance Modeling of Earthen Landfill Covers.” J. Geotech. Geoenviron. Eng., 123(8), 744-754.

Khire, M., Benson, C., and Bosscher, P. (2000). “Capillary Barriers: Design Variables and Water Balance.” J. Geotech. Geoenviron. Eng., 126(8), 695-708.

Kneebone, W. R. and Pepper, I. L. (1984). “Luxury water use by Bermuda grass turf”. Agronomy Journal 76:999-1002.

Klepper, B., & Kaspar, T. C. (1994). “Rhizotrons: their development and use in agricultural research.” *Agronomy journal*, *86*(5), 745-753.

Kano-Nakata, M., Inukai, Y., Wade, L. J., Siopongco, J. D. C., & Yamauchi, A. (2011). “Root development, water uptake, and shoot dry matter production under water deficit conditions in two CSSLs of rice: functional roles of root plasticity.” *Plant Production Science*, *14*(4), 307-317.

Kono, Y., Yamauchi, A., Nonoyama, T., Tatsumi, J., & Kawamura, N. (1987). “A Revised Experimental System of Root-Soil” Interaction for Laboratory Work. *Environment Control in Biology*, *25*(4), 141-151.

Licht, L., Aitchison, E., Schnabel, W., English, M., and Kaempf, M., (2001), “Landfill Capping with Woodland Ecosystems,” *Practice Periodical of azardous, Toxic, and Radioactive Waste Management, Vol. 5, No. 4.*

Labno, C. (2014). “Basic Intensity Quantification with ImageJ.” *Integrated Light Microscopy Core, University of Chicago*.

Lobet, G., Draye, X., & Périlleux, C. (2013). “An online database for plant image analysis software tools.” *Plant methods*, *9*(1), 38.

Lazzari, L. (2008). “Study of spatial variability of soil root zone proper ties using electrical resistivity technique.” Ph.D. Dissertation, University of Basilicata, Potenza, Italy, 107 p

Loperte, A., Satriani, A., Lazzari, L., Amato, M., Celano, G., Lapenna, V., & Morelli, G. (2006). “2D and 3D high resolution geoelectrical tomography for non-destructive determination of the spatial variability of plant root distribution: laboratory experiments and field measurements.” *Geophysical Resource Abstract Wien*, *8*, 06749.

Mulder, J.H., and E.L. Haven. (1995). “Solid Waste Assessment Test “SWAT” Program.” Document No.: 96-1CWP, Report to the Integrated Waste Management Board,

Division of Clean Water, Water Resources Control Board, California Environmental Protection Agency.

Meerdink, J. S., Benson, C. H., & Khire, M. V. (1996). “Unsaturated hydraulic conductivity of two compacted barrier soils.” *Journal of geotechnical engineering*, *122*(7), 565-576.

Malusis, M. A. and Benson, C. H. (2006). “Lysimeter versus Water-Content Sensors for Performance Monitoring of Alternative Earthen Final Covers.” *Unsaturated Soils 2006*: pp. 741-752.

McGuire, P. E., Andraski, B. J., & Archibald, R. E. (2009). “Case study of a full-scale evapotranspiration cover.” *Journal of geotechnical and geoenvironmental engineering*, *135*(3), 316-332.

McKenney, M. S., & Rosenberg, N. J. (1993). Sensitivity of some potential evapotranspiration estimation methods to climate change. *Agricultural and Forest Meteorology*, *64*(1-2), 81-110.

Miura, K. (2006). “Basics of image processing and analysis.” *Centre for Molecular & Cellular Imaging EMBL Heidelberg*.

McDougall, W. B. (1916). “The growth of forest tree roots.” *American Journal of Botany*, *3*(7), 384-392.

Metzner, R., Eggert, A., van Dusschoten, D., Pflugfelder, D., Gerth, S., Schurr, U., & Jahnke, S. (2015). “Direct comparison of MRI and X-ray CT technologies for 3D imaging of root systems in soil: potential and challenges for root trait quantification.” *Plant methods*, *11*(1), 17.

Morelli, G., Zenone, T., Teobaldelli, M., Fischanger, F., Matteucci, M., & Seufert, G. (2007). “Use of ground-penetrating radar (GPR) and electrical resistivity tomography

(ERT) to study tree roots volume in pine forest and poplar plantation." *Napier, New Zealand*, *21*, 1-4.

Nyhan, J. W. (2005). "A seven-year water balance study of an evapotranspiration landfill cover varying in slope for semiarid regions." *Vadose Zone Journal*, *4*(3), 466-480.

Nyhan, J. W., Schofield, T. G., and Starmer, R. H. (1997). "A water balance study of four land fill cover designs varying in slope for semiarid regions." J. Environ. Qual., 26(5), 1385– 1392.

Nixon, W.B., R.J. Murphy and R.I. Stessel, (1997). "An empirical approach to the performance assessment of solid waste landfills." *Waste Management & Research*, 15:607-626

Nagase, A., & Dunnett, N. (2012). "Amount of water runoff from different vegetation types on extensive green roofs: Effects of plant species, diversity and plant structure". *Landscape and urban planning*, *104*(3), 356-363.

Neumann, G., George, T. S., & Plassard, C. (2009). "Strategies and methods for studying the rhizosphere" the plant science toolbox. *Plant and Soil*, *321*(1-2), 431-456.

Ogorzalek, A. S., Bohnhoff, G. L., Shackelford, C. D., Benson, C. H., & Apiwantragoon, P. (2008). "Comparison of field data and water-balance predictions for a capillary barrier cover." Journal of geotechnical and geoenvironmental engineering, 134(4), 470-486.

Othman, M., A, Bonaparte, R., Gross, B., A, and Schmertmann, G., R. (1995). "Design of MSW landfill final cover systems." Landfill Closures ... Environmental Protection and Land Recovery, ASCE, Geotechnical Special Publication No. 53,218-257.

Ottman, M. J., & Timm, H. (1984). "Measurement of viable plant roots with the image analyzing computer." *Agronomy journal*, *76*(6), 1018-1020.

OEPA. (2003). "Sanitary landfill construction facility construction." OAC Chapter 3745-27: Solid & Infectious Waste Regulations, Rule # 374527-08, Ohio Environmental Protection Agency, Columbus, OH.

Plaza-Bonilla, D., Cantero-Martínez, C., Álvaro-Fuentes, J., & Lampurlanés, J. (2012). "Low-cost image analysis method to quantify root surface area." Valencia, Spain: Poster Session. International conference of agricultural engineering, July 8–12.

Pratt, G.C. (2000). "Components of habitat selection, predation risk and biobarrier design for use in managing populations of ground squirrels on low-level radioactive waste landfill caps." MS Thesis, Idaho State University, Pocatello, ID.

Patena, G., & Ingram, K. T. (2000). "Digital acquisition and measurement of peanut root minirhizotron images." *Agronomy Journal*, *92*(3), 541-544.

Pan, W. L., Young, F. L., & Bolton, R. P. (2001). "Monitoring Russian thistle (Salsola iberica) root growth using a scanner-based, portable mesorhizotron." *Weed technology*, *15*(4), 762-766.

Paglis, C. M. (2013). "Application of electrical resistivity tomography for detecting root biomass in coffee trees." *International Journal of Geophysics*, *2013*.

Panissod, C., Michot, D., Benderitter, Y., & Tabbagh, A. (2001). "On the effectiveness of 2D electrical inversion results: an agricultural case study." *Geophysical Prospecting*, *49*(5), 570-576.

Roesler, A.C. and C.H. Benson, (2002). "Field hydrology and model predictions for final covers in the alternative assessment program." Geo Engineering report no. 02-08, University of Wisconsin, Madison, WI.

Ritchie, J.T., and E. Burnett. (1971). "Dryland evaporative flux in a semi humid climate." 2, plant influences. Agron. J. 63:56-62.

Romero, C. C., & Dukes, M. D. (2009). “Turfgrass and ornamental plant evapotranspiration and crop coefficient literature review”. Agricultural and Biological Engineering Department, University of Florida

Rogers, W. S. (1969). “The East Mailing root-observation laboratories.” *Root growth*, 361-376.

Stormont, J. and Morris, C. (1998). “Method to Estimate Water Storage Capacity of Capillary Barriers.” J. Geotech. Geoenviron. Eng., 124(4), 297-302.

Suter, G.W., R.J. Luxmoore, and E.D. Smith. (1993). Compacted soil barriers at abandoned landfills will fail in the long term. Journal of Environmental Quality, Vol. 22, 217-226.

Sala, O. E., Lauenroth W. K., and Parton, W. J., (1992). “Long-term Soil Water Dynamics in The Shortgrass Steppe,” *Ecology, 73 (4*), 1175-1181.

Saravanathiiban, D. S., & Khire, M. V. (2014). “Field-scale unsaturated hydraulic properties of compacted and uncompacted earthen covers.” In *Geo-Congress 2014: Geo-characterization and Modeling for Sustainability* (pp. 1859-1869).

Saravanathiiban, D. S. (2014). “*Preferential flow through earthen landfill covers*.” Ph.D. Dissertation, Michigan State University.

Scanlon, B. R., Reedy, R. C., Keese, K. E., & Dwyer, S. F. (2005). “Evaluation of evapotranspirative covers for waste containment in arid and semiarid regions in the southwestern USA.” *Vadose Zone Journal*, *4*(1), 55-71.

Schwartz, F.W., C.B. Andrews, D.L. Freyberg, C.T. Kincaid, L.F. Konikow, C.R. McKee, D.B. McLaughlin, J.W. Mercer, E.J. Quinn, P.S.C. Rao, B.E. Rittmann, D.D. Runnells, P.K.M van der Heijde, W.J. Walsh, (1990). “Ground water models scientific and regulatory applications.” National Academy Press, Washington, D.C.

Seletchi, E. D., & Duliu, O. G. (2007). “Image Processing and Data Analysis in Computed Tomography.” *Vasa*, *52*, 667-675.

Strunk, R. L. (2009). “An evaluation of the performance of prototype instrumented soil covers at the Regina municipal landfill”. M.S. Thesis, Department of Civil Engineering, University of Saskatchewan, Saskatoon, Saskatchewan

Saini, G. R. (1980). *Pedogenetic and induced compaction in agricultural soils* (p. 32). Research Branch, Agriculture Canada.

Schuurman, J. J., & Goedewaagen, M. A. J. (1965). “*Methods for the examination of root systems and roots”* (pp. 37-41). Wageningen: Centre for agricultural publications and documentation.

Smit, A. L., George, E., & Groenwold, J. (2000). “Root observations and measurements at (transparent) interfaces with soil.” In *Root methods* (pp. 235-271). Springer Berlin Heidelberg.

Soil moisture Equipment Corp. (2011) “Operating instruction of Guelph permeameter.”

Taylor, H.M., D.R. Upchurch and B.L. McMicheal. (1990). “Applications and limitations of rhizotrons and minirhizotrons for root studies.” Plant and Soil. 129:29-35.

Texas Commission on Environmental Quality (TCEQ) (2012). “Guidance for Requesting a Water Balance Alternative Final Cover for a Municipal Solid Waste Landfill.” *Waste Permits Division*, Texas Commission on Environmental Quality, Austin, TX.

Tracy, S. R., Black, C. R., Roberts, J. A., Dodd, I. C., & Mooney, S. J. (2015). “Using X-ray computed tomography to explore the role of abscisic acid in moderating the impact of soil compaction on root system architecture.” *Environmental and Experimental Botany*, *110*, 11-18.

Tardieu, F. (1988). “Analysis of the spatial variability of maize root density.” *Plant and Soil*, *107*(2), 259-266.

Tabbagh, A., Dabas, M., Hesse, A., & Panissod, C. (2000). “Soil resistivity: a non-invasive tool to map soil structure horizonation.” *Geoderma*, *97*(3), 393-404.

U.S. EPA. (1993). “Solid waste disposal facility criteria technical manual.” 40 CFR Part 258, Subpart F, Closure and Post-Closure, Office of Solid Waste and Emergency Response (5306W), U.S. Environmental Protection Agency, Washington, DC.

U.S. EPA. (1991). “*Design and Construction of RCRA/CERCLA Final Covers*.” Washington, D.C.; EPA/625/4-91/025.

U.S. EPA. (1993). “*Presumptive Remedy for CERCLA Municipal Landfill Sites*.” Washington, D.C.: EPA Document No. 540-F-93-035.

U.S. EPA. (1996). “*Application of the CERCLA Municipal Landfill Presumptive Remedy to Military Landfills.”* EPA/540/F-96-020. Office of Solid Waste and Emergency Response, U.S. Environmental Protection Agency.

U.S. EPA. (2003). “Evapotranspiration landfill cover systems fact sheet.” EPA 542-F-03-015, Office of Solid Waste and Emergency Response, U.S. Environmental Protection Agency, Cincinnati.

U.S. Environmental Protection Agency (USEPA) (2006). “Evapotranspiration Landfill Cover Systems Fact Sheet.” *Solid Waste and Emergency Response*, U.S. Environmental Protection Agency, Cincinnati, OH.

U.S. Department of Agriculture, Natural Resources Conservation Service (USDA-NRCS). (2003). “National Soil Survey characterization data.” Soil Survey Laboratory, National Soil Survey Center, Lincoln, Neb.

U.S. Environmental Protection Agency (USEPA). (1992). “U.S. EPA Subtitle D Clarification, 40 CFR 257 & 258, EPA/OSW-FR-92–4146–6.” *Federal Register*, 57(124), 28626–28632.

U.S. EPA. (2004). “Technical Guidance for RCRA/CERCLA Final Covers.” *Solid Waste and Emergency Response*, U.S. Environmental Protection Agency, Cincinnati, OH.

Upchurch, D. R. (1985). “Relationship between observations in mini-rhizotrons and true root length density.” Ph.D. Dissertation, Texas Tech University

Van Genuchten, M. T., Leij, F. J., & Yates, S. R. (1991). “The RETC code for quantifying the hydraulic functions of unsaturated soils.”

Vamerali, T., Bandiera, M., & Mosca, G. (2012). “Minirhizotrons in modern root studies.” In *Measuring roots* (pp. 341-361). Springer Berlin Heidelberg.

Waugh, W. J., Benson, C. H., & Albright, W. H. (2009, January). “Sustainable covers for uranium mill tailings, USA: Alternative design, performance, and renovation”. In Proceedings of 12th International Conference on Environmental Remediation and Radioactive Waste Management (pp. 639-648).

Winkler, W. (1999). “Thickness of Monolithic Covers in Arid and Semi-Arid Climates,” M.S. Thesis, Department of Civil and Environmental Engineering, University of Wisconsin - Madison, 193 p.

Wilson, G.V., W.H. Albright, G.W. Gee, M.J. Fayer, and B.D. Ogan. (1999). “Alternative cover assessment project, phase 1 report.” Final technical report prepared by Desert Research Institute, NV and Pacific Northwest Laboratory, WA for U.S. Environmental Protection Agency.

Webb, S. (2002). Verbal communication. PMTS, Sandia National Laboratories, Albuquerque, NM.

Weaver, J.E. (1920). “Root Development in the Grassland Formation.” Carnegie Institution of Washington, Washington D. C.

Weaver, J. E., Jean, F. C., & Crist, J. W. (1922). “Development and activities of roots of crop plants: a study in crop ecology (No. 316).” Carnegie Institution of Washington.

Wang, J. B., Zhang, X. J., & Wu, C. (2015). “Advances in experimental methods for root system architecture and root development.” *Journal of forestry research*, *26*(1), 23-32.

Zornberg, J. G., LaFountain, L., & Caldwell, J. A. (2003). “Analysis and design of evapotranspirative cover for hazardous waste landfill.” *Journal of Geotechnical and Geoenvironmental Engineering*, *129*(5), 427-438.

Zhu, H., and Zhang, L.M., (2015). “Evaluating suction profile in a vegetated slope considering uncertainty in transpiration.” Comput. Geotech. 63, 112–120

Zhang, L., W. R. Dawes, and G. R. Walker, (2001). “Response of mean annual evapotranspiration to vegetation changes at catchment scale.” Water Resour. Res., 37, 701–708.

Zhang, W., & Sun, C. (2014). “Parametric analyses of evapotranspiration landfill covers in humid regions.” *Journal of Rock Mechanics and Geotechnical Engineering*, *6*(4), 356-365.

Zhu, J., Ingram, P. A., Benfey, P. N., & Elich, T. (2011). “From lab to field, new approaches to phenotyping root system architecture.” *Current opinion in plant biology*, *14*(3), 310-317.

Zenone, T., Morelli, G., Teobaldelli, M., Fischanger, F., Matteucci, M., Sordini, M., ... & Seufert, G. (2008). “Preliminary use of ground-penetrating radar and electrical resistivity tomography to study tree roots in pine forests and poplar plantations.” *Functional Plant Biology*, *35*(10), 1047-1058.

Biographical Information

Md. Jobair Bin Alam graduated with a Bachelor of Science in Civil Engineering from Bangladesh University of Engineering and Technology, Dhaka, Bangladesh in February 2011. After graduation, he started his career as Project Engineer in Orascom Telecom Company with major responsibility of designing of shallow and deep foundation and supervising the construction. On January 2013, he joined Concrete and Steel Technologies Limited, Dhaka, Bangladesh as a design engineer. He served as a Project Coordinator in the same company during that time. Md. Jobair Bin Alam started his graduate studies at The University of Texas at Arlington on spring 2014. As a graduate student, he got the opportunity to work as a graduate research/teaching assistant under supervision of Dr. Sahadat Hossain. The author's research interests include sustainable waste management system, bioreactor landfills, landfills final cover system design, biocell, constitutive modeling of soil, numerical modeling, deep foundation, slope stability analysis, non-destructive testing and geophysical investigation.